



Norwegian University of
Science and Technology

Prefeasibility Study of Piedras Negras Hydropower Plant

Rodrigo Suarez Barrera

Hydropower Development

Submission date: May 2018

Supervisor: Oddbjørn Bruland, IBM

Co-supervisor: Brian Glover, IBM

Norwegian University of Science and Technology
Department of Civil and Environmental Engineering

Prefeasibility Study of Piedras Negras Hydropower Plant

Rodrigo Suárez Barrera

Hydropower Development

Submission date: May 2018

Supervisor: Oddbjørn Bruland

Co-supervisor: Brian Glover

Norwegian University of Science and Technology
Department of Civil and Environmental Engineering

(This page intentionally left blank)

Abstract

Piedras Negras hydropower plant, found in the high altitudes of the Andes mountain range, specifically on the San José river in the Libertador O'Higgins region of Chile, will have a design flow of 10 m³/s, a gross head 281.5 m, 23 MW of installed capacity and 62.3 GWh/year of energy production.

A third of the area of the catchment, from which the flow that will feed the power plant is going to be derived, is covered by the Universidad glacier, which controls the hydrological regime of the San José river, imposing a challenge for the hydrological study which was satisfactorily overcome using the HBV model, a hydrological model popular in the Scandinavian countries. The hydrological study produced a series of 39 years of runoff data with a mean annual discharge of 4.0 m³/s for the San José river at the intake point.

For the design of the hydropower plant itself, three layouts alternatives were analyzed and evaluated from a hydraulic, energy production and costs point of view. All the alternatives considered a flow conduction using pressure pipes and a powerhouse with two Pelton units of varied sizes.

Financially speaking, the most attractive alternative was quoted in 71.3 million of USD with a unit price of energy production of 1,145 USD/MWh.

Although the presence of the glacier in the intake catchment makes this area especially susceptible to the impact of climate change, the results of this evaluation for the lifetime of the power plant showed that under the RCP4.5 scenario, the energy production would increase by 15% while for the most extreme scenario, RCP8.5, this increment would reach 22%. This shows that the installed capacity could be increased to take advantage of the future effects of climate change.

Finally, and due to the characteristics of the project, a detailed analysis of the transient phenomenon in the system is recommended at a future engineering stage as well as a sediment management plan with the goal of extending the lifetime of the electro-mechanical equipment of the power plant, and thus, keeping the operational costs as low as possible.

(This page intentionally left blank)

Acknowledgments

Without my wife Marilu, I would never have taken the initiative to pursue this Master and with it the realization of this Thesis. To you, all my love and recognition for making me a better person every day.

For their infinite patience from the beginning, for sharing their wisdom and for enduring my constant persecution, my professors Brian Glover and Oddbjørn Bruland deserve a statue.

To Tom Jacobsen, who supported me and fed me ideas for an extended period with the noblest intention of just helping me with my endeavor.

To Abebe Girmay Adera who had the patience and the time to sit down with me and teach me in detail how to make climate change analysis from scratch and to Thuat Trinh who with great kindness aided me with the laboratory analysis of the sediment sample.

To my family in Venezuela, who despite the difficult (almost impossible) circumstances of the country have always given me their support and their enthusiasm to continue moving forward.

To the Norwegians in Verkstadloftet, who always included me and made me feel welcomed throughout the year, and even though I still do not know if you consider me as your friend, be sure to know you all are more than friends to me.

To all my friends of Hydropower Development 2016-2018 whom were always there for me and coped with my lousy jokes, especially Ana, Bendik, Debora, Janka, and Javier who were my escape valve and support column during all this time.

Finally, to my friend Rene Ilabaca of Anpac Energía, who in the kindest way made this project available to me and was always able to help and answer all my questions.

To all of you, my deepest and most sincere gratitude.

(This page intentionally left blank)

Table of Contents

| | | |
|----------|---|-----------|
| 1 | INTRODUCTION..... | 1 |
| 2 | PROJECT LOCATION | 5 |
| 3 | HYDROLOGICAL STUDY..... | 9 |
| 3.1 | INTAKE LOCATION | 9 |
| 3.2 | INTAKE WATERSHED DELIMITATION | 10 |
| 3.3 | GAUGING STATIONS AND METEOROLOGICAL DATA | 12 |
| 3.4 | HYDROLOGICAL MODEL | 16 |
| 3.4.1 | Model Structure..... | 16 |
| 3.4.2 | Model Calibration | 20 |
| 3.5 | METEOROLOGICAL BASE DATA FOR HYDROLOGICAL MODELLING | 21 |
| 3.5.1 | Precipitation Data..... | 22 |
| 3.5.2 | Temperature Data..... | 26 |
| 3.5.3 | Evapotranspiration Data..... | 30 |
| 3.5.4 | Calibration Runoff Data..... | 34 |
| 3.6 | CALIBRATION OF HYDROLOGICAL MODEL: MEAN DAILY RUNOFF TIMESERIES | 35 |
| 3.6.1 | Catchment Parameters..... | 35 |
| 3.6.2 | Calibration Results | 39 |
| 3.6.3 | Verification..... | 45 |
| 3.7 | MEAN DAILY RUNOFF TIMESERIES AT INTAKE | 52 |
| 3.7.1 | Catchment Parameters..... | 52 |
| 3.7.2 | Intake Mean Daily Runoff Timeseries Results | 54 |
| 3.8 | FLOOD FREQUENCY ANALYSIS..... | 57 |
| 3.8.1 | Model Calibration | 57 |
| 3.8.2 | Frequency Analysis | 59 |
| 4 | CLIMATE CHANGE ANALYSIS..... | 63 |
| 4.1 | DEFINITIONS AND SCENARIOS | 63 |
| 4.2 | CLIMATE MODELS AND DOWNSCALING | 65 |
| 4.2.1 | Driving Model Selection | 66 |
| 4.2.2 | Regional Climate Model | 67 |
| 4.2.3 | Domain..... | 67 |
| 4.3 | ANALYSIS PROCEDURE..... | 68 |
| 4.3.1 | Node Selection | 68 |
| 4.3.2 | Bias Correction..... | 69 |
| 4.4 | CLIMATE CHANGE RESULTS..... | 73 |
| 4.4.1 | Projected Precipitation | 73 |
| 4.4.2 | Projected Temperature | 76 |
| 4.4.3 | Projected Glacier Melting | 79 |
| 4.4.4 | Projected Intake Mean Daily Runoff Timeseries | 84 |

| | | |
|----------|---|------------|
| 5 | POWER PLANT DESIGN | 89 |
| 5.1 | POWERHOUSE LOCATION | 89 |
| 5.2 | HYDRAULIC STUDY OF SAN JOSÉ RIVER | 94 |
| 5.3 | LANDSLIDE RISK | 100 |
| 5.4 | INTAKE ANALYSIS | 104 |
| 5.5 | SEDIMENT AND SETTLING BASIN..... | 107 |
| 5.5.1 | Preliminary Assessment | 108 |
| 5.5.2 | Settling Basin Design | 112 |
| 5.5.3 | Final Remarks | 116 |
| 5.6 | HEADRACE CONDUIT AND PENSTOCK ALIGNMENT | 118 |
| 5.6.1 | Alignment Criteria..... | 118 |
| 5.6.2 | Alternatives Description..... | 118 |
| 6 | ENERGY PRODUCTION MODEL | 121 |
| 6.1 | TURBINE INFLOW | 121 |
| 6.2 | TURBINE EFFICIENCY AND ACCEPTED FLOW RANGE | 124 |
| 6.3 | GROSS HEAD..... | 125 |
| 6.4 | HEAD LOSSES | 127 |
| 6.4.1 | Frictional Losses | 127 |
| 6.4.2 | Singular Losses | 128 |
| 6.5 | POWER PLANT DESIGN FLOW, NUMBER OF TURBINES, AND THEIR TYPE | 129 |
| 6.6 | OPTIMAL DIAMETER AND TURBINE SIZE COMBINATION..... | 133 |
| 6.6.1 | Optimal Diameter Analysis..... | 134 |
| 6.6.2 | Results | 139 |
| 6.7 | MINIMUM FLOW IMPACT ON ENERGY GENERATION | 143 |
| 6.8 | RESULTS SUMMARY AND FINAL REMARKS | 144 |
| 7 | SURGE CHAMBER AND GOVERNOR STABILITY ASSESSMENT | 149 |
| 7.1 | SURGE CHAMBER | 149 |
| 7.2 | GOVERNOR STABILITY | 152 |
| 7.2.1 | Synchronous Rotational Speed..... | 153 |
| 7.2.2 | Inertia of Electro-Mechanical Elements..... | 155 |
| 7.2.3 | Water and Mechanic Starting Times | 156 |
| 7.2.4 | Wicket, Gate Times, and Governor Stability Results | 158 |
| 7.3 | FINAL REMARKS | 160 |
| 8 | COST ANALYSIS..... | 161 |
| 8.1 | DIRECT COSTS..... | 161 |
| 8.1.1 | Intake..... | 161 |
| 8.1.2 | Settling Basin and Forebay | 161 |
| 8.1.3 | Headrace Conduit and Penstock..... | 162 |

| | | |
|-----------|---|------------|
| 8.1.4 | Powerhouse | 162 |
| 8.2 | INDIRECT COSTS..... | 163 |
| 8.3 | UNFORESEEN EXPENSES..... | 163 |
| 8.4 | RESULTS..... | 164 |
| 8.5 | FINAL REMARKS | 168 |
| 9 | CLIMATE CHANGE IMPACT IN ENERGY PRODUCTION | 171 |
| 10 | RESULTS SUMMARY AND RECOMMENDATIONS..... | 175 |
| 10.1 | RESULTS SUMMARY | 175 |
| 10.2 | RECOMMENDATIONS | 178 |
| 11 | REFERENCES | 181 |
| 12 | APPENDIX | 185 |

| | |
|----------------|--|
| APPENDIX I: | Monthly Summary of Precipitation Data |
| APPENDIX II: | Monthly Summary of Temperature Data |
| APPENDIX III: | Monthly Summary of Calibration Runoff Data |
| APPENDIX IV: | Monthly Summary of Runoff Data at the Intake |
| APPENDIX V: | Flood Runoff per Year at Aquaflow |
| APPENDIX VI: | Monthly Summary of Runoff Data with Climate Change at the Intake |
| APPENDIX VII: | Hydraulic Simulation Results |
| APPENDIX VIII: | Detailed Cost Analysis Results |

List of Figures

- FIGURE 1.1: INSTALLED CAPACITY TIMELINE IN CHILE..... 1
- FIGURE 1.2: TYPE OF POWER PLANTS COMMISSIONED BY DECADE..... 2
- FIGURE 1.3: HISTORICAL ENERGY PRICES IN CHILE..... 3
- FIGURE 2.1: GENERAL LOCATION OF THE PROJECT SITE..... 6
- FIGURE 2.2: VICINITY OF THE PROJECT SECTOR 6
- FIGURE 2.3: PROJECT SECTOR LIMITS 7
- FIGURE 3.1: INTAKE AND WATER RIGHTS LOCATION..... 10
- FIGURE 3.2: PIEDRAS NEGRAS INTAKE WATERSHED..... 11
- FIGURE 3.3: HYSOMETRY CURVE OF INTAKE CATCHMENT 12
- FIGURE 3.4: GAUGING STATIONS LOCATION 14
- FIGURE 3.5: SUMMARY OF AVAILABLE DATA FOR GAUGING STATIONS..... 15
- FIGURE 3.6: HBV MODEL STRUCTURE..... 18
- FIGURE 3.7: LOCATION OF METEOROLOGICAL STATIONS 22
- FIGURE 3.8: PRECIPITATION CORRELATION BETWEEN LA RUFINA AND SAN FERNANDO 23
- FIGURE 3.9: PRECIPITATION CORRELATION BETWEEN LA RUFINA AND RIO TINGUIRIRICA BAJO LOS BRIONES .. 23
- FIGURE 3.10: HISTORICAL PRECIPITATION TREND AT LA RUFINA 25
- FIGURE 3.11: MEAN MONTHLY PRECIPITATION AT LA RUFINA..... 25
- FIGURE 3.12: TEMPERATURE CORRELATION BETWEEN TERMAS DEL FLACO AND EL YESO EMBALSE..... 27
- FIGURE 3.13: TEMPERATURE CORRELATION BETWEEN EL YESO EMBALSE AND LAGUNA LOS CRISTALES 28
- FIGURE 3.14: HISTORICAL TEMPERATURE TREND AT TERMAS DEL FLACO..... 29
- FIGURE 3.15: SEASONAL TEMPERATURE VARIATION AT TERMAS DEL FLACO 30
- FIGURE 3.16: AVERAGE SUNSHINE HOURS FOR PROJECT LOCATION..... 33
- FIGURE 3.17: SEASONAL RUNOFF VARIATION AT AQUAFLOW 35
- FIGURE 3.18: AQUAFLOW GAUGING STATION CATCHMENT..... 36
- FIGURE 3.19: AQUAFLOW CATCHMENT LAND USE..... 37
- FIGURE 3.20: AQUAFLOW CATCHMENT GLACIERS OUTLINE..... 38
- FIGURE 3.21: HYSOMETRIC CURVE OF AQUAFLOW CATCHMENT..... 39
- FIGURE 3.22: TIMESERIES: OBSERVED VS PREDICTED RUNOFF DATA AT AQUAFLOW..... 41
- FIGURE 3.23: WINTER TEMPERATURE AT AQUAFLOW GAUGING STATION 42
- FIGURE 3.24: MEAN DAILY RUNOFF CORRELATION RESULTS FOR AQUAFLOW STATION 43
- FIGURE 3.25: DURATION CURVE: OBSERVED VS PREDICTED RUNOFF DATA AT AQUAFLOW 44
- FIGURE 3.26: SEASONAL VARIATION: OBSERVED VS PREDICTED RUNOFF DATA AT AQUAFLOW 44
- FIGURE 3.27: MEAN ANNUAL RUNOFF: OBSERVED VS PREDICTED RUNOFF DATA AT AQUAFLOW 45
- FIGURE 3.28: COMPARISON BETWEEN AQUAFLOW AND BRIONES CATCHMENTS 46
- FIGURE 3.29: TIMESERIES: OBSERVED VS PREDICTED RUNOFF DATA AT BRIONES..... 49
- FIGURE 3.30: DURATION CURVE: OBSERVED VS PREDICTED RUNOFF DATA AT BRIONES 49
- FIGURE 3.31: SEASONAL VARIATION: OBSERVED VS PREDICTED RUNOFF DATA AT BRIONES 50
- FIGURE 3.32: MEAN ANNUAL RUNOFF: OBSERVED VS PREDICTED RUNOFF DATA AT BRIONES..... 50

| | |
|---|----|
| FIGURE 3.33: MEAN DAILY RUNOFF CORRELATION RESULTS FOR BRIONES STATION | 51 |
| FIGURE 3.34: INTAKE CATCHMENT LAND USE | 53 |
| FIGURE 3.35: INTAKE CATCHMENT GLACIERS OUTLINE..... | 53 |
| FIGURE 3.36: SAN JOSÉ RIVER MEAN DAILY RUNOFF AT INTAKE | 55 |
| FIGURE 3.37: SAN JOSÉ RIVER MEAN DAILY RUNOFF DURATION CURVE AT INTAKE..... | 55 |
| FIGURE 3.38: SAN JOSÉ RIVER MEAN SEASONAL VARIATION CURVE AT INTAKE..... | 56 |
| FIGURE 3.39: SAN JOSÉ RIVER MEAN ANNUAL RUNOFF AT INTAKE | 56 |
| FIGURE 3.40: DURATION CURVE: OBSERVED VS PREDICTED FLOOD RUNOFF DATA AT AQUAFLOW | 58 |
| FIGURE 3.41: NUMBER OF FLOOD EVENTS PER MONTH AT AQUAFLOW | 59 |
| FIGURE 3.42: HISTOGRAM OF FLOOD MAGNITUDES AT AQUAFLOW | 60 |
| FIGURE 3.43: FLOOD FREQUENCY ANALYSIS RESULTS | 61 |
| FIGURE 4.1: RCP PATHWAYS EVOLUTION IN TIME | 65 |
| FIGURE 4.2: SAM-44 DOMAIN FOR REGIONAL CLIMATE MODEL | 68 |
| FIGURE 4.3: REPRESENTATIVE REGIONAL CLIMATE MODEL NODE FOR INTAKE CATCHMENT | 69 |
| FIGURE 4.4: HISTORICAL SEASONAL PRECIPITATION COMPARISON: MODELS VS OBSERVED DATA | 71 |
| FIGURE 4.5: CONSISTENCY PRECIPITATION TEST COMPARISON: MODELS VS OBSERVED DATA..... | 71 |
| FIGURE 4.6: HISTORICAL SEASONAL TEMPERATURE COMPARISON: MODELS VS OBSERVED DATA..... | 72 |
| FIGURE 4.7: CONSISTENCY TEMPERATURE TEST COMPARISON: MODELS VS OBSERVED DATA | 73 |
| FIGURE 4.8: PRECIPITATION SEASONAL VARIABILITY AT LA RUFINA FOR RCP4.5..... | 74 |
| FIGURE 4.9: PRECIPITATION SEASONAL VARIABILITY AT LA RUFINA FOR RCP8.5..... | 74 |
| FIGURE 4.10: PRECIPITATION TREND AT LA RUFINA FOR RCP4.5 | 75 |
| FIGURE 4.11: PRECIPITATION TREND AT LA RUFINA FOR RCP8.5 | 76 |
| FIGURE 4.12: TEMPERATURE SEASONAL VARIABILITY AT TERMAS DEL FLACO FOR RCP4.5 | 77 |
| FIGURE 4.13: TEMPERATURE SEASONAL VARIABILITY AT TERMAS DEL FLACO FOR RCP8.5 | 77 |
| FIGURE 4.14: TEMPERATURE TREND AT TERMAS DEL FLACO FOR RCP4.5..... | 78 |
| FIGURE 4.15: TEMPERATURE TREND AT TERMAS DEL FLACO FOR RCP8.5..... | 79 |
| FIGURE 4.16: CORRELATION BETWEEN TEMPERATURE AND GLACIER MELT | 80 |
| FIGURE 4.17: HISTORICAL EVOLUTION OF GLACIER MELT AND FIELD TEMPERATURE | 81 |
| FIGURE 4.18: ANNUAL GLACIER MELT TREND FOR RCP4.5 | 82 |
| FIGURE 4.19: ANNUAL GLACIER MELT TREND FOR RCP8.5 | 82 |
| FIGURE 4.20: GLACIER MELT SEASONAL VARIABILITY FOR RCP4.5 | 83 |
| FIGURE 4.21: GLACIER MELT SEASONAL VARIABILITY FOR RCP8.5 | 83 |
| FIGURE 4.22: CHANGE IN GLACIER AREA NEAR THE PROJECT SECTOR FOR RCP8.5 | 84 |
| FIGURE 4.23: RUNOFF TREND AT INTAKE FOR RCP4.5..... | 85 |
| FIGURE 4.24: RUNOFF TREND AT INTAKE FOR RCP8.5..... | 85 |
| FIGURE 4.25: RUNOFF SEASONAL VARIABILITY AT INTAKE FOR RCP4.5 | 86 |
| FIGURE 4.26: RUNOFF SEASONAL VARIABILITY AT INTAKE FOR RCP8.5 | 87 |
| FIGURE 4.27: DURATION CURVE AT INTAKE FOR RCP4.5..... | 88 |
| FIGURE 4.28: DURATION CURVE AT INTAKE FOR RCP8.5..... | 88 |
| FIGURE 5.1: INITIAL LOCATION OF RESTITUTION POINT | 90 |

| | |
|---|-----|
| FIGURE 5.2: PERSPECTIVE OF INITIAL LOCATION OF RESTITUTION POINT..... | 91 |
| FIGURE 5.3: PERCENTAGE OF GROSS HEAD VARIATION ALONG THE RIVER ALIGNMENT | 92 |
| FIGURE 5.4: RESTITUTION POINT AND POWERHOUSE LOCATION | 93 |
| FIGURE 5.5: PANORAMIC VIEW OF THE POWERHOUSE LOCATION..... | 93 |
| FIGURE 5.6: SAN JOSÉ RIVER HYDRAULIC MODEL CROSS-SECTIONS | 95 |
| FIGURE 5.7: POWERHOUSE SECTOR HYDRAULIC MODEL CROSS-SECTIONS..... | 95 |
| FIGURE 5.8: SAN JOSÉ RIVER AND FLOODPLAINS CHARACTERISTICS AT INTAKE SECTOR | 97 |
| FIGURE 5.9: SAN JOSÉ RIVER AND FLOODPLAINS CHARACTERISTICS AT POWERHOUSE SECTOR | 97 |
| FIGURE 5.10: SAN JOSÉ RIVER FLOOD FOOTPRINT RESULTS | 98 |
| FIGURE 5.11: POWERHOUSE SECTOR FLOOD FOOTPRINT RESULTS | 99 |
| FIGURE 5.12: SAN JOSÉ RIVER BUFFER ZONE | 100 |
| FIGURE 5.13: POTENTIAL LANDSLIDE AREAS..... | 102 |
| FIGURE 5.14: SATELLITE IMAGE OF POTENTIALLY UNSTABLE SLOPE IN THE LEFT BANK OF SAN JOSÉ RIVER ... | 103 |
| FIGURE 5.15: POTENTIALLY UNSTABLE SLOPE IN THE LEFT BANK OF SAN JOSÉ RIVER PANORAMIC..... | 103 |
| FIGURE 5.16: INTAKE RESERVOIR FOR A 10 M DAM | 105 |
| FIGURE 5.17: AREA-CAPACITY CURVE FOR 10 M INTAKE DAM RESERVOIR | 106 |
| FIGURE 5.18: PANORAMIC VIEW OF THE INTAKE SECTOR..... | 107 |
| FIGURE 5.19: EXAMPLE OF THE ARID TERRAIN UPSTREAM OF THE INTAKE POINT | 108 |
| FIGURE 5.20: LANDSCAPE UPSTREAM OF THE INTAKE POINT..... | 108 |
| FIGURE 5.21: SAN ANDRÉS HPP INTAKE AND REGULATION POND | 109 |
| FIGURE 5.22: SEDIMENTATION JUST UPSTREAM OF SAN ANDRÉS INTAKE..... | 110 |
| FIGURE 5.23: GRANULOMETRIC CURVE OF SEDIMENT SAMPLE TAKEN AT SAN ANDRÉS REGULATION POND ... | 111 |
| FIGURE 5.24: CAMP SEDIMENT REMOVAL EFFICIENCY DIAGRAM | 113 |
| FIGURE 5.25: SETTLING BASIN TYPICAL CROSS SECTION..... | 115 |
| FIGURE 5.26: SHIELD CRITERIA VERIFICATION FOR SEDIMENT MOTION | 116 |
| FIGURE 5.27: POTENTIAL SETTLING BASIN LOCATION AREA..... | 117 |
| FIGURE 5.28: CONDUITS ALTERNATIVES: HORIZONTAL ALIGNMENT..... | 119 |
| FIGURE 5.29: CONDUITS ALTERNATIVES: VERTICAL ALIGNMENT | 120 |
| FIGURE 6.1: CALCULATION FLOWCHART FOR AVAILABLE INFLOW TO THE POWERPLANT..... | 123 |
| FIGURE 6.2: CALCULATION FLOWCHART FOR TURBINE INFLOW | 124 |
| FIGURE 6.3: TURBINE EFFICIENCY CURVES | 125 |
| FIGURE 6.4: STAGE-DISCHARGE CURVE AT POWERHOUSE SECTION | 126 |
| FIGURE 6.5: PENSTOCK DIAMETERS CONSIDERED TO DEFINE THE POWER PLANT DESIGN FLOW..... | 130 |
| FIGURE 6.6: ENERGY PRODUCTION VS POWER PLANT DESIGN FLOW SUMMARY FOR FRANCIS TURBINE | 131 |
| FIGURE 6.7: ENERGY PRODUCTION VS POWER PLANT DESIGN FLOW SUMMARY FOR PELTON TURBINE | 131 |
| FIGURE 6.8: ENERGY PRODUCTION VS NUMBER OF FRANCIS TURBINE UNITS IN THE POWERHOUSE | 132 |
| FIGURE 6.9: ENERGY PRODUCTION VS NUMBER OF PELTON TURBINE UNITS IN THE POWERHOUSE..... | 132 |
| FIGURE 6.10: DESIGN PIEZOMETRIC LINE FOR ALIGNMENT ALTERNATIVES | 135 |
| FIGURE 6.11: DESIGN CONDUIT PRESSURE FOR ALIGNMENT ALTERNATIVES | 135 |
| FIGURE 6.12: CALCULATION FLOWCHART OF STEEL CONDUIT WALL THICKNESS | 136 |

| | |
|--|-----|
| FIGURE 6.13: TOTAL REQUIRED WEIGHT OF STEEL FOR ALIGNMENT ALTERNATIVES CONDUITS..... | 137 |
| FIGURE 6.14: PERCENTAGE OF THE CONDUIT LENGTH IN GRP AND STEEL FOR ALIGNMENT ALTERNATIVES | 139 |
| FIGURE 6.15: OPTIMAL DIAMETER FOR RIVER ALTERNATIVE | 140 |
| FIGURE 6.16: OPTIMAL DIAMETER FOR ROAD ALTERNATIVE | 140 |
| FIGURE 6.17: OPTIMAL DIAMETER FOR LOW-PRESSURE ALTERNATIVE | 141 |
| FIGURE 6.18: TURBINE SIZE COMBINATION FOR RIVER ALTERNATIVE | 141 |
| FIGURE 6.19: TURBINE SIZE COMBINATION FOR ROAD ALTERNATIVE | 142 |
| FIGURE 6.20: TURBINE SIZE COMBINATION FOR LOW-PRESSURE ALTERNATIVE..... | 142 |
| FIGURE 6.21: MINIMUM FLOW VARIATION IMPACT ON ENERGY PRODUCTION | 144 |
| FIGURE 6.22: TURBINE INFLOW DURATION CURVE | 147 |
| FIGURE 6.23: SPILLED VOLUME OF INFLOW DUE TO THE TURBINE SIZE COMBINATION | 147 |
| FIGURE 7.1: SURGE CHAMBER ALIGNMENT FOR ROAD ALTERNATIVE | 151 |
| FIGURE 7.2: SURGE CHAMBER ALIGNMENT FOR LOW-PRESSURE ALTERNATIVE..... | 151 |
| FIGURE 7.3: GORDON STABILITY CURVES | 153 |
| FIGURE 7.4: GOVERNOR STABILITY RESULT FOR RIVER ALTERNATIVE | 159 |
| FIGURE 7.5: GOVERNOR STABILITY RESULT FOR ROAD ALTERNATIVE | 159 |
| FIGURE 7.6: GOVERNOR STABILITY RESULT FOR LOW-PRESSURE ALTERNATIVE..... | 160 |
| FIGURE 8.1: COST RESULTS FOR RIVER ALTERNATIVE..... | 165 |
| FIGURE 8.2: COST RESULTS FOR ROAD ALTERNATIVE | 166 |
| FIGURE 8.3: COST RESULTS FOR LOW-PRESSURE ALTERNATIVE..... | 166 |
| FIGURE 8.4: SORTED UNIT COST RESULTS PER ALTERNATIVE | 168 |
| FIGURE 9.1: TURBINE INFLOW COMPARISON: HISTORICAL VS CLIMATE CHANGE SCENARIOS | 172 |
| FIGURE 9.2: HISTORICAL AND CLIMATE CHANGE ENERGY PRODUCTION FOR RIVER ALTERNATIVE | 172 |
| FIGURE 9.3: HISTORICAL AND CLIMATE CHANGE ENERGY PRODUCTION FOR ROAD ALTERNATIVE | 173 |
| FIGURE 9.4: HISTORICAL AND CLIMATE CHANGE ENERGY PRODUCTION FOR LOW-PRESSURE ALTERNATIVE... | 173 |

List of Tables

| | |
|---|----|
| TABLE 2.1: POWER PLANTS NEAR THE PROJECT SITE..... | 5 |
| TABLE 3.1: INTAKE LOCATION COORDINATES | 10 |
| TABLE 3.2: INTAKE CATCHMENT MORPHOLOGICAL CHARACTERISTICS..... | 12 |
| TABLE 3.3: GAUGING STATIONS | 13 |
| TABLE 3.4: HBV MODEL PARAMETERS | 18 |
| TABLE 3.5: CORRELATION COEFFICIENTS FOR FILLING LA RUFINA MISSING PRECIPITATION DATA..... | 24 |
| TABLE 3.6: CORRELATION COEFFICIENTS FOR FILLING TERMAS DEL FLACO MISSING TEMPERATURE DATA | 26 |
| TABLE 3.7: CORRELATION COEFFICIENTS FOR FILLING EL YESO EMBALSE MISSING TEMPERATURE DATA | 28 |
| TABLE 3.8: OBSERVED POTENTIAL EVAPORATION | 30 |
| TABLE 3.9: POTENTIAL EVAPOTRANSPIRATION RESULTS | 33 |
| TABLE 3.10: AQUAFLOW CATCHMENT AREA DISTRIBUTION BY ELEVATION ZONE | 38 |

| | |
|---|-----|
| TABLE 3.11: CALIBRATED PARAMETERS FOR AQUAFLOW CATCHMENT..... | 40 |
| TABLE 3.12: NASH-SUTCLIFFE COEFFICIENT FOR CALIBRATION PERIOD..... | 41 |
| TABLE 3.13: BRIONES CATCHMENT AREA DISTRIBUTION BY ELEVATION ZONE | 47 |
| TABLE 3.14: COMPARISON BETWEEN AQUAFLOW AND BRIONES PARAMETERS..... | 47 |
| TABLE 3.15: NASH-SUTCLIFFE COEFFICIENT FOR VERIFICATION PERIOD..... | 48 |
| TABLE 3.16: INTAKE CATCHMENT AREA DISTRIBUTION BY ELEVATION ZONE | 54 |
| TABLE 3.17: RUNOFF RESPONSE ROUTINE PARAMETERS COMPARISON: MEAN RUNOFF VS FLOODS..... | 57 |
| TABLE 3.18: FLOOD DISCHARGE VALUES..... | 62 |
| TABLE 4.1: REPRESENTATIVE CONCENTRATION PATHWAYS (RCP) DESCRIPTION | 64 |
| TABLE 4.2: DESCRIPTION OF SELECTED DRIVING MODELS FOR CLIMATE CHANGE ANALYSIS..... | 66 |
| TABLE 4.3: PRECIPITATION DATA BIAS CORRECTION RESULTING MEAN ABSOLUTE ERROR..... | 70 |
| TABLE 4.4: TEMPERATURE DATA BIAS CORRECTION RESULTING MEAN ABSOLUTE ERROR | 72 |
| TABLE 5.1: RESTITUTION LOCATION COORDINATES | 92 |
| TABLE 5.2: INTERNAL FRICTION ANGLE FOR THE PROJECT AREA GEOTECHNICAL UNITS | 101 |
| TABLE 5.3: SETTLING CHAMBER DESIGN RESULTS..... | 115 |
| TABLE 5.4: SUMMARY OF CONDUIT ALTERNATIVES MAIN GEOMETRIC CHARACTERISTICS | 120 |
| TABLE 6.1: MONTHLY MAXIMUM RUNOFF INTAKE ALLOWANCE AND MINIMUM BYPASS FLOW..... | 122 |
| TABLE 6.2: MAXIMUM AND MINIMUM DESIGN FLOW ACCEPTANCE FOR THE TURBINES..... | 125 |
| TABLE 6.3: CONDUITS ROUGHNESS COEFFICIENTS FOR FRICTIONAL LOSSES..... | 128 |
| TABLE 6.4: HEAD LOSSES COEFFICIENTS FOR SINGULAR LOSSES..... | 129 |
| TABLE 6.5: POWER PLANT DESIGN FLOW AND TURBINE TYPE RESULTS FOR PIEDRAS NEGRAS HPP..... | 133 |
| TABLE 6.6: MAXIMUM COMMERCIALY AVAILABLE GRP PIPE DIAMETERS | 138 |
| TABLE 6.7: ENERGY PRODUCTION MODEL RESULTS SUMMARY | 146 |
| TABLE 7.1: SURGE CHAMBER PRE-DIMENSIONING RESULTS | 150 |
| TABLE 7.2: SPEED NUMBER RANGES FOR BEST EFFICIENCY IN TURBINES..... | 154 |
| TABLE 7.3: SYNCHRONOUS ROTATIONAL SPEED AND SPEED NUMBER FOR PELTON TURBINES | 155 |
| TABLE 7.4: TOTAL INERTIA FOR THE TURBO-GENERATOR GROUP..... | 156 |
| TABLE 7.5: HYDRAULIC AND MECHANICAL STARTING TIMES | 157 |
| TABLE 7.6: GATE OPERATION TIME AND GORDON CURVES STABILITY PARAMETERS | 158 |
| TABLE 8.1: COST RESULTS FOR RIVER ALTERNATIVE..... | 164 |
| TABLE 8.2: COST RESULTS FOR ROAD ALTERNATIVE | 164 |
| TABLE 8.3: COST RESULTS FOR LOW-PRESSURE ALTERNATIVE..... | 165 |
| TABLE 8.4: UNIT COST OF GENERATION PER ALTERNATIVE | 167 |
| TABLE 9.1: ENERGY PRODUCTION RESULTS WITH CLIMATE CHANGE..... | 171 |
| TABLE 9.2: ENERGY PRODUCTION INCREMENT WITH CLIMATE CHANGE..... | 174 |
| TABLE 10.1: PIEDRAS NEGRAS HYDROPOWER PLANT RESULTS SUMMARY | 177 |

Abbreviations

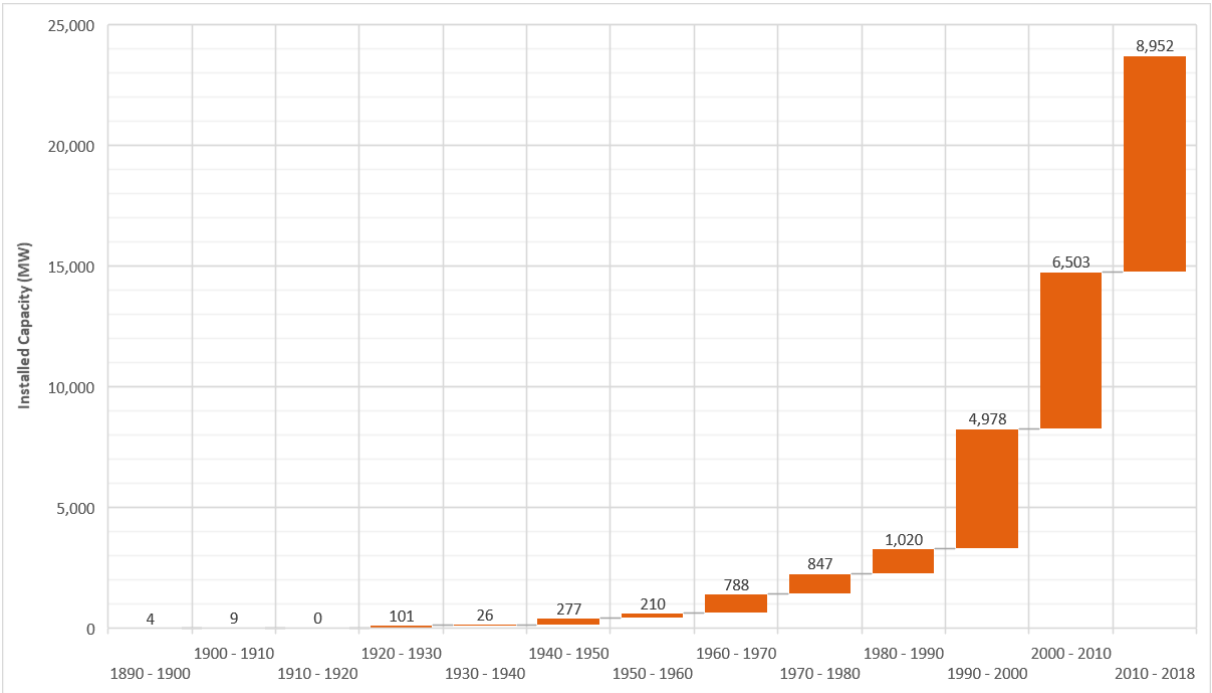
| | |
|--------------|--|
| AR5 | IPCC Fifth Assessment Report |
| ASTER | Advanced Spaceborne Thermal Emission and Reflection Radiometer |
| CAPEX | Capital Expenditure |
| CONAF | National Forestry Corporation |
| CORDEX | Coordinated Regional Climate Downscaling Experiment |
| DGA | General Water Directorate |
| DTM | Digital Terrain Model |
| GCM | General Circulation Model |
| GDEM | Global Digital Elevation Model |
| GIS | Geographical Information System |
| GLIMS | Global Land Ice Measurements from Space |
| GRP | Glass fiber Reinforced Plastics |
| HBV | Hydrologiska Byråns Vattenbalansavdelning |
| HPP | Hydropower Plant |
| ICSU | International Council for Science |
| IOC | Intergovernmental Oceanographic Commission |
| IPCC | Intergovernmental Panel on Climate Change |
| LIDAR | Laser Imaging, Detection and Ranging |
| MOP | Ministry of Public Works |
| mWC | Meter of Water Column |
| NCRE | Non-Conventional Renewable Energies |
| NetCDF | Network Common Data Form |
| NVE | Norges Vassdrags- og Energidirektorat |
| OPEX | Operational Expenditure |
| PEST | Parameter Estimation and Uncertainty Analysis |
| RCA4 | Regional Rossby Center atmospheric model |
| RCM | Regional Climate Models |
| RCP | Representative Concentration Pathways |
| SEA | Environmental Assessment Service |
| SIC | Sistema Interconectado Central |
| SING | Sistema Interconectado del Norte Grande |
| SMHI | Swedish Meteorological and Hydrological Institute |
| UNEP | United Nations Environment Programme |

WCRP..... World Climate Research Program
WMO..... World Meteorological Organization

1 Introduction

Since the arrival of electricity to Chile, at the end of the XIX century, the country has seen, especially in recent times, a considerable increase in its installed generation capacity as can be seen in Figure 1.1.

Figure 1.1: Installed Capacity Timeline in Chile

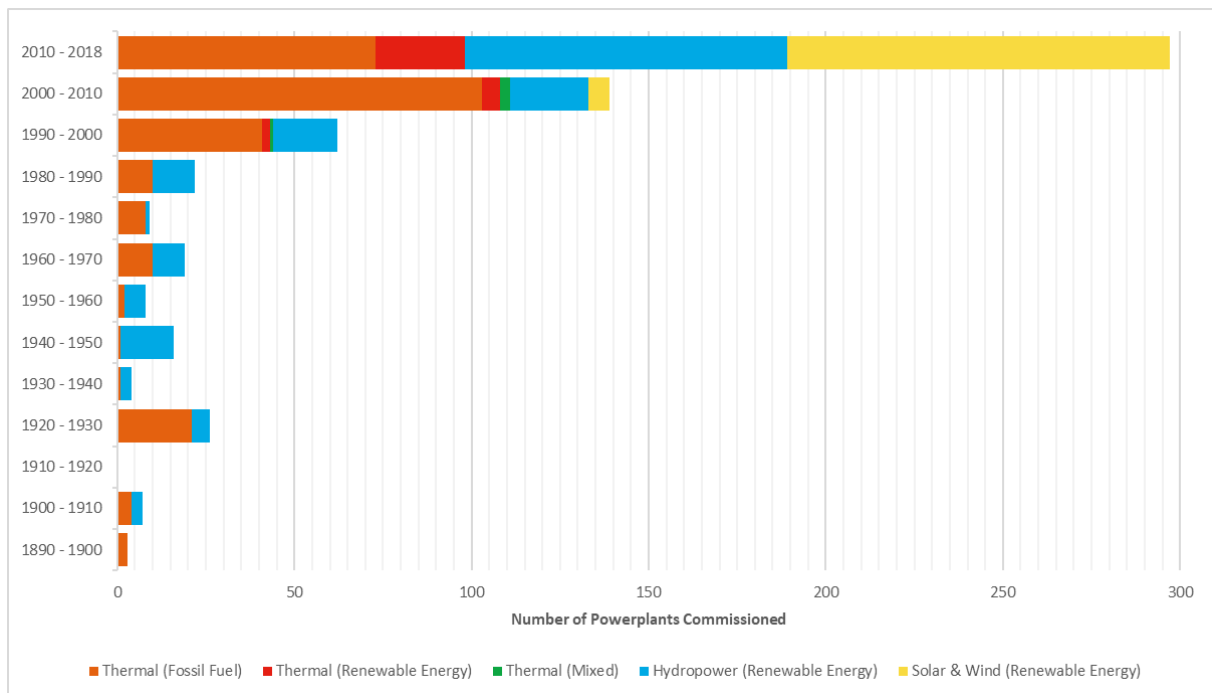


Source: Comisión Nacional de Energía

Historically fossil fuel power plants along with hydropower have primarily dominated the energy generation market in the country. It was not until the mid-1990s that unconventional renewable energies timidly made their way in, breaking the existing monopoly. This first unconventional plant was just a sample of what would begin to happen in the early 2000s, where the drop in the prices of other renewable technologies, such as wind and solar power, caused an exponential growth to such an extent that together they take almost 15% of today’s local generation market.

To illustrate the landscape change in the energy market, Figure 1.2 shows a timeline of the power plants commissioned by decade.

Figure 1.2: Type of Power plants Commissioned by Decade



Source: Comisión Nacional de Energía

It should be mentioned that the continental Chilean electricity system is broken down into four large blocks:

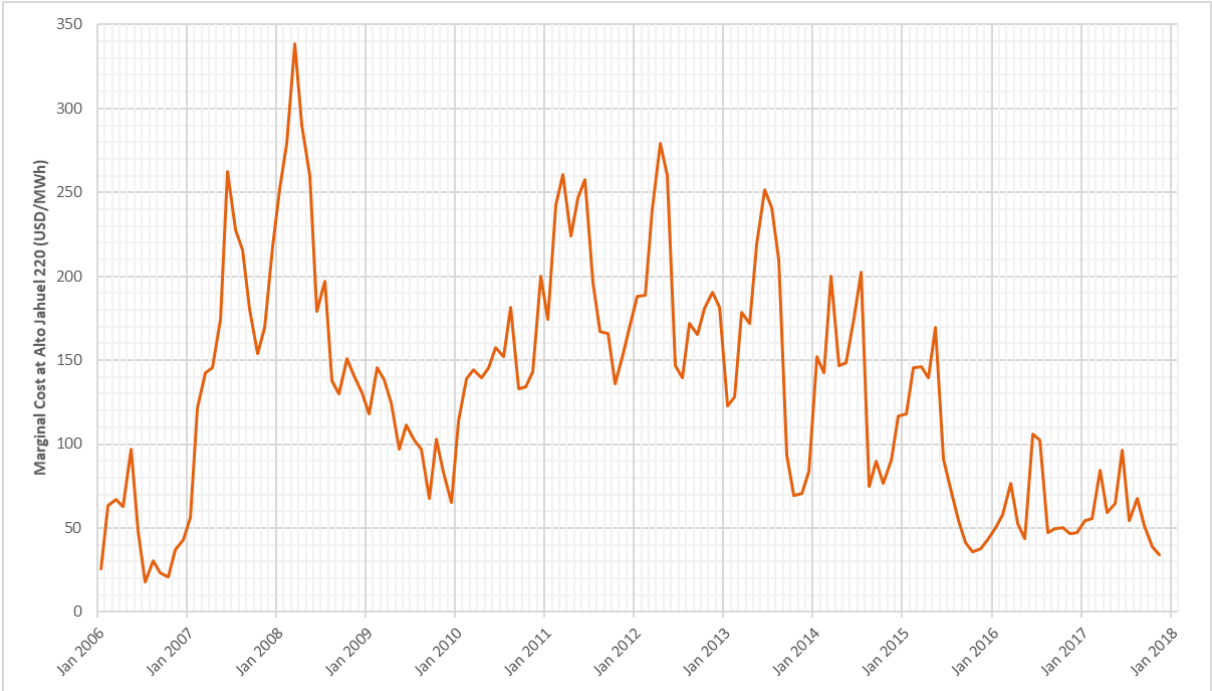
- Central Interconnected System (SIC, Sistema Interconectado Central): The biggest of the blocks, as its name suggests, connects the central part of the country from Atacama region to Los Lagos region.
- Norte Grande Interconnected System (SING, Sistema Interconectado del Norte Grande): Connects the mining regions of the north of the country: Arica y Parinacota, Tarapacá and Antofagasta.
- Aysén and Magallanes: These two systems supply energy for the southern-most part of the country.

Focusing on the SIC, during the period between the beginning of 2000s decade till the middle of 2010s decade, the high prices of energy made Chile an extremely attractive country for international investment in this line of business, this caused an explosion of new energy projects especially in the field Non-Conventional Renewable Energies (NCRE) such as run-of-river hydropower plants along with solar and wind power plants.

Despite the above, the central government feared that this explosion in the energy market prices could get out of control, this led to the adoption in 2014 of a roadmap whose main objective was to reduce the energy prices while keeping the diversification of the generation market towards renewable energies (Ministerio de Energía, 2014).

The combination of the government policy in conjunction with the NCRE boom and the international drop in fuel prices (Tercera, 2017), along with the interconnection between SIC and SING, caused a considerable drop in energy sales prices. As an example of this, the average energy price went from 153 USD/MWh on average in 2013 to 60 USD/MWh in 2017 as can be seen in Figure 1.3.

Figure 1.3: Historical Energy Prices in Chile



Source: Systept

Years of soaring prices that helped the development of new hydroelectric projects created a mindset in the developers that any project, regardless of its size or characteristics, would be profitable once built. This vision was severely changed after mid-2015 when energy prices plummeted, causing many projects in execution to become not economically attractive in brief time.

This then stands for a new challenge to which the Norwegian developers have been comfortable with: Creating profitable hydropower projects in an austere economic environment. It is this situation that provoked the genesis of this Master Thesis: Applying Norwegian expertise to the development of a medium-sized hydropower plant in the central region of Chile.

In this regard, the primary goal of this Master Thesis is to show the criteria used and calculations applied to the pre-feasibility study of Piedras Negras hydropower plant owned by Anpac Energía. This document covers the entire design process including the hydrological and hydraulic analysis of San José river, alternatives definition of the layout of the power plant project, hydraulic design of the main works, and cost estimation of the project.

2 Project Location

The project site is in the VI Region of Libertador General Bernardo O'Higgins, Chile, approximately 54 kilometers east of the city of San Fernando as is shown in Figure 2.1.

The intake of the project will be located on the San José river. The river source occurs in the high peaks of the Andes mountain range and in its watershed are important geographical landmarks such as Torres del Brujo, Universidad glacier and the summit of El Portillo (4,817 masl). Also, is worth to mention that the intake basin, on its eastern side, defines the boundary between Chile and Argentina.

Just downstream of the study area, San José flows into the Portillo river, who then becomes Azufre river, one of the main tributaries of the Tinguiririca river.

Near the project, other hydroelectric power plants such as La Higuera, La Confluencia, and the closest one to the site, San Andrés can be found as is shown in Figure 2.2. Table 2.1 summarizes the main characteristics of these hydropower plants.

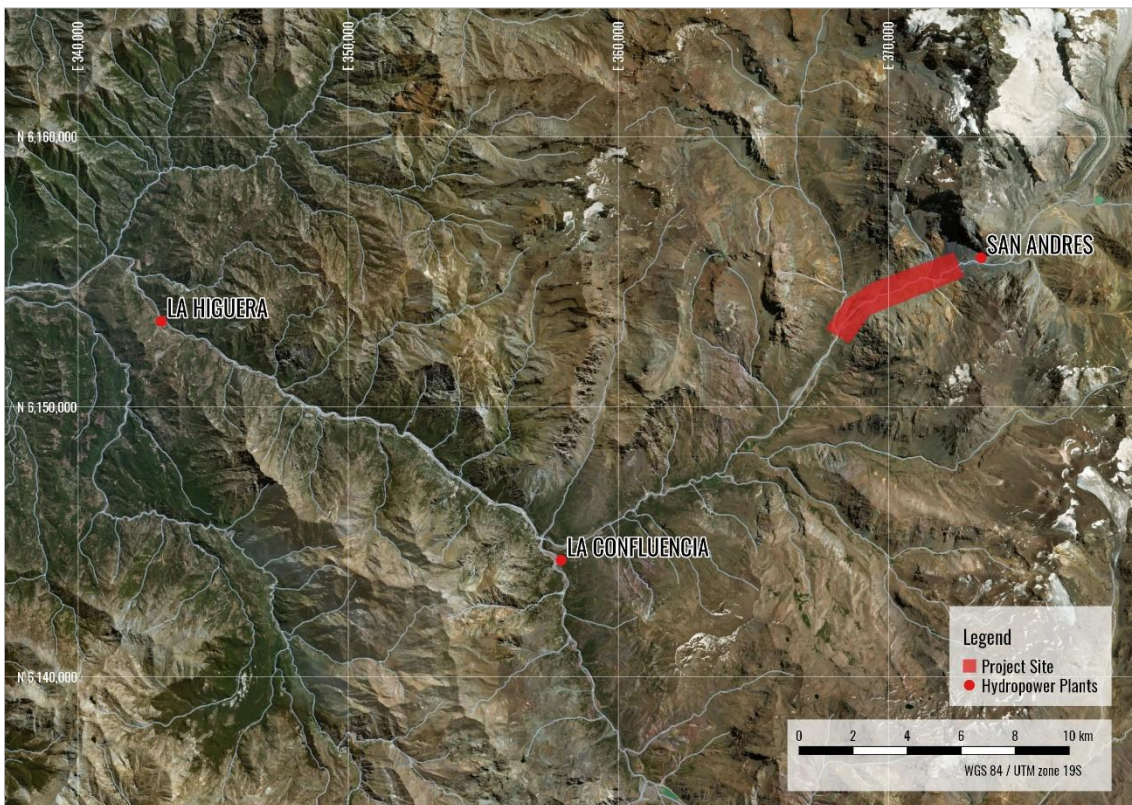
Table 2.1: Power plants Near the Project Site

| | La Higuera | La Confluencia | San Andrés |
|---------------------------------|---------------------------|---------------------------|-------------------|
| Owner | Pacific Hydro & Statkraft | Pacific Hydro & Statkraft | HydroChile S.A. |
| Operating Since | 2011 | 2011 | 2014 |
| Design Flow (m ³ /s) | 50 | 50 | 10.3 |
| Gross Head (m) | 372 | 344 | 480 |
| Number of Units | 2 | 2 | 2 |
| Installed Capacity (MW) | 155.0 | 163.2 | 40.3 |
| Energy Production (GWh/year) | 761 | 672 | 158 |

Figure 2.1: General Location of the Project Site



Figure 2.2: Vicinity of the Project Sector



The river sector to study has a length of approximately 9.5 km and is found at an elevation between 1,500 masl and 1,815 masl approximately. The site can be accessed by a road that is in good condition and that currently works as an access road to San Andres hydropower plant.

In general, due to its altimetric location, the project sector is arid without the presence of vegetation, meaning it does not have agricultural development or significant human settlements as it can be seen in Figure 2.3. This ground condition causes that along the course of the river many alluvial fans can be seen, which presumes that the flow has the potential to carry many sediments when precipitation events out of the ordinary occur.

Figure 2.3: Project Sector Limits



(This page intentionally left blank)

3 Hydrological Study

3.1 Intake Location

The first step of the hydrological study consisted in defining the precise place where the intake of the power plant will be found.

According to current Chilean legislation this point is defined according to the water right (Derecho de Agua) issued by the General Water Directorate (DGA, Dirección General de Aguas), the governmental entity responsible for the water resources management in Chile and part of the Ministry of Public Works (MOP, Ministerio de Obras Públicas).

The water right not only defines the location of the works but also the greatest amount of water per month to be used by the power plant, as well as a first estimate of the ecological flow that should be allowed to by-pass the intake.

In the case of the Piedras Negras HPP, there are two water rights issued five years apart: DGA-435/1999 and DGA-462/2004.

Because the coordinates that outline the location of a water right are defined using maps with large scales, the DGA allows the location to have a range of movement to adjust it to the reality of the project. Usually, this *error threshold* varies between 100 m up to 150 m around the designated point. This means that the power plant intake can be located within the range of error of both issued rights.

However, just upstream of the aforementioned rights, there is another right owned by a third party and identified with the number DGA-41/2013, meaning that the intake of the Piedras Negras HPP must be located downstream of the coordinates defined by this last right with the idea of not interfering with it.

The final coordinates of the intake are included in Table 3.1 and its final location is shown in Figure 3.1.

Table 3.1: Intake Location Coordinates

| | N (m) | E (m) | Elevation (masl) |
|-----------------|--------------|--------------|-------------------------|
| Intake Location | 6,155,198 | 372,547 | 1,815 |

Datum: WGS 84 / UTM zone 19S

Figure 3.1: Intake and Water Rights Location



3.2 Intake Watershed Delimitation

Due to the extension of the project area, for the delimitation of the drainage basin to the intake point, it was decided to use a Geographical Information System (GIS) software, Quantum GIS (QGIS) which has built-in algorithms for this purpose.

In this sense, the topographic information was obtained using the Advanced Spaceborne Thermal Emission and Reflection Radiometer (ASTER) Global Digital Elevation Model (GDEM) open sourced data, whose spatial resolution is 30 m (METI & NASA, 2011).

The intake watershed is shown in Figure 3.2, the hypsometric curve is shown in Figure 3.3 and its main parameters are included in Table 3.2.

Figure 3.2: Piedras Negras Intake Watershed

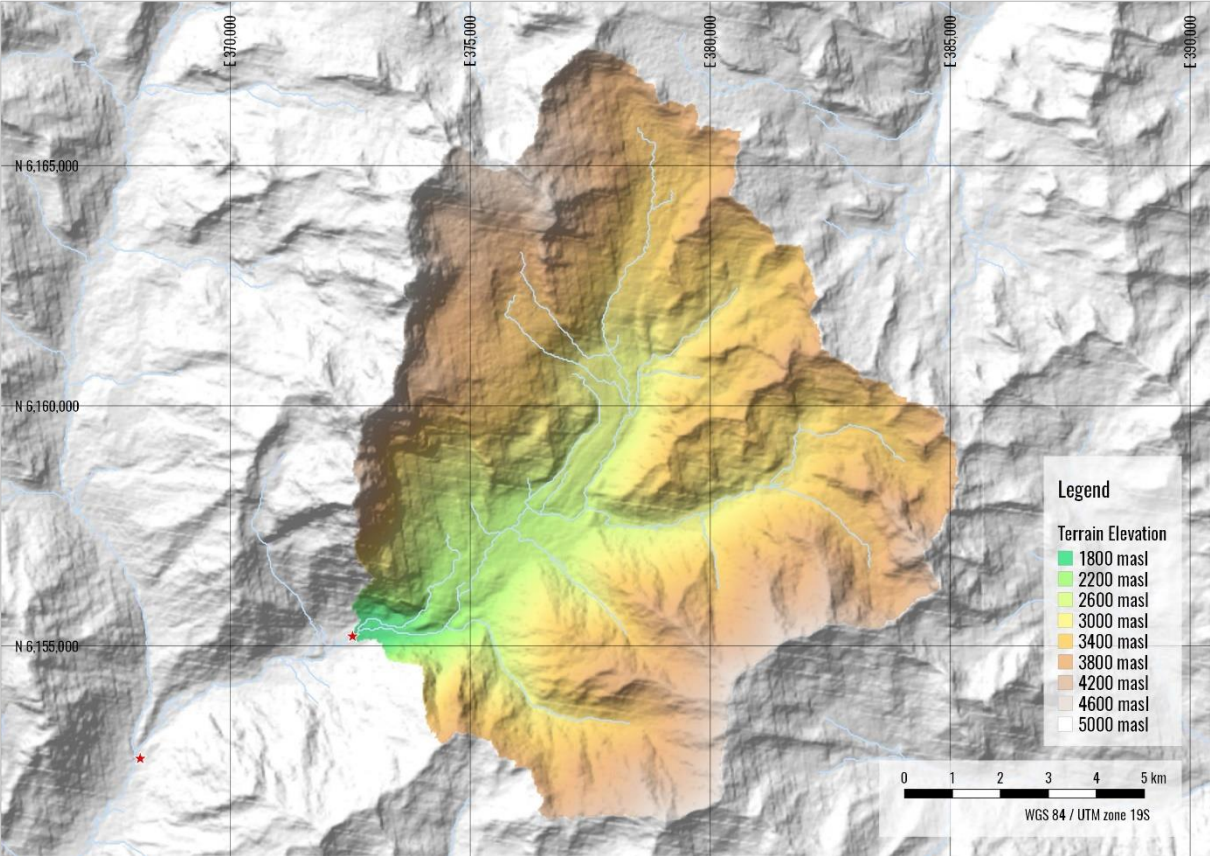


Figure 3.3: Hypsometry Curve of Intake Catchment

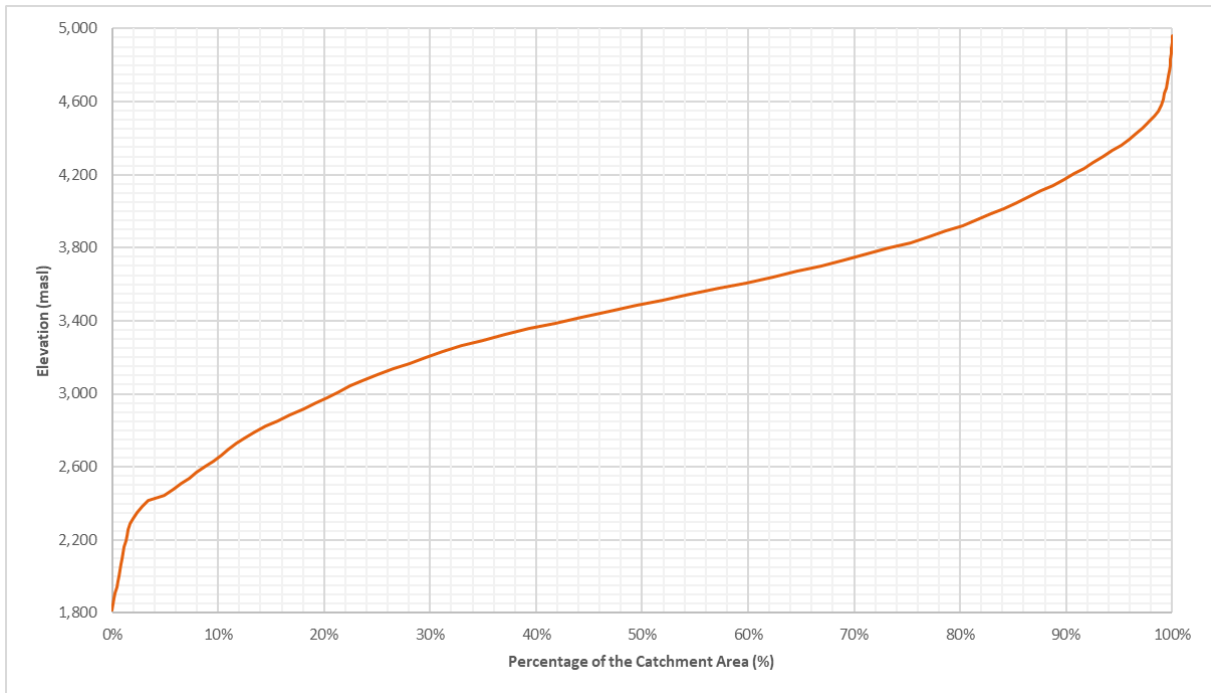


Table 3.2: Intake Catchment Morphological Characteristics

| Parameter | Value |
|-------------------------|-------|
| Area (km ²) | 127.8 |
| Mean Slope | 58.5% |
| Mean Elevation (masl) | 3,489 |
| Longest Flow Path (km) | 20.2 |
| Outlet Elevation (masl) | 1,815 |

3.3 Gauging Stations and Meteorological Data

To carry out the hydrological study, a total of 19 meteorological and fluvimetric measurement stations were reviewed.

18 of these stations are owned by the DGA, so their data is of public nature and was compiled using the tools developed by the team of the Center for Climate and Resilience Research - CR2 of Chile (CR2, n.d.).

The additional station, called "Aquaflow" is private and was located at the downstream end of the study area, therefore it is the closest to the project.

Table 3.3 includes a summary of the type of data considered for this study, while Figure 3.4 shows their location compared to the intake of the power plant.

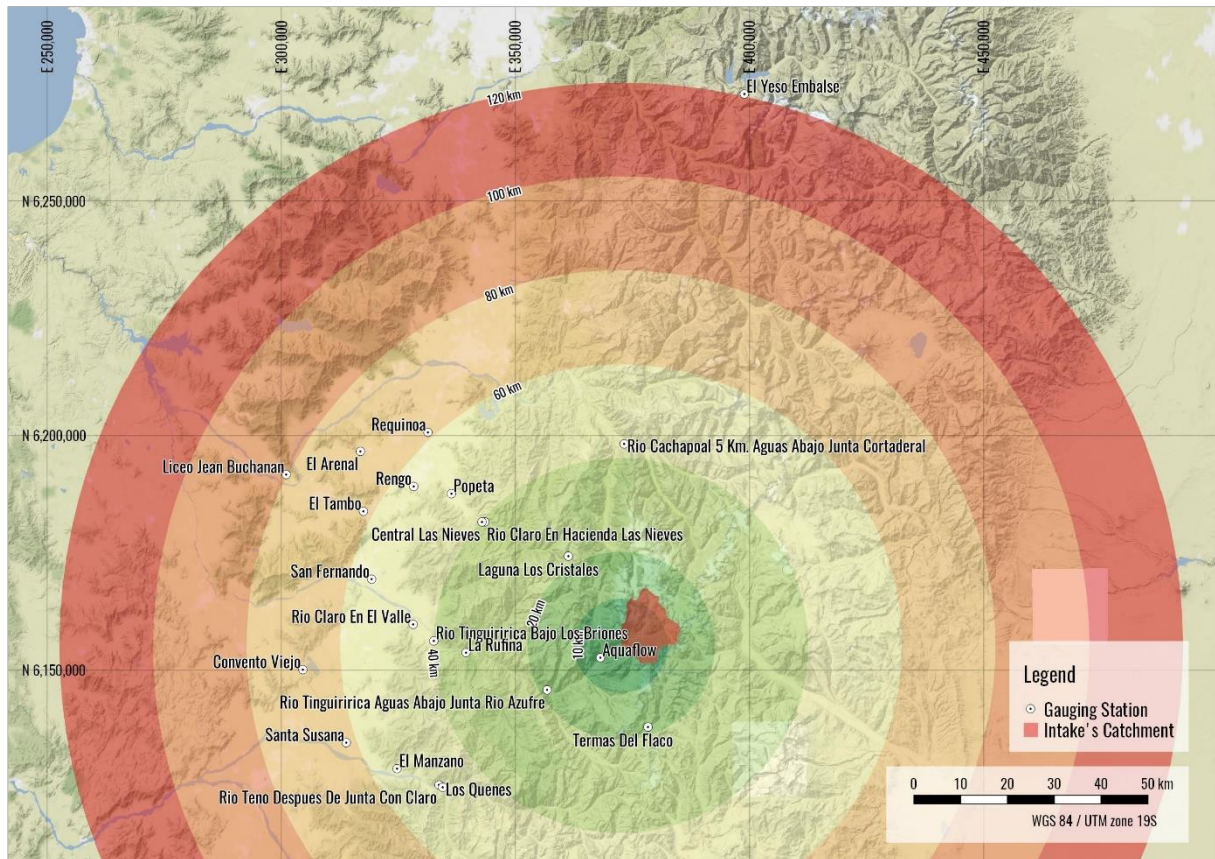
Table 3.3: Gauging Stations

| Gauging Station Name | Measured Data | Elevation (masl) | N (m) | E (m) |
|--|---------------|------------------|-----------|---------|
| Aquaflow | F – P | 1,500 | 6,152,623 | 368,126 |
| Central Las Nieves | P | 773 | 6,181,566 | 342,841 |
| Convento Viejo | T | 246 | 6,150,081 | 304,583 |
| El Arenal | ET | 256 | 6,196,602 | 316,866 |
| El Manzano | P | 643 | 6,128,972 | 324,700 |
| El Tambo | ET | 243 | 6,183,828 | 317,515 |
| El Yeso Embalse | T | 2,475 | 6,272,785 | 398,880 |
| La Rufina | P | 693 | 6,153,706 | 339,421 |
| Laguna Los Cristales | P – T | 2,319 | 6,174,272 | 361,292 |
| Liceo Jean Buchanan | ET | 172 | 6,191,668 | 301,015 |
| Los Queñes | P | 758 | 6,124,993 | 334,446 |
| Popeta | P – T | 488 | 6,187,588 | 336,305 |
| Rengo | P – T | 297 | 6,189,129 | 328,252 |
| Requínoa | ET | 369 | 6,200,655 | 331,293 |
| Rio Cachapoal 5 Km. Aguas Abajo Junta Cortaderal | P | 1,228 | 6,198,201 | 373,199 |
| Rio Claro en El Valle | F – P | 492 | 6,159,727 | 328,136 |
| Rio Claro en Hacienda Las Nieves | P – T | 708 | 6,181,576 | 343,447 |
| Rio Teno Después de Junta Con Claro | F – P | 645 | 6,125,500 | 333,642 |
| Rio Tinguiririca Aguas Abajo Junta Rio Azufre | F | 1,026 | 6,145,771 | 356,752 |
| Rio Tinguiririca Bajo Los Briones | F – P – T | 646 | 6,156,209 | 332,543 |
| San Fernando | P | 351 | 6,169,366 | 319,268 |
| Santa Susana | P | 412 | 6,134,516 | 313,854 |

| Gauging Station Name | Measured Data | Elevation (masl) | N (m) | E (m) |
|----------------------|---------------|------------------|-----------|---------|
| Termas del Flaco | T | 2,533 | 6,137,852 | 378,291 |

For measured data: F: Flow, P: Precipitation, T: Temperature, ET: Evapotranspiration
Datum: WGS 84 / UTM zone 19S

Figure 3.4: Gauging Stations Location



One of the most important aspects evaluated on the stations shown is the extension of the data and the number of gaps that each station owns. In this sense, Figure 3.5 includes a summary of the number of days per year that the stations do not have data, that is, the smaller the number (the greener the color) the more complete the year is.

Figure 3.5: Summary of Available Data for Gauging Stations

| | 1970 | 1971 | 1972 | 1973 | 1974 | 1975 | 1976 | 1977 | 1978 | 1979 | 1980 | 1981 | 1982 | 1983 | 1984 | 1985 | 1986 | 1987 | 1988 | 1989 | 1990 | 1991 | 1992 | 1993 | 1994 | 1995 | 1996 | 1997 | 1998 | 1999 | 2000 | 2001 | 2002 | 2003 | 2004 | 2005 | 2006 | 2007 | 2008 | 2009 | 2010 | 2011 | 2012 | 2013 | 2014 | 2015 | 2016 | 2017 | | | |
|--|------|------|------|------|------|------|------|------|------|------|------|------|------|------|------|------|------|------|------|------|------|------|------|------|------|------|------|------|------|------|------|------|------|------|------|------|------|------|------|------|------|------|------|------|------|------|------|------|---|---|--|
| Rain Stations | | | | | | | | | | | | | | | | | | | | | | | | | | | | | | | | | | | | | | | | | | | | | | | | | | | |
| Rio Cochapal 5 Km. Aguas Abajo Junta Coratobal | | | | | | | | | | | | | | | | | | | | | | | | | | | | | | | | | | | | | | | | | | | | | | | | | | | |
| Ringo | 164 | 0 | 0 | 0 | 0 | 0 | 0 | 0 | 0 | 0 | 0 | 0 | 0 | 0 | 0 | 0 | 0 | 0 | 0 | 0 | 0 | 0 | 0 | 0 | 0 | 0 | 0 | 0 | 0 | 0 | 0 | 0 | 0 | 0 | 0 | 0 | 0 | 0 | 0 | 0 | 0 | 0 | 0 | 0 | 0 | 0 | 0 | 0 | | | |
| Papeta | 0 | 0 | 1 | 0 | 0 | 30 | 0 | 0 | 0 | 0 | 0 | 0 | 0 | 0 | 0 | 0 | 0 | 0 | 0 | 0 | 0 | 0 | 0 | 0 | 0 | 0 | 0 | 0 | 0 | 0 | 0 | 0 | 0 | 0 | 0 | 0 | 0 | 0 | 0 | 0 | 0 | 0 | 0 | 0 | 0 | 0 | 0 | 0 | 0 | | |
| Rio Claro En Hacienda Las Nuevas | | | | | | | | | | | | | | | | | | | | | | | | | | | | | | | | | | | | | | | | | | | | | | | | | | | |
| Central Las Nuevas | 30 | 1 | 395 | 123 | | | | | | | | | | | | | | | | | | | | | | | | | | | | | | | | | | | | | | | | | | | | | | | |
| Laguna Los Chitabos | | | | | | | 120 | | | | | | | | | | | | | | | | | | | | | | | | | | | | | | | | | | | | | | | | | | | | |
| San Fernando | 242 | 0 | 0 | 0 | 0 | 0 | 0 | 0 | 0 | 0 | 0 | 0 | 0 | 0 | 0 | 0 | 0 | 0 | 0 | 0 | 0 | 0 | 0 | 0 | 0 | 0 | 0 | 0 | 0 | 0 | 0 | 0 | 0 | 0 | 0 | 0 | 0 | 0 | 0 | 0 | 0 | 0 | 0 | 0 | 0 | 0 | 0 | 0 | | | |
| Rio Claro El Valle | | | | | | | | | | | | | | | | | | | | | | | | | | | | | | | | | | | | | | | | | | | | | | | | | | | |
| Rio Tinguirica Bajo Los Briones | | | | | | | | | | | | | | | | | | | | | | | | | | | | | | | | | | | | | | | | | | | | | | | | | | | |
| San Isidro | 0 | 0 | 2 | 1 | 0 | 0 | 0 | 0 | 0 | 0 | 0 | 0 | 0 | 0 | 0 | 0 | 0 | 0 | 0 | 0 | 0 | 0 | 0 | 0 | 0 | 0 | 0 | 0 | 0 | 0 | 0 | 0 | 0 | 0 | 0 | 0 | 0 | 0 | 0 | 0 | 0 | 0 | 0 | 0 | 0 | 0 | 0 | 0 | 0 | | |
| La Infirnia | | | | | | | | | | | | | | | | | | | | | | | | | | | | | | | | | | | | | | | | | | | | | | | | | | | |
| San Isidro | 354 | 246 | 364 | 31 | 0 | 0 | 0 | 0 | 0 | 0 | 0 | 0 | 0 | 0 | 0 | 0 | 0 | 0 | 0 | 0 | 0 | 0 | 0 | 0 | 0 | 0 | 0 | 0 | 0 | 0 | 0 | 0 | 0 | 0 | 0 | 0 | 0 | 0 | 0 | 0 | 0 | 0 | 0 | 0 | 0 | 0 | 0 | 0 | 0 | | |
| El Progreso | | | | | | | | | | | | | | | | | | | | | | | | | | | | | | | | | | | | | | | | | | | | | | | | | | | |
| Rio Teno Despues De Junta Coratobal | 0 | 0 | 2 | 1 | 272 | 0 | 0 | 0 | 0 | 0 | 0 | 0 | 0 | 0 | 0 | 0 | 0 | 0 | 0 | 0 | 0 | 0 | 0 | 0 | 0 | 0 | 0 | 0 | 0 | 0 | 0 | 0 | 0 | 0 | 0 | 0 | 0 | 0 | 0 | 0 | 0 | 0 | 0 | 0 | 0 | 0 | 0 | 0 | | | |
| Los Oufes | | | | | | | | | | | | | | | | | | | | | | | | | | | | | | | | | | | | | | | | | | | | | | | | | | | |
| Aquiflow | | | | | | | | | | | | | | | | | | | | | | | | | | | | | | | | | | | | | | | | | | | | | | | | | | | |
| Temperature Stations | | | | | | | | | | | | | | | | | | | | | | | | | | | | | | | | | | | | | | | | | | | | | | | | | | | |
| El Veso Embalse | 71 | | | | | | 71 | 5 | 2 | 1 | 1 | 0 | 0 | 0 | 0 | 0 | 0 | 0 | 0 | 0 | 0 | 0 | 0 | 0 | 0 | 0 | 0 | 0 | 0 | 0 | 0 | 0 | 0 | 0 | 0 | 0 | 0 | 0 | 0 | 0 | 0 | 0 | 0 | 0 | 0 | 0 | 0 | 0 | 0 | | |
| Termas Del Fiac | | | | | | | | | | | | | | | | | | | | | | | | | | | | | | | | | | | | | | | | | | | | | | | | | | | |
| Ringo | 30 | 0 | 1 | 7 | 6 | 0 | 8 | 9 | 3 | 39 | 72 | 0 | 0 | 0 | 0 | 0 | 0 | 0 | 0 | 0 | 0 | 0 | 0 | 0 | 0 | 0 | 0 | 0 | 0 | 0 | 0 | 0 | 0 | 0 | 0 | 0 | 0 | 0 | 0 | 0 | 0 | 0 | 0 | 0 | 0 | 0 | 0 | 0 | 0 | | |
| Papaya | 60 | 0 | 0 | 4 | 31 | 215 | | | | | | | | | | | | | | | | | | | | | | | | | | | | | | | | | | | | | | | | | | | | | |
| Rio Claro En Hacienda Las Nuevas | | | | | | | | | | | | | | | | | | | | | | | | | | | | | | | | | | | | | | | | | | | | | | | | | | | |
| Laguna Los Chitabos | | | | | | | | | | | | | | | | | | | | | | | | | | | | | | | | | | | | | | | | | | | | | | | | | | | |
| Rio Tinguirica Bajo Los Briones | | | | | | | | | | | | | | | | | | | | | | | | | | | | | | | | | | | | | | | | | | | | | | | | | | | |
| Convento Viejo | 243 | 37 | 39 | 25 | 19 | 2 | 6 | 3 | 1 | 1 | 5 | 1 | 0 | 0 | 0 | 0 | 0 | 0 | 0 | 0 | 0 | 0 | 0 | 0 | 0 | 0 | 0 | 0 | 0 | 0 | 0 | 0 | 0 | 0 | 0 | 0 | 0 | 0 | 0 | 0 | 0 | 0 | 0 | 0 | 0 | 0 | 0 | | | | |
| Flow Stations | | | | | | | | | | | | | | | | | | | | | | | | | | | | | | | | | | | | | | | | | | | | | | | | | | | |
| Rio Tinguirica Bajo Los Briones | 61 | 0 | 2 | 1 | 8 | 1 | 182 | 94 | 0 | 31 | 0 | 0 | 299 | 0 | 360 | 0 | 212 | 210 | 0 | 0 | 53 | 66 | 2 | 158 | 24 | 16 | 2 | 43 | 14 | 0 | 0 | 0 | 0 | 0 | 0 | 0 | 0 | 0 | 0 | 0 | 0 | 0 | 0 | 0 | 0 | 0 | 0 | 0 | 0 | 0 | |
| Rio Tinguirica Agua Abajo Junta Rio Anifre | 134 | 9 | 147 | 87 | 140 | 84 | 33 | 99 | 19 | 0 | 234 | 212 | 203 | 33 | 0 | 77 | | | | | | | | | | | | | | | | | | | | | | | | | | | | | | | | | | | |
| Rio Teno Despues De Junta Con Claro | 0 | 1 | 36 | 0 | 29 | 41 | 26 | 0 | 8 | 19 | 8 | 57 | 56 | 0 | 1 | 0 | 74 | 92 | 0 | 0 | 0 | 0 | 0 | 0 | 0 | 0 | 0 | 0 | 0 | 0 | 0 | 0 | 0 | 0 | 0 | 0 | 0 | 0 | 0 | 0 | 0 | 0 | 0 | 0 | 0 | 0 | 0 | 0 | | | |
| Rio Claro En El Valle | 120 | 0 | 0 | 0 | 0 | 0 | 0 | 0 | 0 | 0 | 0 | 0 | 0 | 0 | 0 | 0 | 0 | 0 | 0 | 0 | 0 | 0 | 0 | 0 | 0 | 0 | 0 | 0 | 0 | 0 | 0 | 0 | 0 | 0 | 0 | 0 | 0 | 0 | 0 | 0 | 0 | 0 | 0 | 0 | 0 | 0 | 0 | 0 | | | |
| Aquiflow | | | | | | | | | | | | | | | | | | | | | | | | | | | | | | | | | | | | | | | | | | | | | | | | | | | |

3.4 Hydrological Model

Due to the lack of a fluviometric gauging station at the intake location, it was decided to use a hydrological model with the aim of obtaining a historical series of daily average flows to simulate not only the energy production but also the hydraulic behavior of San José river.

To achieve this goal, the HBV model (Hydrologiska Byråns Vattenbalansavdelning) developed in 1976 by Dr. Sten Bergström at the Swedish Meteorological and Hydrological Institute (SMHI) was chosen.

The HBV model is a conceptual precipitation-runoff model which is used to simulate runoff processes in catchments based on precipitation, air temperature and potential evapotranspiration data. The model calculates snow accumulation, snowmelt, effective evapotranspiration, soil moisture storage capacity, surface and groundwater runoff (Killingtveit & Sælthun, 1995).

It is worth to mention that the HBV has been applied in more than 40 countries with such different climatic conditions as for example Sweden, Zimbabwe, India and Colombia (Swedish Meteorological and Hydrological Institute, n.d.).

3.4.1 Model Structure

The structure of the HBV model is divided into four main items:

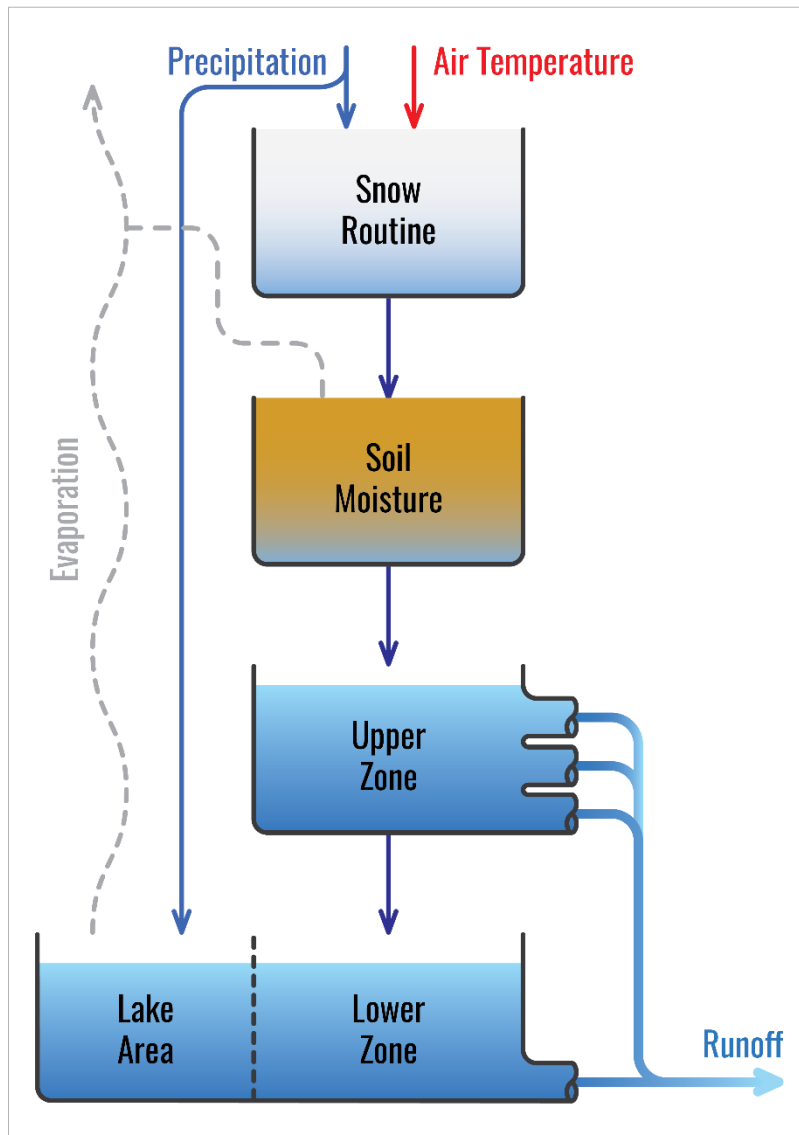
- **Meteorological Corrections:** The temperature and the precipitation are adjusted to consider the elevation difference between the gauging station and the catchment. Along with the elevation, the precipitation data is also corrected in case its liquid or solid (snow). For temperature, an added correction is carried out depending if it was a cloudless day or it had precipitation.
- **Snow Routine:** One of the main reasons the HBV model was selected for this catchment was due to the existence of this module. This routine computes the snow cover distribution, snow water equivalent, liquid water content in the snowpack and the snow melt in the catchment solely based on the corrected meteorological data. It should be mentioned that the snow behavior is highly dependent on the elevation. To obtain results as exact as possible the catchment was divided into 10 elevation zones, and for each one

of these elevations, an uneven snow distribution was considered to take into consideration wind drift or vegetation.

- **Soil Moisture Routine:** The water outflow from the snow routine feeds the soil routine. This module simulates the progressive saturation of the soil, and thus, the water storage in it. Also, it calculates the amount of water that evaporates and goes back to the atmosphere (actual evapotranspiration) leaving a net precipitation as the result.
- **Runoff Response Routine:** It transforms the net precipitation produced in the soil moisture routine into a runoff. The runoff response function consists of two linear tanks:
 - **The upper zone:** Its input comes directly from the soil moisture routine and conceptually is the quick runoff components both from overland flow and from groundwater drained through more superficial channels or interflow. For the case of this project, this linear tank had tree outlets.
 - **The lower zone:** Stands for the groundwater and lake storage that contributes to base flow in the catchment. Its input is the water that percolates from the upper zone and by direct precipitation on lakes.

The standard structure of the HBV model is graphically presented in Figure 3.6:

Figure 3.6: HBV Model Structure



Each of the routines shown in Figure 3.6 makes use of several parameters for the achievement of the simulation. In Table 3.4 a list of said parameters is shown accompanied by a brief description of them.

Table 3.4: HBV Model Parameters

| Routine | Parameter | Description |
|----------------------------|------------------|--|
| Meteorological Corrections | RCORR | Precipitation correction factor for rain |
| | SCORR | Precipitation correction factor for snow |
| | TX (°C) | Threshold temperature rain - snow |

| Routine | Parameter | Description |
|-------------------------|---------------------|---|
| | TCGRAD (°C/100m) | Temperature lapse rate on clear days |
| | TPGRAD (°C/100m) | Temperature lapse rate on overcast days |
| | PGRAD (%/100m) | Relative increase in precipitation per 100 m in elevation |
| Snow Routine | CX (mm/d·°C) | Degree-day factor for snowmelt in forest-free part |
| | CXN (mm/d·°C) | Degree-day factor for snowmelt in forested part |
| | TS (°C) | Threshold melt/freeze in forest-free part |
| | TSN (°C) | Threshold melt/freeze in forested part |
| | CFR (mm/d·°C) | Refreeze coefficient |
| | LWMAX | Max relative part liquid water in snow |
| | NDAY | Day number for snow to ice conversion |
| | CGLAC | Adjustment of CX for glacier melting |
| Soil Moisture Routine | FC (mm) | Field capacity |
| | FCDEL | Minimum soil moisture filling for potential evaporation |
| | BETA | Non-linearity in soil water retention |
| | INFMAX (mm/h) | Infiltration capacity |
| Runoff Response Routine | KUZ2 (1/day) | Outlet coefficient for fast surface runoff |
| | KUZ1 (1/day) | Outlet coefficient for medium fast surface runoff |
| | KUZ (1/day) | Outlet coefficient for slow surface runoff |
| | KLZ (1/day) | Outlet coefficient for groundwater runoff |
| | PERC (mm/day) | Constant percolation rate to groundwater storage |
| | UZ2 (mm) | Threshold between medium fast and fast surface runoff |
| | UZ1 (mm) | Threshold between slow and medium fast surface runoff |

For this Thesis, PINEHBV V1.0 model developed by Dr. Ing. Trond Rinde was used.

3.4.2 Model Calibration

Like any mathematical model and considering the number of parameters in it, in principle, the HBV model needs not only meteorological data to work, but also fluviometric data which will serve as a reference to obtain the correct combination of parameters that characterize in the best way possible the catchment under analysis. In this context, the *model calibration* is a procedure “to determine the set of free parameters in the model that gives the best possible correspondence between observed and simulated runoff for a catchment” (Killingtveit & Sælthun, 1995).

In this regard, it is recommended to have at least five years of measured runoff data to perform a calibration (Killingtveit & Sælthun, 1995).

To evaluate the quality of the calibration, the main parameter used was the model efficiency coefficient proposed by Nash and Sutcliffe in 1970, which is defined as (Krause, Boyle, & Bäse, 2005):

$$E = 1 - \frac{\sum_{i=0}^n (O_i - P_i)^2}{\sum_{i=0}^n (O_i - \bar{O})^2}$$

Where:

E : Nash-Sutcliffe efficiency coefficient.

O_i : Observed runoff at a specific time (m^3/s).

P_i : Predicted runoff at a specific time (m^3/s).

\bar{O} : Average value of all observed runoff data (m^3/s).

The range of Nash-Sutcliffe coefficient lies between 1.0 (perfect fit) and $-\infty$. A coefficient lower than zero indicates that the mean value of the observed runoff would have been better at prediction than the model (Krause et al., 2005). Normal values during the HBV model calibration are within the range of 0.6 to 0.9 (Killingtveit & Sælthun, 1995).

One important aspect to ponder is that the Nash-Sutcliffe coefficient can overestimate the model performance during peak flows and underestimate it during low flow conditions (Krause et al., 2005).

For this reason, it was decided to additionally use the cumulative difference in the water balance and the visual comparison of the observed and predicted duration curve.

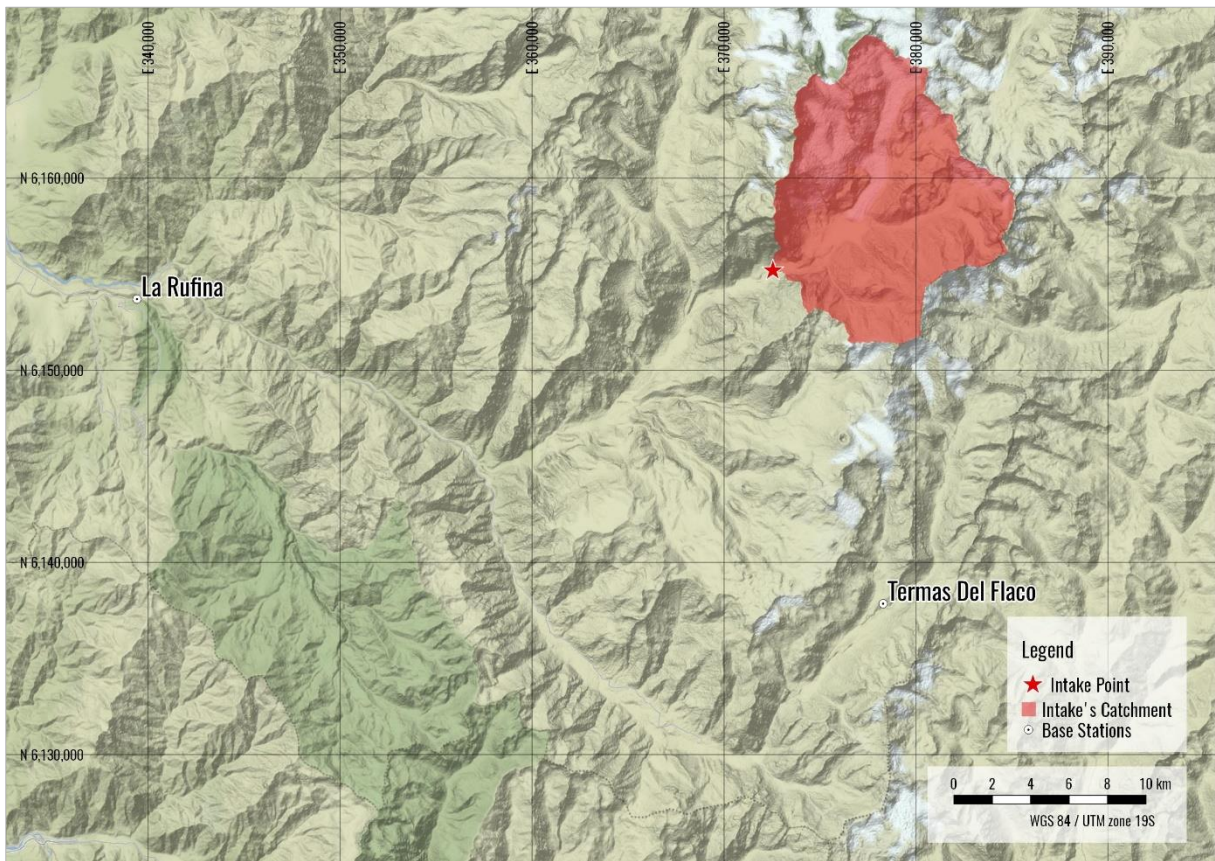
3.5 Meteorological Base Data for Hydrological Modelling

Although the calibration of the model requires at least five years of flow data, the main goal of using a hydrological model to obtain a time series of runoff data long enough to reduce as much as possible the uncertainty of the San José river behavior, and therefore, Piedras Negras HPP energy production.

Because HBV uses precipitation and temperature data to generate runoff, it is important to select a climatological measurement stations that are representative of catchment conditions, in other words, that are closest to it and that have a broad historical data and with an amount of missing data that can be filled keeping the measurement error as low as possible.

Looking at the locations of the meteorological stations in Figure 3.4 and the summary of their available data showed in Figure 3.5, for precipitation and temperature “La Rufina” and “Termas del Flaco” were picked respectively as base stations for the hydrological modeling of the intake catchment. As a reference, Figure 3.7 shows the location of both stations compared to the intake catchment.

Figure 3.7: Location of Meteorological Stations



3.5.1 Precipitation Data

As said the base station selected is “La Rufina” This station has an exceptionally long and complete historical timeseries starting from 1929, nevertheless, for this Thesis only the period from January 1970 till September 2017 was considered.

For the almost 48 years of data series, less than 2% was missing. To fill these gaps, two stations were picked: San Fernando and Rio Tinguiririca Bajo Los Briones. Based on daily values, monthly correlations were calculated individually for both stations and combined.

Figure 3.8 and Figure 3.9 shows the data correlation between La Rufina, San Fernando, and Rio Tinguiririca Bajo Los Briones respectively.

Figure 3.8: Precipitation Correlation Between La Rufina and San Fernando

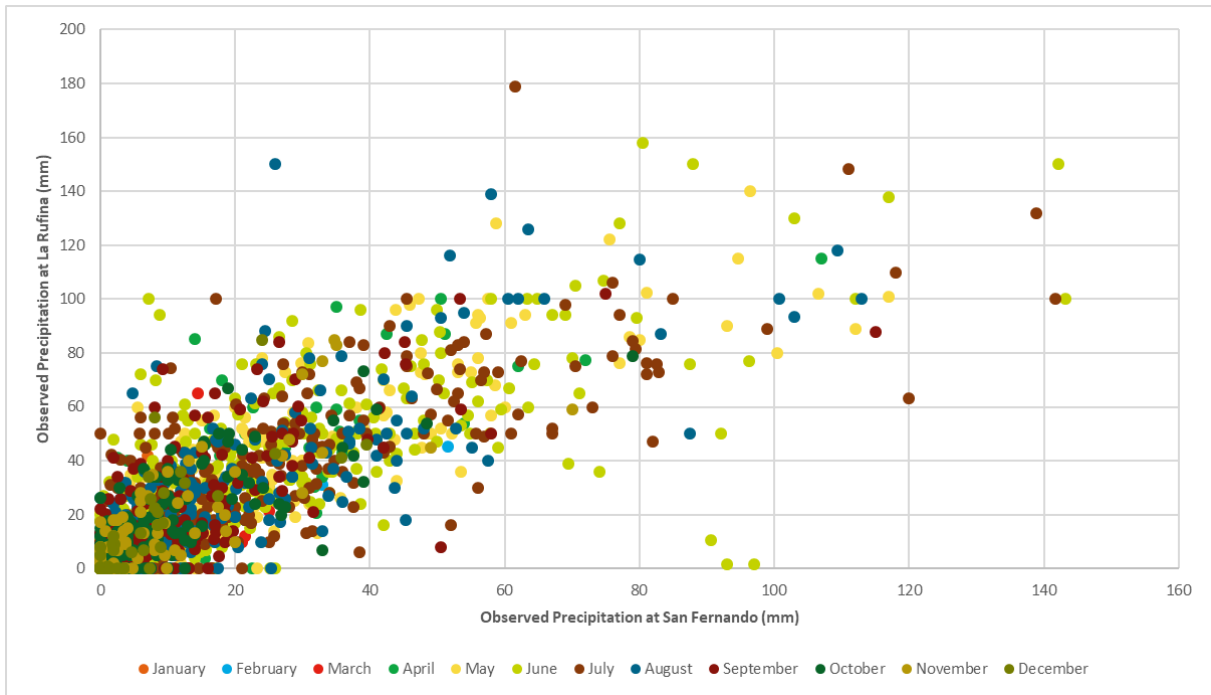
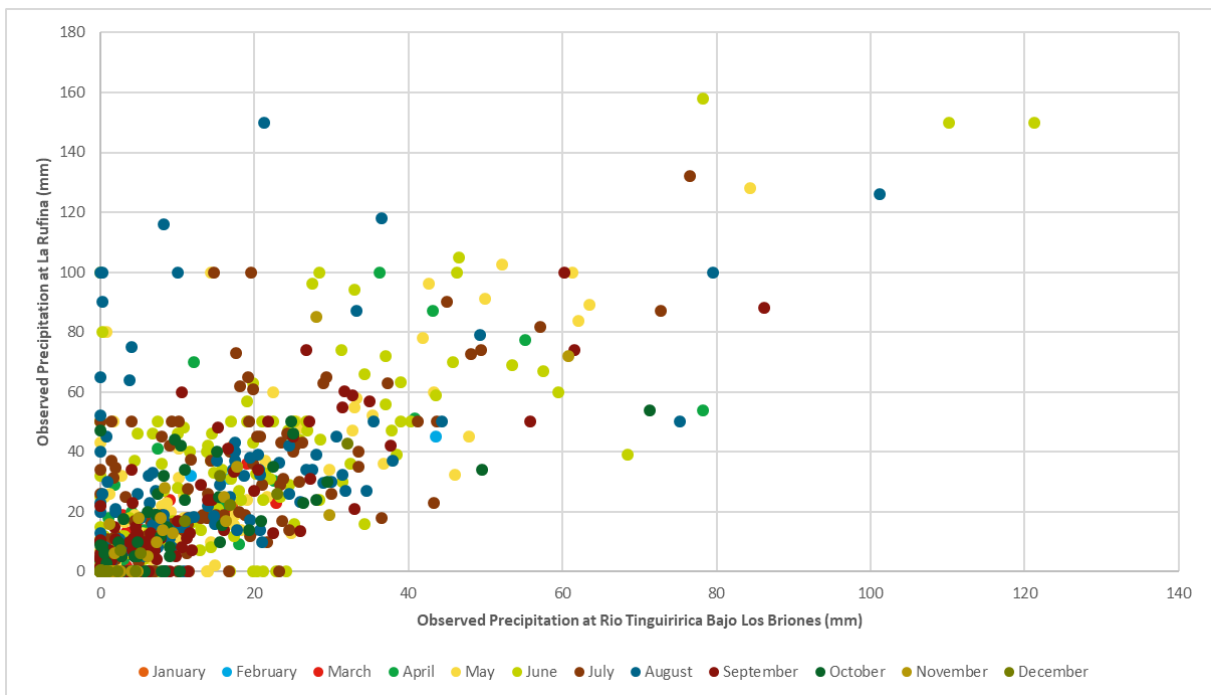


Figure 3.9: Precipitation Correlation Between La Rufina and Rio Tinguiririca Bajo Los Briones



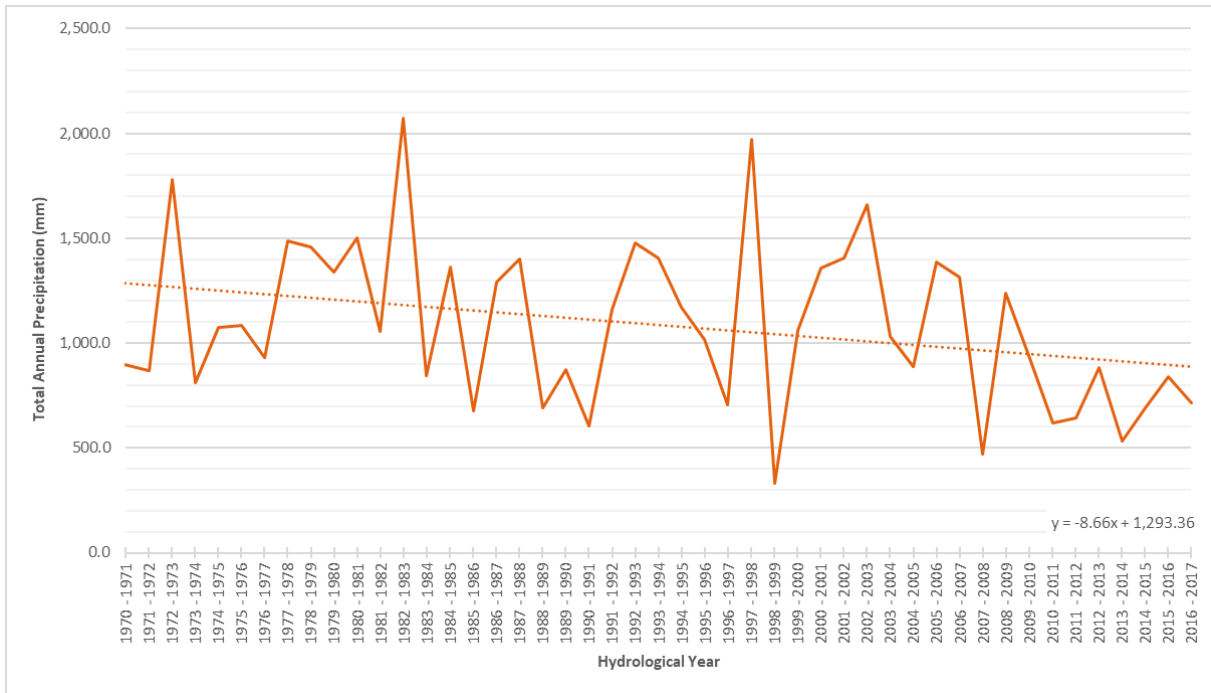
Also, Table 3.5 includes the monthly coefficient of correlation (R^2) for the individual stations and for the combination of them. The red-boldded values show the picked station used to fill the missing data by month.

Table 3.5: Correlation Coefficients for Filling La Rufina Missing Precipitation Data

| Month | San Fernando | Rio Tinguiririca Bajo Los Briones | San Fernando and Rio Tinguiririca Bajo Los Briones Combined |
|-----------|--------------|-----------------------------------|---|
| January | 0.70 | 0.89 | 0.89 |
| February | 0.72 | 0.85 | 0.85 |
| March | 0.66 | 0.81 | 0.86 |
| April | 0.79 | 0.71 | 0.78 |
| May | 0.84 | 0.78 | 0.86 |
| June | 0.72 | 0.71 | 0.80 |
| July | 0.77 | 0.68 | 0.77 |
| August | 0.75 | 0.46 | 0.73 |
| September | 0.70 | 0.81 | 0.81 |
| October | 0.72 | 0.61 | 0.76 |
| November | 0.75 | 0.78 | 0.88 |
| December | 0.73 | 0.95 | 0.96 |

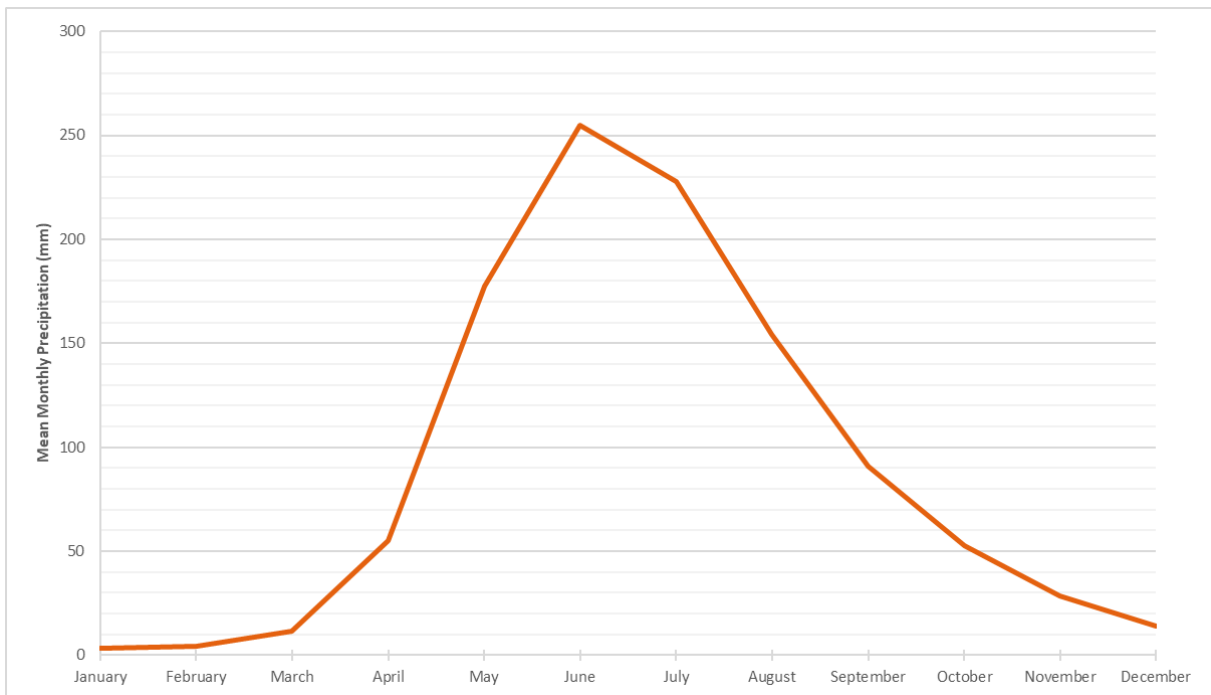
The complete precipitation timeseries yielded a mean annual precipitation of 1,077 mm. Now considering the hydrological years (from April 1st till March 31st), it can be seen in Figure 3.10 that La Rufina has a decreasing precipitation trend at a rate of about 9 mm annually from 1970 to 2017.

Figure 3.10: Historical Precipitation Trend at La Rufina



Finally, for reference, the average seasonal behavior of the station is shown in Figure 3.11.

Figure 3.11: Mean Monthly Precipitation at La Rufina



The precipitation data used in the HBV model is included in Appendix I.

3.5.2 Temperature Data

The temperature data was one of the biggest challenges for the realization of this Thesis.

A reduced number of temperature measurement stations are in the upper part of the Andes mountain range, which means that most of the data available are not representative of the conditions of the catchment under study.

As an anecdote, normally the government offices responsible for the collection of climatic data report the minimum, average and maximum temperature, however, it was discovered during the execution of this Thesis that, for unknown reasons, the amount of average data is significantly less than extreme data (minimum and maximum).

The elevation and its proximity to the area under study was one of the main reasons why the station "Termas del Flaco" was chosen as base temperature station. But as it is possible to see in Figure 3.5, this station only has 18 years of data (from 1999 to 2017), which is why it was required to fill the missing data using another station with which it had a high correlation.

After analyzing the available stations, and their monthly correlation coefficient included in Table 3.6, it was decided to use "El Yeso Embalse" for this purpose. The correlation between both stations can be seen in Figure 3.12.

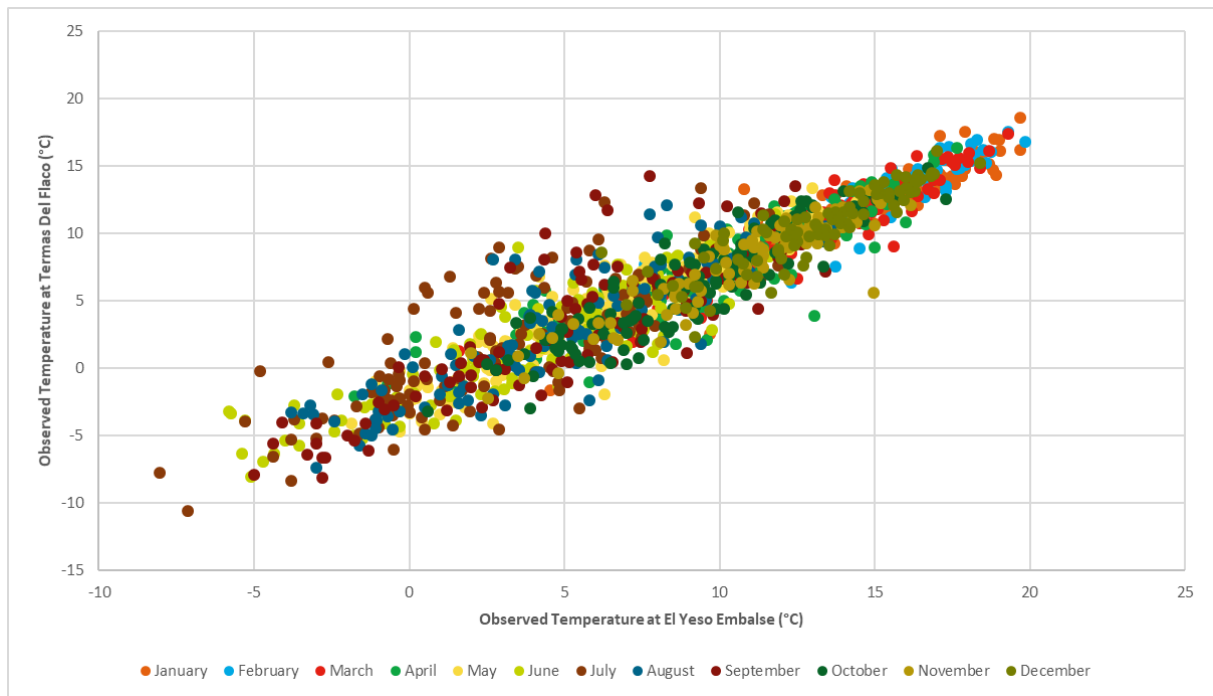
Table 3.6: Correlation Coefficients for Filling Termas del Flaco Missing Temperature Data

| Month | El Yeso Embalse | Rengo | Rio Claro En Hacienda Las Nieves | Rio Tinguiririca Bajo Los Briones | Convento Viejo |
|----------|-----------------|-------|----------------------------------|-----------------------------------|----------------|
| January | 0.81 | 0.38 | 0.68 | 0.58 | 0.32 |
| February | 0.85 | 0.38 | 0.55 | 0.51 | 0.17 |
| March | 0.87 | 0.29 | 0.22 | 0.21 | 0.32 |
| April | 0.78 | 0.10 | 0.54 | 0.32 | 0.17 |
| May | 0.85 | 0.00 | 0.31 | 0.22 | 0.01 |
| June | 0.78 | 0.01 | 0.24 | 0.13 | 0.00 |
| July | 0.61 | 0.04 | 0.47 | 0.28 | 0.01 |

| Month | El Yeso Embalse | Rengo | Rio Claro En Hacienda Las Nieves | Rio Tinguiririca Bajo Los Briones | Convento Viejo |
|-----------|-----------------|-------|----------------------------------|-----------------------------------|----------------|
| August | 0.73 | 0.34 | 0.43 | 0.25 | 0.23 |
| September | 0.73 | 0.45 | 0.76 | 0.48 | 0.53 |
| October | 0.82 | 0.39 | 0.00 | 0.00 | 0.41 |
| November | 0.83 | 0.62 | 0.00 | 0.00 | 0.58 |
| December | 0.78 | 0.40 | 0.00 | 0.00 | 0.45 |

Note: The red-bolded values show the picked station used to fill the missing data.

Figure 3.12: Temperature Correlation Between Termas del Flaco and El Yeso Embalse



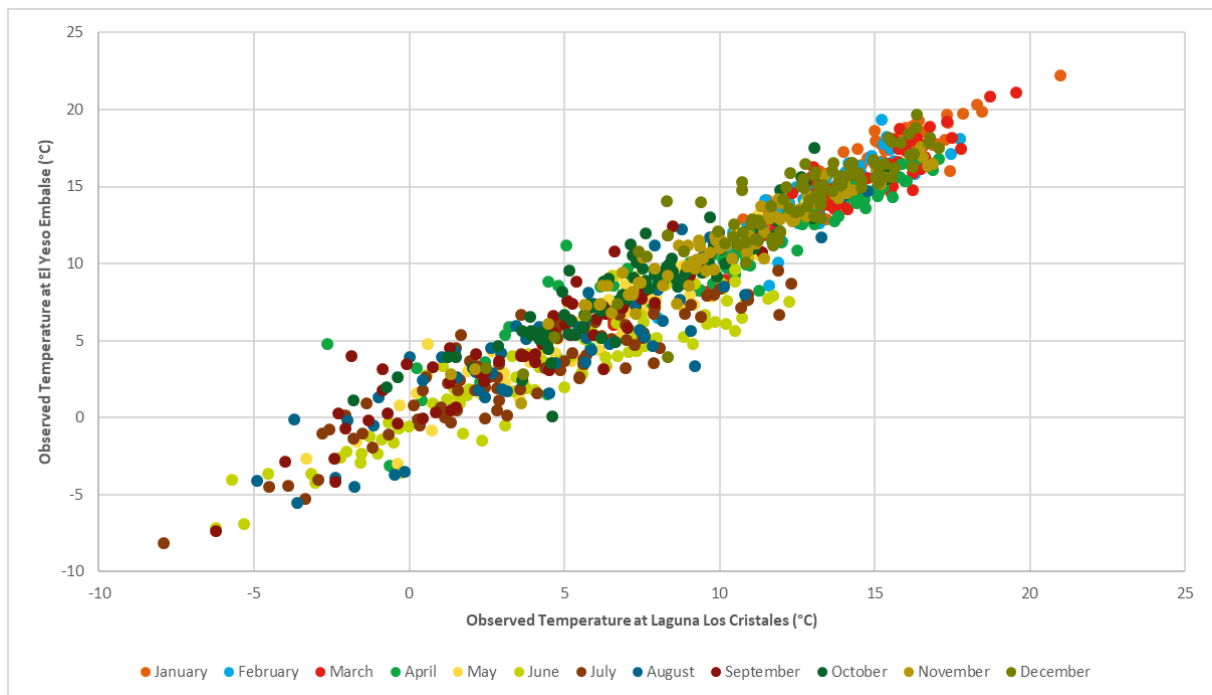
El Yeso Embalse has good data continuity between the end of 1977 and the beginning of 2016, however, in this last year, there is a 25% of missing data. To fill it, and after calculating the monthly correlation coefficient included in Table 3.7, "Laguna Los Cristales" station was chosen due to its good correlation as Figure 3.13 shows.

Table 3.7: Correlation Coefficients for Filling El Yeso Embalse Missing Temperature Data

| Month | Rengo | Rio Claro En Hacienda Las Nieves | Laguna Los Cristales | Rio Tinguiririca Bajo Los Briones | Convento Viejo |
|-----------|-------|----------------------------------|----------------------|-----------------------------------|----------------|
| January | 0.18 | 0.40 | 0.78 | 0.34 | 0.16 |
| February | 0.20 | 0.46 | 0.78 | 0.36 | 0.23 |
| March | 0.09 | 0.35 | 0.90 | 0.26 | 0.27 |
| April | 0.18 | 0.48 | 0.88 | 0.21 | 0.21 |
| May | 0.06 | 0.46 | 0.89 | 0.35 | 0.06 |
| June | 0.09 | 0.48 | 0.86 | 0.26 | 0.04 |
| July | 0.10 | 0.46 | 0.82 | 0.28 | 0.08 |
| August | 0.27 | 0.39 | 0.81 | 0.30 | 0.24 |
| September | 0.31 | 0.62 | 0.85 | 0.49 | 0.35 |
| October | 0.34 | 0.65 | 0.85 | 0.59 | 0.39 |
| November | 0.44 | 0.66 | 0.92 | 0.58 | 0.42 |
| December | 0.41 | 0.59 | 0.82 | 0.53 | 0.42 |

Note: The red-boldd values show the picked station used to fill the missing data.

Figure 3.13: Temperature Correlation Between El Yeso Embalse and Laguna Los Cristales



The complete temperature timeseries yielded a mean annual temperature at Termas del Flaco of 6.5 °C. With the filled data it can be seen that the temperature at the station location has a slightly increasing trend of 0.02 °C/year between 1978 and 2017 as shown in Figure 3.14. The station seasonal variation is also shown in Figure 3.15.

Figure 3.14: Historical Temperature Trend at Termas del Flaco

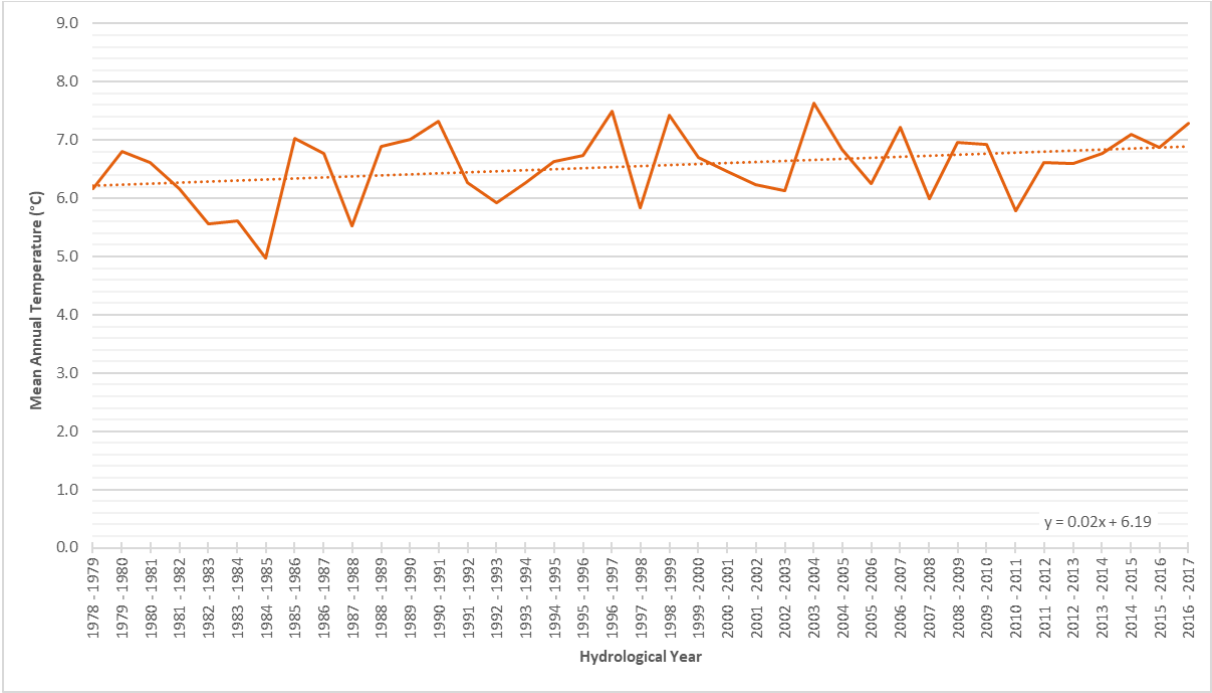
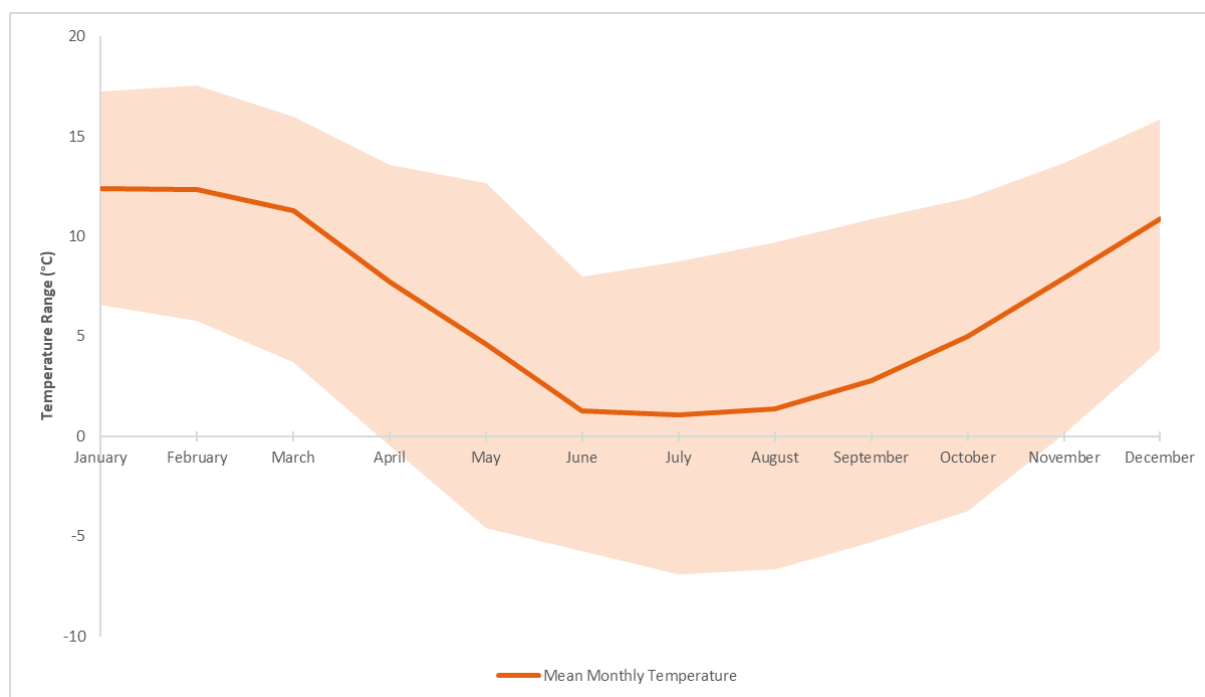


Figure 3.15: Seasonal Temperature Variation at Termas del Flaco



The temperature data used in the HBV model is included in Appendix II.

3.5.3 Evapotranspiration Data

In addition to rainfall and temperature, the HBV model needs potential evaporation data to be applied in the soil moisture and lower zone routines.

In most cases, this measurement is scanty or simply non-existent, but as can be seen in Table 3.3, near the project area four stations were found with measured data. The average potential evaporation data per month for these stations is included in Table 3.8.

Table 3.8: Observed Potential Evaporation

| Month | El Tambo (mm/day) | El Arenal (mm/day) | Liceo Jean Buchanan (mm/day) | Requinoa (mm/day) |
|----------|-------------------|--------------------|------------------------------|-------------------|
| January | 3.3 | 0.9 | 0.0 | 5.4 |
| February | 2.9 | 0.7 | 0.0 | 4.8 |
| March | 2.2 | 0.6 | 0.0 | 3.3 |

| Month | El Tambo (mm/day) | El Arenal (mm/day) | Liceo Jean Buchanan (mm/day) | Requinoa (mm/day) |
|-----------|----------------------|-----------------------|------------------------------------|----------------------|
| April | 1.5 | 0.3 | 0.0 | 1.8 |
| May | 1.2 | 0.2 | 0.0 | 1.4 |
| June | 1.0 | 0.1 | 0.0 | 1.2 |
| July | 1.0 | 0.1 | 0.0 | 1.0 |
| August | 1.1 | 0.2 | 0.0 | 1.6 |
| September | 1.4 | 0.3 | 0.0 | 2.8 |
| October | 2.2 | 0.9 | 0.0 | 3.2 |
| November | 3.1 | 1.2 | 0.3 | 4.9 |
| December | 3.5 | 1.3 | 0.7 | 5.5 |

It can be seen in Table 3.8 data that there is a significant discrepancy in the measured data between stations, especially with El Arenal and Liceo Jean Buchanan. It should also be considered that, due to the location of the measurement stations, the data may overestimate the phenomena with what might occur in the high altitudes of the Andean mountain range

That is why, for the HBV model, it was chosen to use the Thornthwaite method to calculate the potential evapotranspiration due to its simplicity and proven results. This method states (Pascual-ferrer & Candela, 2015).

$$EPot = 16 \cdot \left(\frac{10 \cdot t}{I} \right)^\alpha \cdot \frac{N}{12} \cdot \frac{d}{30}$$

With:

$$I = \sum_{i=1}^{12} \left(\frac{t}{5} \right)^{1.514}$$

$$\alpha = 675 \cdot 10^{-9} \cdot I^3 - 771 \cdot 10^{-7} \cdot I^2 + 1,792 \cdot 10^{-5} \cdot I + 0.49239$$

Where:

- EPot*: Potential evapotranspiration (mm/month).
t: Mean monthly temperature (°C).
I: Annual heat index
N: Sunshine hours for each month (h).
d: Number of days for each month (d).

To calculate the sunshine hours for each month, the following expression was applied (Kirk, 1994):

$$N = 0.133 \cdot \cos^{-1}(-\tan \gamma \cdot \tan \delta)$$

With:

$$\delta = 0.39637 - 22.9133 \cdot \cos \psi + 4.02543 \cdot \sin \psi - 0.3872 \cdot \cos 2 \cdot \psi + 0.052 \cdot \sin 2 \cdot \psi$$

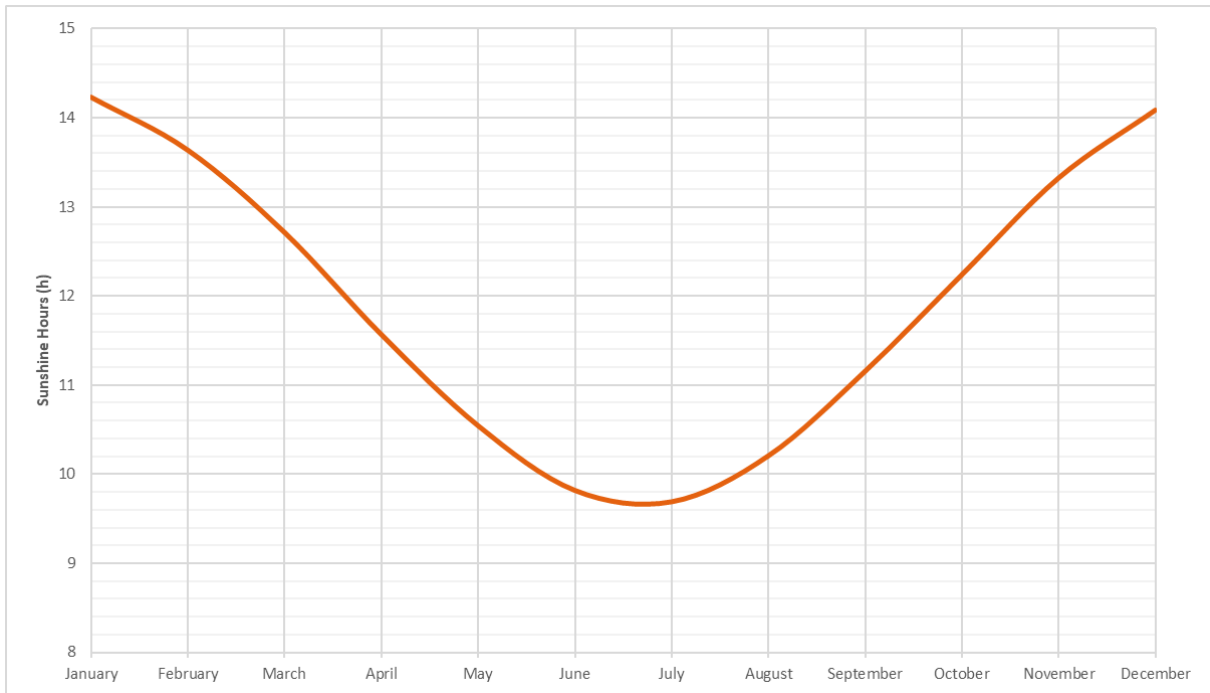
$$\psi = 360^\circ \cdot \frac{d}{365}$$

Where:

- N*: Sunshine hours (h).
γ: Location latitude (°).
δ: Solar declination (°).
d: Day number, ranging from 0 on 1 January to 364 on 31 December.

Considering the project is found at a latitude of -34.7°, the result for the average sunshine hours is shown in Figure 3.16.

Figure 3.16: Average Sunshine Hours for Project Location



With these input, Table 3.9 summarizes the results obtained from the application of the Thornthwaite method:

Table 3.9: Potential Evapotranspiration Results

| Month | Number of Days | Mean Daylength (h) | Mean Temperature (°C) | Monthly Heat Index | Potential Evaporation (mm/d) |
|-----------|----------------|--------------------|-----------------------|--------------------|------------------------------|
| January | 31 | 14 | 12.4 | 3.9 | 2.8 |
| February | 28 | 14 | 12.3 | 3.9 | 2.7 |
| March | 31 | 13 | 11.3 | 3.4 | 2.3 |
| April | 30 | 12 | 7.7 | 1.9 | 1.5 |
| May | 31 | 11 | 4.6 | 0.9 | 0.9 |
| June | 30 | 10 | 1.3 | 0.1 | 0.3 |
| July | 31 | 10 | 1.1 | 0.1 | 0.2 |
| August | 31 | 10 | 1.4 | 0.1 | 0.3 |
| September | 30 | 11 | 2.8 | 0.4 | 0.6 |
| October | 31 | 12 | 5.0 | 1.0 | 1.1 |
| November | 30 | 13 | 7.9 | 2.0 | 1.8 |

| Month | Number of Days | Mean Daylength (h) | Mean Temperature (°C) | Monthly Heat Index | Potential Evaporation (mm/d) |
|----------|----------------|--------------------|-----------------------|--------------------|------------------------------|
| December | 31 | 14 | 10.9 | 3.2 | 2.5 |

3.5.4 Calibration Runoff Data

As mentioned in the Title 3.4, to obtain a combination of parameters for the hydrological model that best represent the fluvial behavior of the catchment, it is first necessary to compare known measured river runoff with the ones predicted by the model.

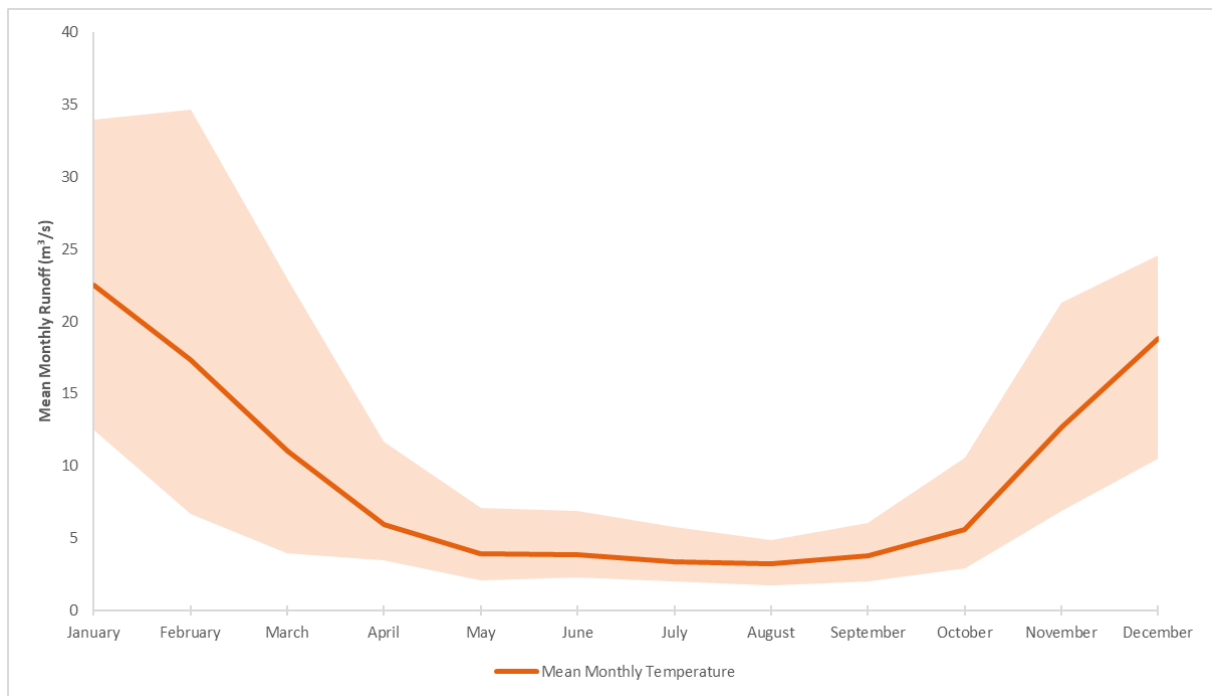
For this reason, it was decided to use the observed data from the Aquaflow station found at the downstream limit of the study area as can be seen in Figure 3.4.

This private station has a little more than five years of records from November 2009 to July 2015, but for calibration purposes, the data used ranged from April 1, 2010, to March 31, 2015, sticking in this way the hydrological calendar.

During this period there was a little less than 3% of missing data which was filled using a joint correlation between the stations Rio Tinguiririca Bajo Los Briones and Rio Claro En El Valle.

The mean observed runoff value for this station was of 9.3 m³/s and its seasonal variation is shown in Figure 3.17.

Figure 3.17: Seasonal Runoff Variation at Aquaflow



The runoff data used for calibration is included in Appendix III.

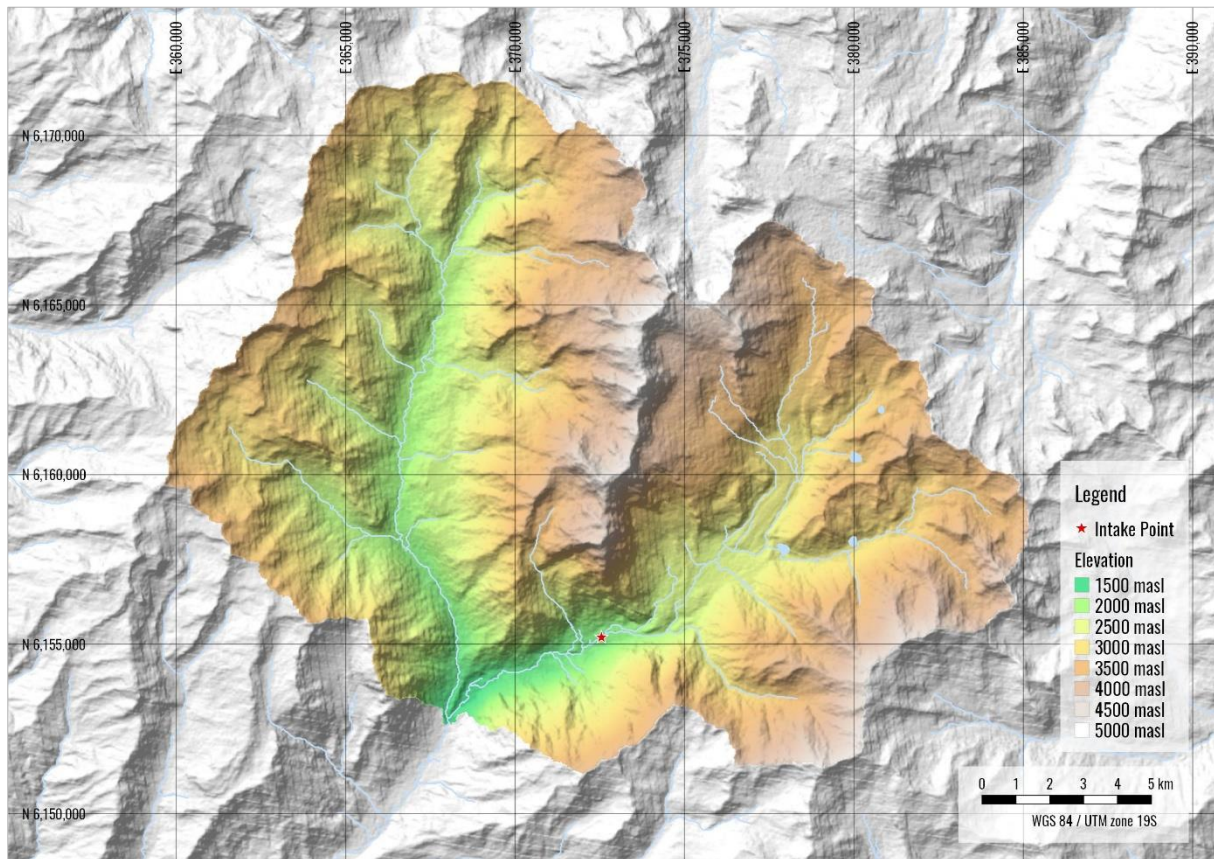
3.6 Calibration of Hydrological Model: Mean Daily Runoff Timeseries

3.6.1 Catchment Parameters

The first step to perform the calibration process is to obtain the morphological parameters of the catchment to be calibrated, which in this case is the one draining to the Aquaflow gauge station.

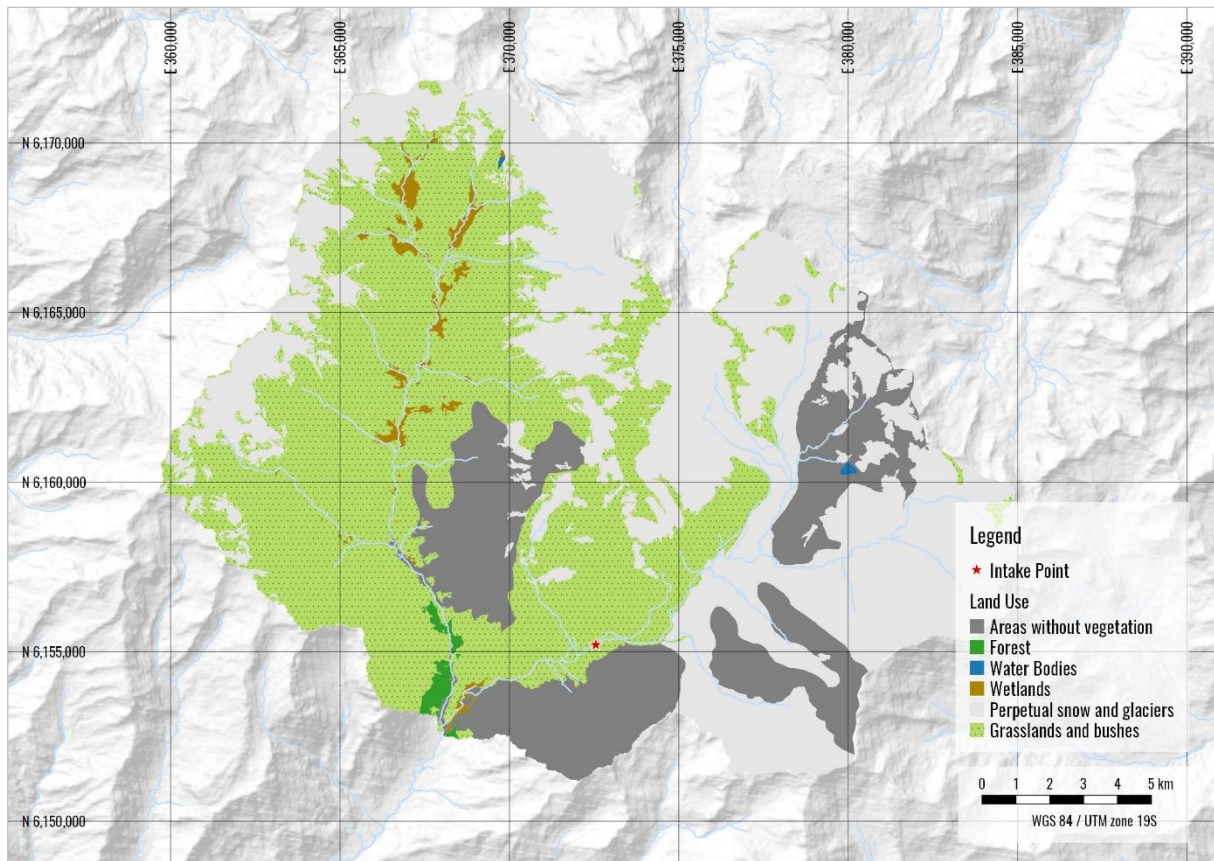
The delimitation of the catchment was done using the same data and procedure explained in the Title 3.2. For reference, Aquaflow catchment is shown in Figure 3.18.

Figure 3.18: Aquaflo Gauging Station Catchment



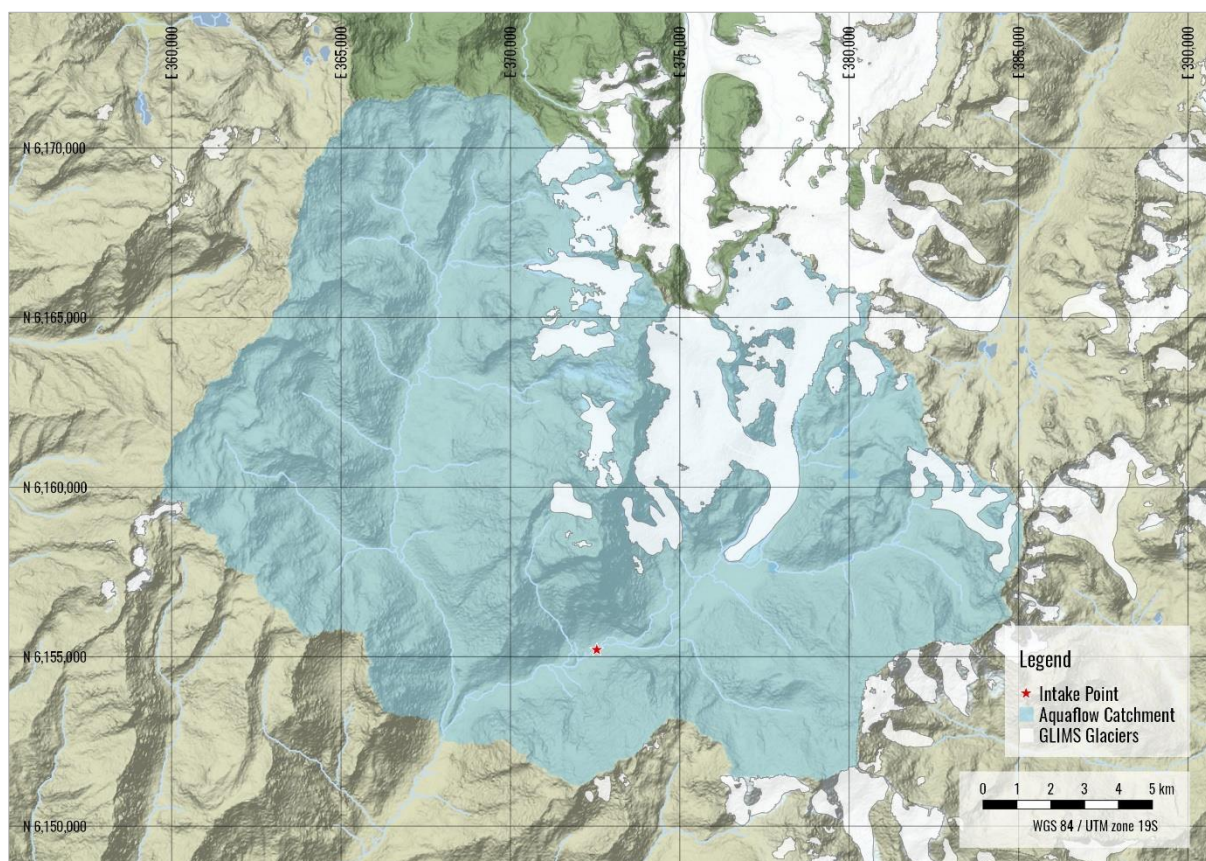
With the idea getting the percentage of the area of the catchment occupied by forest areas, the cadaster of land uses and vegetational resources, developed by the National Forestry Corporation (CONAF, Corporación Nacional Forestal) in 2013 was used (Corporación Nacional Forestal, n.d.). Figure 3.19 shows the different land uses in the catchment.

Figure 3.19: Aquaflow Catchment Land Use



Although the land use information provided by CONAF includes glaciers, it does not distinguish between these ice bodies and perpetual snow. That is why to specifically extract the glacier area of the catchment, the data developed by the Global Land Ice Measurements from Space (GLIMS) team was used (Raup et al., 2007). Figure 3.20 shows the outline of the Universidad glacier over the limit of the catchment.

Figure 3.20: Aquaflow Catchment Glaciers Outline



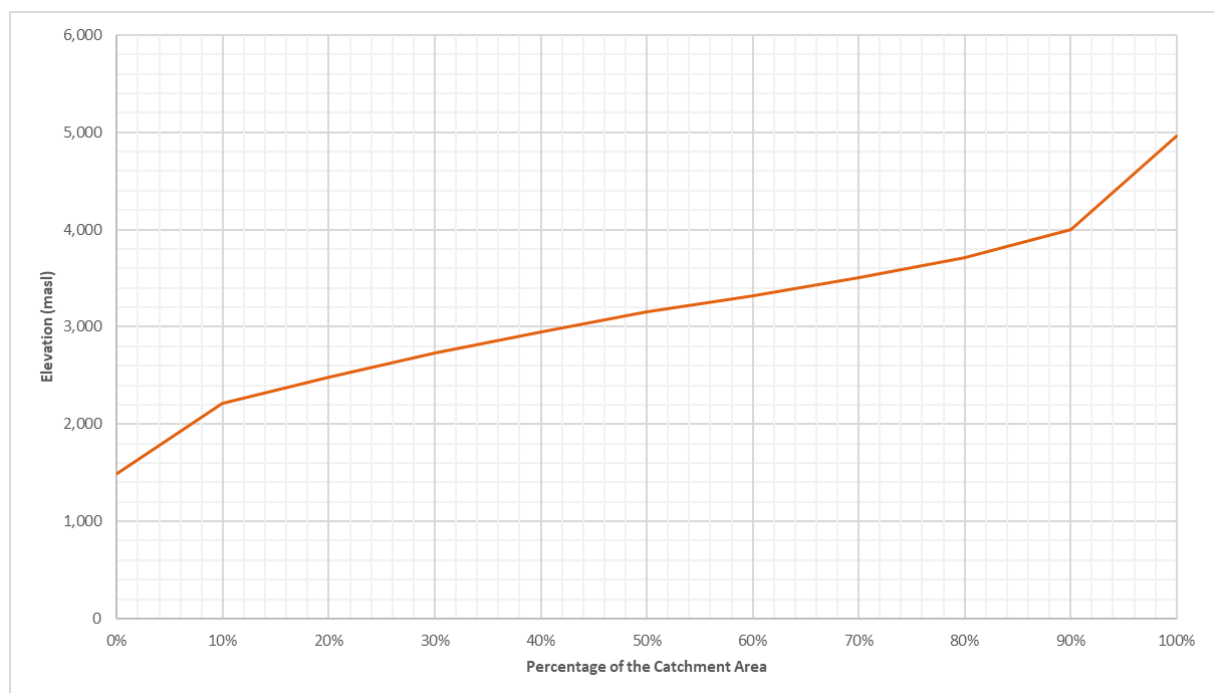
With this information, and dividing the basin into 10 elevation zones, Table 3.10 includes the area distribution by elevation zone and Figure 3.21 shows the hypsometric curve of the catchment.

Table 3.10: Aquaflow Catchment Area Distribution by Elevation Zone

| | Max. Elevation (masl) | Catchment Area (km ²) | Glacier Area (km ²) | Lakes Area (km ²) |
|---------|--------------------------|--------------------------------------|------------------------------------|----------------------------------|
| Outlet: | 1,488 | - | - | - |
| Zone 1: | 2,217 | 32.41 | 0.00 | 0.00 |
| Zone 2: | 2,485 | 32.50 | 0.10 | 0.00 |
| Zone 3: | 2,731 | 32.41 | 1.23 | 0.09 |
| Zone 4: | 2,950 | 32.59 | 2.71 | 0.05 |
| Zone 5: | 3,151 | 32.47 | 1.19 | 0.02 |
| Zone 6: | 3,324 | 32.32 | 2.20 | 0.13 |
| Zone 7: | 3,502 | 32.47 | 6.58 | 0.00 |

| | Max. Elevation (masl) | Catchment Area (km²) | Glacier Area (km²) | Lakes Area (km²) |
|----------|----------------------------------|--|--|--|
| Zone 8: | 3,708 | 32.58 | 11.02 | 0.00 |
| Zone 9: | 4,002 | 32.52 | 13.87 | 0.00 |
| Zone 10: | 4,962 | 32.54 | 9.73 | 0.00 |
| | Total | 324.8 | 48.6 | 0.3 |
| | Catchment Percentage | 100% | 14.97% | 0.09% |

Figure 3.21: Hypsometric Curve of Aquaflow Catchment



3.6.2 Calibration Results

In total, five hydrological years of data were used for calibration, starting from April 1, 2010, to March 31, 2015.

For the parameters calibration, an iterative supervised autocalibration was applied by using the Model-Independent Parameter Estimation and Uncertainty Analysis (PEST) algorithm integrated to the PINEHBV software.

The resulting calibration parameters for the catchment are included in Table 3.11.

Table 3.11: Calibrated Parameters for Aquaflo Catchment

| Routine | Parameter | Value |
|----------------------------|----------------------------|--------------|
| Meteorological Corrections | RCORR | 1.600 |
| | SCORR | 2.500 |
| | TX (°C) | 8.000 |
| | TCGRAD (°C/100m) | -0.76 |
| | TPGRAD (°C/100m) | -0.40 |
| | PGRAD (%/100m) | 5.80% |
| Snow Routine | CX (mm/d ^o ·C) | 3.798 |
| | CXN (mm/d ^o ·C) | 3.381 |
| | TS (°C) | 4.250 |
| | TSN (°C) | 5.330 |
| | CFR (mm/d ^o ·C) | 0.01 |
| | LWMAX | 0.07 |
| | NDAY | 270 |
| | CGLAC | 4.5 |
| Soil Moisture Routine | FC (mm) | 180.6 |
| | FCDEL | 1.0 |
| | BETA | 1.240 |
| | INFMAX (mm/h) | 50.0 |
| Runoff Response Routine | KUZ2 (1/day) | 0.134 |
| | KUZ1 (1/day) | 0.100 |
| | KUZ (1/day) | 0.060 |
| | KLZ (1/day) | 0.035 |
| | PERC (mm/day) | 1.650 |
| | UZ2 (mm) | 150.00 |
| | UZ1 (mm) | 71.13 |

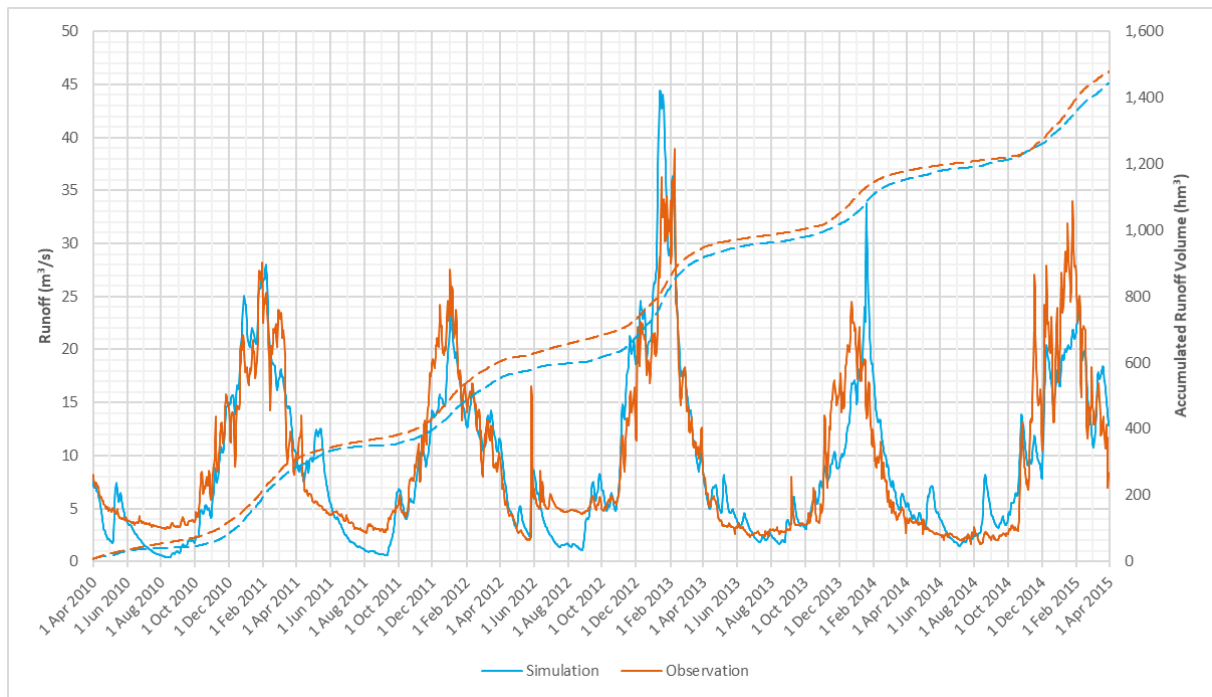
With these parameters, the resulting Nash-Sutcliffe model efficiency coefficient is shown in Table 3.12:

Table 3.12: Nash-Sutcliffe Coefficient for Calibration Period

| Season | Nash - Sutcliffe |
|---------------------------|------------------|
| Annual | 0.81 |
| Summer Season (Oct - Mar) | 0.68 |
| Winter Season (Apr - Sep) | -0.67 |

The annual result shows that overall, the model does a decent job at predicting the runoff of the catchment with a mean absolute error of $\pm 2.42 \text{ m}^3/\text{s}$, nevertheless, in the winter season, the resulting efficiency coefficient yields a negative value. The reason for this can be better explained after looking at Figure 3.22:

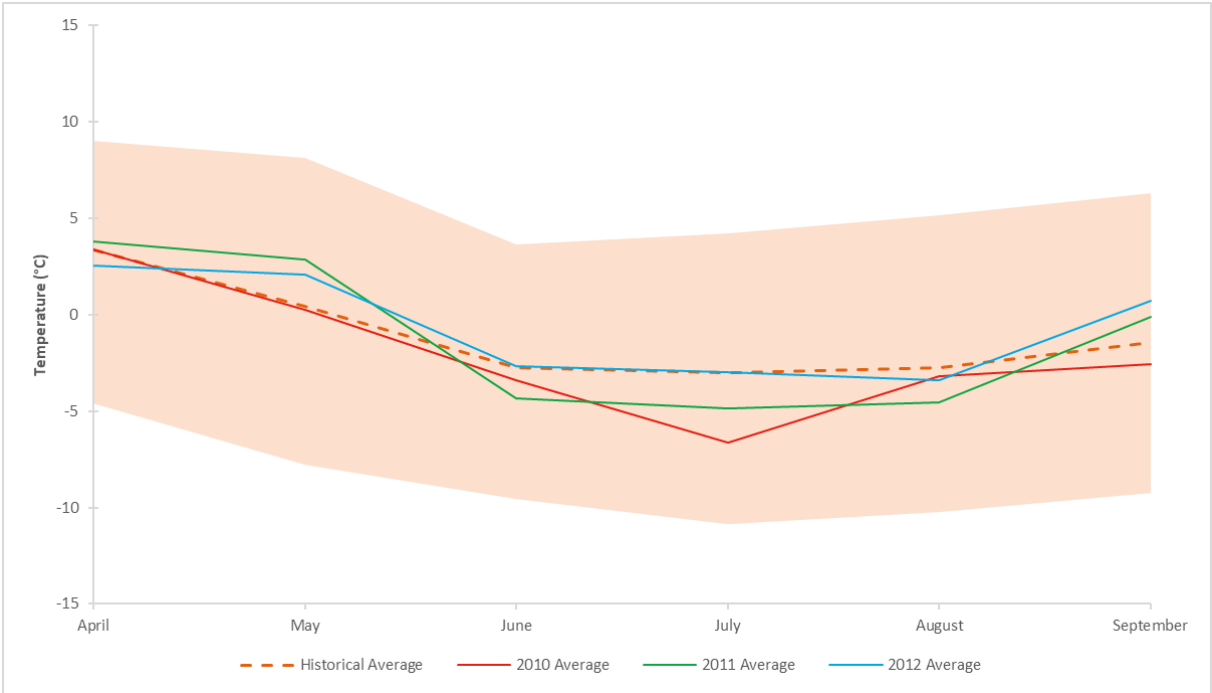
Figure 3.22: Timeseries: Observed vs Predicted Runoff Data at AquafLOW



As its title says, Figure 3.22 is a comparison between the observed (in orange) and predicted (in blue) runoff values at AquafLOW gauging stations. Looking at the first three winter seasons (2010, 2011 and 2012) it is possible to see the simulated runoff values are significantly lower than the measured ones.

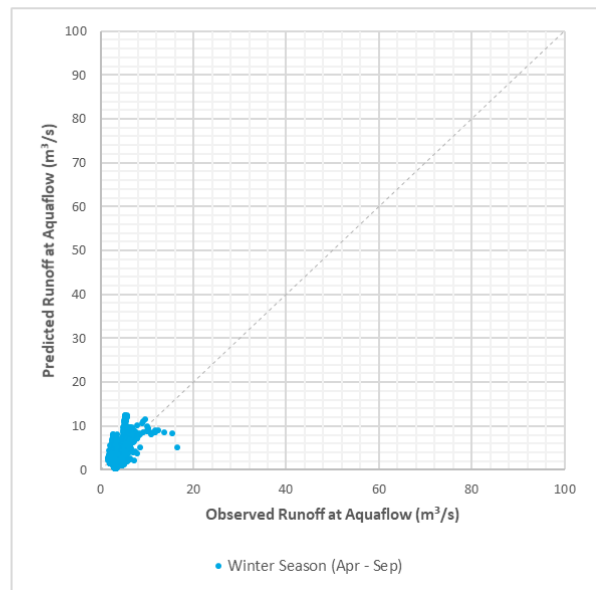
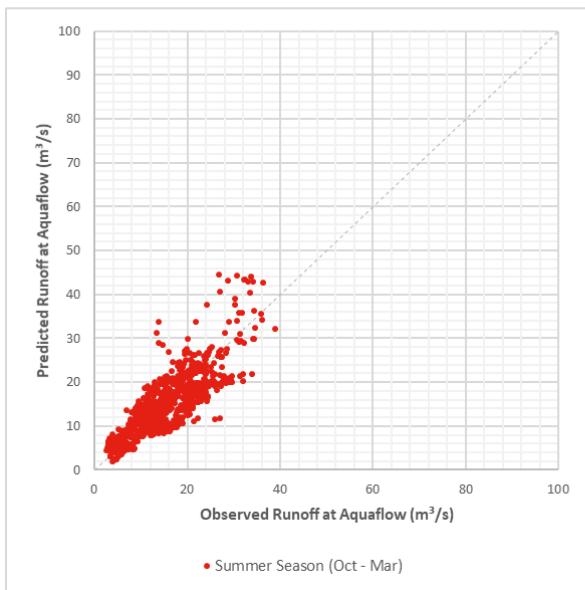
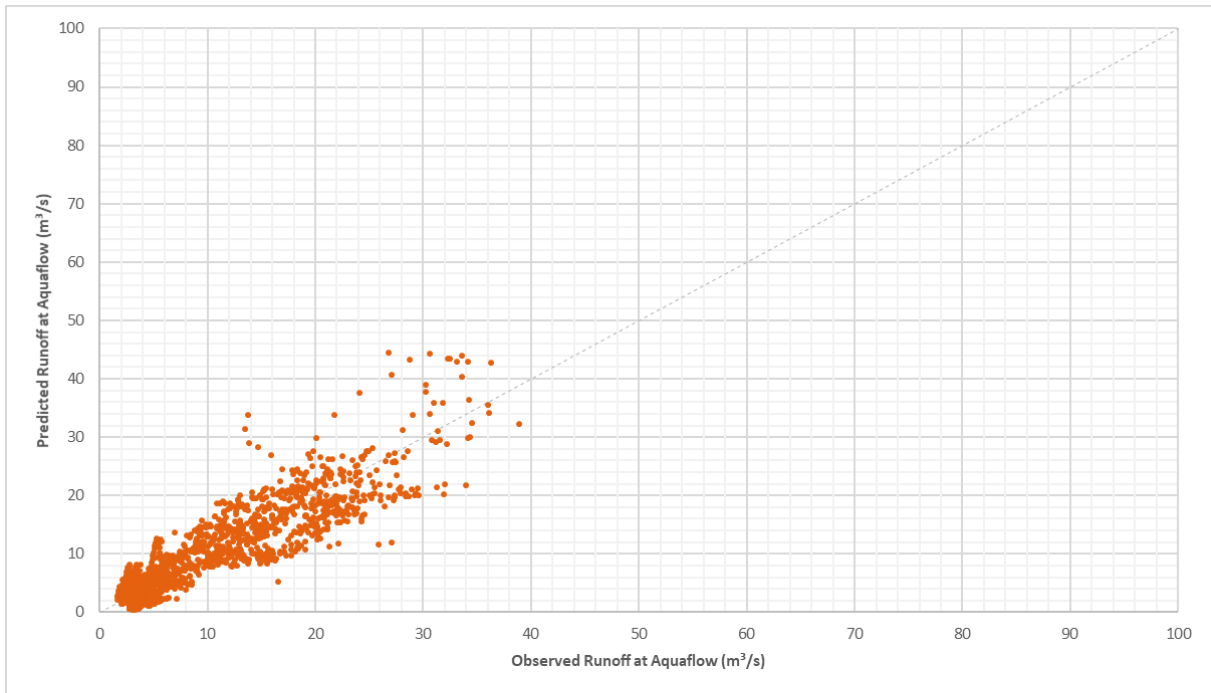
During these winter seasons lower than average temperature was present in the gauging station location as Figure 3.23 shows, reaching average values of -4.0 °C during June, July, and August. This could have provoked ice formation in San José river, causing backwater effects in the river reach resulting in an alteration of the normal stage-discharge curve of the control section in the river (World Meteorological Organization, 2010), and thus, delivering an overestimation on the discharge of the river on these periods. This observed overestimation is driving the model efficiency coefficient to its negative value.

Figure 3.23: Winter Temperature at AquafLOW Gauging Station



The annual, summer season and winter season correlation between the observed and the predicted runoff values at the AquafLOW gauging station are shown in Figure 3.24.

Figure 3.24: Mean Daily Runoff Correlation Results for Aquaflow Station



Finally, the duration curve, average seasonal variation and the mean daily runoff are shown in Figure 3.25, Figure 3.26 and Figure 3.27 respectively.

Figure 3.25: Duration Curve: Observed vs Predicted Runoff Data at Aquaflow

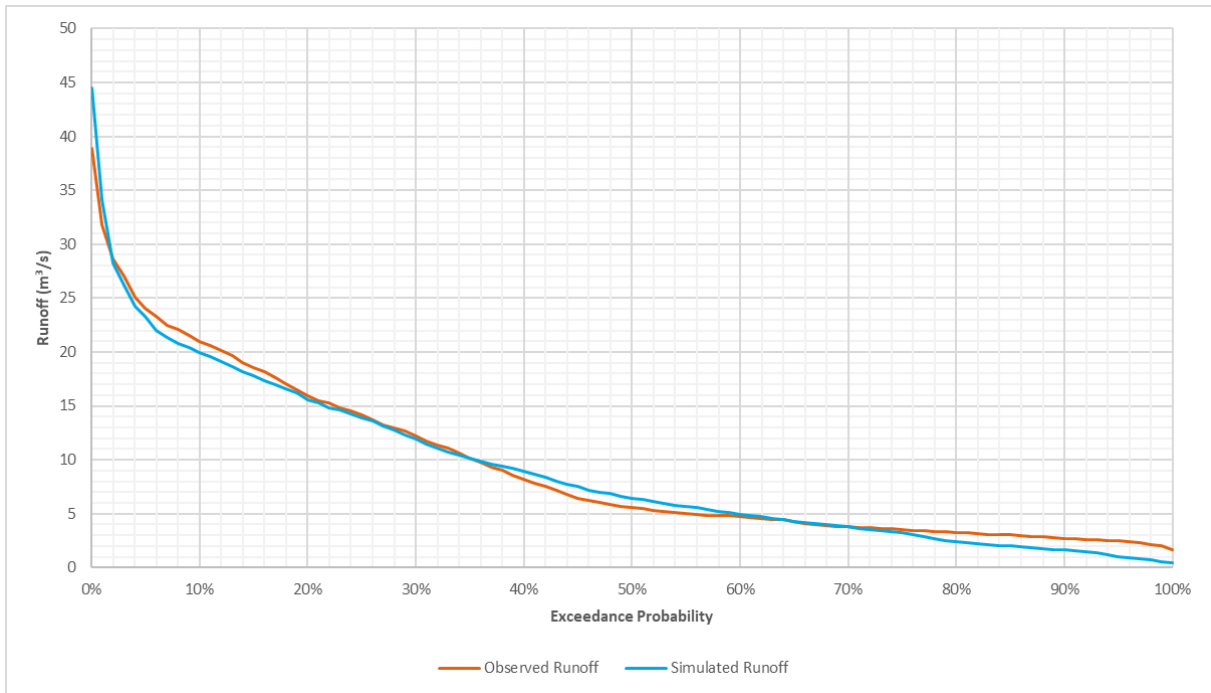


Figure 3.26: Seasonal Variation: Observed vs Predicted Runoff Data at Aquaflow

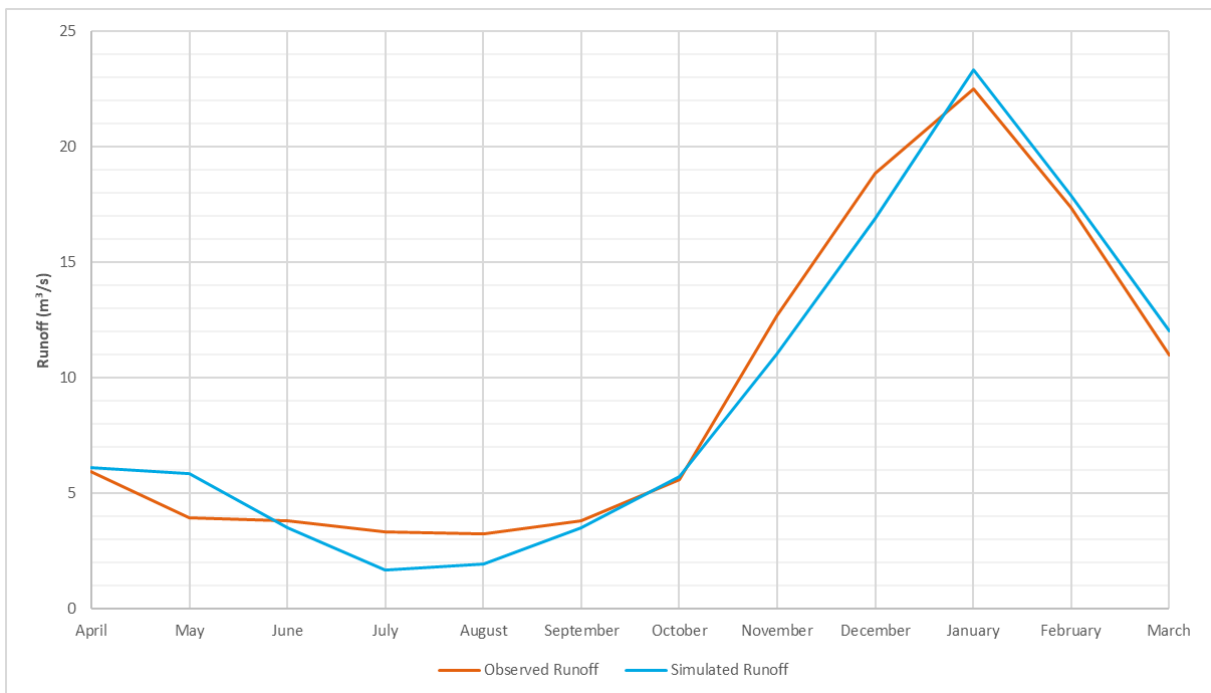


Figure 3.27: Mean Annual Runoff: Observed vs Predicted Runoff Data at Aquaflow

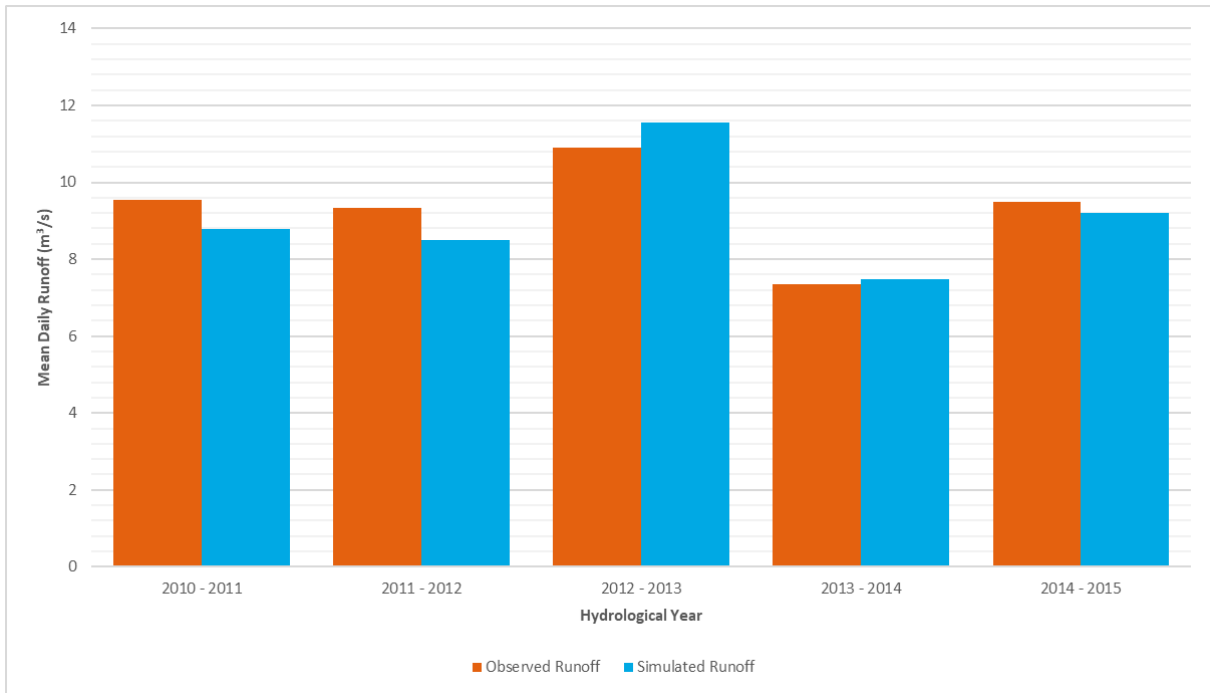


Figure 3.25 and Figure 3.26 shows the same phenomena described before about the runoff overestimation for the winter season measurements. Looking in the duration curve at the flows with an exceedance probability around 10% shows that the model underestimates the magnitude of frequent flood events.

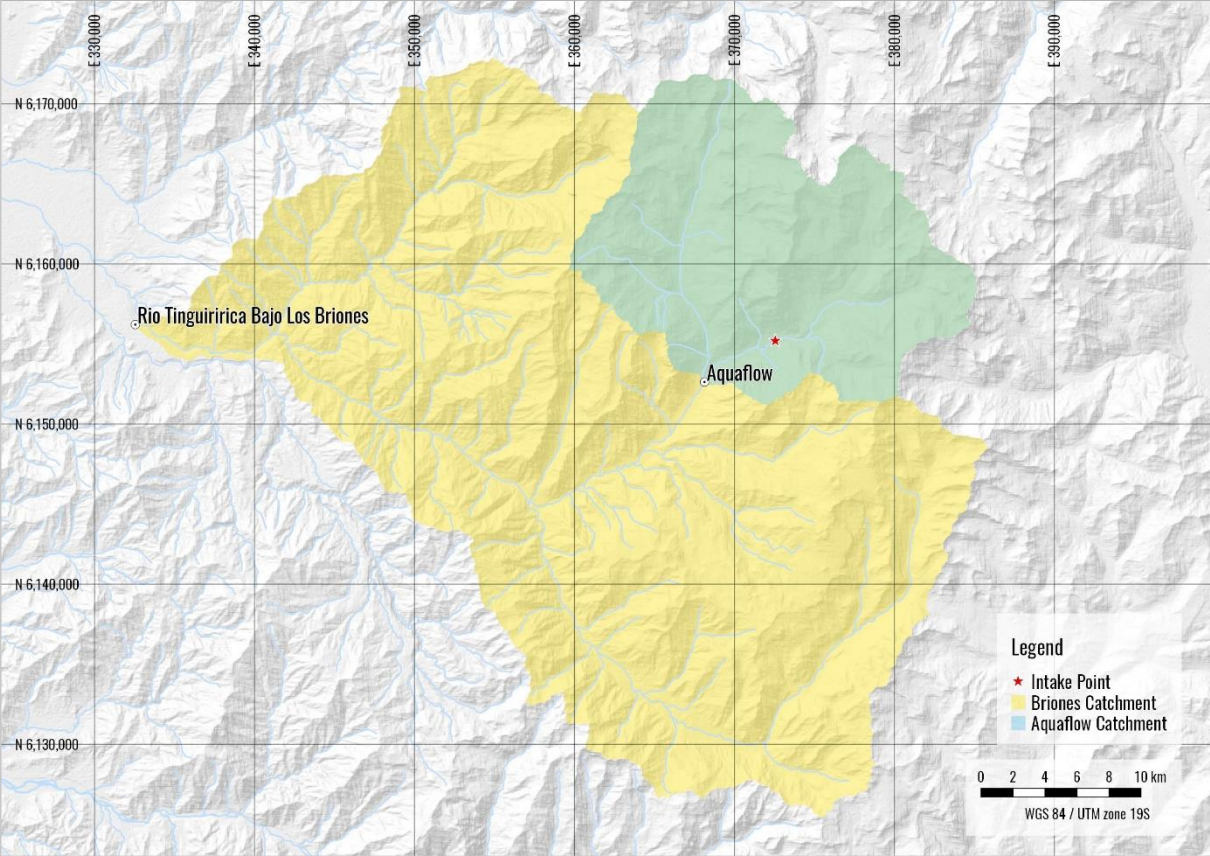
After assessing results from the calibration, it can be said that overall the model yields good mean daily runoff prediction results, suitable for modeling the energy production of Piedras Negras HPP.

3.6.3 Verification

Since Aquaflow gauging station has only five years of runoff records, it was decided to use the "Rio Tinguiririca Bajo Los Briones" (Briones) station to carry out the calibration verification, due to the quality and extension of its fluviometric record. Regarding this, the considered verification period starts from April 1, 1999, till March 31, 2017, meaning 18 years of runoff data.

This imposes a challenge because this station is approximately 46 km downstream of the station to be verified, meaning a difference in elevation of almost 1,000 m and a draining basin four times larger than that of Aquaflow as is shown in Figure 3.28.

Figure 3.28: Comparison Between Aquaflow and Briones Catchments



Due to this situation, a re-calibration of some of the meteorological correction parameters (SCORR, RCORR and TX), and the parameters linked to the temperature in the snow routine (CX, CXN, TS and TSN) had to be done. The rest of the parameters from the soil moisture and runoff response routines were left the same. Briones catchment parameters and a comparison between Aquaflow calibrated parameters and the re-calibrated Briones parameters are included in Table 3.13 and Table 3.14 respectively.

Table 3.13: Briones Catchment Area Distribution by Elevation Zone

| | Max. Elevation (masl) | Catchment Area (km²) | Glacier Area (km²) | Lakes Area (km²) |
|----------|----------------------------------|--|--|--|
| Outlet: | 565 | - | - | - |
| Zone 1: | 1,437 | 144.47 | 0.00 | 0.00 |
| Zone 2: | 1,811 | 144.28 | 0.00 | 0.00 |
| Zone 3: | 2,170 | 144.49 | 0.00 | 0.00 |
| Zone 4: | 2,427 | 144.63 | 0.00 | 0.00 |
| Zone 5: | 2,662 | 144.63 | 0.34 | 0.00 |
| Zone 6: | 2,886 | 144.23 | 2.05 | 0.09 |
| Zone 7: | 3,160 | 144.84 | 2.33 | 0.17 |
| Zone 8: | 3,444 | 144.26 | 3.03 | 0.15 |
| Zone 9: | 3,700 | 144.83 | 20.69 | 0.03 |
| Zone 10: | 4,962 | 144.68 | 45.37 | 0.00 |
| | Total | 1445.3 | 73.8 | 0.4 |
| | Catchment Percentage | 100% | 5.11% | 0.03% |

Table 3.14: Comparison Between Aquaflo and Briones Parameters

| Routine | Parameter | Calibrated Aquaflo Values | Re-Calibrated Briones Values |
|-------------------------------|---------------------|--------------------------------------|---|
| Meteorological Corrections | RCORR | 1.600 | 1.435 |
| | SCORR | 2.500 | 1.588 |
| | TX (°C) | 8.000 | 4.844 |
| | TCGRAD (°C/100m) | -0.76 | -0.76 |
| | TPGRAD (°C/100m) | -0.40 | -0.40 |
| | PGRAD (%/100m) | 5.80% | 5.80% |
| Snow Routine | CX (mm/d°·C) | 3.798 | 4.487 |
| | CXN (mm/d°·C) | 3.381 | 4.185 |
| | TS (°C) | 4.250 | 7.456 |
| | TSN (°C) | 5.330 | 7.890 |

| Routine | Parameter | Calibrated Aquaflow Values | Re-Calibrated Briones Values |
|-------------------------|----------------------------|---------------------------------------|---|
| | CFR (mm/d ^o .C) | 0.01 | 0.01 |
| | LWMAX | 0.07 | 0.07 |
| | NDAY | 270 | 270 |
| | CGLAC | 4.5 | 4.5 |
| Soil Moisture Routine | FC (mm) | 180.6 | 180.6 |
| | FCDEL | 1.0 | 1.0 |
| | BETA | 1.240 | 1.240 |
| | INFMAX (mm/h) | 50.0 | 50.0 |
| Runoff Response Routine | KUZ2 (1/day) | 0.134 | 0.134 |
| | KUZ1 (1/day) | 0.100 | 0.100 |
| | KUZ (1/day) | 0.060 | 0.060 |
| | KLZ (1/day) | 0.035 | 0.035 |
| | PERC (mm/day) | 1.650 | 1.650 |
| | UZ2 (mm) | 150.00 | 150.00 |
| | UZ1 (mm) | 71.13 | 71.13 |

The resulting Nash-Sutcliffe model efficiency coefficient is shown in Table 3.12:

Table 3.15: Nash-Sutcliffe Coefficient for Verification Period

| Season | Nash - Sutcliffe |
|---------------------------|-------------------------|
| Annual | 0.52 |
| Summer Season (Oct - Mar) | 0.58 |
| Winter Season (Apr - Sep) | 0.27 |

The following Figures graphically summarizes the verification results:

Figure 3.29: Timeseries: Observed vs Predicted Runoff Data at Briones

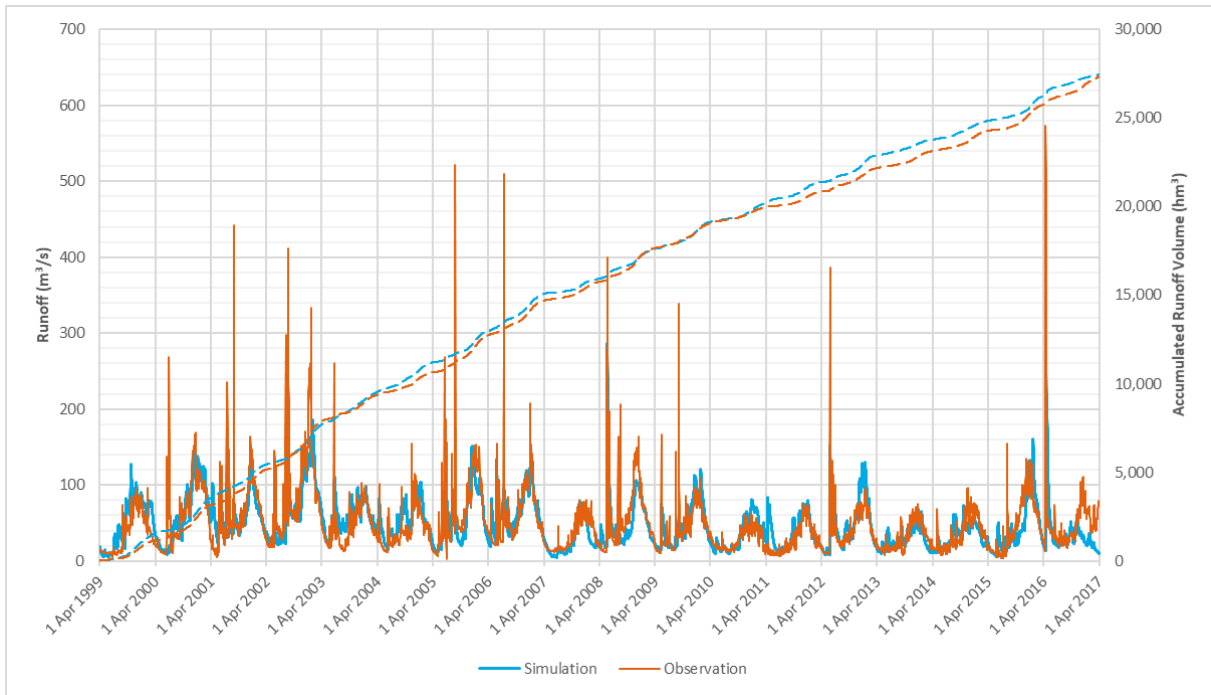


Figure 3.30: Duration Curve: Observed vs Predicted Runoff Data at Briones

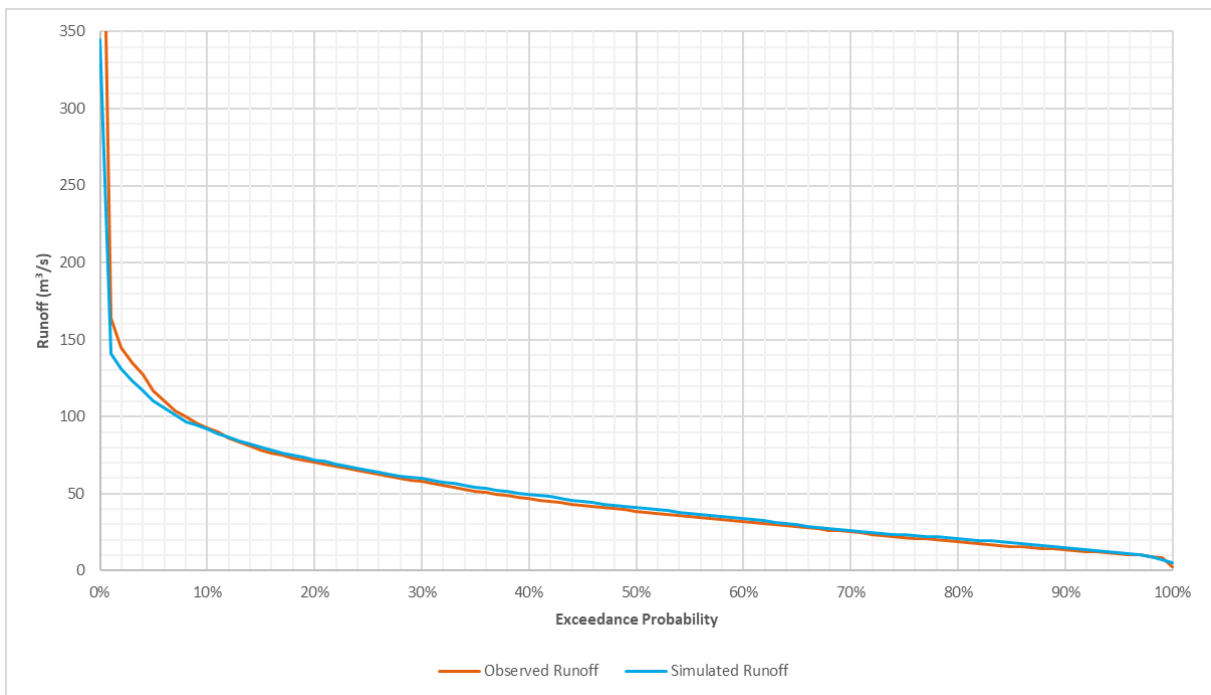


Figure 3.31: Seasonal Variation: Observed vs Predicted Runoff Data at Briones

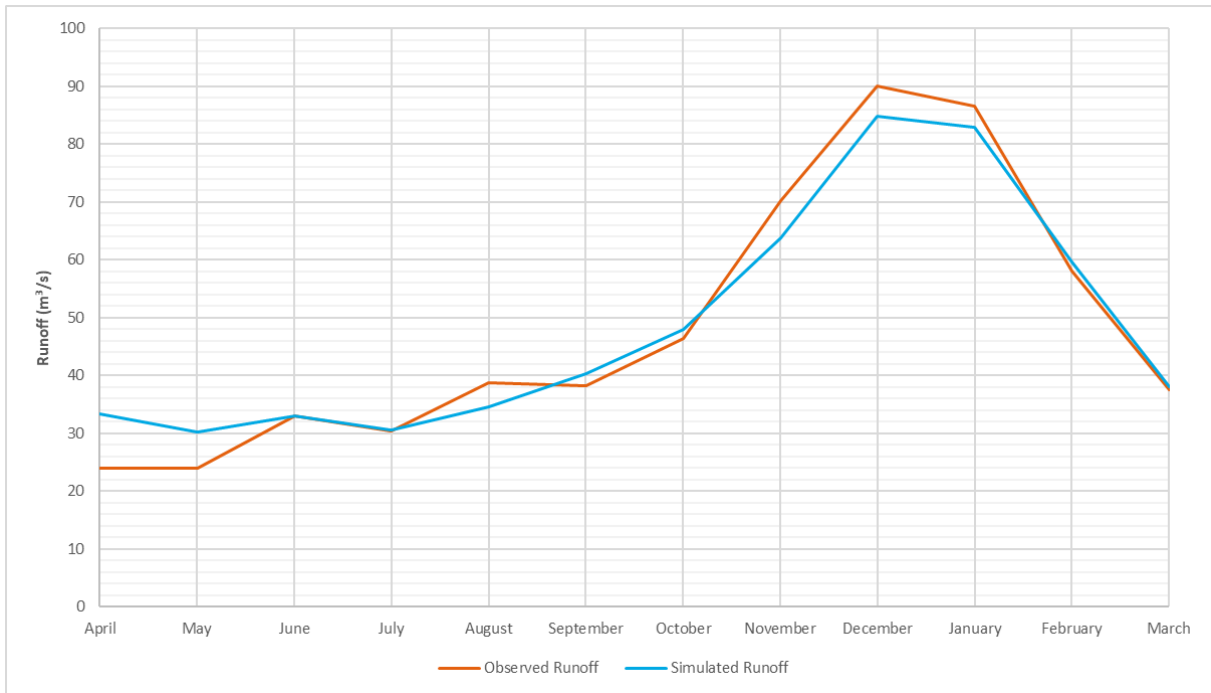


Figure 3.32: Mean Annual Runoff: Observed vs Predicted Runoff Data at Briones

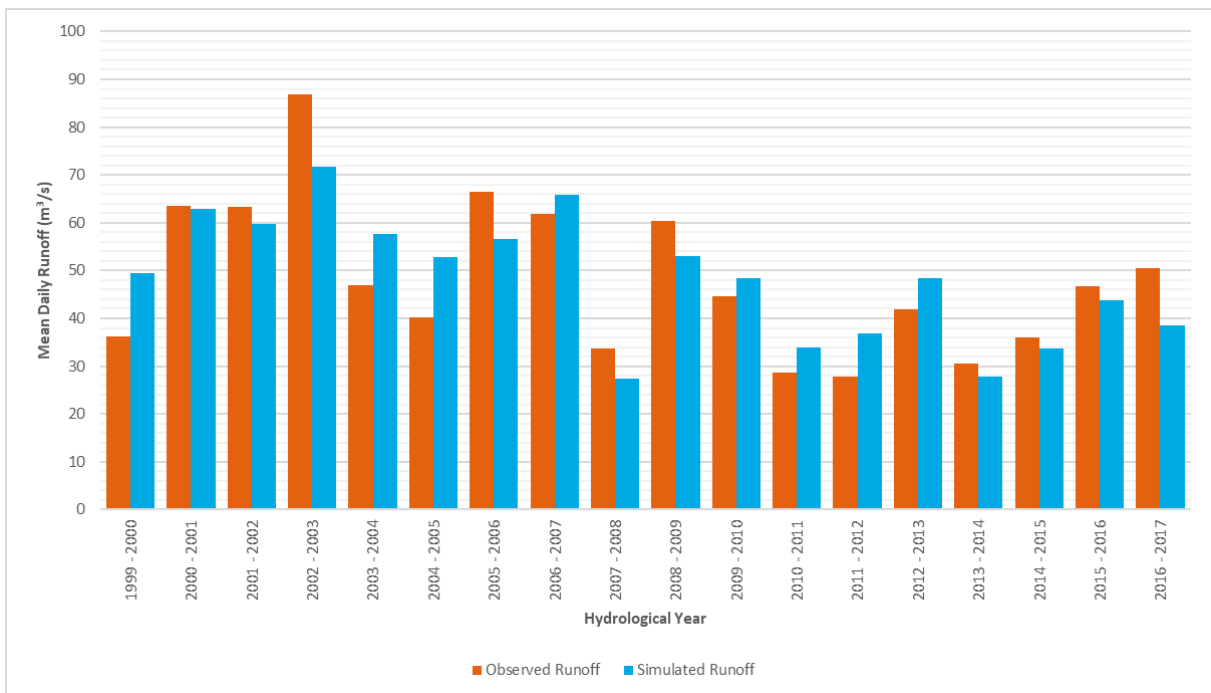
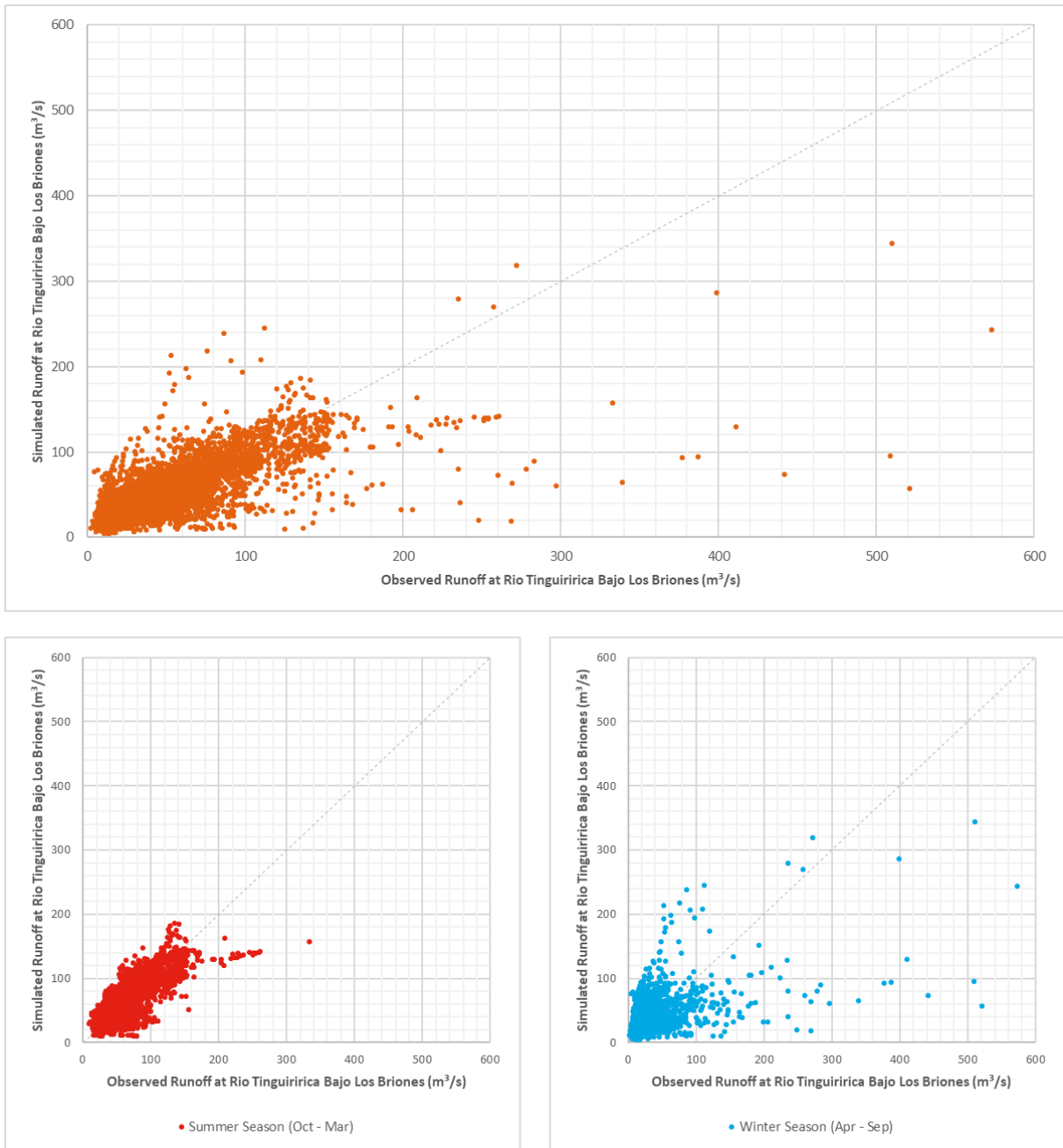


Figure 3.33: Mean Daily Runoff Correlation Results for Briones Station



As exposed in Table 3.15, the resulting Nash-Sutcliffe coefficient is outside the limits usually recommended for this type of models. Despite this, the result was expected due to the differences in the characteristics already commented between the calibration and validation basins and to the considered verification period being almost four times longer than the calibration one, which exposes the model to greater variations in the basin behavior.

However, and observing Figure 3.30 and Figure 3.31, a good follow-up of the predicted to the measured runoff is generally observed, both in duration and in seasonality.

For the reasons stated, it is considered that the verification finds that the model has a correct performance for the desired purposes.

3.7 Mean Daily Runoff Timeseries at Intake

During the calibration process, a precipitation, temperature and observed runoff timeseries ranging from 2010 till 2015 were used. Nevertheless, and as mentioned before, the idea of using a hydrological model for the project is to have an extended timeseries of runoff values for the San José river, this with the idea of decreasing the uncertainty of the energy production simulation.

Although precipitation data begins in January 1970, the greatest restriction comes from the temperature data, which start continuously from 1978 onwards. Therefore, the hydrological model will be used for the period from April 1, 1978, until March 31, 2017, that is, 39 years in total.

3.7.1 Catchment Parameters

Following the same procedure presented on the Title 3.6 and considering the catchment delimitation already done in the Title 3.2, a new set of parameters had to be collected to simulate the intake catchment. In this regard, Figure 3.34 shows the catchment land use and Figure 3.35 the glaciers outline.

Figure 3.34: Intake Catchment Land Use

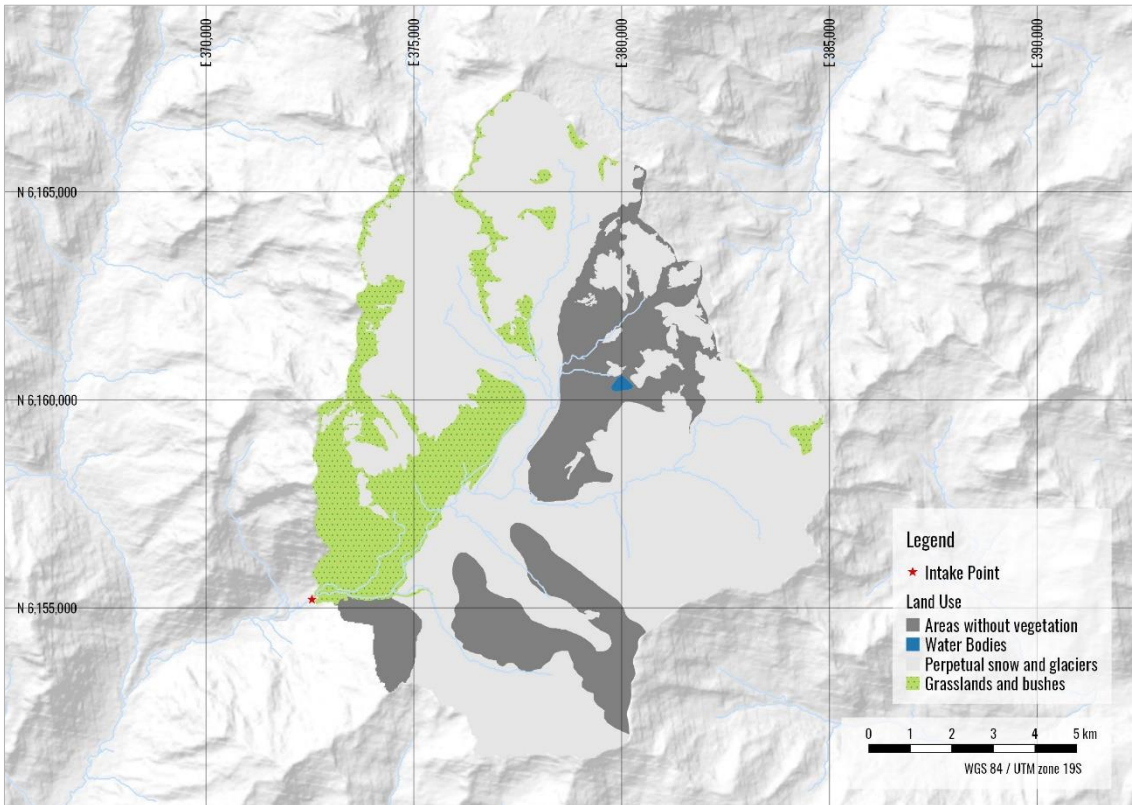
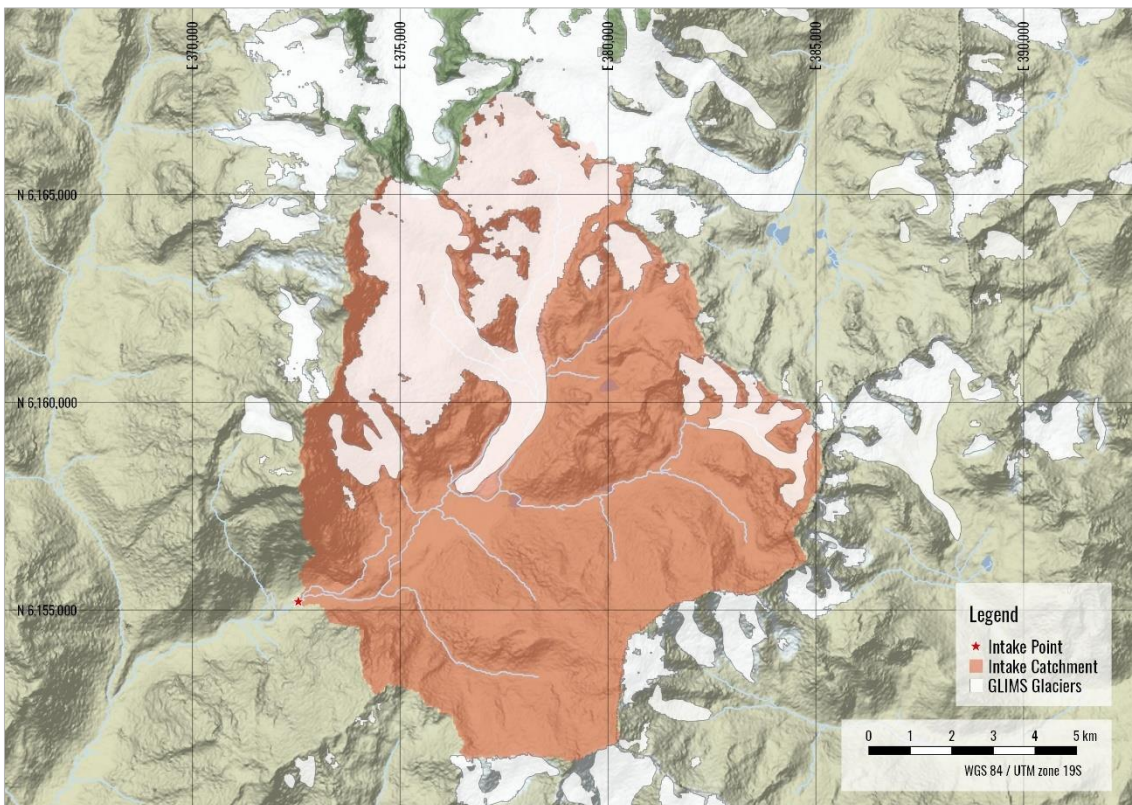


Figure 3.35: Intake Catchment Glaciers Outline



With this information, and dividing the basin into 10 elevation zones, Table 3.16 area distribution by elevation zone of the catchment.

Table 3.16: Intake Catchment Area Distribution by Elevation Zone

| | Max. Elevation (masl) | Catchment Area (km²) | Glacier Area (km²) | Lakes Area (km²) |
|----------|----------------------------------|--|--|--|
| Outlet: | 1,814 | - | - | - |
| Zone 1: | 2,650 | 12.76 | 0.77 | 0.06 |
| Zone 2: | 2,970 | 12.77 | 3.39 | 0.08 |
| Zone 3: | 3,207 | 12.80 | 1.48 | 0.01 |
| Zone 4: | 3,365 | 12.78 | 2.47 | 0.13 |
| Zone 5: | 3,488 | 12.72 | 4.31 | 0.00 |
| Zone 6: | 3,609 | 12.81 | 5.21 | 0.00 |
| Zone 7: | 3,747 | 12.78 | 5.06 | 0.00 |
| Zone 8: | 3,917 | 12.79 | 4.63 | 0.00 |
| Zone 9: | 4,179 | 12.81 | 4.88 | 0.00 |
| Zone 10: | 4,962 | 12.82 | 4.12 | 0.00 |
| | Total | 127.8 | 36.3 | 0.3 |
| | Catchment Percentage | 100% | 28.41% | 0.22% |

3.7.2 Intake Mean Daily Runoff Timeseries Results

Using the calibrated parameters included in Table 3.11, and the catchment parameters in Table 3.16, the mean average runoff of the San José river at the intake location is 4.0 m³/s, and a summary of the resulting runoff series are graphically shown next.

Figure 3.36: San José River Mean Daily Runoff at Intake

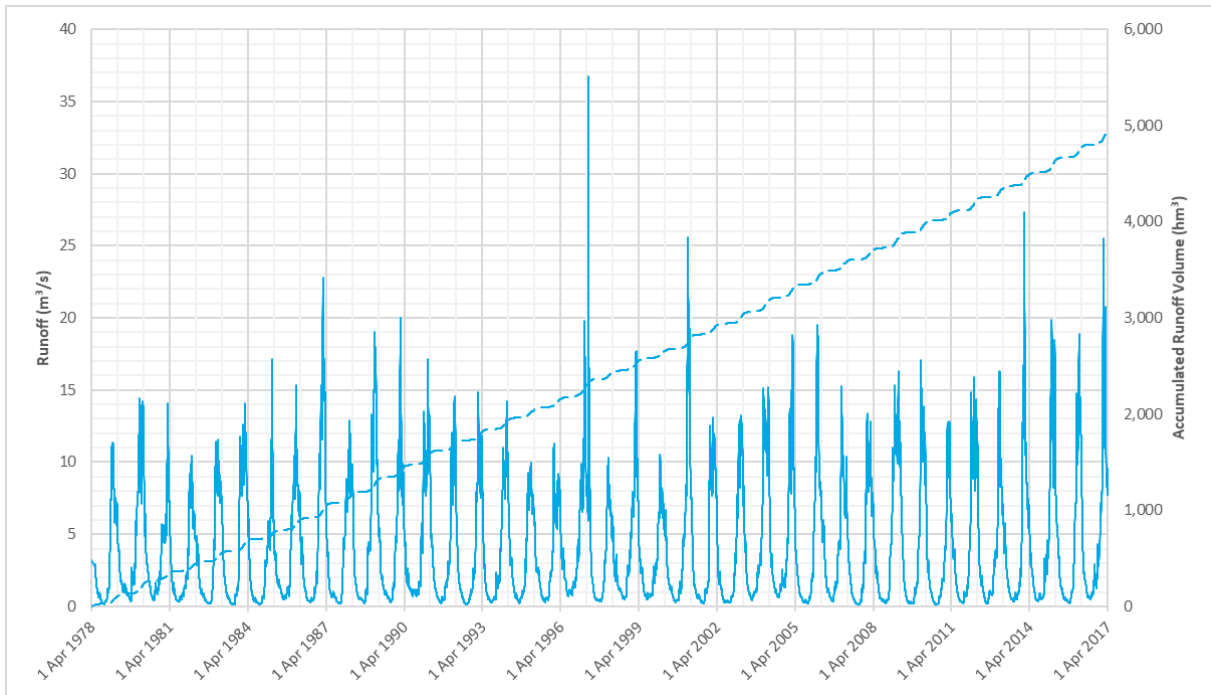


Figure 3.37: San José River Mean Daily Runoff Duration Curve at Intake

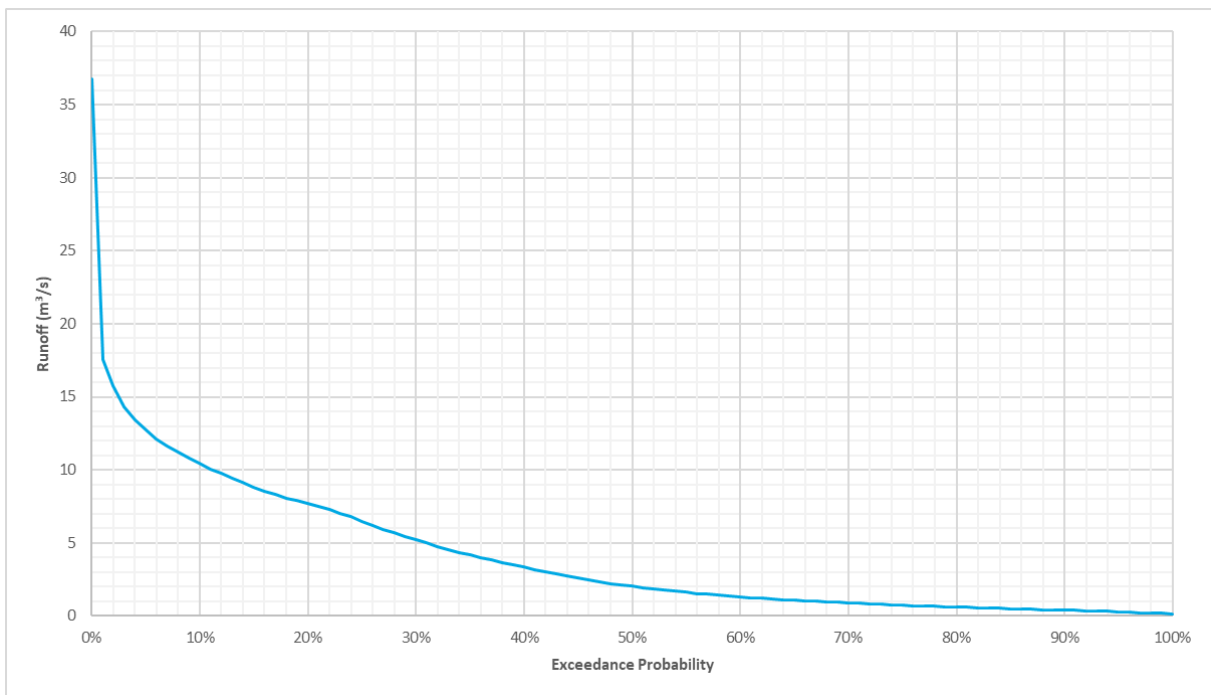


Figure 3.38: San José River Mean Seasonal Variation Curve at Intake

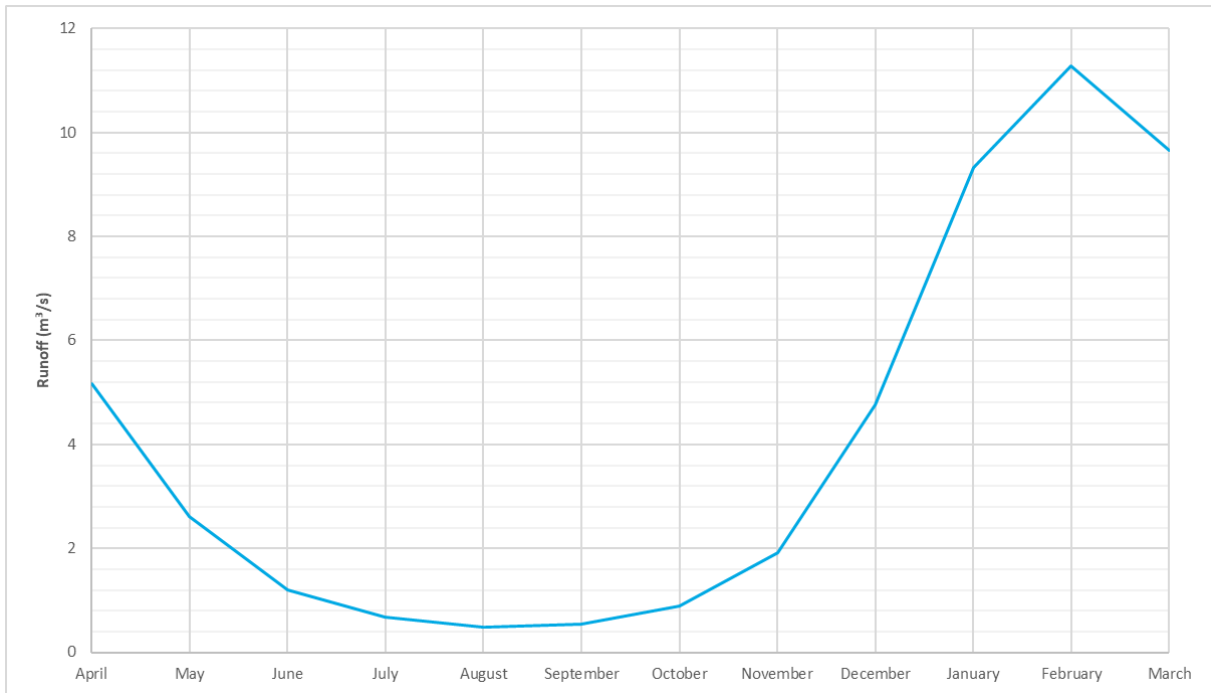
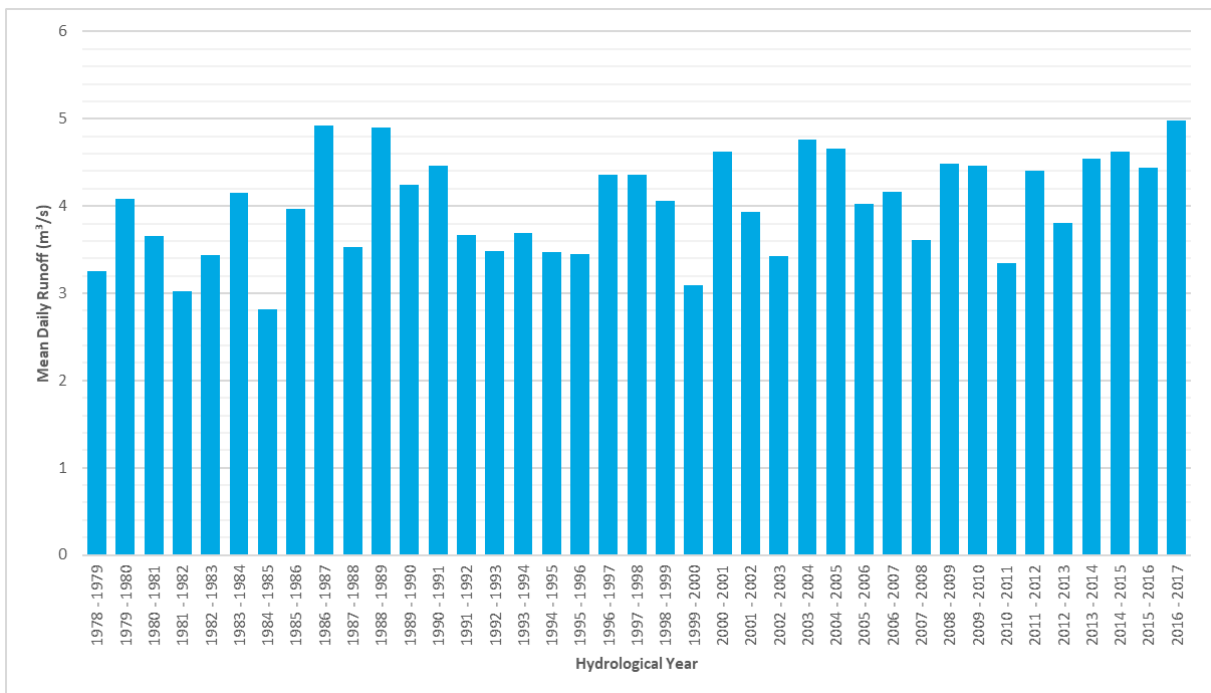


Figure 3.39: San José River Mean Annual Runoff at Intake



From Figure 3.38 it can be seen that the average runoff during winter season (1.8 m³/s) increases more than three times during the summer season (6.3 m³/s), this shows that the behavior of the San José river at the intake location is highly dependent on the snow and glacier cover of the

basin, offering a significant increase in spring flows due to the melting of these elements, and substantially decreasing its magnitude in the autumn due to the snow accumulation. This reiterates that the choice of the HBV model with its routine specifically dedicated to the simulation of the snow behavior was the right one.

The resulting runoff data is included in Appendix IV.

3.8 Flood Frequency Analysis

3.8.1 Model Calibration

Another goal of extending the runoff timeseries of the San José river was to be able to perform a flood frequency analysis with the idea of simulating the hydraulic behavior of the river during these events and establish safe boundaries for the placement of the powerhouse and other important works such as the headrace conduit.

Because this defines a different objective from the one contemplated for the mean daily runoff (Title 3.6.2), in whose results it was mentioned that the floods that occur more frequently were underestimated, it was decided to manually adjust the runoff response routine parameters so that the predicted runoff floods were better fitted to those observed in detriment of the base flows.

A comparison between the runoff response routine for the mean daily and the resulting flood timeseries is included in Table 3.17.

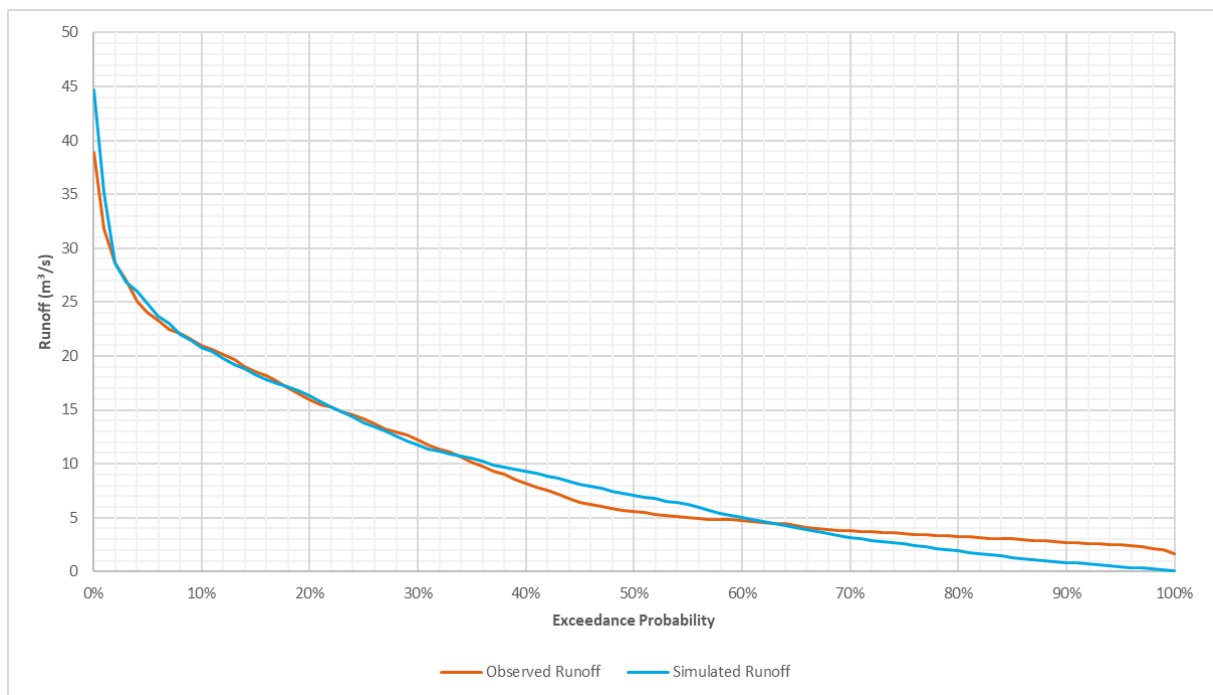
Table 3.17: Runoff Response Routine Parameters Comparison: Mean Runoff vs Floods

| Routine | Parameter | Mean Daily Runoff Values | Flood Frequency Analysis Values |
|-------------------------|------------------|---------------------------------|--|
| Runoff Response Routine | KUZ2 (1/day) | 0.134 | 0.102 |
| | KUZ1 (1/day) | 0.100 | 0.100 |
| | KUZ (1/day) | 0.060 | 0.100 |
| | KLZ (1/day) | 0.035 | 0.100 |
| | PERC (mm/day) | 1.650 | 1.650 |

| Routine | Parameter | Mean Daily Runoff Values | Flood Frequency Analysis Values |
|---------|-----------|--------------------------|---------------------------------|
| | UZ2 (mm) | 150.00 | 148.00 |
| | UZ1 (mm) | 71.13 | 31.00 |

With these changes, Figure 3.40 shows the resulting duration curve. It must be remembered to focus the attention on how the predicted runoff below an exceedance probability of 30% fits the observed values, considering these as flood flows.

Figure 3.40: Duration Curve: Observed vs Predicted Flood Runoff Data at Aquaflow



Since as mentioned the idea is to generate a safety boundary for the location of the powerhouse and the conduit, it was decided to work directly with Aquaflow station catchment due to its proximity to the potential area where said work will be located and, for the rest of the river reach located upstream, these resulting flood flows would be slightly overestimated which adds a safety factor to the hydraulic simulation of these events.

3.8.2 Frequency Analysis

Considering only the maximum flows of each simulated year, in Figure 3.41, it can be observed the flood events occur mostly between December and January, coinciding with the thaw season. Similarly, in the Figure 3.42 shows its common to expect flood flows between 25 and 30 m³/s.

Figure 3.41: Number of Flood Events per Month at Aquaflow

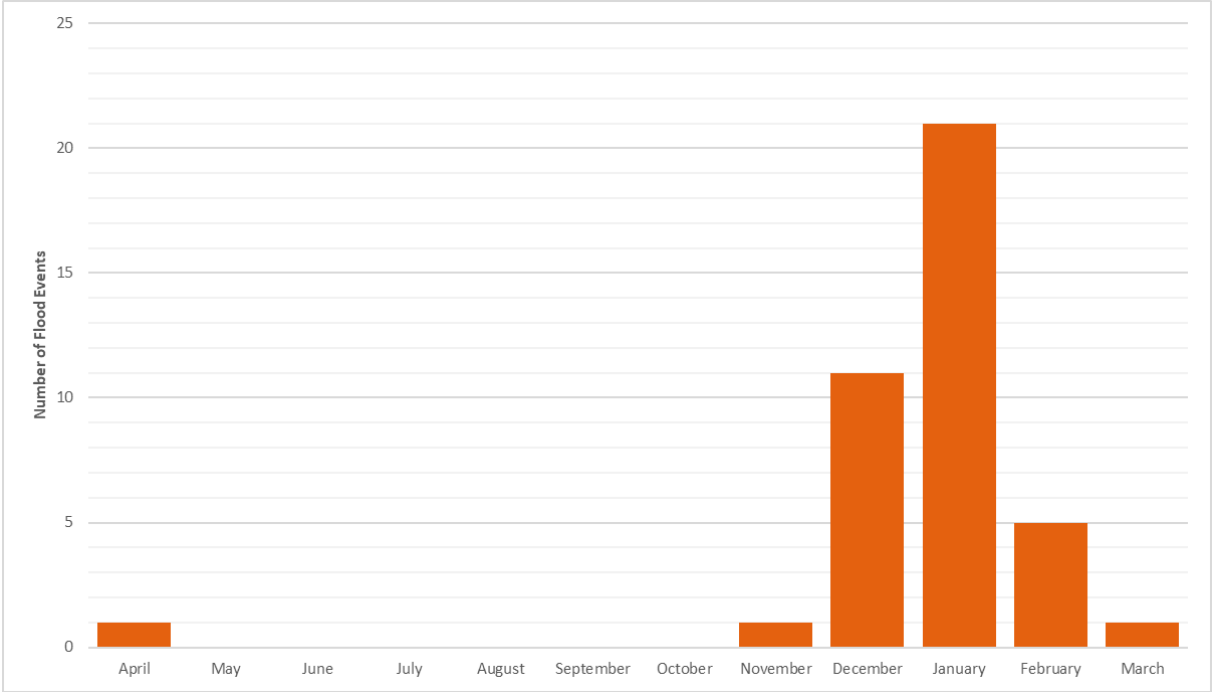
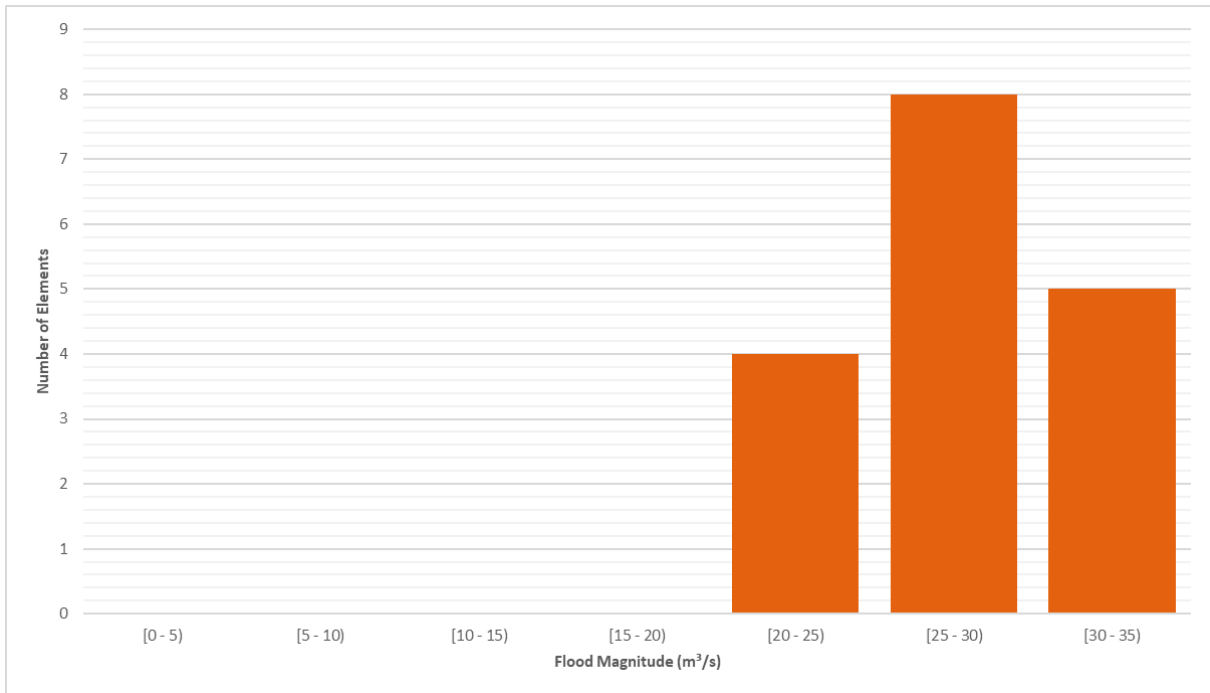


Figure 3.42: Histogram of Flood Magnitudes at Aquaflow



The resulting maximum flood discharge per year is included in Appendix V.

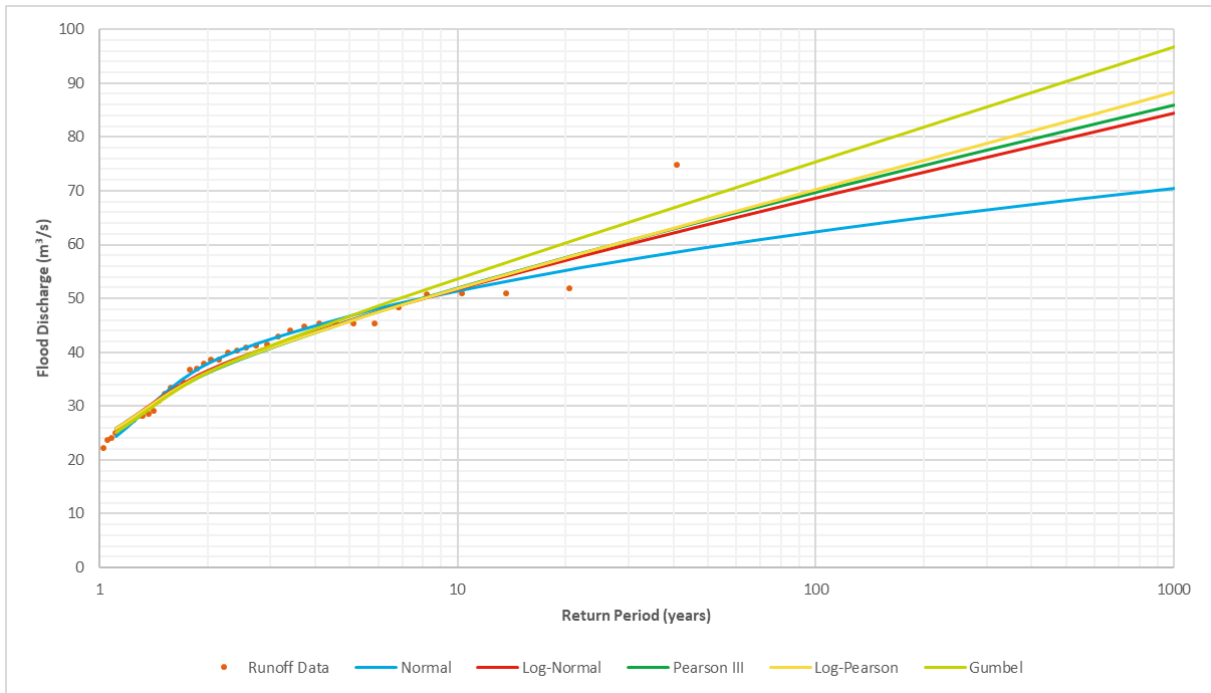
With the resulting series of maximum flows per year, the next step consisted in performing a frequency analysis for the floods. This was done using the following statistical distributions: Normal, Log-Normal, Pearson Type III, Log-Pearson, and Gumbel. All were considered for a flood return period of 1, 2, 5, 10, 20, 25, 50, 100, 200, 500 and 1,000 years.

It is appropriate to mention that according to current Chilean legislation (Ministerio de Justicia, 2018), for this type of infrastructure it must be considered a return period of 100 years for the hydraulic design and 200 years to verify the design.

Due to this, and even though mathematical correlation indicators such as the coefficient of determination (R^2) and the mean squared error were calculated, the final choice of flood discharges values for each return period was made by visually assessing which distribution is best suited for each return period, especially for the values needed by the Chilean legislation.

In this regard, Figure 3.43 shows the observed values and each of the mentioned statistical distributions.

Figure 3.43: Flood Frequency Analysis Results



Looking at Figure 3.43, for the return periods up to five years, the Normal distribution results were chosen, from 10 years onwards, Gumbel distribution yields better results. Table 3.18 includes the selected resulting flood discharge values for each of the mentioned return periods.

Table 3.18: Flood Discharge Values

| Return Period (years) | Flood Discharge (m³/s) |
|----------------------------------|--|
| 1 | 24.3 |
| 2 | 37.9 |
| 5 | 46.7 |
| 10 | 53.7 |
| 20 | 60.3 |
| 25 | 62.4 |
| 50 | 68.9 |
| 100 | 75.4 |
| 200 | 81.8 |
| 500 | 90.3 |
| 1,000 | 96.7 |

4 Climate Change Analysis

As part of the scope of this Thesis not only the historical hydrological behavior of the catchment under study was analyzed, but also the impact that the changes occurring worldwide in the weather patterns will have on the future hydrology when the Piedras Negras HPP is in full operation.

This is considered of vital importance for this project if it is kept in mind that an important percentage of the basin that drains into the intake is controlled by Universidad glacier.

The criteria and the analysis made to evaluate this point will be explained next.

4.1 Definitions and Scenarios

In 1988 the United Nations Environment Programme (UNEP) and the World Meteorological Organization (WMO) established the Intergovernmental Panel on Climate Change (IPCC), the leading international body whose main objective is to provide the world with a clear scientific view on the current state of knowledge in climate change and its potential environmental and socio-economic impacts (WMO, 2018).

On IPCC Fifth Assessment Report (AR5), the last assessment report to date, IPCC defines (Flato et al., 2013):

“Climate change refers to a change in the state of the climate that can be identified (e.g., by using statistical tests) by changes in the mean and/or the variability of its properties, and that persists for an extended period, typically decades or longer. Climate change may be due to natural internal processes or external forcings such as modulations of the solar cycles, volcanic eruptions, and persistent anthropogenic changes in the composition of the atmosphere or in land use. Note that the Framework Convention on Climate Change (UNFCCC), in its Article 1, defines climate change as: “a change of climate which is attributed directly or indirectly to human activity that alters the composition of the global atmosphere and which is in addition to natural climate variability observed over comparable time periods”. The UNFCCC thus makes

a distinction between climate change attributable to human activities altering the atmospheric composition, and climate variability attributable to natural causes”.

Bearing in mind that the UN definition itself attributes climate change to the effects that humankind has had on the atmosphere, and considering that one of the main drivers of climate change is the concentration of greenhouse gases, it should be considered that there are many variables and factors linked to the future emissions of greenhouse gases that can alter the development of this effect on the atmosphere. The scientific evidence for warming of the climate system is unequivocal but there is no consensus on a unique evolution path climate change is going to follow.

In this regard, the IPCC in the AR5 defined four Representative Concentration Pathways (RCP) which describes four climate futures depending on the greenhouse emission in the years to come. The RCPs are named after the expected change in the net (incoming minus outgoing) radiative flux at the top of atmosphere for the year 2100 (Flato et al., 2013).

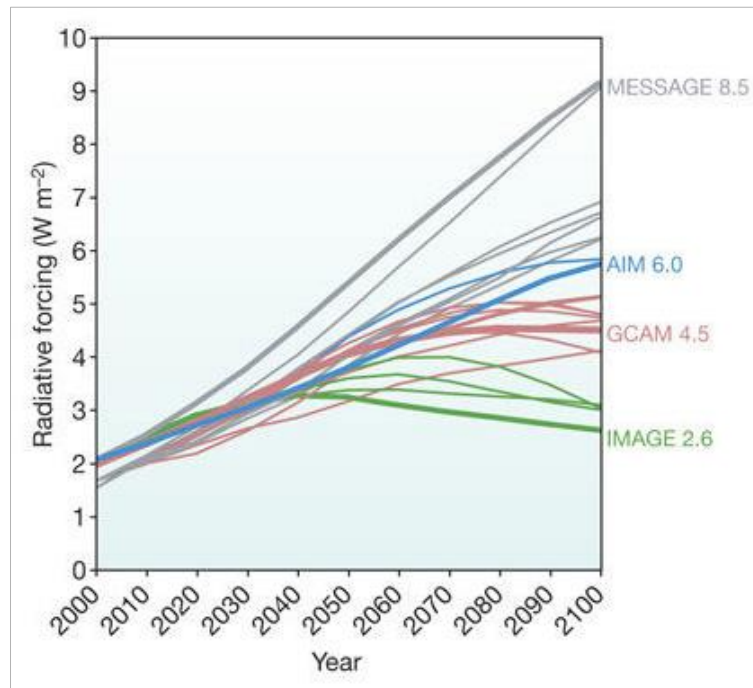
To describe the four RCPs scenarios, their descriptions are included in Table 4.1 (Moss et al., 2010):

Table 4.1: Representative Concentration Pathways (RCP) Description

| Name | Radiative Forcing | Concentration (p.p.m.) | Pathway |
|-------------|---|--|---------------------------------|
| RCP8.5 | >8.5 W/m ² in 2100 | >1,370 CO ₂ -equiv. in 2100 | Rising |
| RCP6.0 | ~6 W/m ² at stabilization after 2100 | ~850 CO ₂ -equiv. (at stabilization after 2100) | Stabilization without overshoot |
| RCP4.5 | ~4.5 W/m ² at stabilization after 2100 | ~650 CO ₂ -equiv. (at stabilization after 2100) | Stabilization without overshoot |
| RCP2.6 | Peak at ~3 W/m ² before 2100 and then declines | Peak at ~490 CO ₂ -equiv. before 2100 and then declines | Peak and decline |

In Table 4.1 it is mentioned that each RCP evolves in time in a differentiated way. Figure 4.1 shows the pathway contemplated for each of these scenarios.

Figure 4.1: RCP Pathways Evolution in Time



Source: (Moss et al., 2010)

It is important to mention that for the purposes of this Thesis, it was considered that RCP2.6 would be not representative of the future conditions of the catchment for being an optimistic climate change scenario. For this reason, and with the idea of obtaining an envelope of the future climatic effects, it was chosen to work only with the RCP4.5 and the RCP8.5 scenarios.

4.2 Climate Models and Downscaling

Each of the RCP scenarios discussed in the earlier point has been included in the so-called General Circulation Model (GCM), which are mathematical models of the global climate where the physical processes that affect the oceans and the planet atmosphere are simulated.

The way of working on these models is to divide the whole planet into rectangular cells. Each cell will represent in a mathematical way the average geomorphological characteristics of its location and will simulate the climatic processes of interest. In other words, a piece of the planet is represented in each cell of the model.

However, in the case of the GCMs, since it covers the entire planet, said cells can have a size of hundreds of kilometers at a time. The consequence of this for the case study of a specific

catchment is that the resolution is so low that the climatic results are not representative of the in-situ conditions.

This means that, for the data to be usable, a process called “downscaling” must be carried out, which consists in taking specific GCM cells and subdivide it (increase its resolution) to obtain data that is representative of the region of interest.

There are many procedures to perform downscaling. In the case of this Thesis, it was decided to work directly with the regional models integrated into the Coordinated Regional Climate Downscaling Experiment (CORDEX), one of the largest projects of the World Climate Research Program (WCRP) which is sponsored by the WMO, the International Council for Science (ICSU) and the Intergovernmental Oceanographic Commission (IOC) of UNESCO.

Using a GCM as a driving model and choosing a specific region of the planet (or domain), CORDEX takes the diving model data and uses it as input for a Regional Climate Models (RCM), which is a high resolution climatic model, meaning each cell has a maximum size of tens of kilometers (European Network for Earth System modelling, 2016).

In this sense, the following was considered for the study of climate change.

4.2.1 Driving Model Selection

To minimize the uncertainty in the study of climate change, it was decided to use a total of five driving models. The idea was to obtain a range of results and an average with which the climate change impact on the energy production of Piedras Negras HPP was assessed.

In this regard, Table 4.2 includes a summary of the considered driving models.

Table 4.2: Description of Selected Driving Models for Climate Change Analysis

| Model Name | Model ID | Country of Origin | Developing Institution |
|-------------------------|------------------|--------------------------|--------------------------------------|
| MPI- Earth System Model | MPI-M-MPI-ESM-LR | Germany | Max-Planck-Institut für Meteorologie |

| Model Name | Model ID | Country of Origin | Developing Institution |
|---|---------------------------|-------------------|--|
| Model for Interdisciplinary Research on Climate | MIROC-MIROC5 | Japan | The University of Tokyo Center for Climate System Research, National Institute for Environmental Studies, Japan, Japan Agency for Marine-Earth Science and Technology Frontier Research Center for Global Change |
| Norwegian Earth System Model | NCC-NorESM1-M | Norway | UNI Bjerknes Center for Climate Research, The Norwegian Meteorological Institute |
| CSIRO-MK3.6.0 | CSIRO-QCCCE-CSIRO-Mk3-6-0 | Australia | Commonwealth Scientific and Industrial Research Organization |
| Geophysical Fluid Dynamics Laboratory Earth System Models | NOAA-GFDL-GFDL-ESM2M | USA | National Oceanic and Atmospheric Administration |

4.2.2 Regional Climate Model

Once the driving models are chosen, it is necessary to select an RCM that will work with the resulting GCM data.

In this sense, it was decided to work with the Regional Rossby Center atmospheric model (RCA4), developed by the SMHI, the same institute that created the HBV. The choice of this model is due to its wide use and acceptance within the climate research community.

4.2.3 Domain

As mentioned before, the domain refers to the region of the planet to which the driving model downscaling process will be carried out.

Since Chile is the country in which the project is found, it was chosen to work with the SAM-44 domain, which covers the entire South American region with a separation between nodes of 0.44°, approximately 50 km, as can be seen in Figure 4.2.

Figure 4.2: SAM-44 Domain for Regional Climate Model



4.3 Analysis Procedure

The information downloaded from the CORDEX portal consisted of historical and future daily data of surface temperature and precipitation for the commented domain.

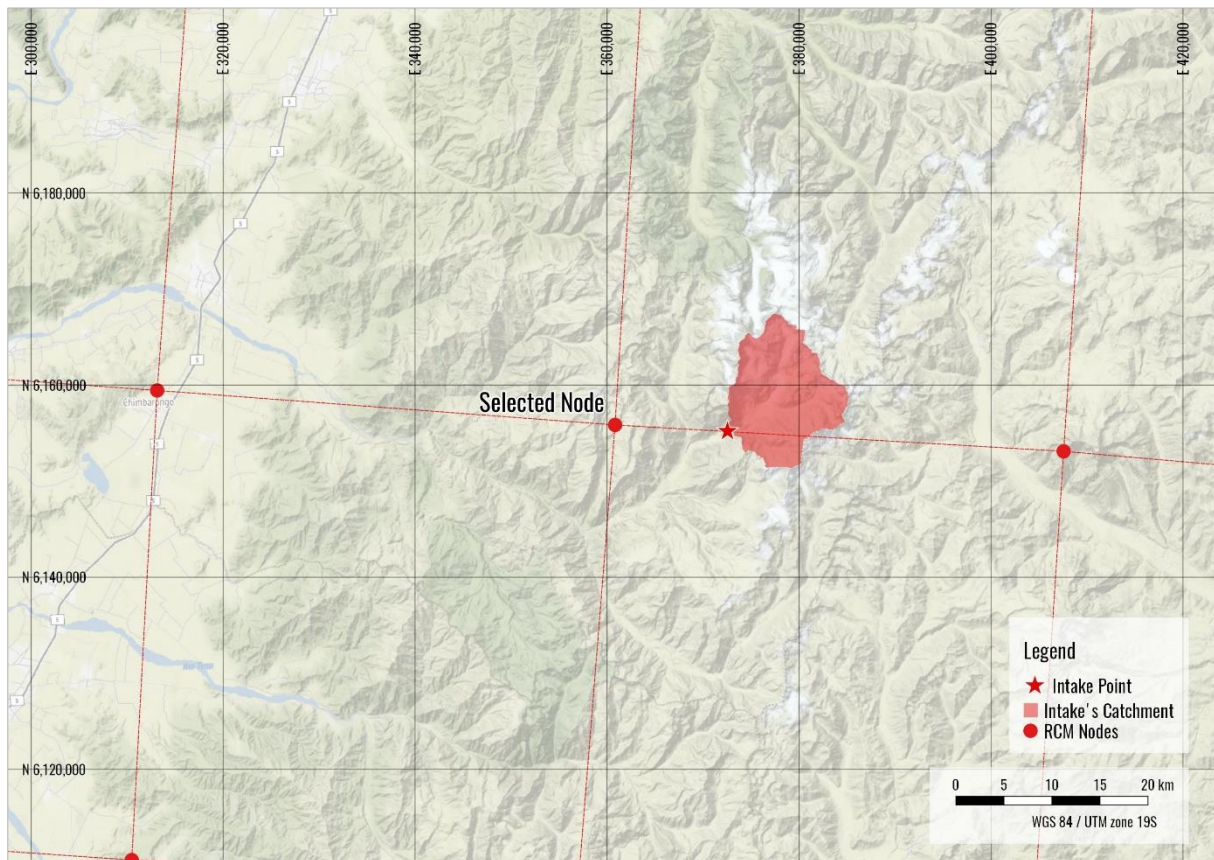
These data from the climate models are stored in Network Common Data Form (NetCDF) files, with extension ".nc". This file type is designed to hold a large amount of data both spatial and temporal, which is translated in that each node of the domain shown in Figure 4.2 holds a timeseries of the climatic data of interest.

4.3.1 Node Selection

The first step for the analysis of the data consisted in selecting a node that was representative of the basin that drains towards the intake. This had to be done because due to the catchment size none of the RCM nodes of the domain were located within its limits.

The closest node was chosen as shown in Figure 4.3.

Figure 4.3: Representative Regional Climate Model Node for Intake Catchment



4.3.2 Bias Correction

To address the assessment of climate change, so far it has been discussed on the use of climatic models, both GCMs and RCM. Like any mathematical model, the results must be compared and adjusted with observed data to ensure that the analysis adheres to the local reality.

This process of adjusting the results of the models is called “bias correction”, and in general terms, the process consists of comparing historical data from both the climate models and the observations made in-situ and use this comparison to calculate statistical correction factors which will then be applied to the future climate change data in the area.

There are several methods to perform bias correction, however, the employed in this Thesis involved a script programmed by Abebe Girmay Adera, M. Sc. in RStudio which uses a

statistical transformation package for post-processing climate model output named QMap. This package estimates the values of the quantile-quantile relation of observed and modeled time series for regularly spaced quantiles using local linear least square regression (Gudmundsson, 2016).

The bias correction factors were computed using 24 years of historical data from January 1981 till December 2005.

4.3.2.1 Precipitation

Considering all the driving models from Table 4.2, the resulting mean absolute error from the bias correction process for each of them is included in Table 4.3.

Table 4.3: Precipitation Data Bias Correction Resulting Mean Absolute Error

| Model ID | Mean Absolute Error (mm) |
|---------------------------|---------------------------------|
| MPI-M-MPI-ESM-LR | 5.7 |
| MIROC-MIROC5 | 5.6 |
| NCC-NorESM1-M | 5.5 |
| CSIRO-QCCCE-CSIRO-Mk3-6-0 | 5.8 |
| NOAA-GFDL-GFDL-ESM2M | 5.6 |

To graphically see the results of the bias correction, Figure 4.4 shows the seasonal average and the dispersion of the driving models vs the observed precipitation while Figure 4.5 shows a consistency test using a double mass curve to compare the models with the observed data.

Figure 4.4: Historical Seasonal Precipitation Comparison: Models vs Observed Data

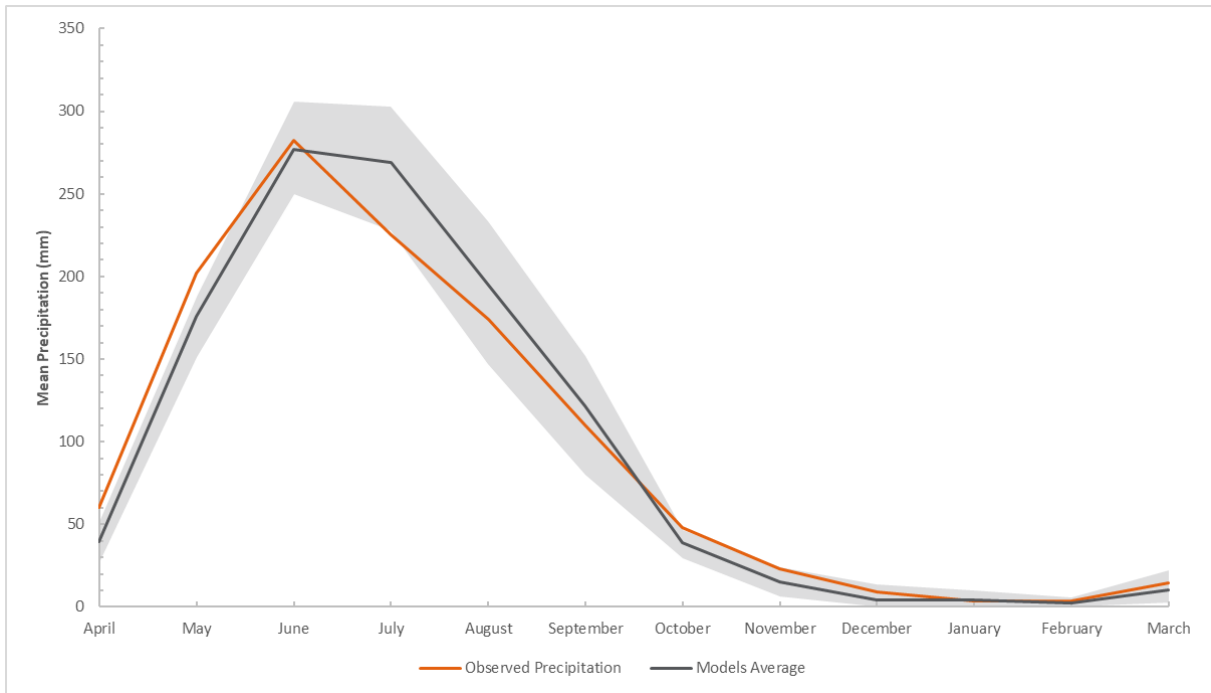
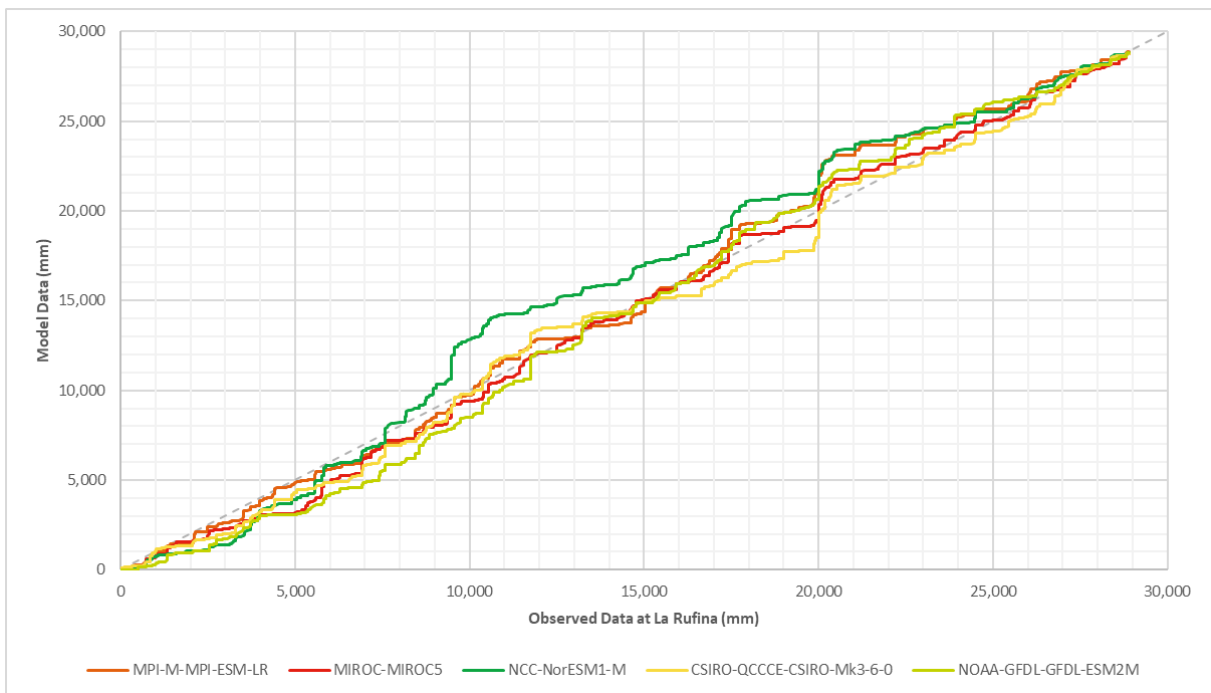


Figure 4.5: Consistency Precipitation Test Comparison: Models vs Observed Data



4.3.2.2 Temperature

Similar to the results obtained for precipitation, Table 4.4 includes the resulting mean absolute error from the bias correction process, Figure 4.6 shows the seasonal average and the dispersion of the driving models vs the observed temperature and Figure 4.7 shows a consistency test using a double mass curve to compare the models with the observed data.

Table 4.4: Temperature Data Bias Correction Resulting Mean Absolute Error

| Model ID | Mean Absolute Error (°C) |
|---------------------------|--------------------------|
| MPI-M-MPI-ESM-LR | 3.5 |
| MIROC-MIROC5 | 3.5 |
| NCC-NorESM1-M | 3.3 |
| CSIRO-QCCCE-CSIRO-Mk3-6-0 | 3.3 |
| NOAA-GFDL-GFDL-ESM2M | 3.3 |

Figure 4.6: Historical Seasonal Temperature Comparison: Models vs Observed Data

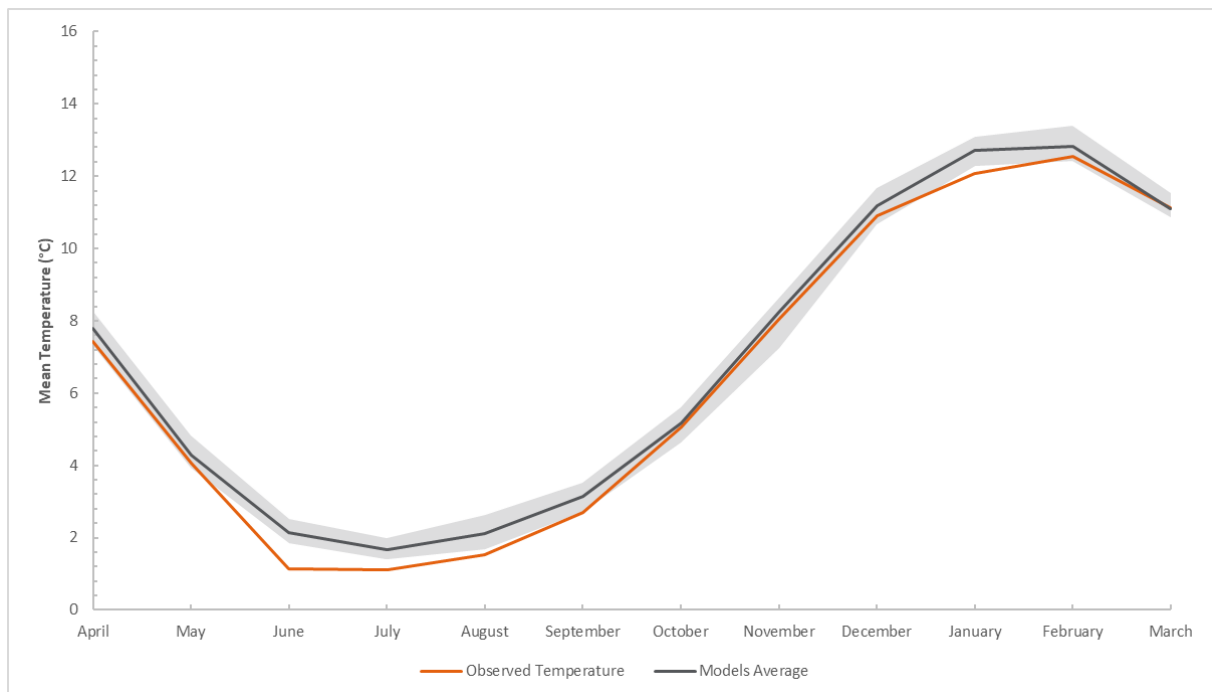
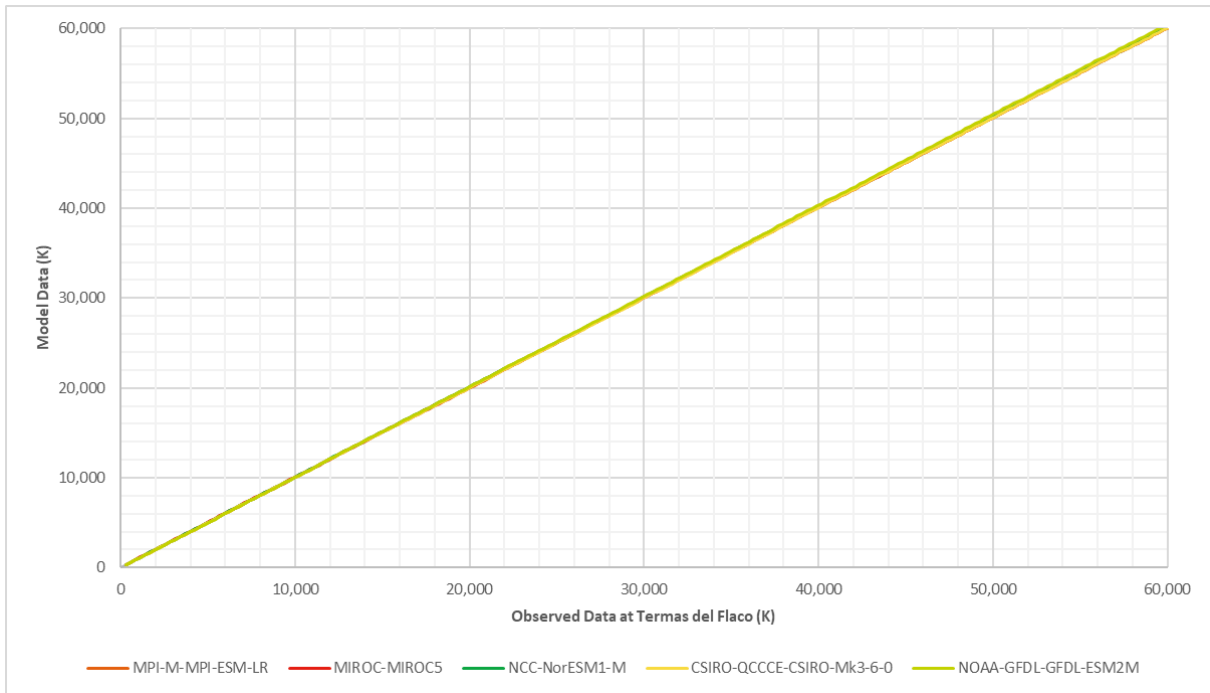


Figure 4.7: Consistency Temperature Test Comparison: Models vs Observed Data



4.3.2.3 Final Remarks

Observing the bias correction results both from precipitation and temperature, it can be said that the behavior of the models closely resembles the observed values, with an average error of ± 5.6 mm for the precipitation and ± 3.4 °C for temperature, error values which are acceptable for this study. Therefore, the bias correction process was satisfactory, and the model data was considered ready to use for the next stage.

4.4 Climate Change Results

The climate change analysis for each of the driving models included in Table 4.2 covered 50 years of data, starting from January 2021 till December 2070. This period was chosen to cover the potential lifetime of Piedras Negras HPP.

4.4.1 Projected Precipitation

To visualize the projected behavior of the precipitation, Figure 4.8 and Figure 4.9 compare the historical seasonal variation with the projected for the RCP4.5 and RCP8.5 scenarios respectively.

Figure 4.8: Precipitation Seasonal Variability at La Rufina for RCP4.5

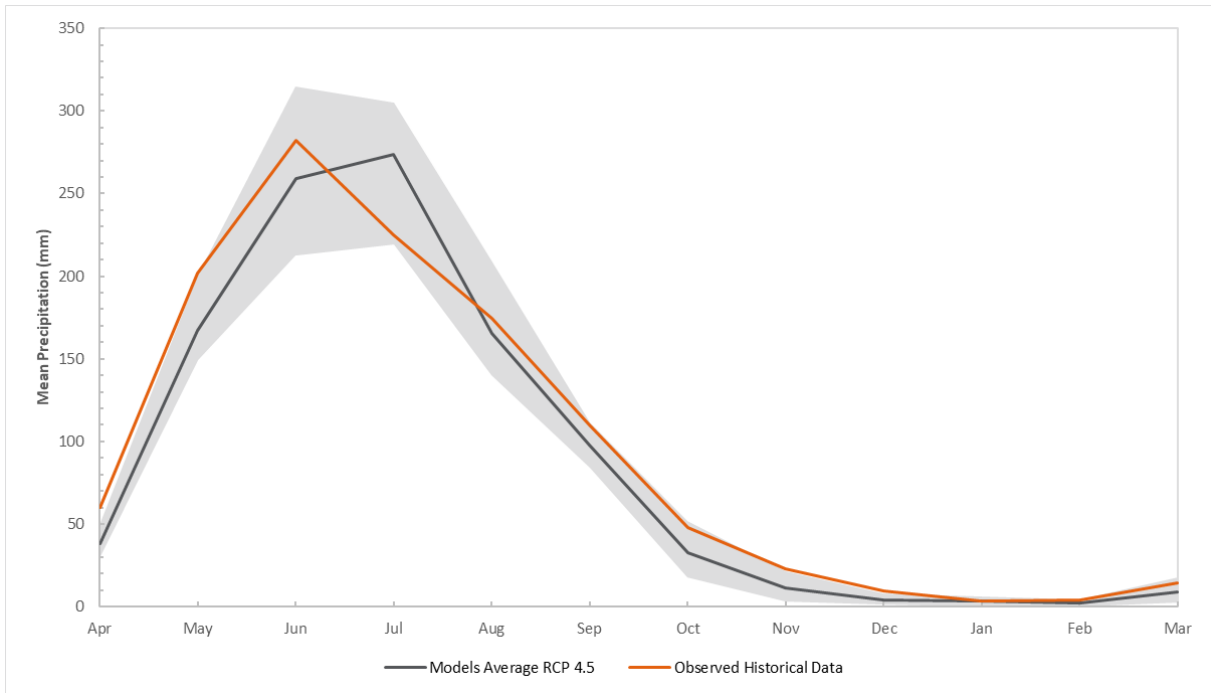
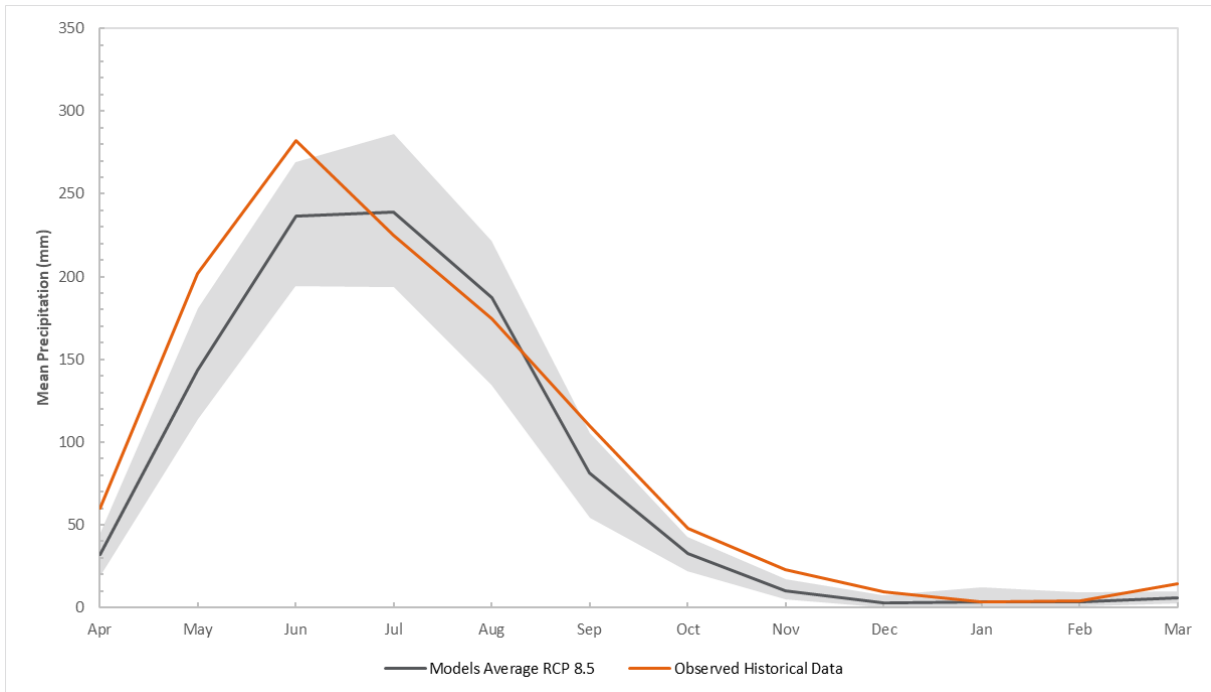


Figure 4.9: Precipitation Seasonal Variability at La Rufina for RCP8.5



It is interesting to see how in both scenarios the wet season reduces its duration with a delayed arrival and an early beginning of the drought season. It is also possible to observe a 23% and

28% reduction in the amount of precipitation on average for RCP4.5 and RCP8.5 respectively in comparison with the observed historical data.

Now, looking at the projected precipitation trend from 2021 to 2070, shown in Figure 4.10 and Figure 4.11 for RCP4.5 and RCP8.5 respectively, it is observed that for the first scenario the trend is practically flat but showing a slight increase of 0.2 mm/yr, while for the RCP8.5 the downward trend is appreciable with an average decrease of 2.3 mm/yr.

Figure 4.10: Precipitation Trend at La Rufina for RCP4.5

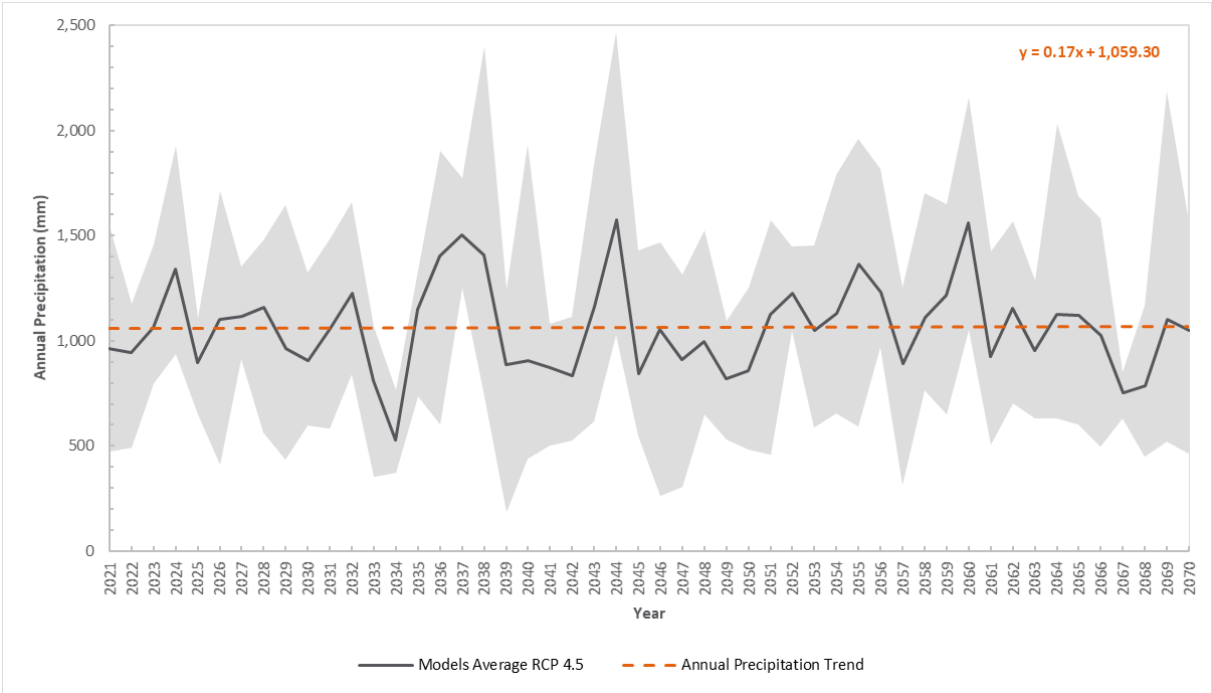
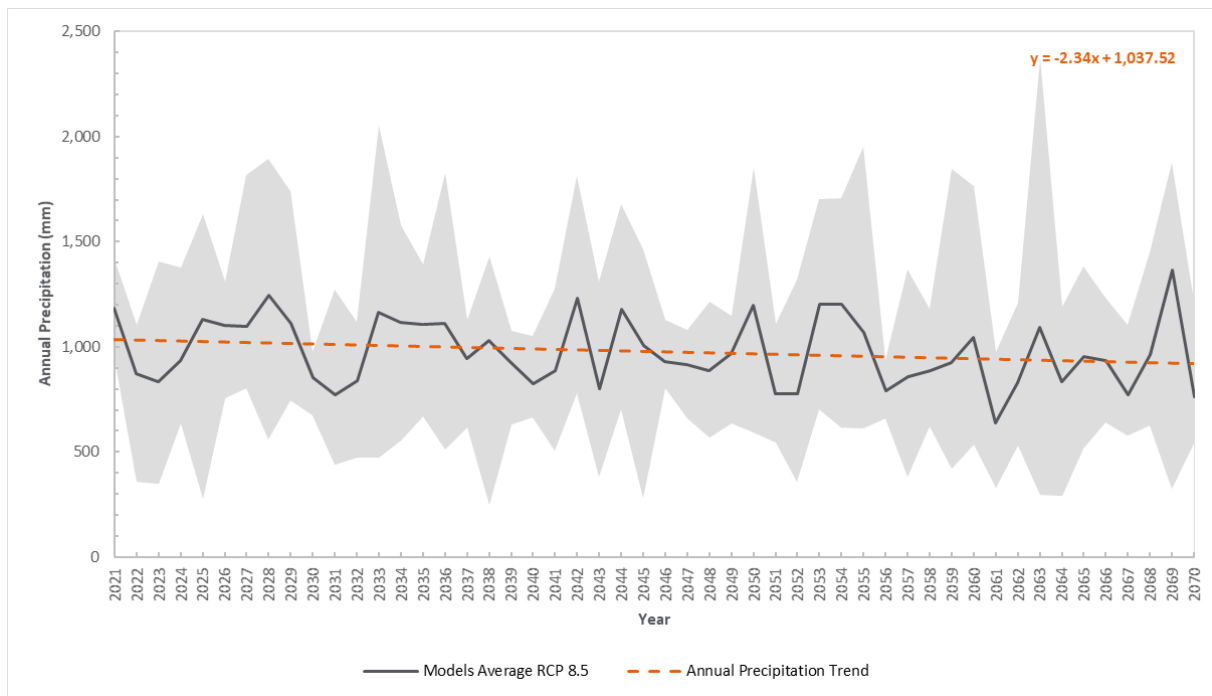


Figure 4.11: Precipitation Trend at La Rufina for RCP8.5



4.4.2 Projected Temperature

Regarding the seasonal variability of the RCP4.5 and RCP8.5 scenarios, it is possible to observe that the driving models have less dispersion of results among themselves, that is, the temperature predicted for future scenarios converge more closely to the average, indicating more agreement between the models as can be seen in the Figure 4.12 and Figure 4.13 respectively.

Figure 4.12: Temperature Seasonal Variability at Termas del Flaco for RCP4.5

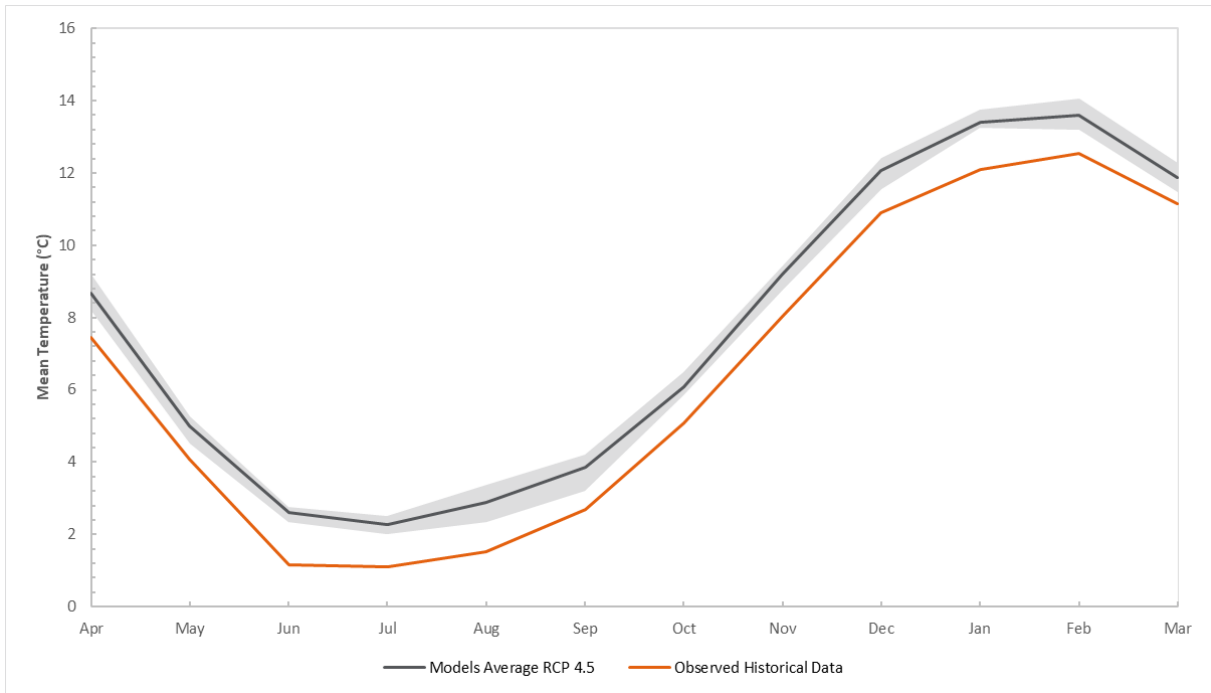
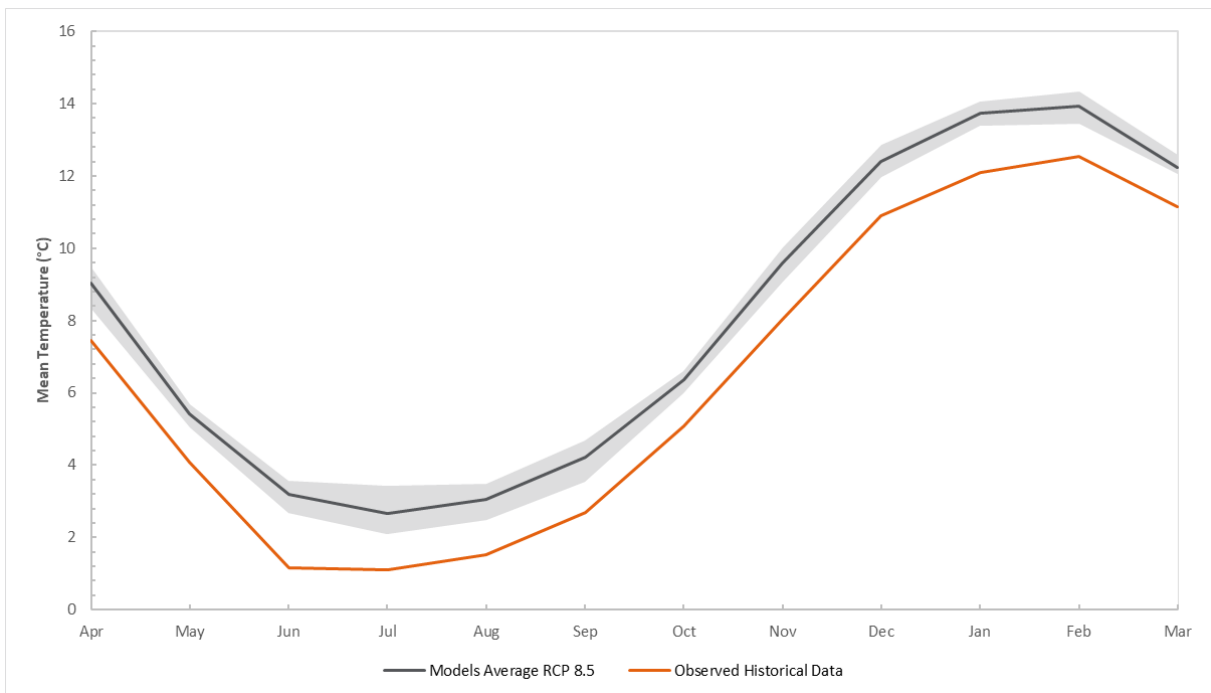


Figure 4.13: Temperature Seasonal Variability at Termas del Flaco for RCP8.5



Comparing the future temporal variability with the historical one as shown in Figure 4.12 and Figure 4.13, it is possible to determine that in the RCP4.5 scenario the temperature would

increase by 40% or 1.1 °C on average; for the RCP8.5 this increase is of 52% or 1.5 °C on average.

In a basin whose flow regime is highly linked to the snow and glacier conditions of the sector, this expected increase in temperature is indicative of more extreme fluvial conditions. A higher temperature leads to a more accelerated melting of the snow and glacier area, that is, the basin will reduce its storage capacity, affecting the base flows, and as there will be an increase in both the exposed terrain and liquid precipitation, potentially increasing the floods events with respect to the historically observed.

Now, observing future trends, both scenarios show a gradual increase in the temperatures of the sector, with rates of 0.02 °C/yr and 0.03 °C/yr for the RCP4.5 and RCP8.5 scenarios respectively as depicted in Figure 4.14 and Figure 4.15.

Figure 4.14: Temperature Trend at Termas del Flaco for RCP4.5

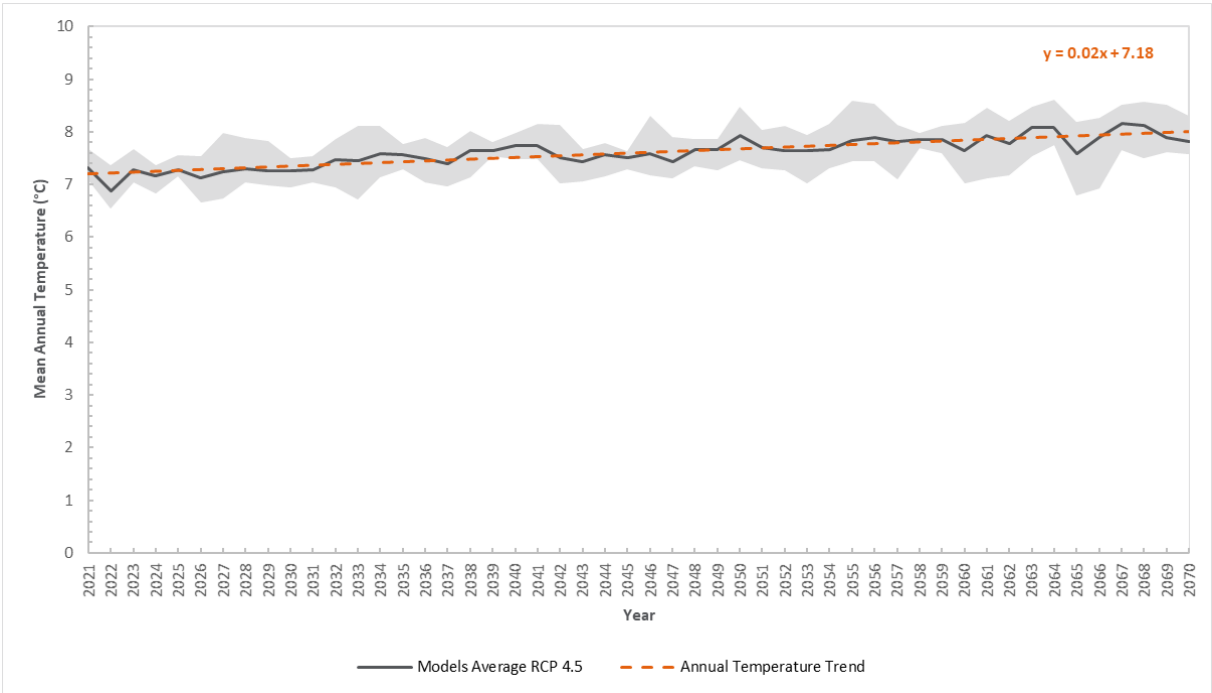
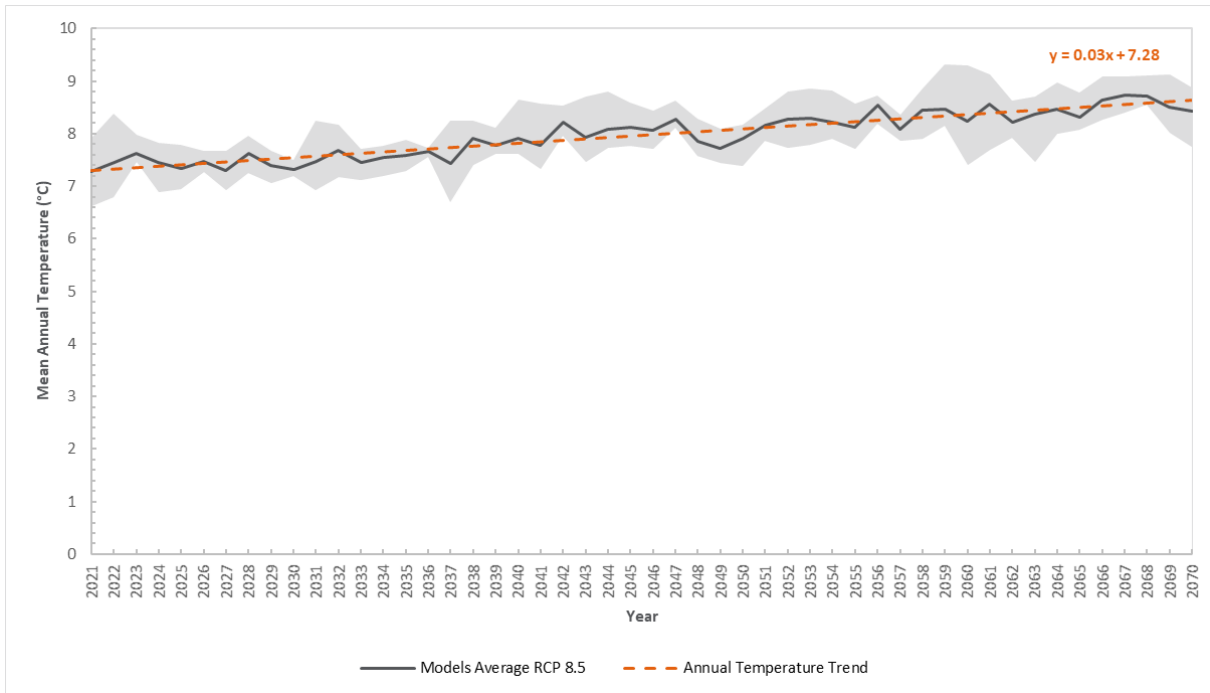


Figure 4.15: Temperature Trend at Termas del Flaco for RCP8.5



4.4.3 Projected Glacier Melting

As has already been mentioned, one of the most critical issues in the analysis of climate change in the study area is the impact that this phenomenon will have on the Universidad glacier, which covers almost 30% of the drainage basin to the intake.

According to (Cuffey & Paterson, 2010): In comparison with other types of streamflow, glacier runoff has unusual features such as large diurnal fluctuations and maximum flow during summer. Glaciers act as reservoirs that store water in solid form in cool summers and release copious amounts in hot dry summers when water from other sources is in short supply.

It is possible to see for the case of Piedras Negras HPP how this statement is fulfilled. Taking the historical results of the glacial melt obtained from the HBV model, it is possible to see that during the summer months (October - March) the glacial melting is almost 10 times the value obtained during the winter months (April - September).

It is proper to remember that the HBV does not focus on glaciers modeling but instead on the runoff of the catchment. As an example, these ice bodies can vary in size over the years, either

shrinking or growing, but for the HBV model, their physical extension is constant over time. Despite the limitations that this model has in this respect, as it was seen in Title 3.6.2, the predictions of runoff in the basin under study were reproduced in a satisfactory manner showing that the results of glacial melting are equally satisfactory.

The melting of snow and glacier within the snow routine of the HBV model is based on the temperature of the sector. This can be clearly observed in the Figure 4.16 and Figure 4.17: The first shows the exponential correlation between temperature and glacial melting and the second shows the seasonal evolution that these variables have had in the 80s, 90s and 00s decades.

Figure 4.16: Correlation Between Temperature and Glacier Melt

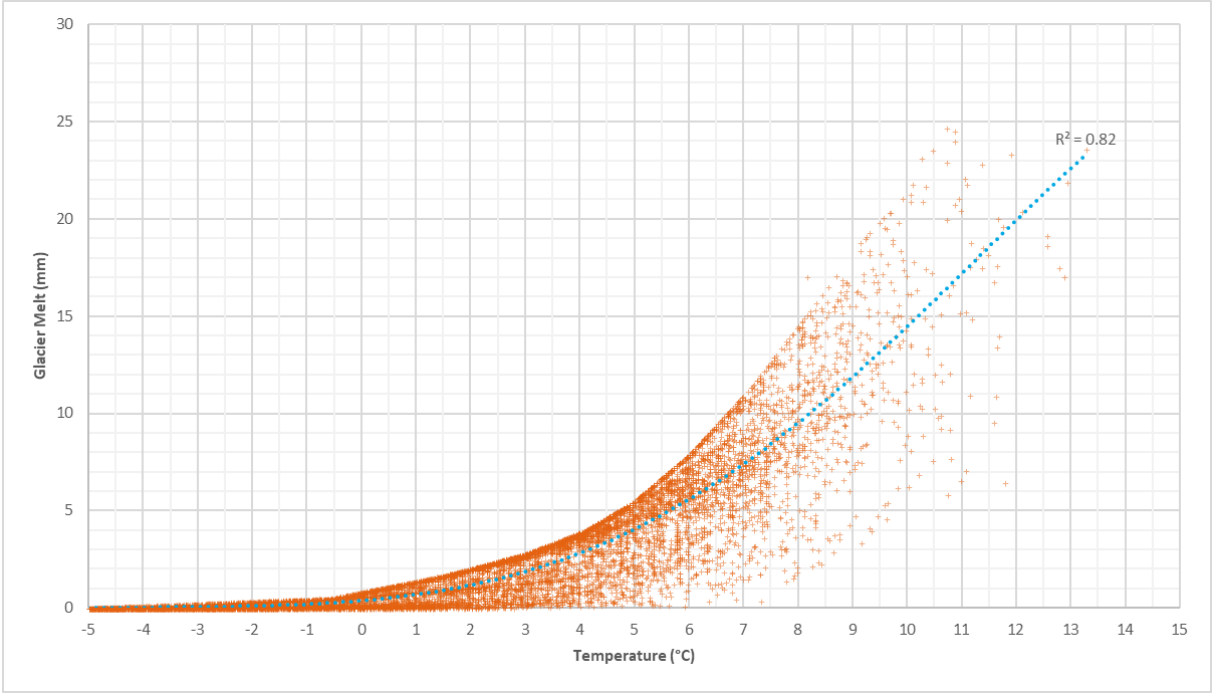
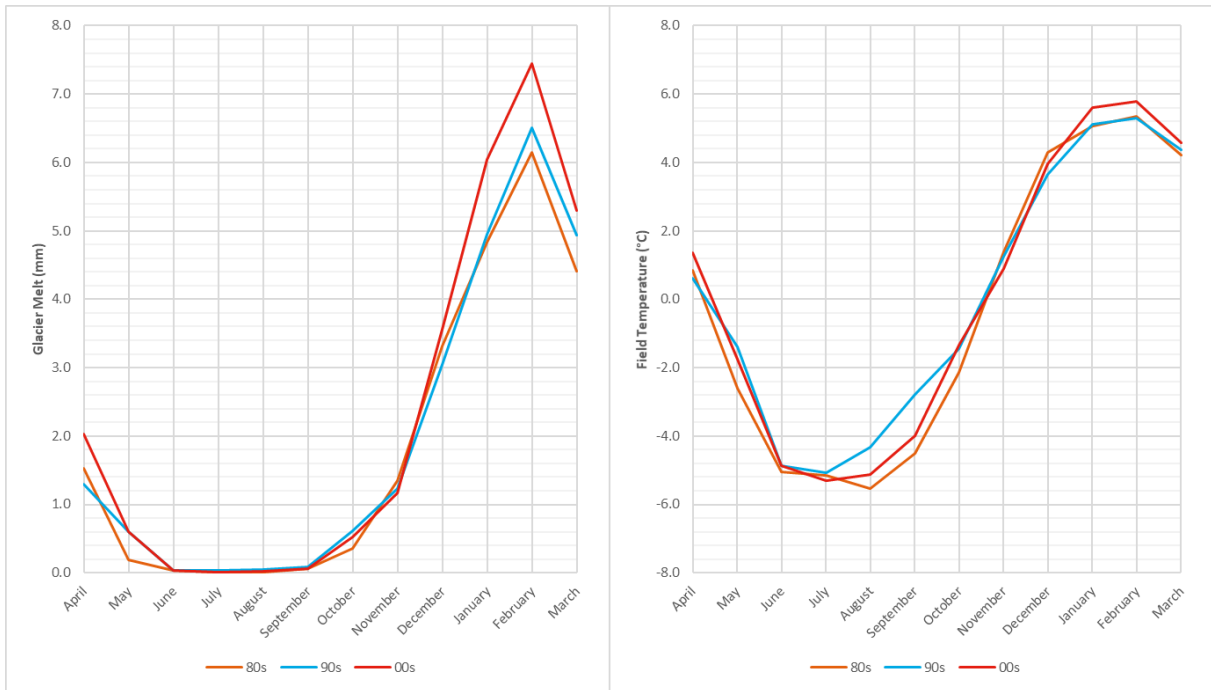


Figure 4.17: Historical Evolution of Glacier Melt and Field Temperature



Considering the studied scenarios of climate change, it is possible to predict that the glacial melt will increase with time following the trend of the temperature of the sector. This can be seen clearly in Figure 4.18 and Figure 4.19, where for RCP4.5 glacier melting increase at a rate of 206 mm/yr while for RCP8.5 this value is even higher at 396 mm/yr.

Figure 4.18: Annual Glacier Melt Trend for RCP4.5

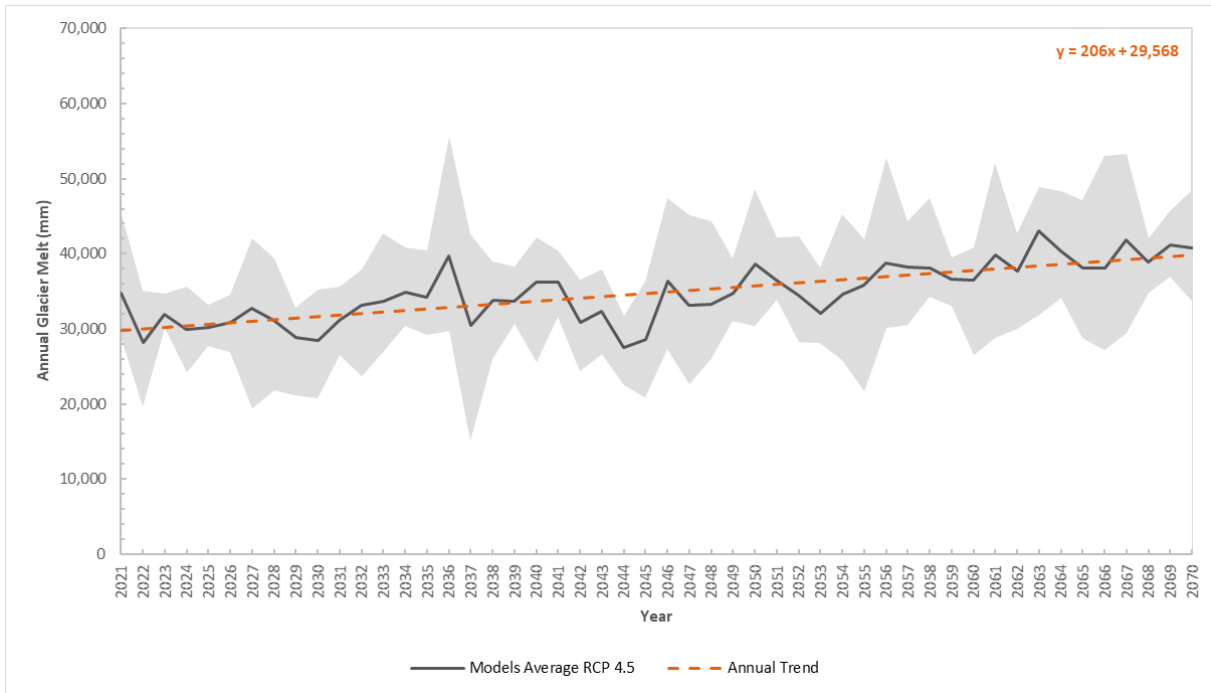
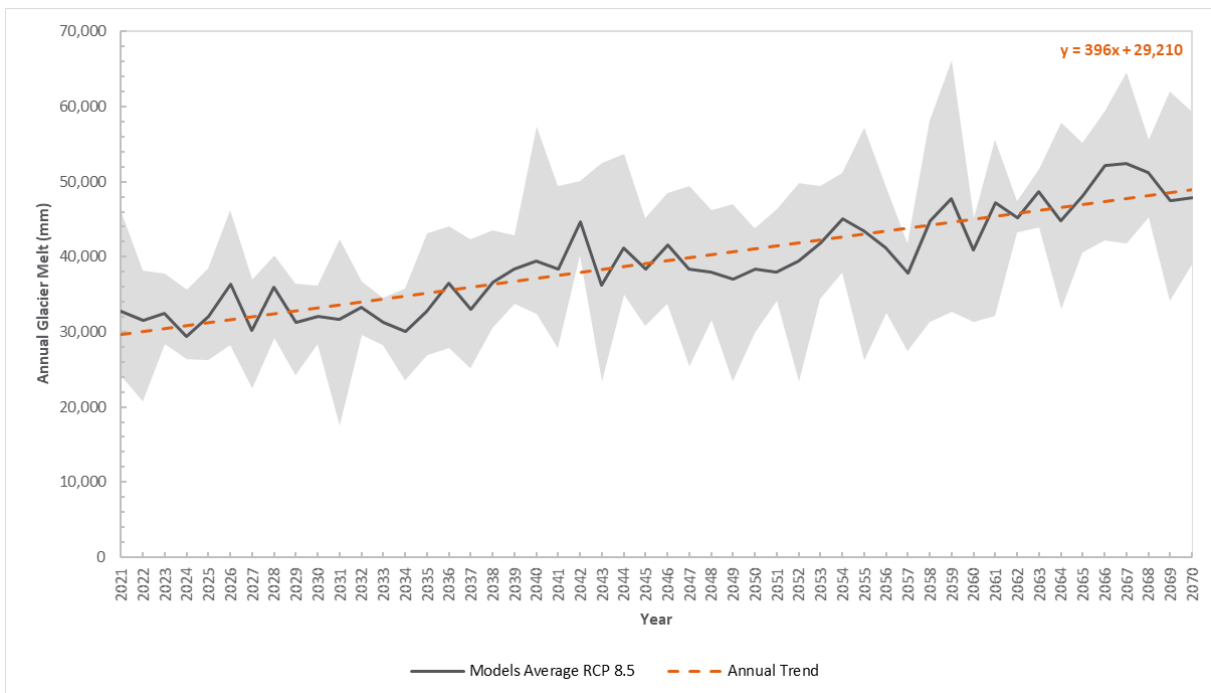


Figure 4.19: Annual Glacier Melt Trend for RCP8.5



If we compare the historical seasonal variation with the expected from the climatic change model results (Figure 4.20 and Figure 4.21), an average increase of the glacial melt of 36% is expected for RCP4.5 and 69% for RCP8.5.

Figure 4.20: Glacier Melt Seasonal Variability for RCP4.5

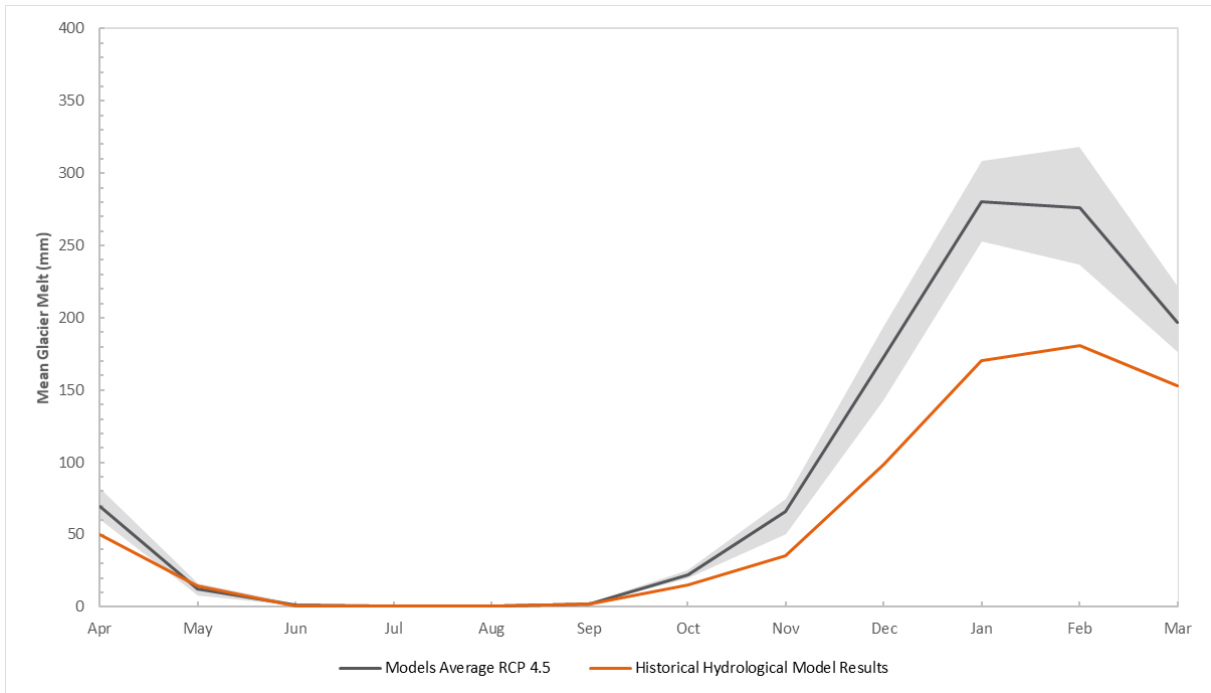
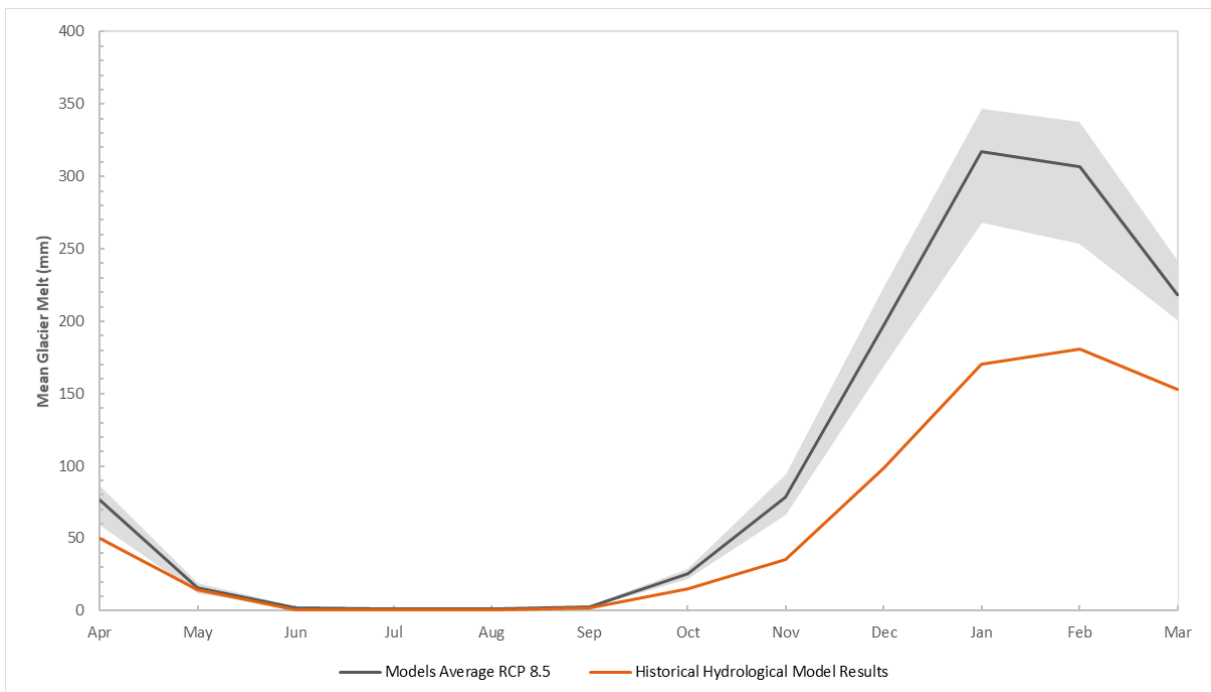


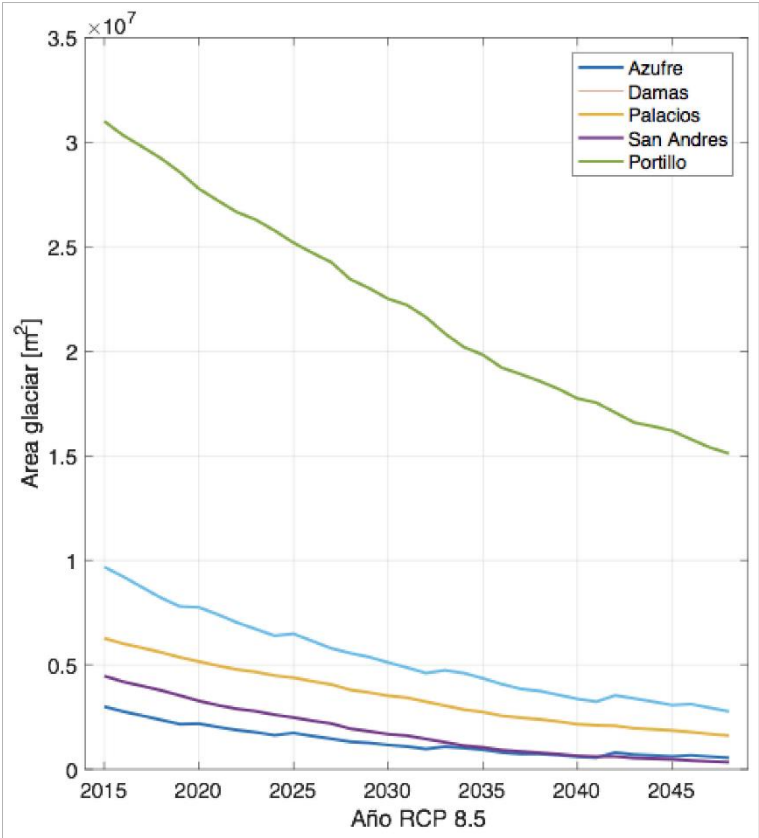
Figure 4.21: Glacier Melt Seasonal Variability for RCP8.5



With the results presented, it is possible to affirm that climate change will significantly affect the Universidad glacier, causing an appreciable increase in its rate of melting during the spring-summer season, which will potentially lead to a reduction in its size in the years come.

This last point was studied in more detail in the reference by (Cortes, McPhee, & Baldo, 2017), where the behavior of the glaciers in the nearby area was modeled, arriving at conclusions that point in the same direction and projecting glacial area losses of up to 50% compared to today situation. The evolution of the area loss for the glaciers in the sector is shown in Figure 4.22.

Figure 4.22: Change in Glacier Area Near the Project Sector for RCP8.5



Source: (Cortes et al., 2017)
 Note: Years in the horizontal axis. Glacier Area ($m^2 \cdot 10^7$) in the vertical axis.

4.4.4 Projected Intake Mean Daily Runoff Timeseries

Projecting the annual runoff volume of the San José river, for both scenarios, RCP4.5 and RCP8.5, the result shows an upward trend in the years to come, with a rate of 317 hm³/yr for

the first scenario and 580 hm³/yr for the second as shown in Figure 4.23 and Figure 4.24 respectively.

Figure 4.23: Runoff Trend at Intake for RCP4.5

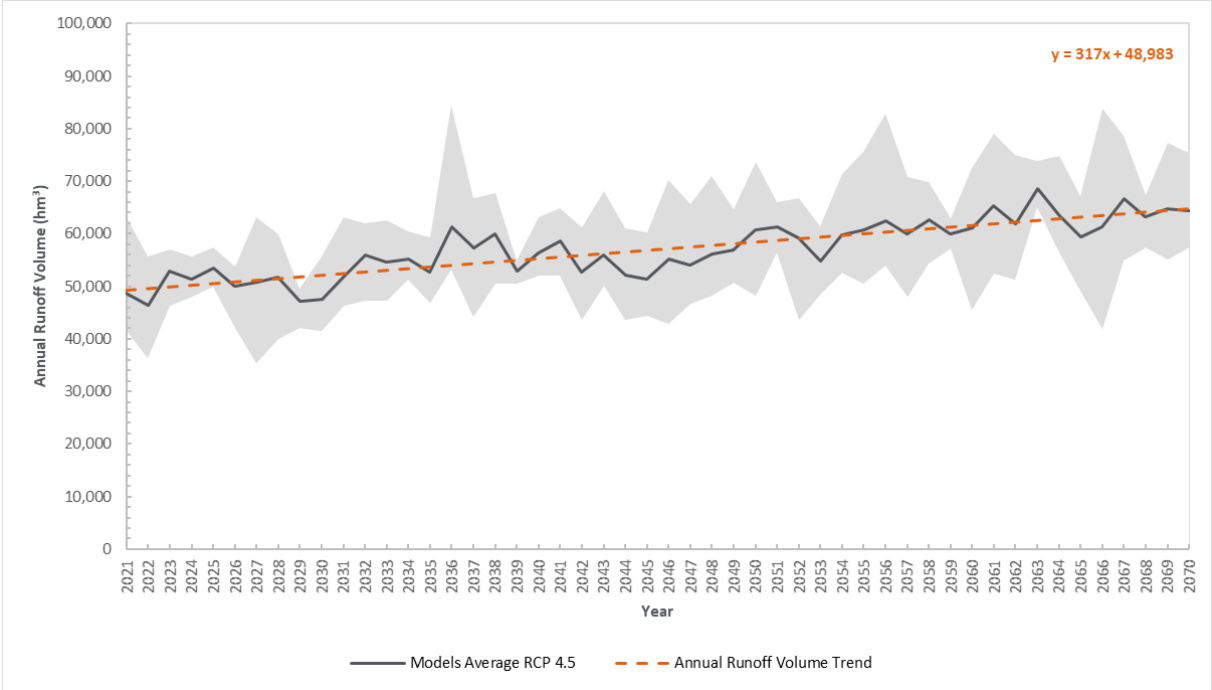


Figure 4.24: Runoff Trend at Intake for RCP8.5



Regarding seasonal variability, the increase in temperatures will cause an early arrival of the wet season, and an increase in the mean annual runoff of 25% (from 4.0 m³/s to 5.0 m³/s) for RCP4.5 and 38% (from 4.0 m³/s to 5.5 m³/s) for RCP8.5 as shown in Figure 4.25 and Figure 4.26 respectively.

Figure 4.25: Runoff Seasonal Variability at Intake for RCP4.5

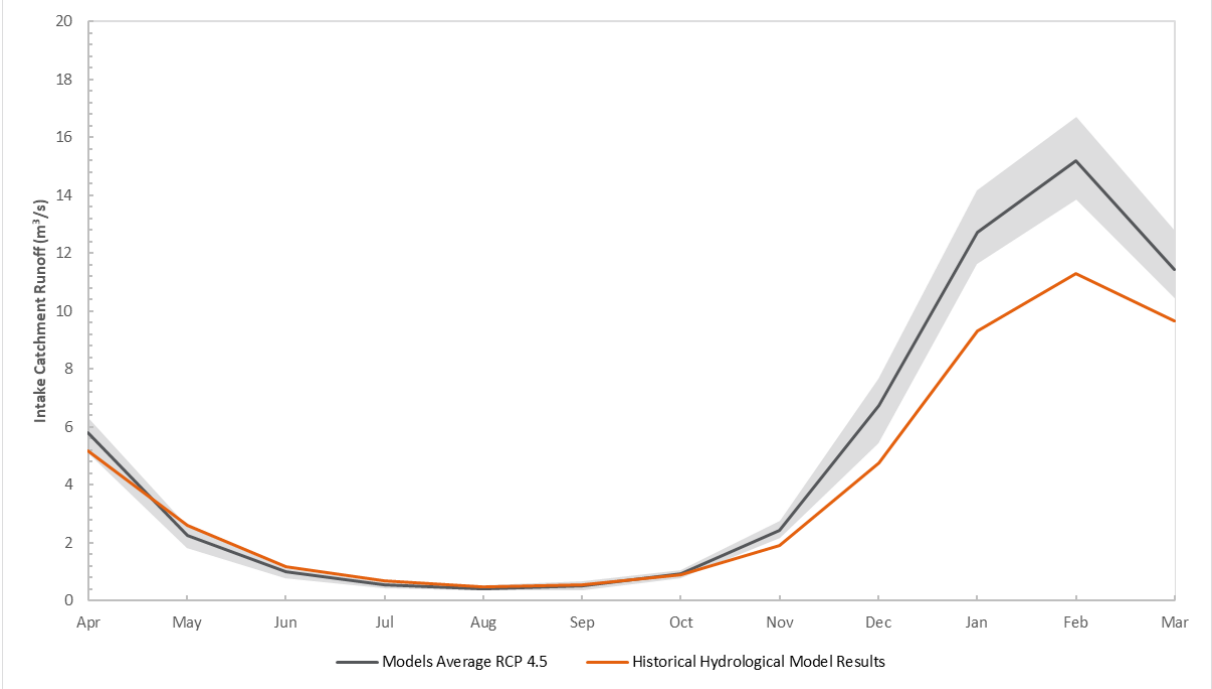
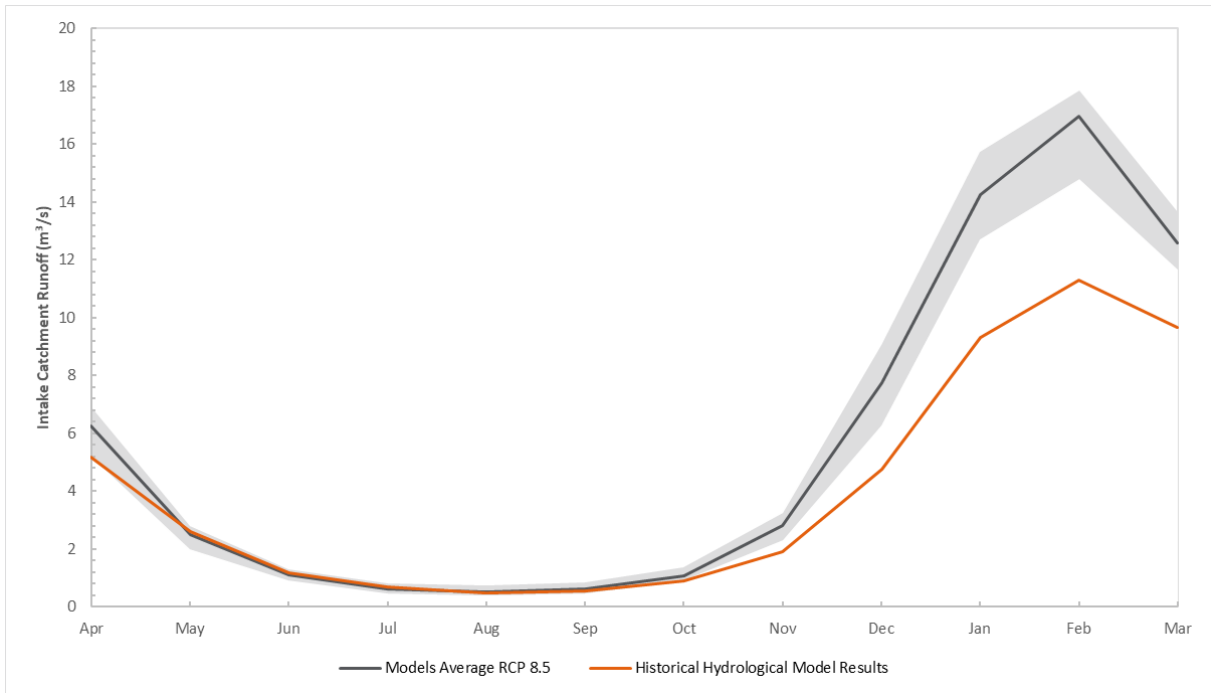


Figure 4.26: Runoff Seasonal Variability at Intake for RCP8.5



As mentioned in Title 4.4.3, the early melting of both the snow and glacier area, along with an increase in the frequency of liquid precipitation due to the rise in temperatures, will cause a greater area of the basin to be saturated and exposed to said precipitation, which foresees that flood events increase in magnitude as the durations curves in Figure 4.27 and Figure 4.28 shows.

Figure 4.27: Duration Curve at Intake for RCP4.5

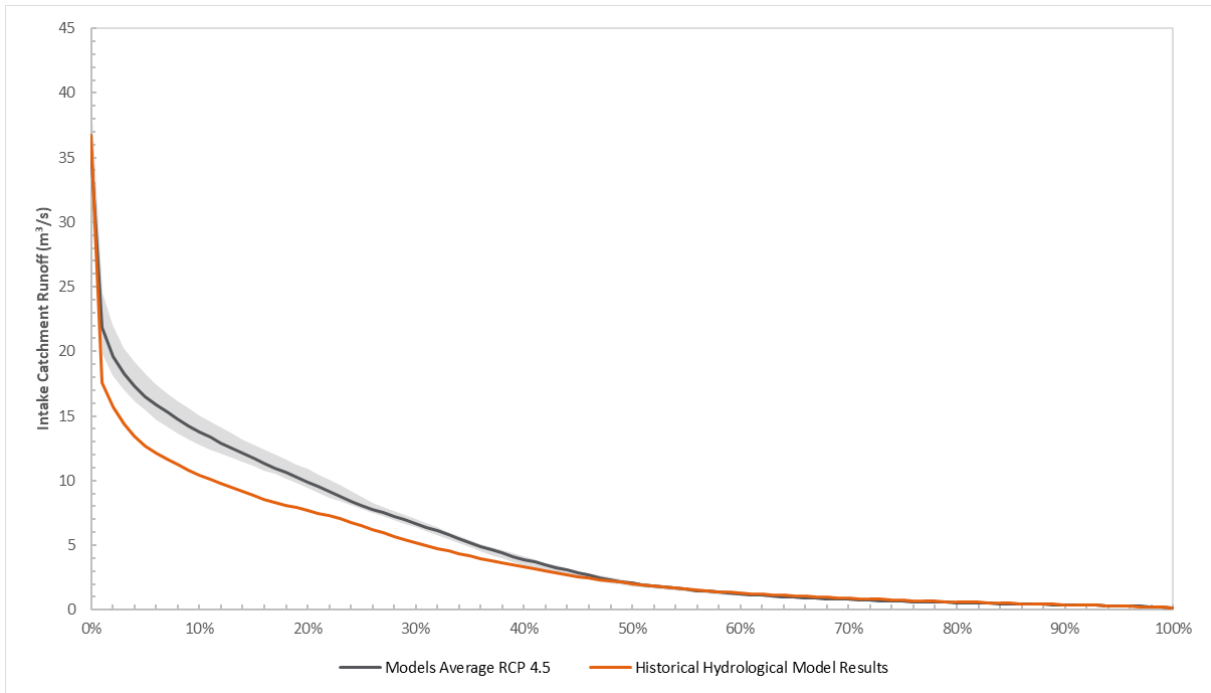
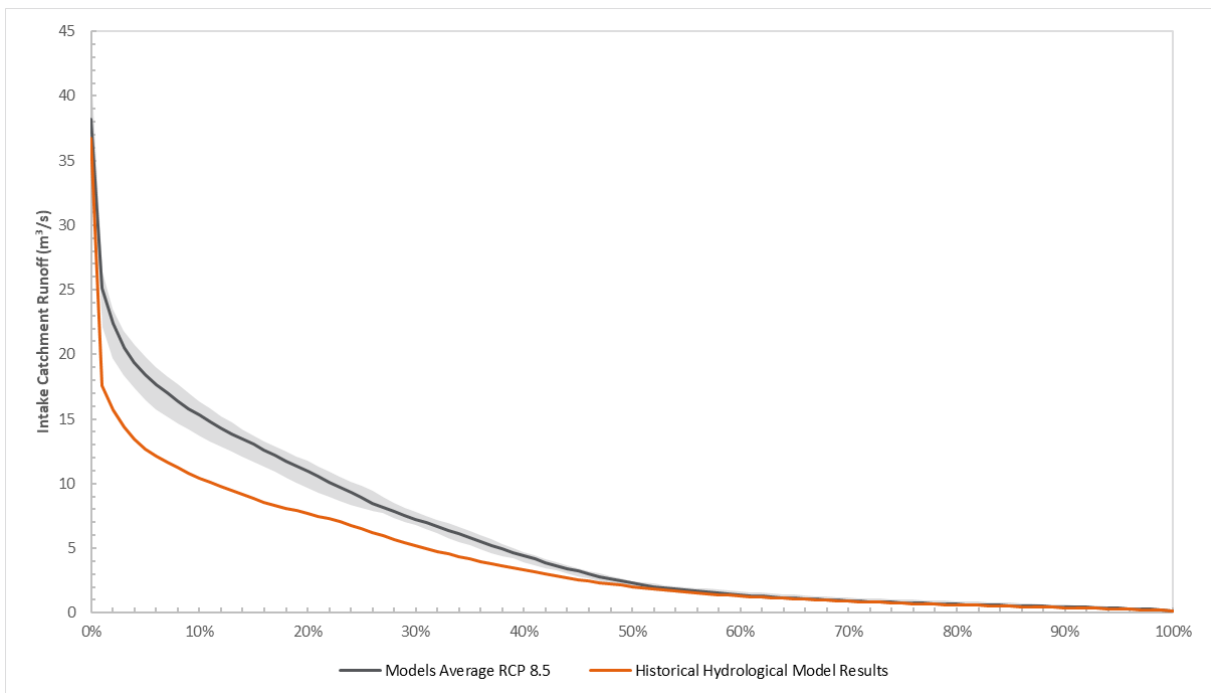


Figure 4.28: Duration Curve at Intake for RCP8.5



The projected runoff data with climate change is included in Appendix VI.

5 Power Plant Design

Once the entire hydrological base of the project was analyzed, the hydroelectric power plant was designed as such. It should be remembered that until now only the location of the intake has been defined, but not the powerhouse, a topic that will be resolved next.

5.1 Powerhouse Location

As mentioned in the Intake Location chapter (Title 3.1), in Chile both the point of intake and restitution (powerhouse) are tentatively defined at the time of requesting the water right to the DGA

Initially, the coordinates contained in the water rights belonging to Anpac Energía (owners of the Piedras Negras HPP) were considered upstream and downstream limits of the project as shown in Figure 2.3. Recalling that from these points the DGA allows a location *error threshold* of 100 m to 150 m around it, in the case of the powerhouse, it was considered in principle to locate it at the downstream end of this *error threshold*, as shown in the Figure 5.1, to make the most of the gross head that the topography offers.

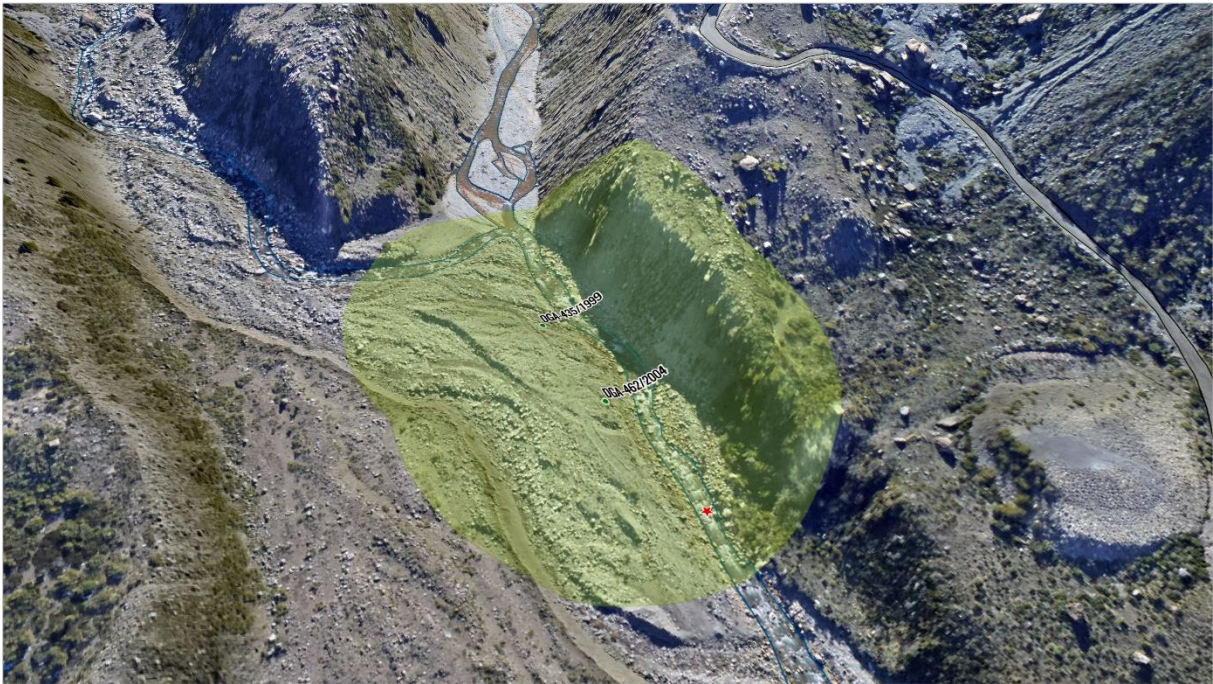
Figure 5.1: Initial Location of Restitution Point



Looking at Figure 5.1, especially focusing in the green *error threshold* area, it was decided that this sector was not suitable for locating the powerhouse since it potentially exposed this structure to the flood flows from Portillo river, whose alignment at the confluence points directly to the left bank of the San José river, where the powerhouse should be located.

Another aspect that made this sector to be considered not suitable is the local topography. As mentioned, due to the characteristics of the place and its accessibility, the left bank of the San José river was considered to locate the powerhouse, however, this sector has pronounced slopes of loose material, which during the site visit were considered unstable to any intervention, potentially increasing the risk and the cost of constructing this structure in said place. To illustrate this point, a perspective from the downstream end of the commented sector can be seen in Figure 5.2.

Figure 5.2: Perspective of Initial Location of Restitution Point



In this sense, the decision was taken to find another location for the powerhouse that would give security to the infrastructure, easy access, and low constructive complexity. It should be mentioned that changing the restitution point established in the water rights also translates into the modification of this legal document issued by the DGA. One of the fundamental aspects that this government bureau evaluates when granting a water right is that there are no conflicts with third parties, for this reason, it is discarded to move the restitution point downstream since this type of conflict could arise causing the rejection of this request.

Moving the restitution point upstream reduces the hydropower plant gross head and therefore its energy production capacity. To evaluate this impact, Figure 5.3 shows the percentage variation of the gross head along the river alignment considering the total gross head to the initial restitution point.

Figure 5.3: Percentage of Gross Head Variation Along the River Alignment



Approximately 850 m upstream of the sector originally chosen, there is an alluvial esplanade with scarce vegetation on the left bank of the river and that has the right conditions to establish the powerhouse. Figure 5.3 shows that in this sector approximately 9% of the original gross head is lost, which is 30 m of difference in elevation, however, this sector significantly reduces the risk to which the structure will be subjected, and since it is an esplanade, it will also reduce the constructive complexity as well as the costs derived from cutting the topography. Another point to evaluate this location is the proximity to the power line coming from the San Andrés HPP (Figure 2.2), which would ease the connection of the power plant to the electrical grid.

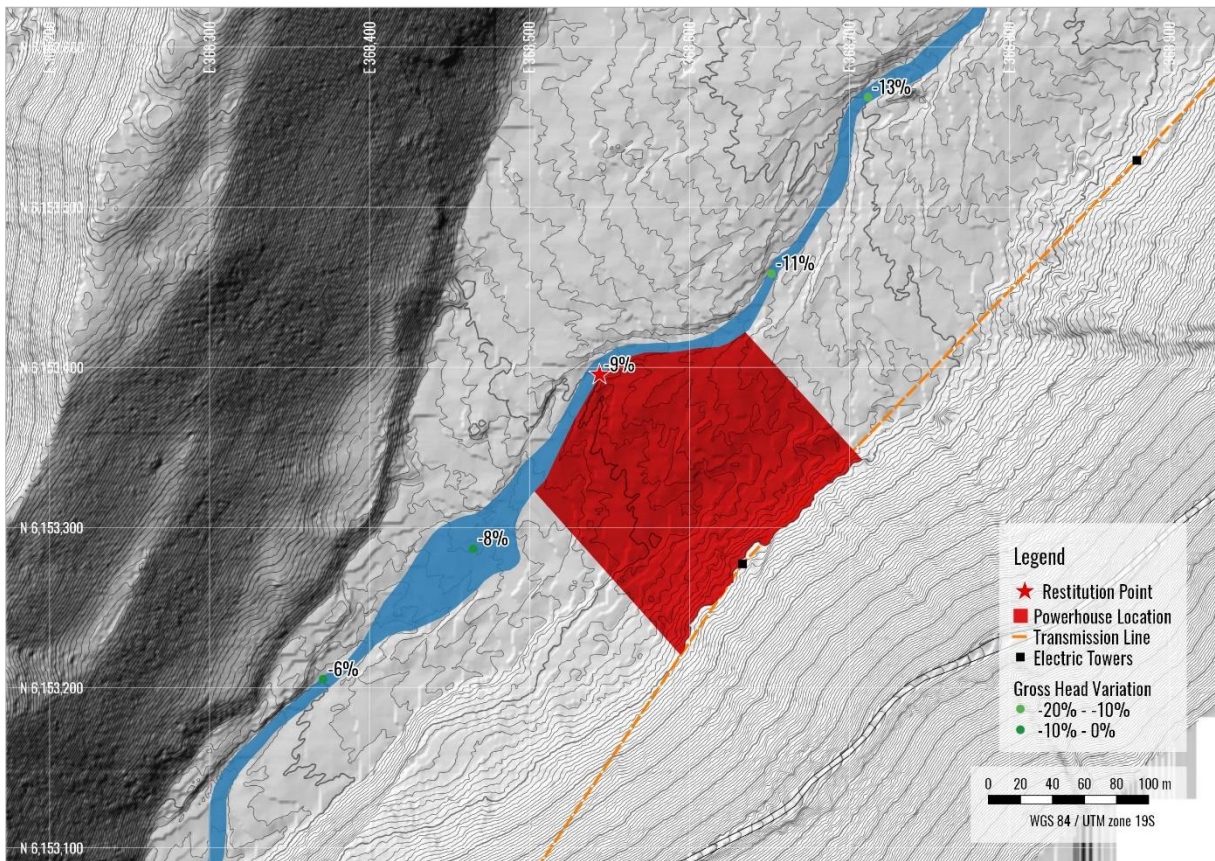
The final coordinates of the restitution point are included in Table 5.1 and its location along with the powerhouse sector is shown in Figure 5.4.

Table 5.1: Restitution Location Coordinates

| | N (m) | E (m) | Elevation (masl) |
|----------------------|--------------|--------------|-------------------------|
| Restitution Location | 6,153,395 | 368,544 | 1,530 |

Datum: WGS 84 / UTM zone 19S

Figure 5.4: Restitution Point and Powerhouse Location



As a reference, a panoramic picture of the selected powerhouse location is shown in Figure 5.5. The picture was taken in January 2018 from the road found on the left side of the river.

Figure 5.5: Panoramic View of the Powerhouse Location



Note: The river flows from the right end to the left end of the picture.

5.2 Hydraulic Study of San José River

As mentioned in Title 3.7, with the objective of establishing a safety boundary around the river to locate main works of the Piedras Negras HPP (i.e.: Powerhouse, penstock, etc.), a one-dimensional hydraulic simulation of the flooding behavior of the San José river was carried out using the HEC-RAS 5.0.3 model.

One-dimensional hydraulic models calculate the flow characteristics by calculating an energy balance between adjacent cross-sections. According to (USACE, 2016) and (Goodell, 2012), the cross sections must meet four fundamental requirements:

1. Its alignment must be perpendicular to the expected flow lines.
2. They should not intersect each other.
3. They should extend across the entire floodplain.
4. They should be drawn looking in the downstream direction.

In this sense, and with the aim of reducing as much as possible the inaccuracies of the results, two hydraulic models were carried out:

- The first covers the entire San José river, starting approximately 100 m upstream of the intake and ending 650 m downstream of the powerhouse sector. It has a total of 57 cross-sections located every 100 m along the center line of the river. The location and identification of the cross-section are shown in Figure 5.6.
- The second focuses on the powerhouse sector and the esplanade where it will be found. The first section is located 650 m downstream of the restitution point and the last section is 850 m upstream from this point. A total of 61 sections were considered located every 25 m along the center line of the river. The location and identification of the cross-section are shown in Figure 5.7.

Figure 5.6: San José River Hydraulic Model Cross-Sections

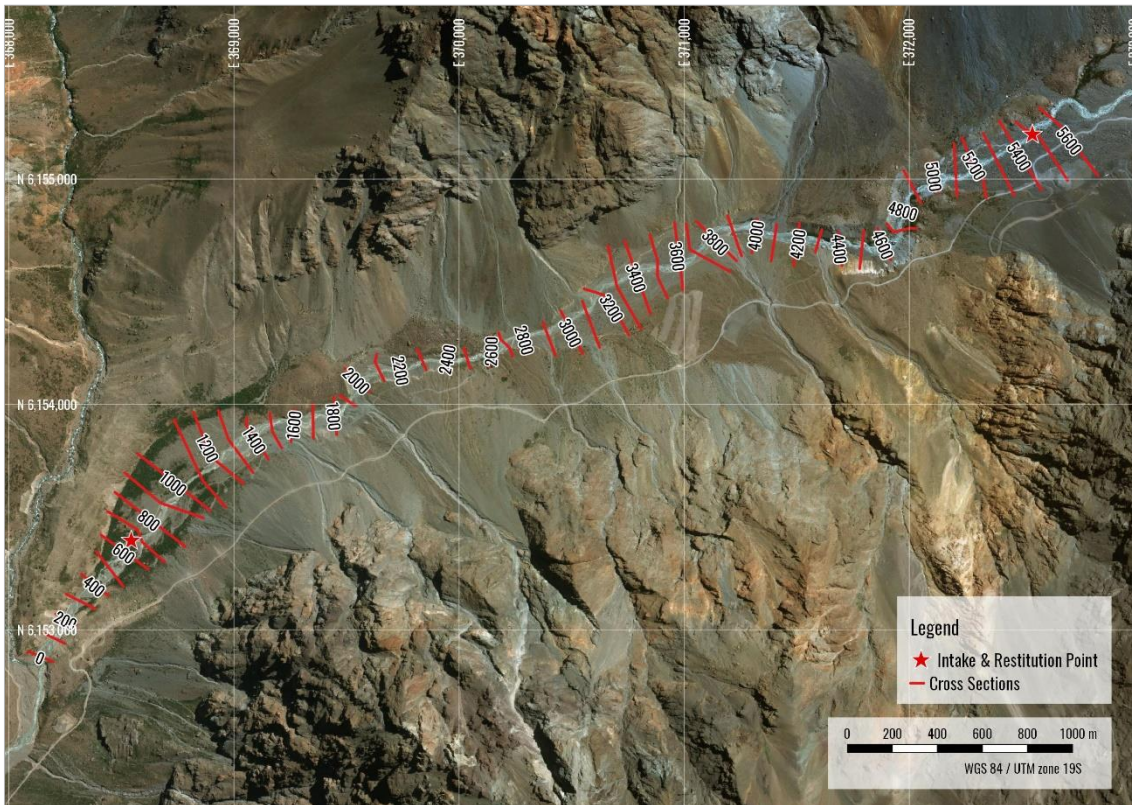
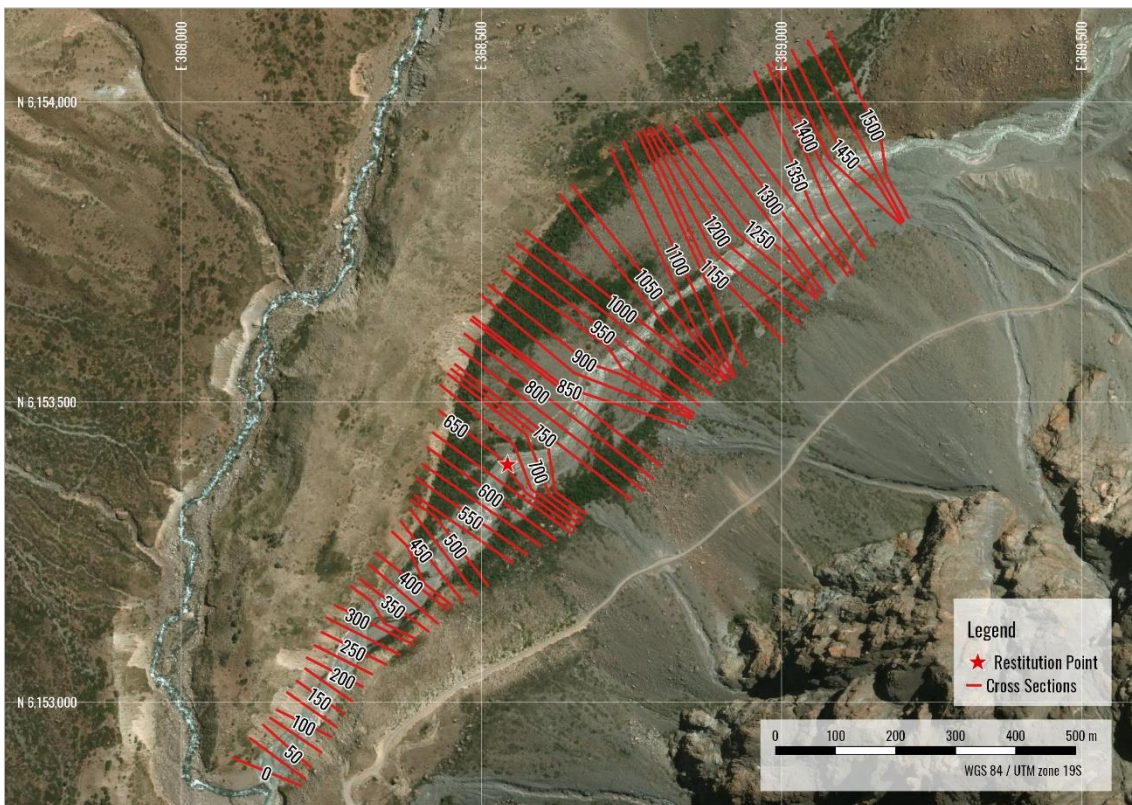


Figure 5.7: Powerhouse Sector Hydraulic Model Cross-Sections



The topographic information used to draw the cross-sections comes from a LIDAR (Laser Imaging, Detection and Ranging) survey with contour lines every 1 m, from which a DTM (Digital Terrain Model) was generated in QGIS. It is important to note that the survey did not include a bathymetry of the river bed.

The Manning roughness coefficients for the main river channel and the floodplains were assigned according to the characteristics seen in the terrain and through the descriptions of (Chow, 1959), resulting:

- Main Channel: $n = 0.040$ - Mountain streams, no vegetation in the channel, banks usually steep, trees and brush along banks submerged at high stages with a bottom of gravels, cobbles, and few boulders.
- Floodplains: $n = 0.080$ - Mean value between the high value of mountain streams, no vegetation in the channel, banks usually steep, trees and brush along banks submerged at high stages with a and normal value of floodplain with medium to dense brush, in summer.

As a reference, Figure 5.8 and Figure 5.9 shows the characteristics of the main channel and the floodplains.

Figure 5.8: San José River and Floodplains Characteristics at Intake Sector



Figure 5.9: San José River and Floodplains Characteristics at Powerhouse Sector



The flood discharges considered for both models are those included in Table 3.18.

With these parameters, the flood footprints for the average flow and the floods of 5, 100 and 200 years of return period are shown in Figure 5.10 and Figure 5.11 for the entire river and the powerhouse sector respectively.

Figure 5.10: San José River Flood Footprint Results

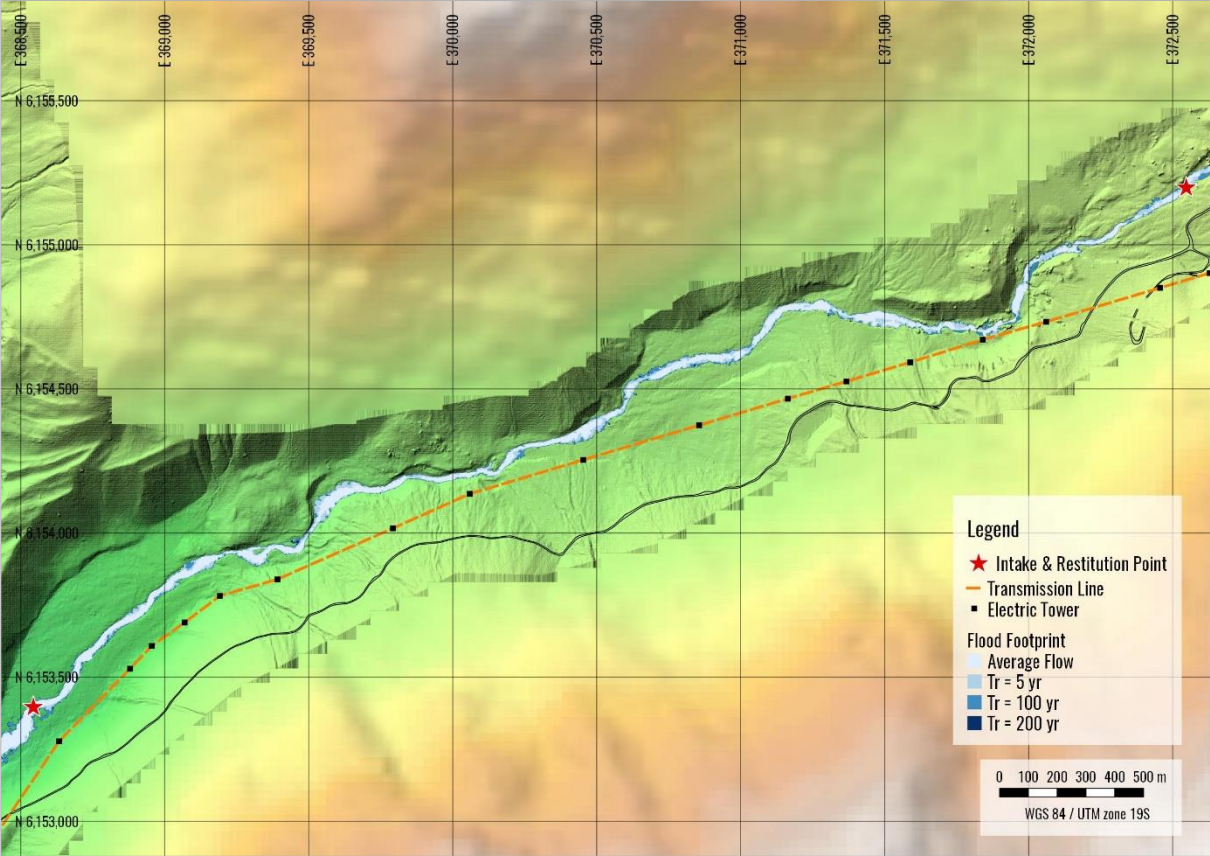
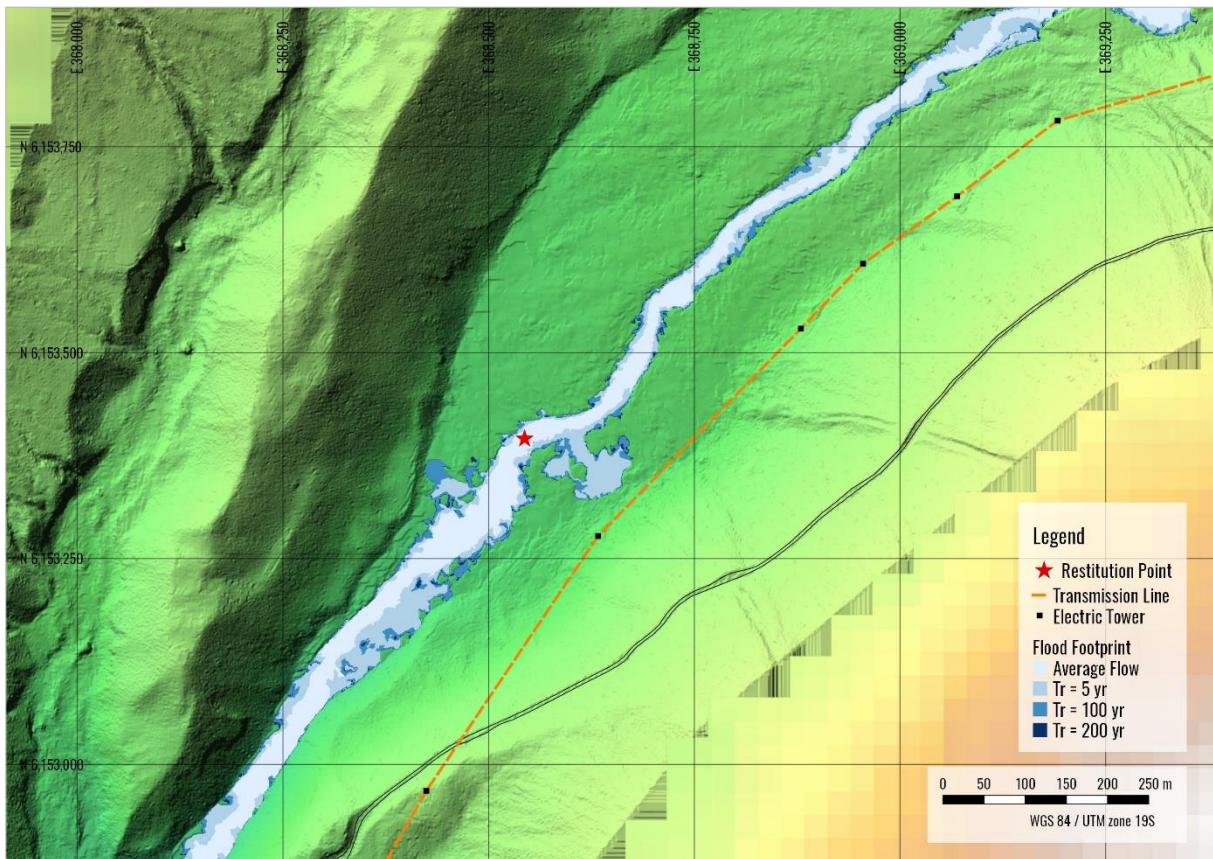


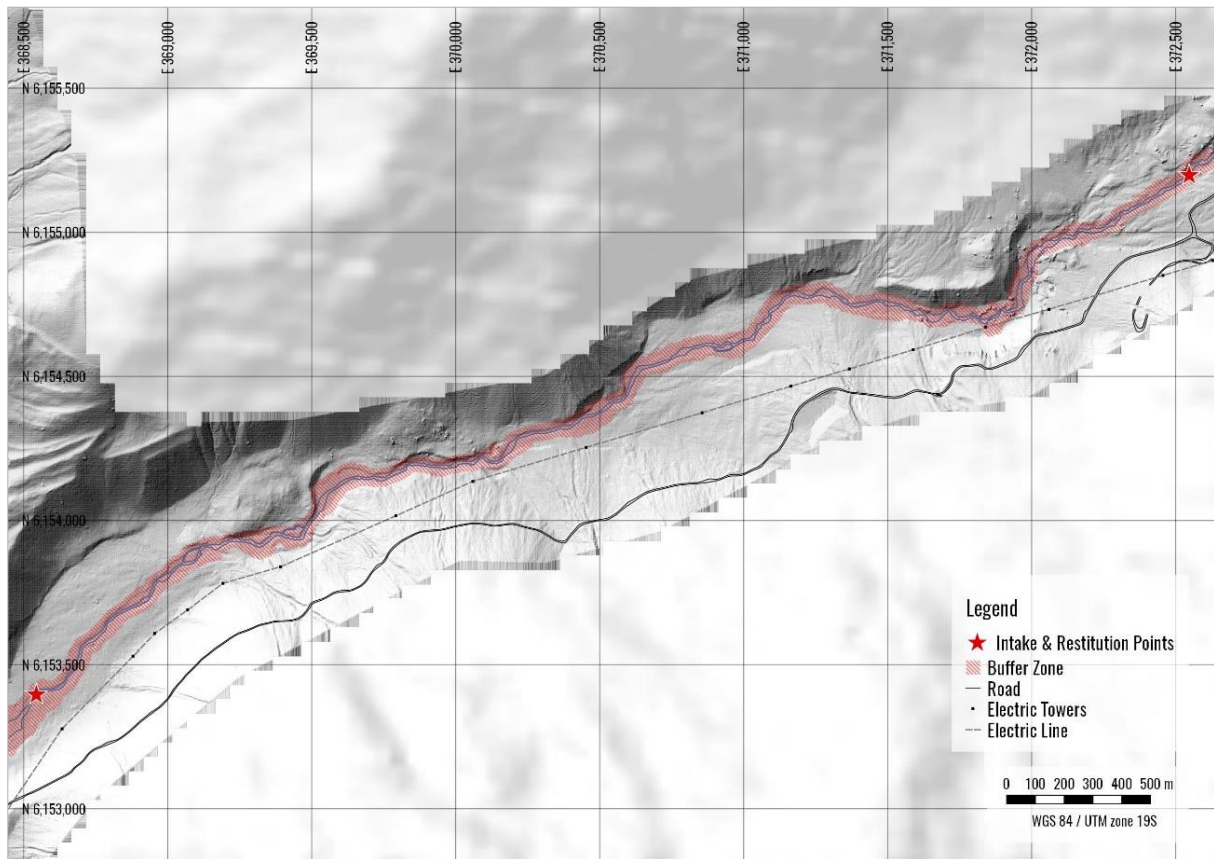
Figure 5.11: Powerhouse Sector Flood Footprint Results



It is noticeable the Figure 5.11 that the sector considered to establish the powerhouse is prone to flooding from a flood with a 5 of return period. Nevertheless, a small depression on the topography caused said overflow. This is considered easily solved by the protection works that the powerhouse should consider during its design and construction, which is why the selected location is kept as definitive.

As mentioned, part of the goal of this hydraulic analysis was to generate a safety boundary around the river outside of which it is considered safe to allocate any type of conveyance structure for the power plant. In this sense, the external limit of the footprint for the 100 years return period flood event was considered and added a safety distance of 20 m. The resulting buffer zone is shown in Figure 5.12.

Figure 5.12: San José River Buffer Zone



The hydraulic results tables are included in Appendix VII.

5.3 Landslide Risk

As part of the risk analysis carried out, it was analyzed which areas of the sector under study show the greatest risk of landslide.

To evaluate this, first the largest extension of the DTM with a spatial resolution of 1 m generated from the LIDAR topography was used, this DTM covers a strip of approximately 330 m around the San José river in its entire length. For the rest of the study area, the DTM from the ASTER GDEM program with a cell resolution of 30 m was considered.

The risk assessment was carried out considering two fundamental factors: Soil as the superficial material and a terrain slope equal to or greater to the internal friction angle of the said soil material.

The angle of internal friction was obtained from the geological and geotechnical reports made by the company Xoren Earth (Xoren Earth, 2018b, 2018a). In said reports, the results of a geological mapping and laboratory analysis of several trial pits in the sector are presented. A summary of the recommended values of the internal friction angle of the materials in the area is included in Table 5.2.

Table 5.2: Internal Friction Angle for the Project Area Geotechnical Units

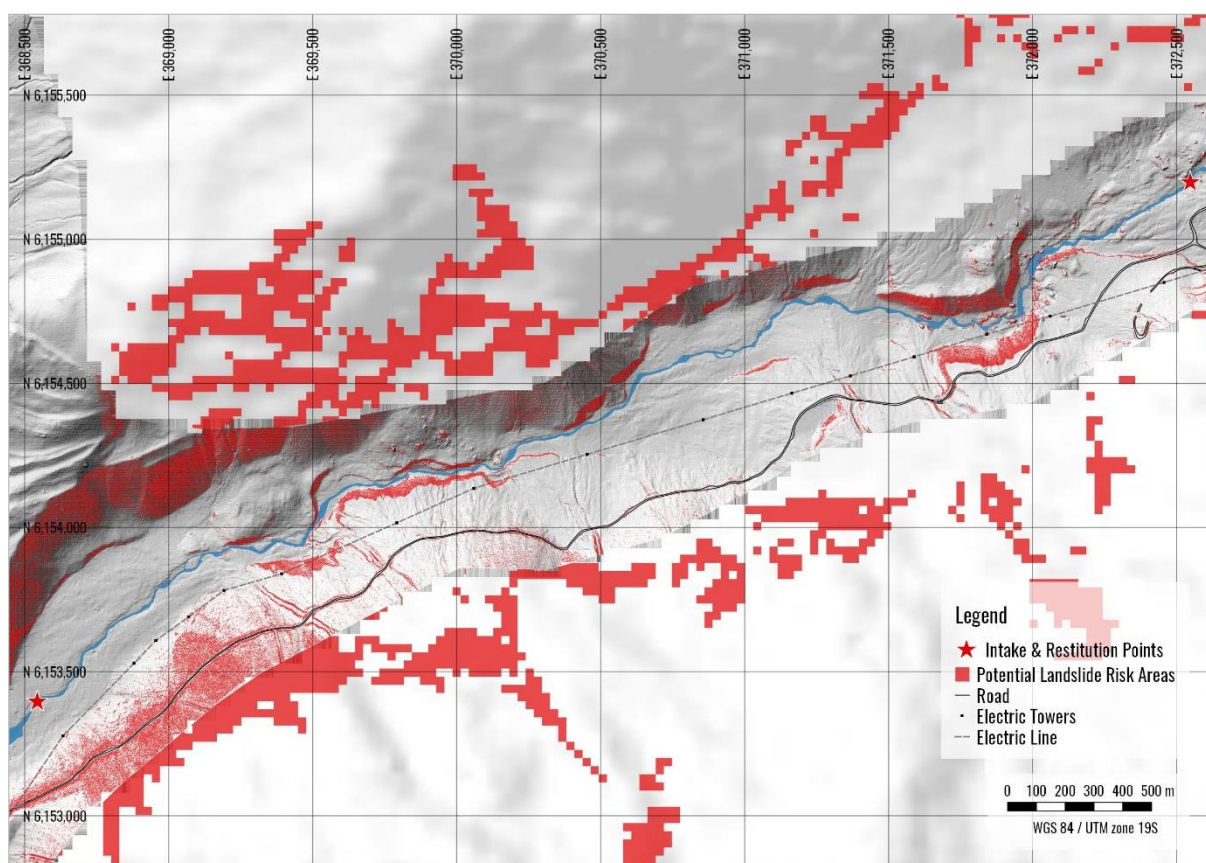
| Geotechnical Unit | Internal Friction Angle (°) |
|--------------------------|------------------------------------|
| Fluvial Deposits | 34 – 39 |
| Fluvioglacial Deposits | 30 – 33 |
| Alluvial Deposits | 34 – 39 |
| Colluvial Deposits | 34 – 39 |
| Moraine Deposits | 32 – 35 |

Source: (Xoren Earth, 2018b)

Looking at the values in Table 5.2, for this risk assessment analyze, a mean value of 34° was considered for the internal friction angle.

Using satellite imagery to delineate the terrain soil cover, Figure 5.13 shows in red the areas where the terrain slope is equal to or larger than 34°, implying there is a potential risk of landslide occurrence.

Figure 5.13: Potential Landslide Areas



Looking at the intake and powerhouse sectors, there is no potential risk of landslides in the vicinity.

A potentially unstable area next to the access road to San Andrés HPP is seen approximately 850 m downstream of the intake point. In this sector it is perceived how the river changes its direction towards the south, undermining what would originally be its left bank, causing the potentially unstable slope. A satellite image and a panoramic view taken on the upstream end of this of this eroded bank can be seen in Figure 5.14 and Figure 5.15 respectively.

Figure 5.14: Satellite Image of Potentially Unstable Slope in the Left Bank of San José River



Note: The river flows from the right end to the left end of the picture.

Figure 5.15: Potentially Unstable Slope in the Left Bank of San José River Panoramic



Note: The river flows from the right end to the left end of the picture.

After visiting the site and looking at this specific place, it was decided that any intervention to this slope will increase the potential risk of landslide. To avoid this, it was considered passing through this sector by its base or through the ridge.

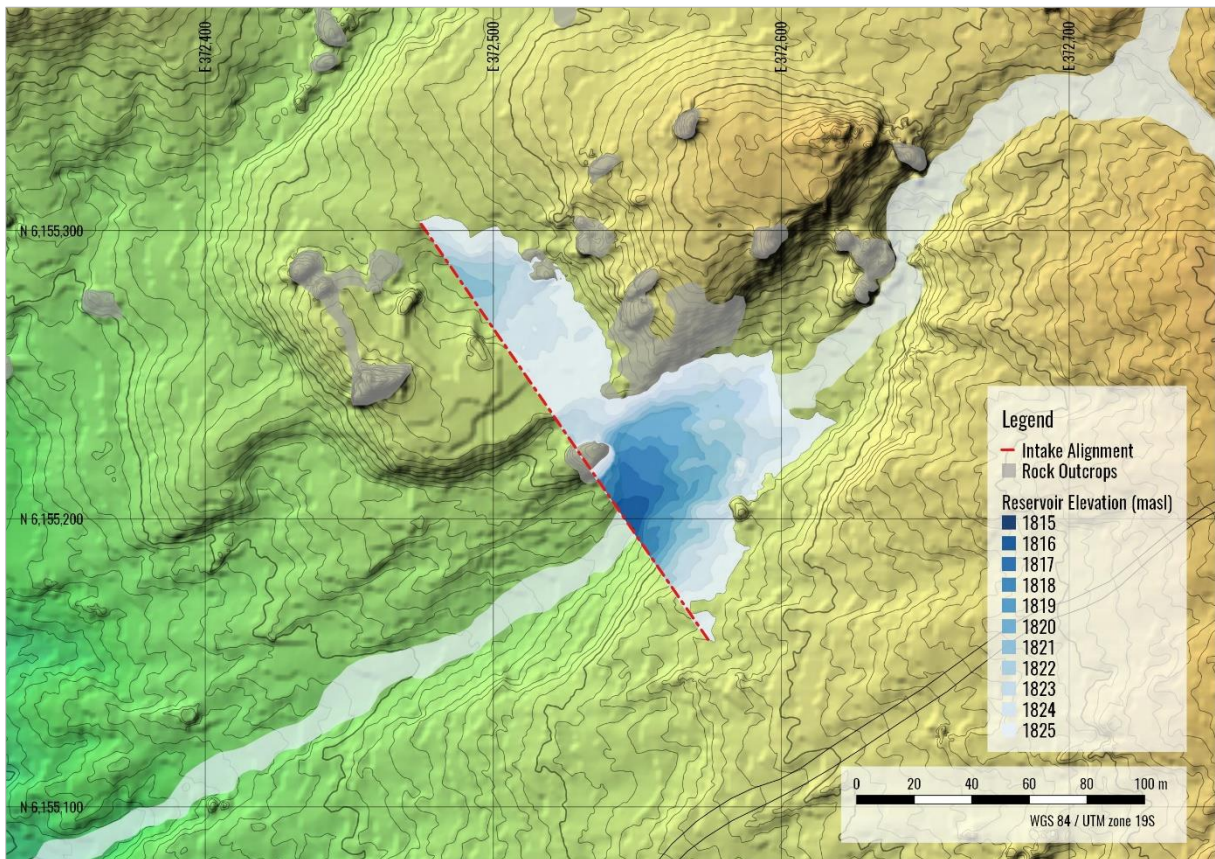
5.4 Intake Analysis

In addition to defining its location as described in Title 3.1, one of the first analyzes made to the intake sector was to evaluate the feasibility of building a medium-size dam which would fulfill three main functions:

- Create a regulated reservoir volume that allows hydropeaking and the production of firm power.
- Use this reservoir as a primary sediment trap.
- Grant submergence to the headrace conduit without the need of building a structure for this sole purpose.

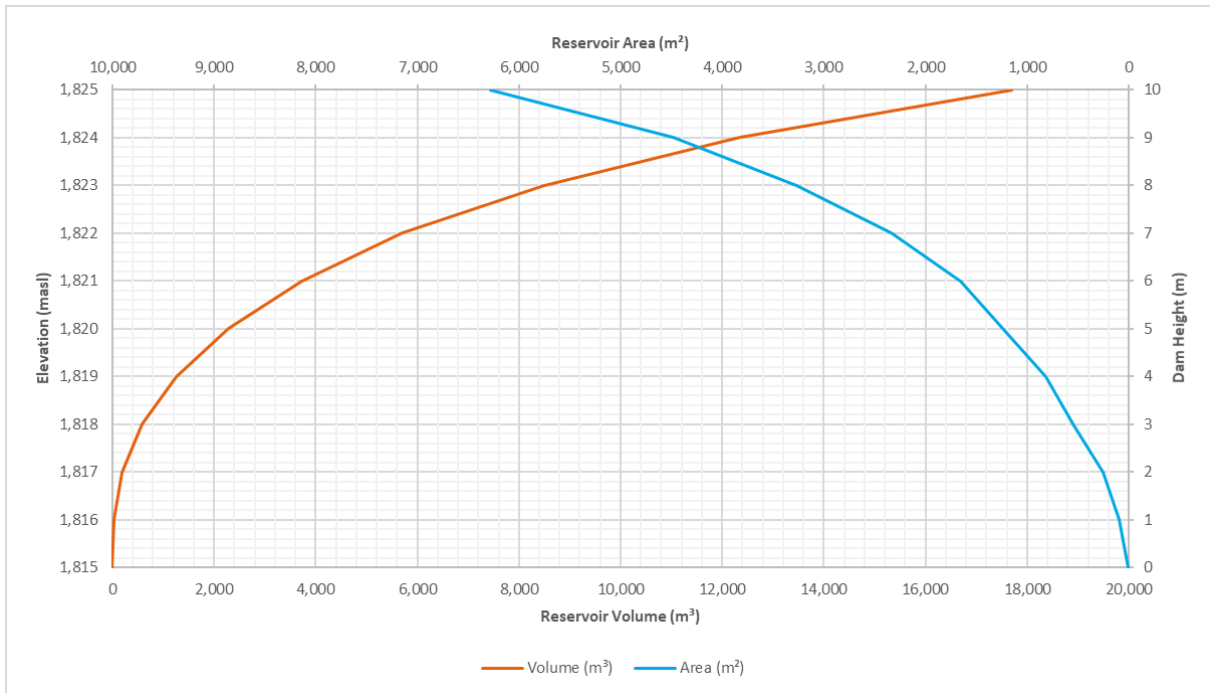
To evaluate this possibility, an alignment of what would be the dam axis was first defined, which takes advantage of rock outcrops present in the sector. Considering a 10 m high dam, Figure 5.16 shows a plan view of the alignment and the resulting reservoir.

Figure 5.16: Intake Reservoir for a 10 m Dam



When looking at Figure 5.16, and despite having a relatively high dam, the first impression it gives is that the reservoir is not large enough to achieve the expected functions. This is confirmed when looking at the area-capacity curve of the reservoir, shown in Figure 5.17, on which the gross storage volume resulted in 17.7 thousand m^3 .

Figure 5.17: Area-Capacity Curve for 10 m Intake Dam Reservoir



Observing Figure 5.18, where the dam sector is shown from the downstream side, the first thing that jumps into sight is the large amount and size of the sediment in the area. This suggests after a flood event, the gross volume of storage of the reservoir would be filled by this material, entailing a high maintenance cost of the reservoir and its impracticality to regulate flows.

Figure 5.18: Panoramic View of the Intake Sector



Note: As a reference, the intake alignment passes through the rock in the center towards the right end of the picture. The river flows from the right end to the left end of the picture.

It is for these reasons that the construction of a dam to create a regulation reservoir for Piedras Negras HPP was discarded. Instead, a typical for run-of-the-river power plant intake scheme, with a low diversion dam and a lateral intake structure was considered for further analysis and for CAPEX (Capital Expenditure) purposes.

5.5 Sediment and Settling Basin

From the beginning of this document it has been emphasized that one of the biggest challenges of this project is the sediments and its management, basically because of the characteristics of the project site, which due to its geographical and elevated location shows arid characteristics and the absence of vegetation that gives protection against soil erosion from precipitation or melting events.

An example of this is the considerable number of alluvial fans and loose material that can be seen both in the satellite image shown in Figure 5.19 and in Figure 5.20 that shows a panoramic view of the upstream sector from the intake point.

Figure 5.19: Example of the Arid Terrain Upstream of the Intake Point

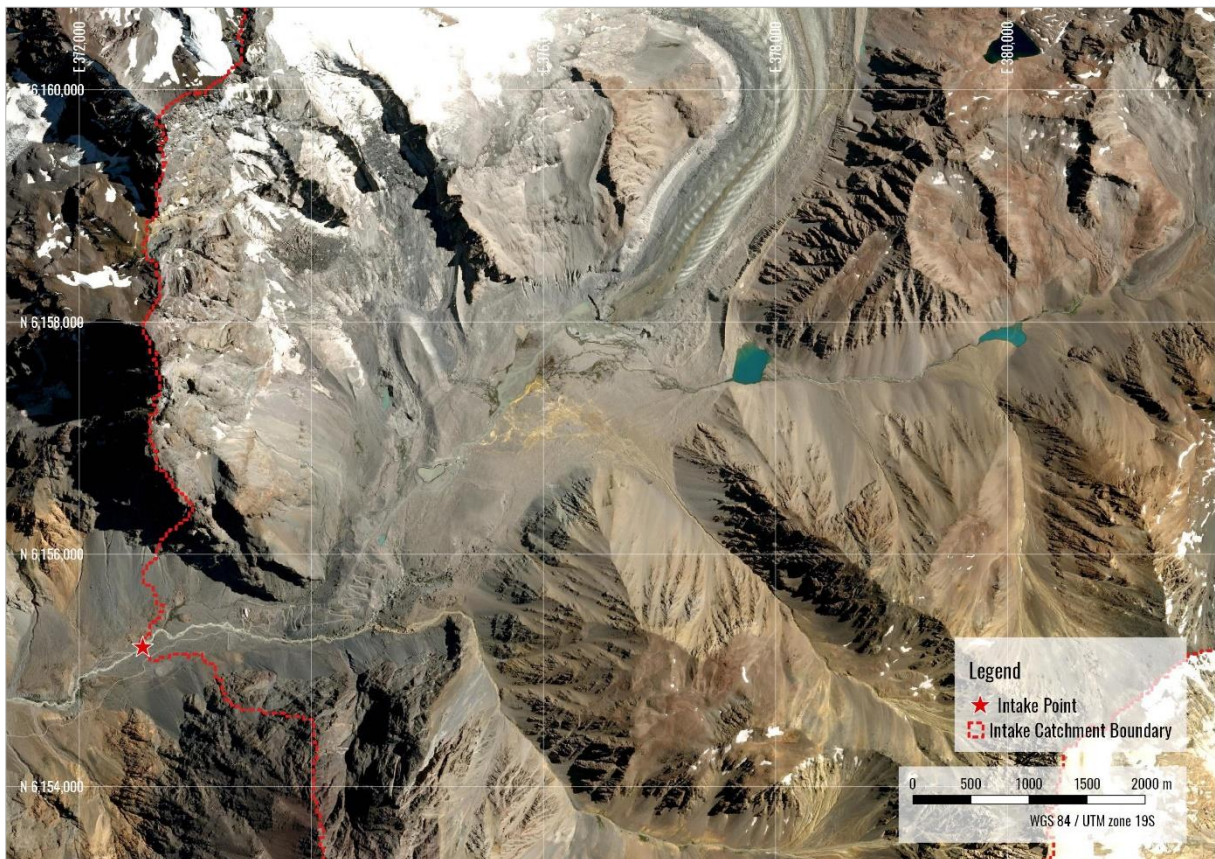


Figure 5.20: Landscape Upstream of the Intake Point



5.5.1 Preliminary Assessment

With the idea of doing a preliminary evaluation of this topic, during the site visit, it was also visited San Andrés HPP, whose intake is found approximately 3.8 km upstream from the intake point of Piedras Negras HPP (Figure 2.2).

San Andrés is a run-of-the-river HPP operating since 2014. Has a gross head of 480 m and a design flow of 10.3 m³/s. The design flow is derived from the intake, through a rectangular channel to a regulation pond where it is then conducted through a GRP penstock to the powerhouse. Inside the powerhouse, there are two vertical axis Pelton units with an installed capacity of 20 MW each (ARCADIS Geotécnica, 2010).

As a reference, Figure 5.21 shows a satellite image of the intake structure and the regulation pond.

Figure 5.21: San Andrés HPP Intake and Regulation Pond

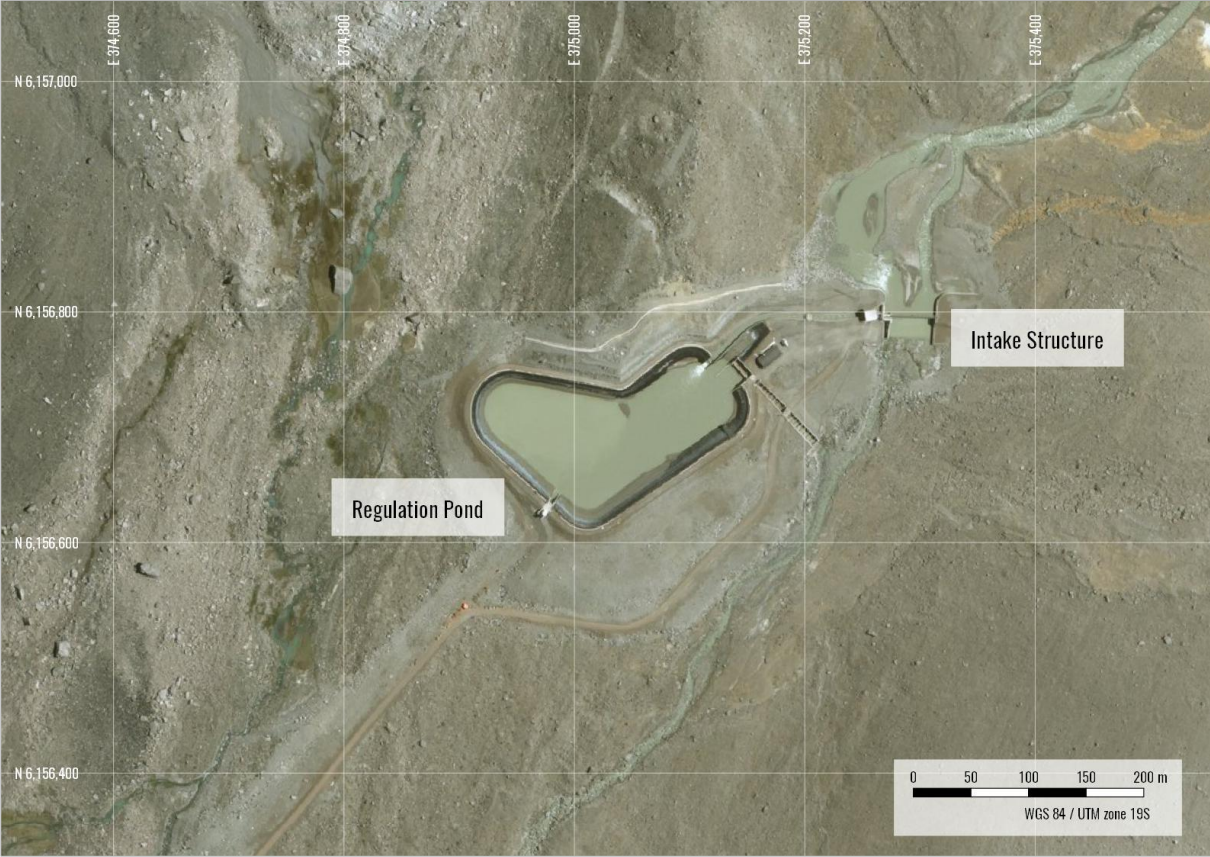


Figure 5.22 shows a photo taken from the top of the intake section where is seen how after three years of operation the sector immediately upstream from the derivation dam is almost entirely sedimented.

Figure 5.22: Sedimentation Just Upstream of San Andrés Intake



The regulation pond has a surface area of 1.9 ha and a total storage capacity of 115,000 m³ (ARCADIS Geotécnica, 2010). Although its main aim is to allow hydropeaking operation, its dimensions allow it to also perform a de-sanding task of the flow coming from the intake.

During the visit, one of the operators of the plant commented that the pond is cleaned by a floating dredger at the beginning of the wet season, which runs from November to April of each year. He also showed that at the end of each season, i.e. after April, the runners of the Pelton turbines must be changed due to the abrasive effect of the sediment particles remaining in the flow.

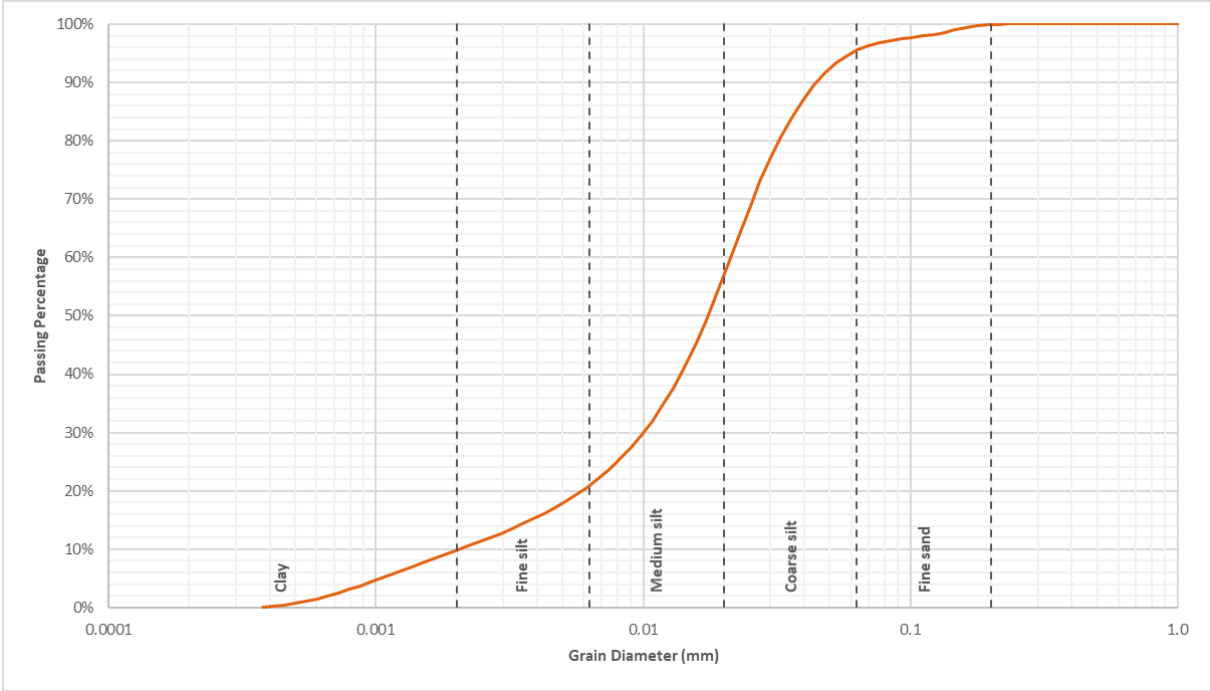
The information provided by the plant operator, summed to the geometry of the regulation pond, made me believe initially that this pond did not offer the adequate conditions for the sedimentation of the required size particles. Regarding this point, there are several empirical criteria in the technical literature on what should be the smallest size of the particle to sediment to reduce the abrasive effect on the electro-mechanical equipment of the power plant depending on its gross head. In this regard, and as a reference, (Bouvard, 1984) suggests that any particle with a diameter equal to or bigger than 0.15 mm should be removed from the flow for power plants with heads greater than 300 m, which is the case of San Andrés.

To test this hypothesis, a sediment sample was collected next to the discharge of the headrace channel to the regulation pond. Being next to the discharge and considering that the flow showed some turbulence, it was contemplated that the sediment deposited here would have a larger particle size than in the rest of the pond, where the velocity of the water is nearly zero.

The sample was subjected to a granulometric analysis using a laser scattering tool. To minimize measurement errors, the analysis was repeated five times and the average result was adopted.

The resulting sediment granulometric curve is shown in Figure 5.23.

Figure 5.23: Granulometric Curve of Sediment Sample Taken at San Andrés Regulation Pond



Observing Figure 5.23, and considering that the $d_{90} = 0.045 \text{ mm}$, it can be concluded that the sediment sample is free of grains larger than 0.15 mm. It is also important to note that 86% of the weight of the sampled sediment is within the range of silt (0.063 mm to 0.002 mm). This fact suggests that, in the case of the San Andres HPP, the problem of abrasion of the turbine runner is produced by the quartz concentration in the remaining suspended sediment rather than in the particles with enough size to settle.

This in principle rules out the hypothesis that the regulation pond does not have a good sedimentation efficiency, however, it must also be taken into consideration that a single sample taken at a unique location of the pond and at a unique moment of operation may not be conclusive for this purpose, but it gives insights on the challenges that Piedras Negras HPP must face.

5.5.2 Settling Basin Design

For practical purposes, the particle size of the sampled sediment (silt) is outside the range usually considered for a classic design of a settling basin for a hydropower power plant, basically because any alteration of the flow regime will cause the resuspension of the deposited material.

However, and for CAPEX purposes, a settling basin design was made considering the following criteria:

- Total design flow: 10 m³/s.
- Number of settling chambers: 2
- Size of the particle to settle: 0.20 mm
- Water density: 999.7 kg/m³ (at 10°C)
- Water kinematic viscosity: 1.31 · 10⁻⁶ m²/s (at 10°C)
- Sediment density: 2,650 kg/m³

To estimate the grain settling velocity, the equation proposed by (Ferguson & Church, 2004) was applied, which states:

$$w = \frac{R \cdot g \cdot D^2}{C_1 \cdot \nu + (0.75 \cdot C_2 \cdot R \cdot g \cdot D^3)^{0.5}}$$

With:

$$R = \frac{\rho_s - \rho_w}{\rho_w}$$

Where:

w : Particle's fall velocity (m/s)

R : Submerged specific gravity.

g : Gravitational acceleration (m/s²).

D : Particle's diameter (m)

- C_1 : Constant in Stokes' equation for laminar settling.
- C_2 : Constant drag coefficient for particle Reynolds numbers exceeding 1000.
- ν : Water kinematic viscosity (m^2/s).
- ρ_s : Density of the sediment (kg/m^3).
- ρ_w : Density of the water (kg/m^3).

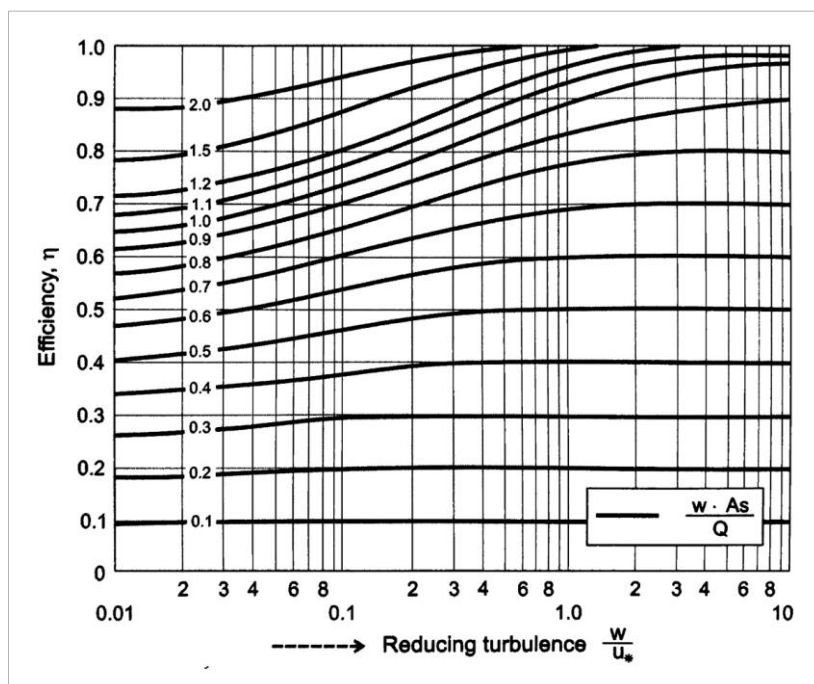
Regarding C_1 and C_2 parameters, and following the suggestion made by (Ferguson & Church, 2004) for natural sands where nominal diameters are used, the adopted values were in $C_1 = 20$ and $C_2 = 1.1$.

Under these conditions, the grain settling velocity is:

$$w = 0.02 \text{ m/s}$$

To do the dimensioning of the settling basin itself, the method proposed by Camp (Camp, 1946) was applied in which the sediment removal efficiency is calculated by using the following diagram shown in Figure 5.24.

Figure 5.24: Camp Sediment Removal Efficiency Diagram



To use this diagram, two expressions must be calculated:

$$\frac{w}{U_*} \text{ and } \frac{w \cdot A_s}{Q}$$

With:

$$U_* = \sqrt{g \cdot R_h \cdot S} = n \cdot V \cdot \sqrt{\frac{g}{\sqrt[3]{R_h}}}$$

Where:

- w : Particle's fall velocity (m/s)
- U_* : Shear velocity (m/s).
- A_s : Superficial wetted area of the settling chamber (m²).
- Q : Settling chamber design flow (m³/s).
- g : Gravitational acceleration (m/s²).
- R_h : Settling chamber hydraulic radius (m).
- S : Flow's energy line slope (m/m).
- n : Manning's roughness coefficient.
- V : Mean flow velocity in the settling chamber (m/s).

It should be noted the superficial wetter area is calculated with the width and length of each settling chamber, while the mean flow velocity is calculated with the width of the settling chamber and the depth of the flow, this results in a volume that defines the smallest dimensions of the structure.

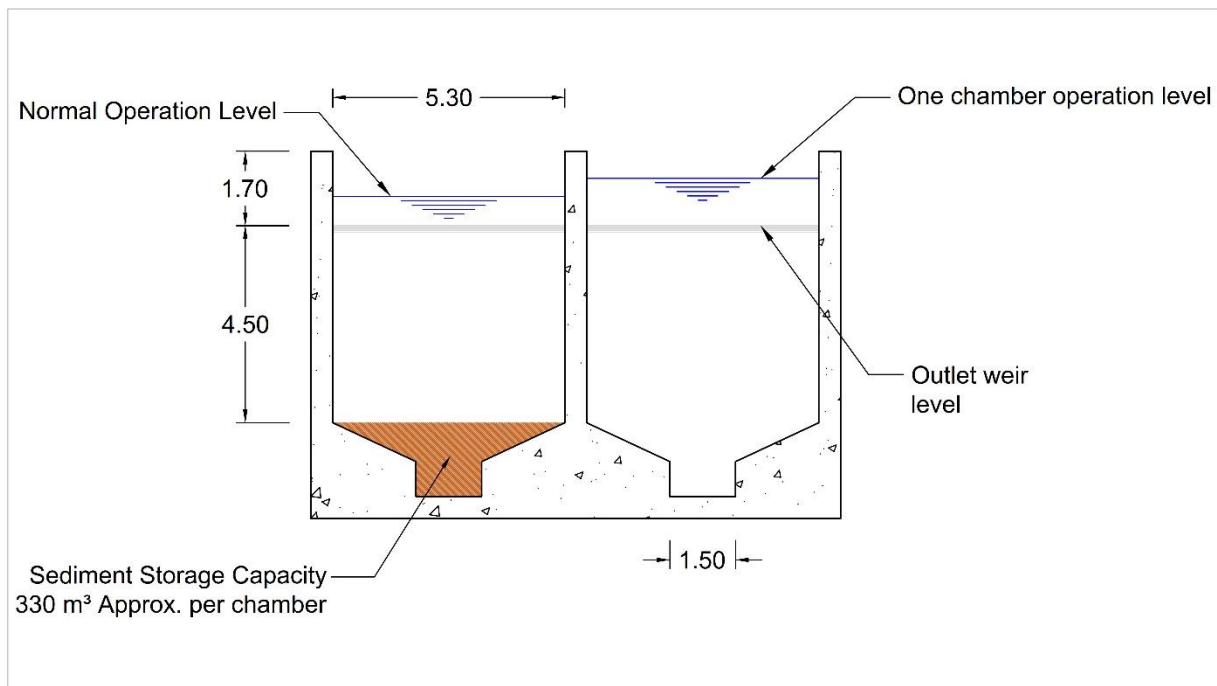
Considering a settling chamber design flow of $Q = 5 \text{ m}^3/\text{s}$, and a Manning roughness coefficient of $n = 0.018$, the results the design conditions, and when only one of the chambers is in use are included in Table 5.3.

Table 5.3: Settling Chamber Design Results

| Item | Normal Operation | One Chamber in Operation |
|--|------------------|--------------------------|
| Chamber discharge (m ³ /s) | 5.0 | 10.0 |
| Settling chamber length (m) | 80.0 | 80.0 |
| Settling chamber width (m) | 5.30 | 5.30 |
| Settling chamber depth (m) | 4.50 | 4.50 |
| Superficial area [A_s] (m ²) | 424 | 424 |
| Cross-sectional area (m ²) | 23.9 | 23.9 |
| Hydraulic radius (m) | 14.3 | 14.3 |
| Mean flow velocity [V] (m/s) | 0.21 | 0.42 |
| Shear velocity [U_*] (m/s) | 0.008 | 0.015 |
| $w \cdot A_s / Q$ | 1.51 | 0.75 |
| w / U_* | 2.34 | 1.17 |
| Sediment Removal Efficiency [η] | 100% | 73% |

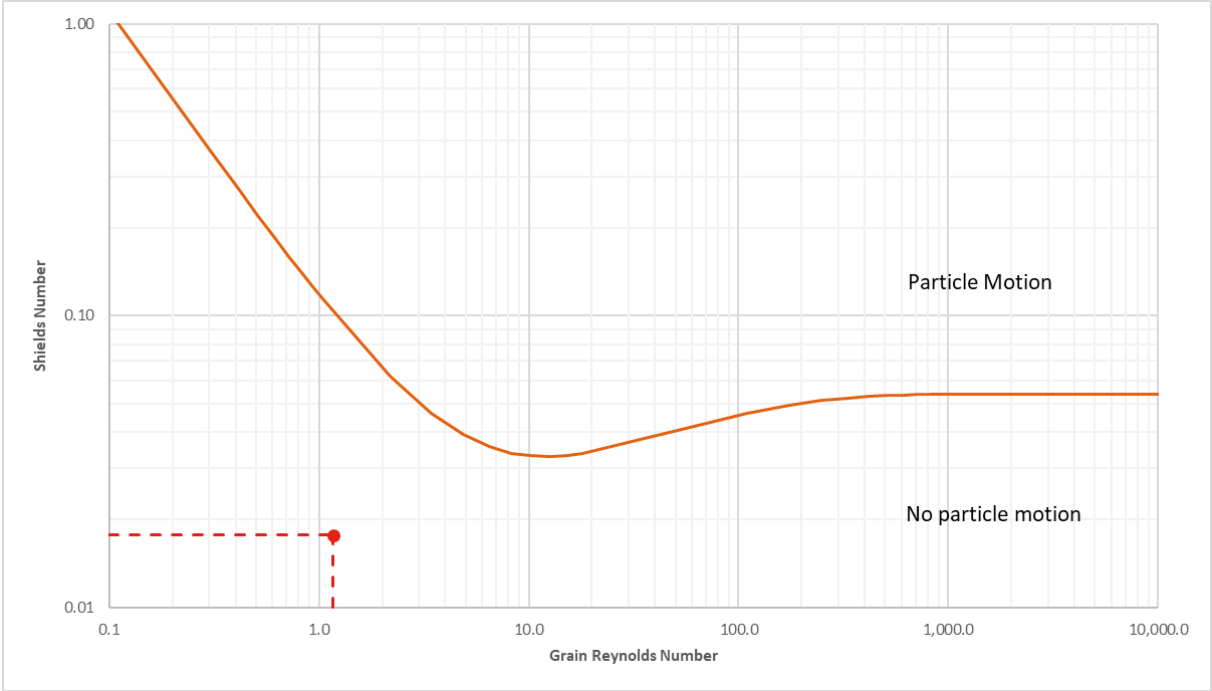
As a reference, Figure 5.25 shows a typical cross-section of the settling basin.

Figure 5.25: Settling Basin Typical Cross Section



To verify that in the design condition the sediment already decanted does not suffer from resuspension, the Shields criterion was applied. Under these conditions, with a particle Reynolds number of 1.16 and a Shield number equal to 0.018, Figure 5.26 shows that particles with a diameter equal to or greater than 0.20 mm do not move under the hydraulic conditions in the settling chamber.

Figure 5.26: Shield Criteria Verification for Sediment Motion



5.5.3 Final Remarks

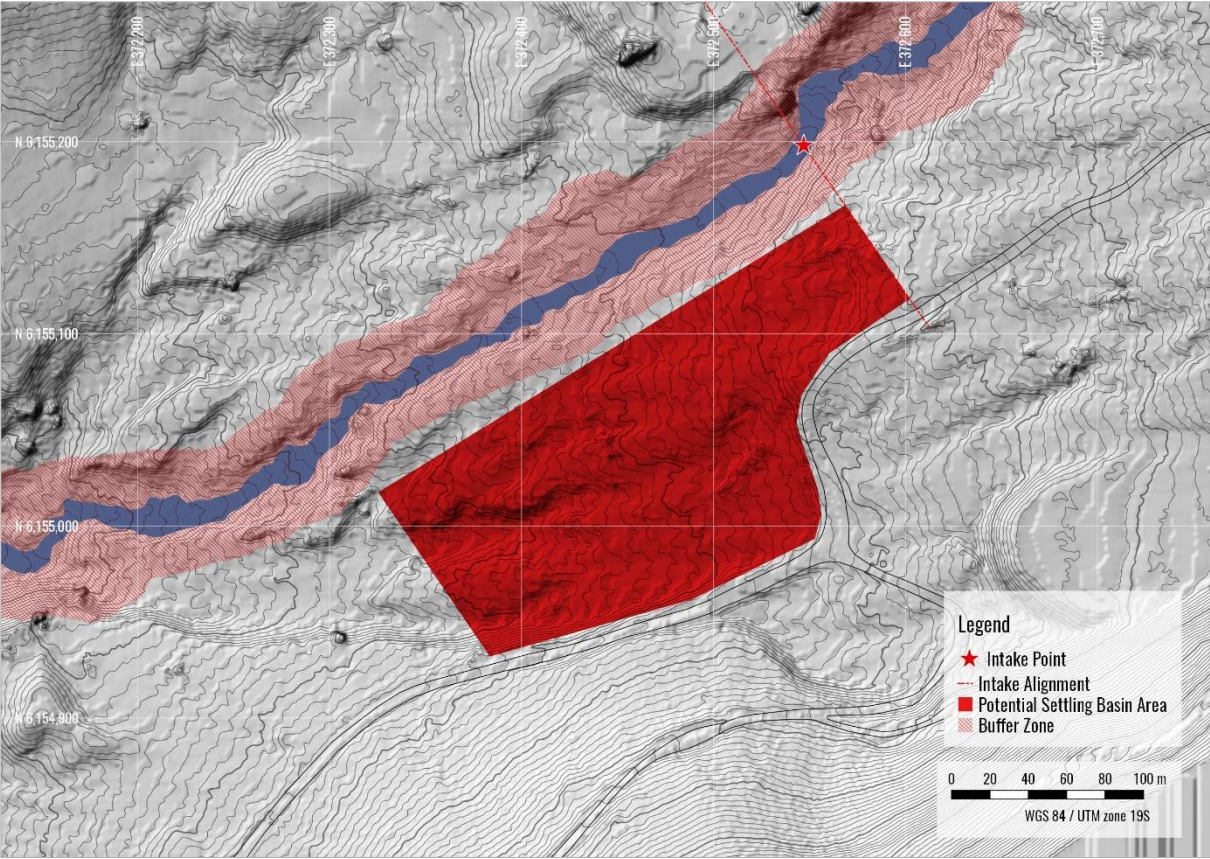
Although a settling basin design was made to sediment particles with diameters equal to or greater than 0.20 mm, after what has been seen in San Andrés HPP, it is known that the basin design will help to reduce but not end the abrasion problems that may exist in Piedras Negras HPP.

In this regard, another possibility to reduce this problem is to build a larger settling basin. As shown in Figure 5.27, near the intake site there is an esplanade that could allocate a pond with a surface up to 3 ha approximately. This pond could be designed specifically to optimize the sediment settling of the inflow, however, and due to its possible dimensions, it could also be used as a reservoir to allow hydropeaking.

Nevertheless, during the operation of the future plant, should be foreseen the use of specially designed turbines to deal with the type of sediment in San José river. This type of technology varies among suppliers, but it is usual for the runners to have a coating of resistant materials such as tungsten carbide.

Regardless of all the above, the final intake design must consider a gravel excluder to keep clear of sediments the sector right next to the intake section. Also, it should be considered in the OPEX (Operational Expenditure) a routinely cost for repairing and changing the turbines runners.

Figure 5.27: Potential Settling Basin Location Area



5.6 Headrace Conduit and Penstock Alignment

5.6.1 Alignment Criteria

One of the most relevant aspects for hydroelectric generation projects is the definition of the headrace conduit and the penstock layout. These alignments can have an important impact on the final cost of the project if constructive issues such as cut and fill, pipe fittings, anchor blocks, etc. are considered.

Similarly, if an alignment with the least possible number of bends is considered, from the hydraulic point of view this would result also in reduced head losses directly affecting the production of energy, and therefore the economic benefits obtained from the power plant.

Therefore, the following criteria were considered when tracing both the horizontal and vertical alignments of the conduits:

- All conduits were considered closed and flowing under pressure.
- To protect the pipes against vandalism, vehicle load or the freezing weather effects, the complete alignment is buried with the top of the pipe found at a minimum of 1.50 m below the surface.
- Changes of direction (vertices) were minimized as much as possible both in horizontal and vertical alignment.
- Terrain excavation was minimized as much as possible.
- To avoid air pockets, only positive slopes (downhill) was considered.

5.6.2 Alternatives Description

With these criteria, and with the idea of having a good evaluation of the possible alignments, a total of three alternatives were developed contemplating the same intake point and location of the powerhouse. These alternatives are:

1. **River Alternative:** Takes advantage of the floodplains of the San José river to allocate the alignment of the conduit, following the river slope and always staying out of the buffer zone set up in the hydraulic study (Title 5.2). Elevation-wise, of the three alternatives this is the lowest one, making the whole alignment to be at high pressure.

2. **Road Alternative:** As the name suggests, the alignment considers the conduit buried under the existing access road to San Andrés HPP. A big part of the alignment develops in a medium to low pressure, and near the powerhouse location, a high-pressure section follows the greatest slope of the terrain. A surge chamber will be found at the start point of the high-pressure section.
3. **Low-Pressure Alternative:** The highest altitude alternative. The alignment tries to keep an almost horizontal slope by following the elevation of the contour line at the outlet of the settling basin. Most of the conduit goes in low pressure, followed by a high-pressure section going down the greatest slope of the terrain to the powerhouse. A surge chamber will be found at the start point of the high-pressure section.

The horizontal and vertical alignment of the three alternatives are shown in Figure 5.28 and Figure 5.29 respectively.

Figure 5.28: Conduits Alternatives: Horizontal Alignment

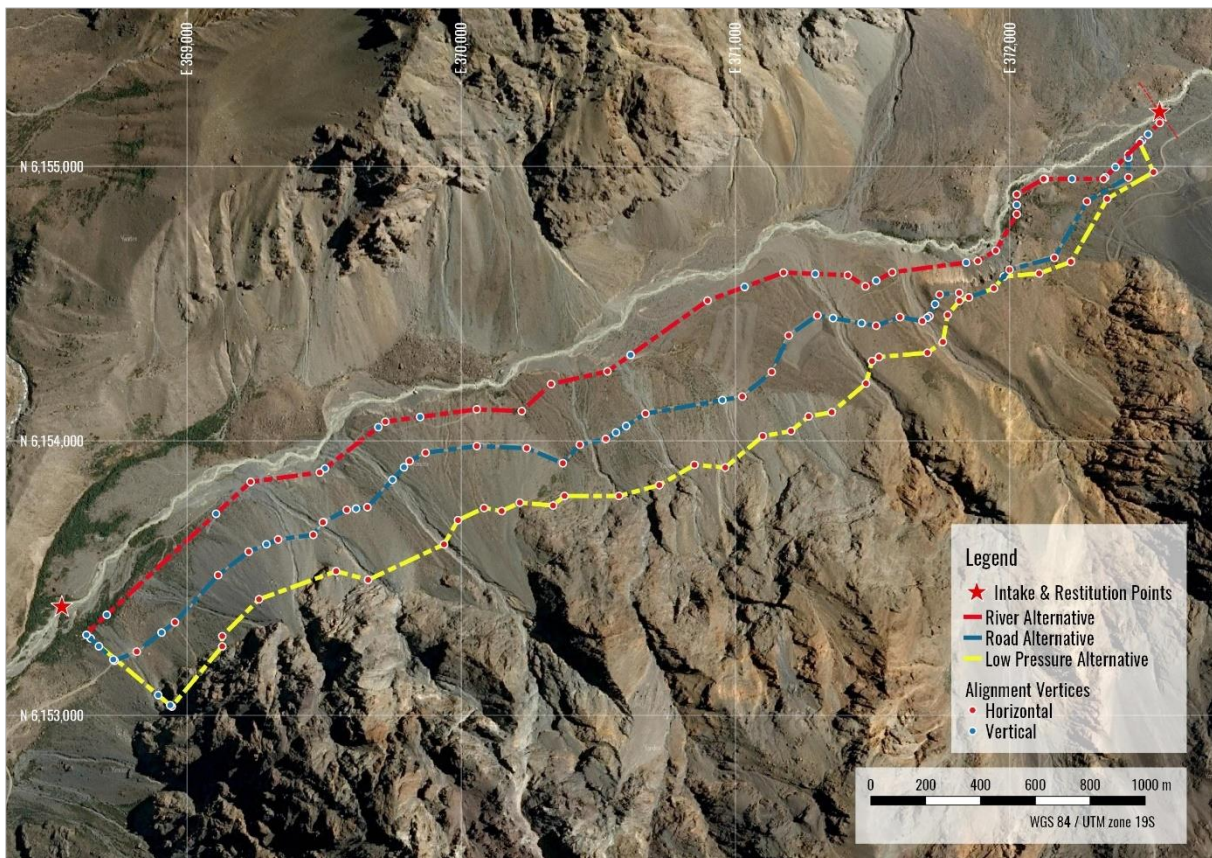
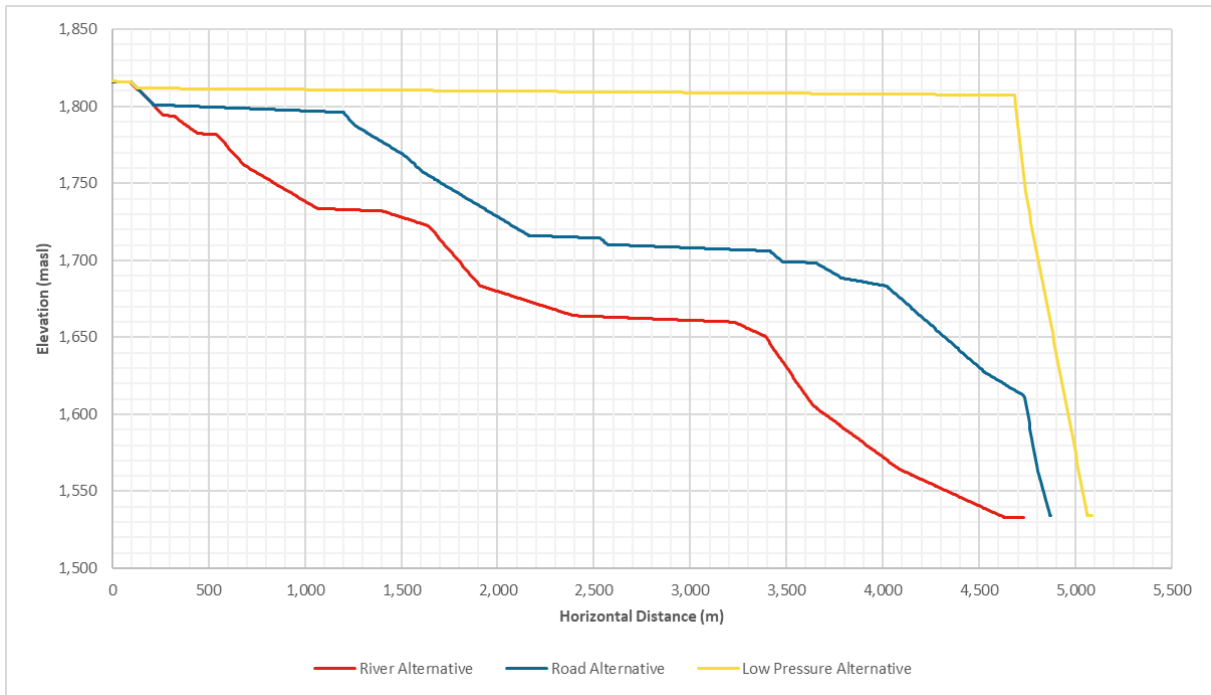


Figure 5.29: Conduits Alternatives: Vertical Alignment



A summary of the main characteristics of each alternative is included in Table 5.4.

Table 5.4: Summary of Conduit Alternatives Main Geometric Characteristics

| Element | River Alternative | Road Alternative | Low-Pressure Alternative |
|---------------------------------|-------------------|------------------|--------------------------|
| Headrace Conduit Length (m) | 0 | 4,743 | 4,684 |
| Penstock Length (m) | 4,747 | 158 | 493 |
| Number of Horizontal Vertices | 19 | 36 | 36 |
| Number of Vertical Vertices | 16 | 18 | 5 |
| Average Excavation Depth (m) | 3.8 | 4.0 | 3.3 |
| Total Length (m) | 4,747 | 4,901 | 5,177 |
| Total Number of Vertices | 35 | 54 | 41 |

Note: Excavation value for low-pressure alternative only considers the section inside the LIDAR DTM.

6 Energy Production Model

To simulate the energy production of Piedras Negras HPP, a mathematical model was created which takes into consideration the following input parameters:

- Water surface elevation at intake point.
- Turbine centerline elevation or water surface elevation at restitution point.
- Hydrological river inflow timeseries.
- Hydrological intake restrictions (ecological flow, maximum intake capacity, etc.)
- Conduits size and length.
- Frictional and singular flow energy losses for each discharge in the timeseries.
- Turbine efficiency curve.
- Up to four turbines of equal or different installed capacities.

With these inputs, the model simulated the energy production for each day of the hydrological timeseries and allowed the user to test the production impact of a range of power plant design flows and the number and size of the turbine units in the powerhouse.

The goal of testing a variety of these parameters is to find the combination that maximizes the energy production of the power plant.

6.1 Turbine Inflow

In Title 3.7, as shown, an HBV model was set up and calibrated to produce a historical series of 39 years of mean daily runoff at the intake point of Piedras Negras HPP. However, the totality of this runoff cannot be exploited due to the restrictions imposed by the water rights issued by the DGA.

The net amount of water that the Piedras Negras power plant can take for energy production is governed by the provisions of the water rights DGA435, issued on June 8, 1999, and DGA462 issued on November 3, 2004. The first is a non-consumptive right, of eventual and continuous exercise, the second is non-consumptive, of eventual and discontinuous exercise. According to (Ministerio de Justicia, 2018), the definition of each of these terms is:

- Article 14: Non-consumptive use allows water to be used without consuming it and to retribute it in the manner decided by the act of acquisition or constitution of the right.
- Article 18: Eventual exercise only empower to use the water at the times in which the matrix discharge has a surplus after the water rights of permanent exercise have been already supplied.
- Article 19: Continuous exercise are those that allow using the water in an uninterrupted form during the twenty-four hours of the day. The rights of discontinuous exercise only allow the use of water during certain periods.

Although it is not usual to have water rights categorized only as eventual, in conversations with Anpac Energía the author of this document was informed that for practical purposes, both water rights should be considered as permanent and continuous.

In this regard, Table 6.1 includes the greatest monthly intake allowance each water right allows and the minimum flow the intake should let it pass.

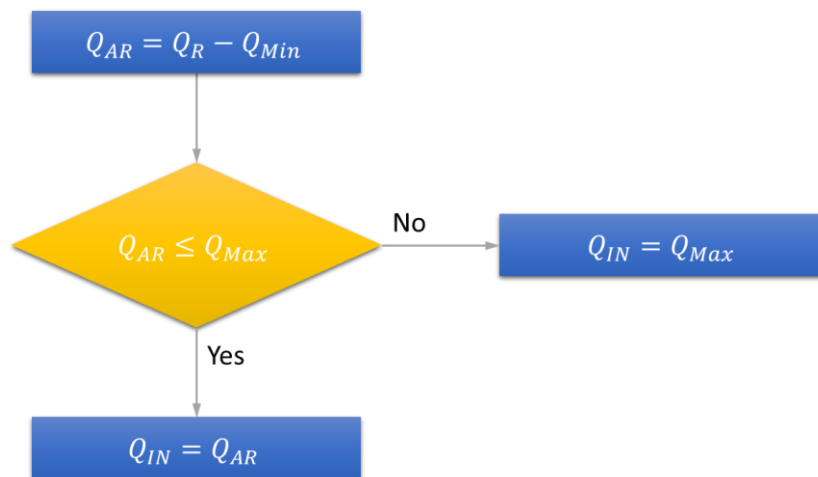
Table 6.1: Monthly Maximum Runoff Intake Allowance and Minimum Bypass Flow

| Month | Maximum Intake Allowance | | Minimum Bypass Flow | | Maximum Intake Allowance (m ³ /s) | Minimum Bypass Flow (m ³ /s) |
|-----------|----------------------------|----------------------------|----------------------------|----------------------------|--|---|
| | DGA462 (m ³ /s) | DGA435 (m ³ /s) | DGA462 (m ³ /s) | DGA435 (m ³ /s) | | |
| January | 6.99 | 7.80 | 0.47 | 0.47 | 14.79 | 0.94 |
| February | 2.21 | 7.80 | 0.47 | 0.47 | 10.01 | 0.94 |
| March | | 7.80 | | 0.47 | 7.80 | 0.47 |
| April | | 7.80 | | 0.47 | 7.80 | 0.47 |
| May | | 7.80 | | 0.47 | 7.80 | 0.47 |
| June | | 7.80 | | 0.47 | 7.80 | 0.47 |
| July | | 7.80 | | 0.47 | 7.80 | 0.47 |
| August | | 7.80 | | 0.47 | 7.80 | 0.47 |
| September | | 7.80 | | 0.47 | 7.80 | 0.47 |
| October | | 7.80 | | 0.47 | 7.80 | 0.47 |

| Month | Maximum Intake Allowance | | Minimum Bypass Flow | | Maximum Intake Allowance (m ³ /s) | Minimum Bypass Flow (m ³ /s) |
|----------|----------------------------|----------------------------|----------------------------|----------------------------|--|---|
| | DGA462 (m ³ /s) | DGA435 (m ³ /s) | DGA462 (m ³ /s) | DGA435 (m ³ /s) | | |
| November | 0.52 | 7.80 | 0.47 | 0.47 | 8.32 | 0.94 |
| December | 5.74 | 7.80 | 0.47 | 0.47 | 13.54 | 0.94 |

Considering the information exposed in Table 6.1, the flowchart to calculate the available inflow to the power plant is shown in Figure 6.1.

Figure 6.1: Calculation Flowchart for Available Inflow to the Powerplant



Where:

Q_{AR} : Available runoff in the river (m³/s).

Q_R : Mean daily river runoff (m³/s).

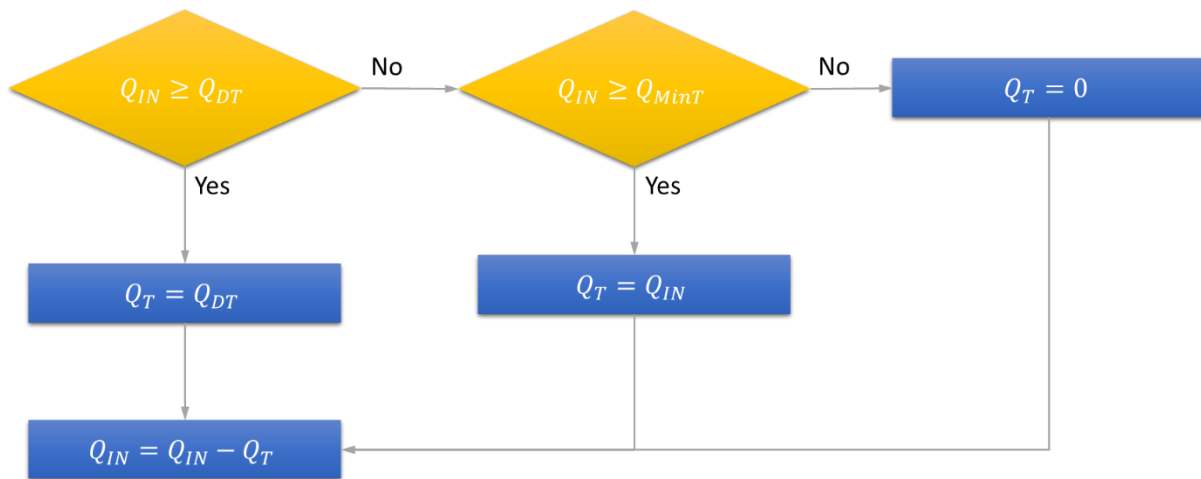
Q_{Min} : Minimum bypass flow (Table 6.1) (m³/s).

Q_{Max} : Maximum intake allowance (Table 6.1) (m³/s).

Q_{IN} : Available inflow to the power plant (m³/s).

Finally, the flow accepted by each turbine was calculated following the process Figure 6.2 shows.

Figure 6.2: Calculation Flowchart for Turbine Inflow



Where:

Q_{IN} : Available inflow to the power plant or to the next turbine unit (m^3/s).

Q_{DT} : Maximum accepted flow by the turbine (design flow) (m^3/s).

Q_{MinT} : Minimum accepted flow by the turbine (m^3/s).

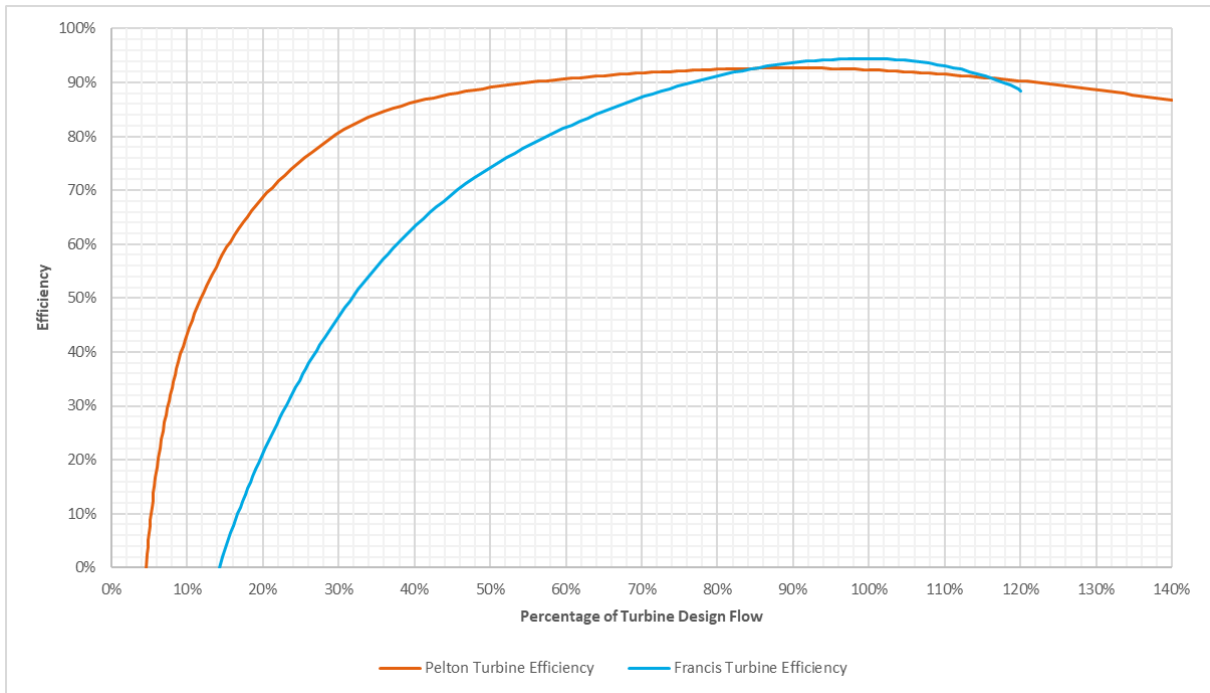
Q_T : Net inflow to the turbine (m^3/s).

6.2 Turbine Efficiency and Accepted Flow Range

Due to the characteristics of the project, two types of turbines were evaluated: Pelton and Francis.

In this regard, Figure 6.3 shows the efficiency curves considered for each type of turbine (Brekke, 1995).

Figure 6.3: Turbine Efficiency Curves



Source: (Brekke, 1995)

It should be mentioned that in the model the generator or transformer efficiencies were not considered, only the turbine efficiency was used for energy production calculation.

Regarding the accepted flow for each type of turbine, Table 6.2 includes the values considered for the model

Table 6.2: Maximum and Minimum Design Flow Acceptance for the Turbines

| Turbine Type | Minimum Percentage of the Turbine Design Flow Accepted | Maximum Percentage of the Turbine Design Flow Accepted |
|---------------------|---|---|
| Francis | 30% | 100% |
| Pelton | 15% | 100% |

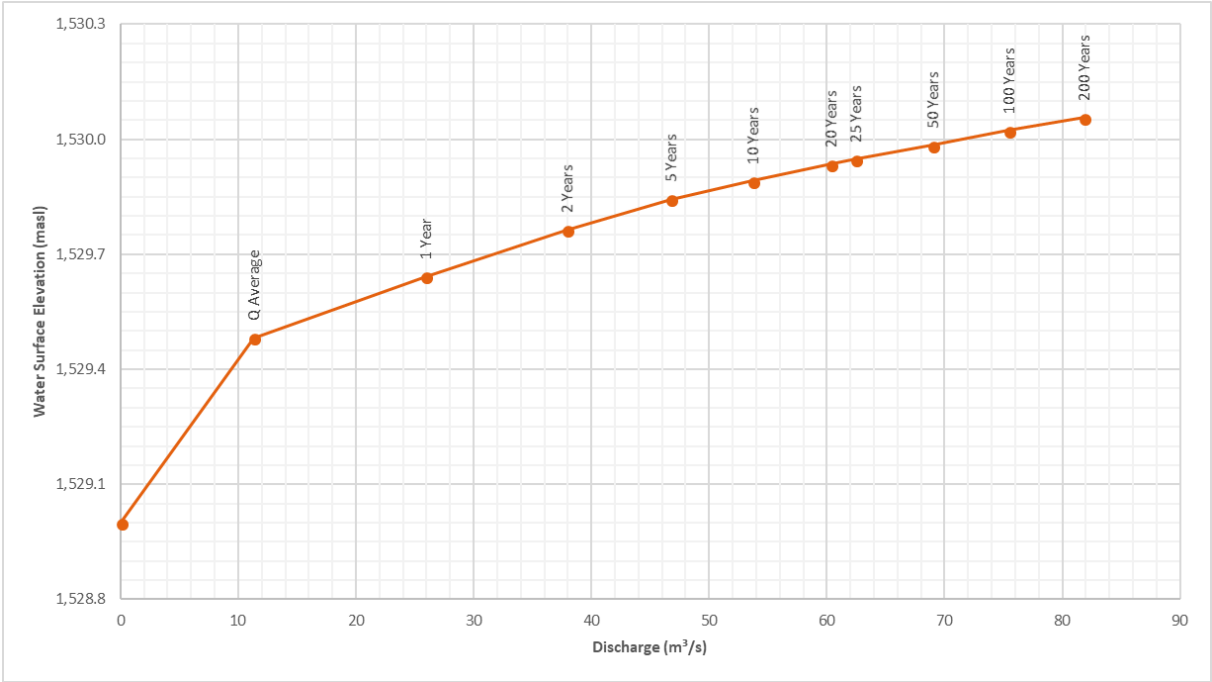
6.3 Gross Head

In Title 3.1, where the location of the intake point was defined, it was indicated that the elevation of said point is 1,815 masl, however, and for the purposes of estimating the gross head, it was decided to lower this elevation a couple of meters to consider the water surface

elevation at the discharge of the settling basin, that is, in the energy production model the intake level was set at 1,813 masl.

In the case of the powerhouse, using the hydraulic model of the San José river described in Title 5.2, a stage-elevation curve was generated for this sector of the river. This is shown in Figure 6.4.

Figure 6.4: Stage-Discharge Curve at Powerhouse Section



When simulating a powerhouse with Francis turbines, and considering the river daily average flows at the powerhouse sector, the stage-discharge curve shown in Figure 6.4 was directly applied to obtain the gross head for each date of the historical runoff timeseries.

In the case of Pelton turbines, it was considered that the centerline of the turbine would be found 1.50 m above the water surface level reached for a flood event with a return period of 50 years, that is, 1,531.5 masl, resulting in a constant gross head equal to 281.5 m.

6.4 Head Losses

The total head losses were calculated for each day of the historical timeseries of discharges admitted to the turbines considering separately the frictional losses and the singular losses as explained next.

6.4.1 Frictional Losses

For the calculation of frictional losses, it was first necessary to define what materials would be used for the pipes. In this regard, steel, and GRP (Glass fiber Reinforced Plastics) were considered for this purpose.

The adopted value of the frictional losses was an average of the results of the Manning and Hazen-Williams equations, which states:

- Manning Equation for Circular Conduits:

$$h_f = 10.2936 \cdot n^2 \cdot \frac{Q^2 \cdot L}{D^{16/3}}$$

- Hazen–Williams for Circular Conduits:

$$h_f = 10.6743 \cdot \left(\frac{Q}{C}\right)^{1.8519} \cdot \frac{L}{D^{4.8705}}$$

Where:

- h_f : Frictional head loss (m).
 n : Manning roughness coefficient.
 C : Hazen–Williams roughness coefficient.
 Q : Discharge in the conduit (m³/s).
 L : Conduit length (m).
 D : Conduit internal diameter (m).

The adopted values for the roughness coefficients are included in Table 6.3.

Table 6.3: Conduits Roughness Coefficients for Frictional Losses

| Conduit Material | Manning Coefficient | Hazen–Williams Coefficient |
|------------------|---------------------|----------------------------|
| Steel | 0.012 | 120 |
| GRP | 0.010 | 140 |

6.4.2 Singular Losses

The singular head losses were calculated by using the following equation:

$$h_s = K \cdot \frac{V^2}{2 \cdot g} \approx 0.0826 \cdot \frac{K \cdot Q^2}{D^4}$$

Where:

- h_s : Singular head losses (m).
- K : Head loss coefficient.
- V : Flow velocity in the conduit (m/s).
- Q : Discharge in the conduit (m³/s).
- D : Conduit internal diameter (m).

For each of the vertices of the three alternatives shown in Figure 5.28, the deflection angle of the conduit, that is, the angle needed to change the flow direction was fixed to a nominal value. This angle was used to define the head loss coefficient.

In addition to the vertices of each alternative, the other elements considered for the singular losses were: Conduit entrance, penstock branching and emergency butterfly valve at the inlet of the turbines.

The adopted coefficients of losses are included in Table 6.4 (Méndez, 1995)(Mays, 1999).

Table 6.4: Head Losses Coefficients for Singular Losses

| Element | Head Loss Coefficient |
|----------------------------------|------------------------------|
| Inlet Emergency Butterfly Valve | 0.400 |
| Penstock Branches | 0.200 |
| Penstock Entrance | 0.260 |
| Vertex with Deflection Angle 5° | 0.024 |
| Vertex with Deflection Angle 10° | 0.044 |
| Vertex with Deflection Angle 15° | 0.062 |
| Vertex with Deflection Angle 20° | 0.088 |
| Vertex with Deflection Angle 25° | 0.158 |
| Vertex with Deflection Angle 30° | 0.165 |
| Vertex with Deflection Angle 35° | 0.189 |
| Vertex with Deflection Angle 40° | 0.209 |
| Vertex with Deflection Angle 45° | 0.284 |
| Vertex with Deflection Angle 60° | 0.268 |
| Vertex with Deflection Angle 65° | 0.292 |
| Vertex with Deflection Angle 70° | 0.312 |
| Vertex with Deflection Angle 85° | 0.335 |
| Vertex with Deflection Angle 90° | 0.342 |

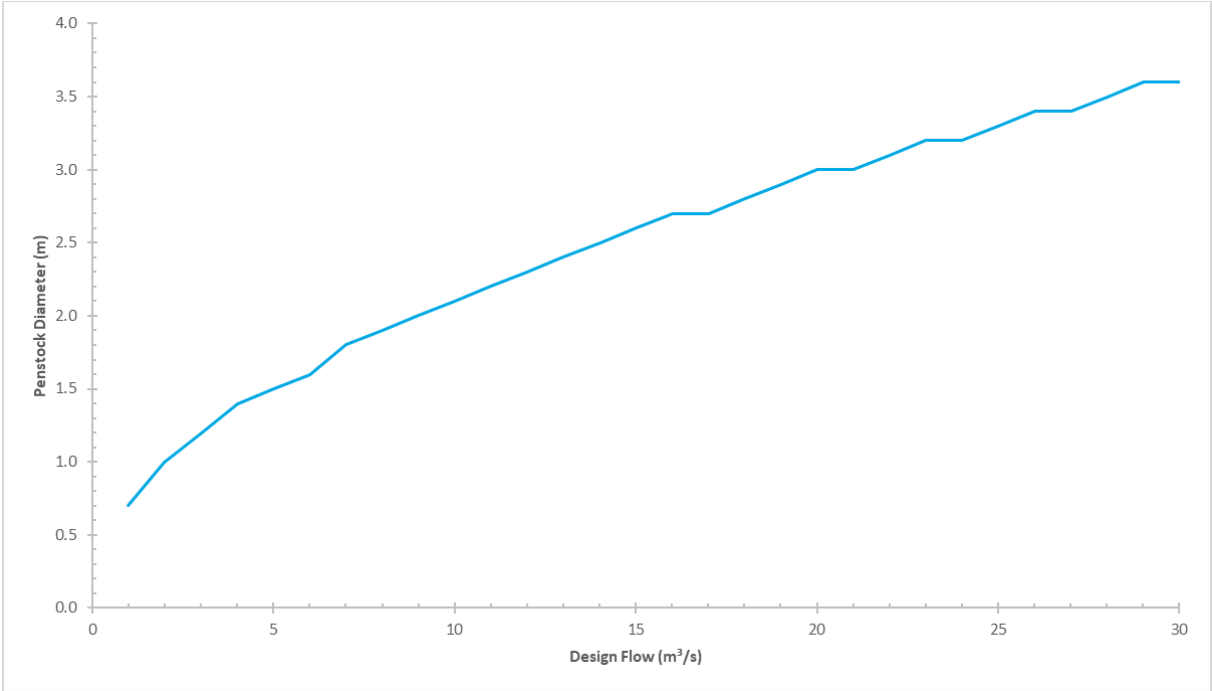
6.5 Power Plant Design Flow, Number of Turbines, and their Type

To define the design flow and type of turbine of Piedras Negras HPP, the energy production of the river alternative was simulated evaluating a range of design flows between 1 m³/s and 30 m³/s.

The design flow adopted for the power plant corresponded to the greater flow that generated a marginal increase in the energy production equal to or greater than 1%.

For the penstock, pipe diameters that resulted in flow velocities of 3.0 m/s, depending on the tested design flow, were considered. The resulting diameters values were rounded to immediately highest 0.10 m multiple (i.e.: 1.75 m to 1.80 m). These diameters are shown for reference in Figure 6.5.

Figure 6.5: Penstock Diameters Considered to Define the Power Plant Design Flow



Regarding the turbines, this exercise was carried out considering Pelton or Francis turbines of equal size in the powerhouse. A different number of turbines were tested, the value that yielded the greatest marginal energy production increment was chosen. In an analogous way, the type of turbine that delivered the highest energy production would be selected to continue with the rest of the analyzes.

With these considerations, Figure 6.6 and Figure 6.7 shows the energy production results from varying the design flow while Figure 6.8 and Figure 6.9 shows the energy production impact of having a different number of units in the powerhouse for both Francis and Pelton turbines respectively. Finally, a summary of the numerical values from these Figures are included in Table 6.5.

Figure 6.6: Energy Production vs Power Plant Design Flow Summary for Francis Turbine

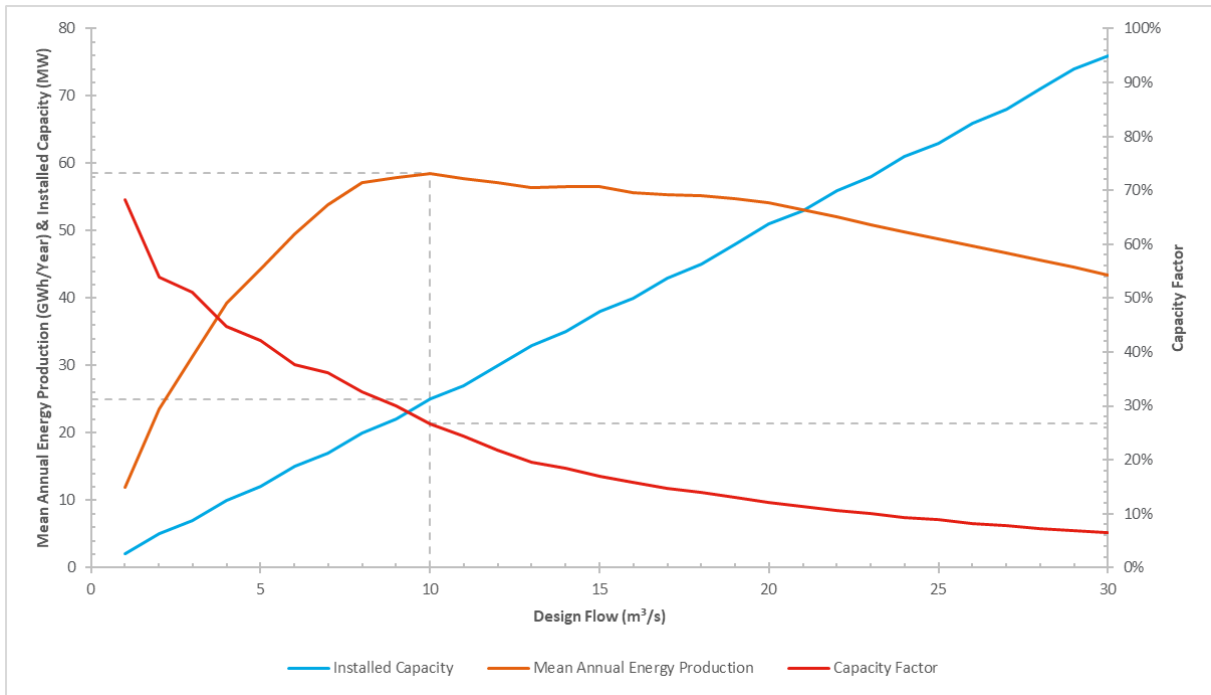


Figure 6.7: Energy Production vs Power Plant Design Flow Summary for Pelton Turbine

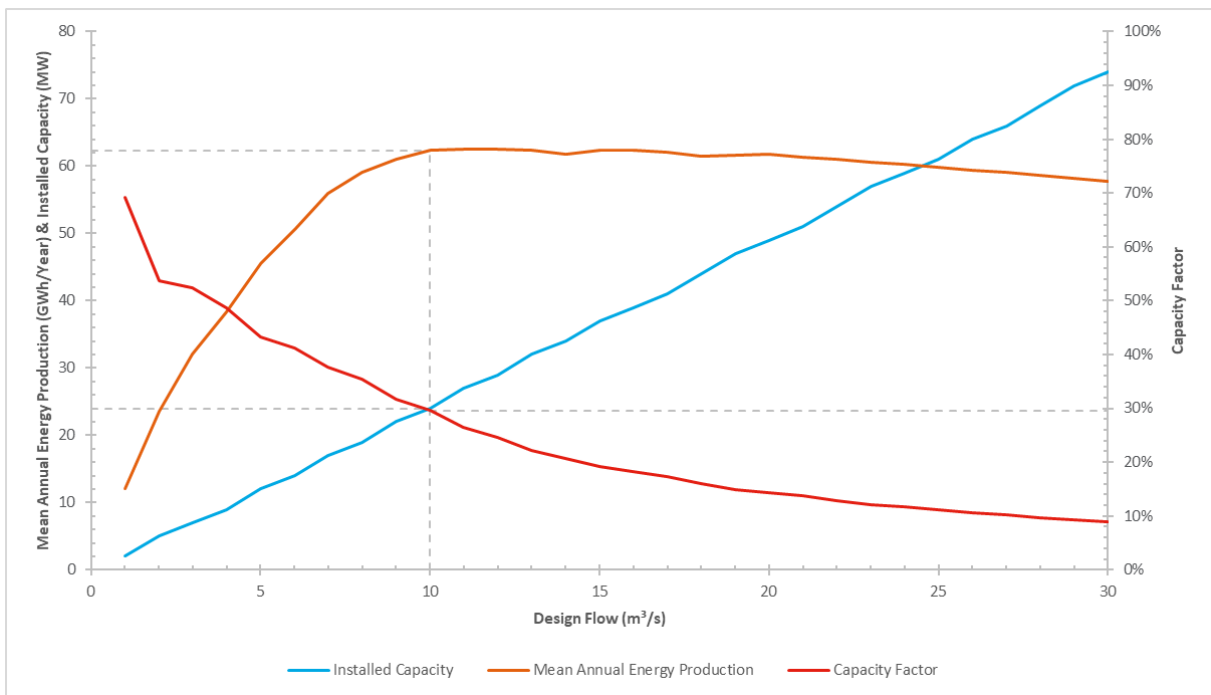


Figure 6.8: Energy Production vs Number of Francis Turbine Units in the Powerhouse

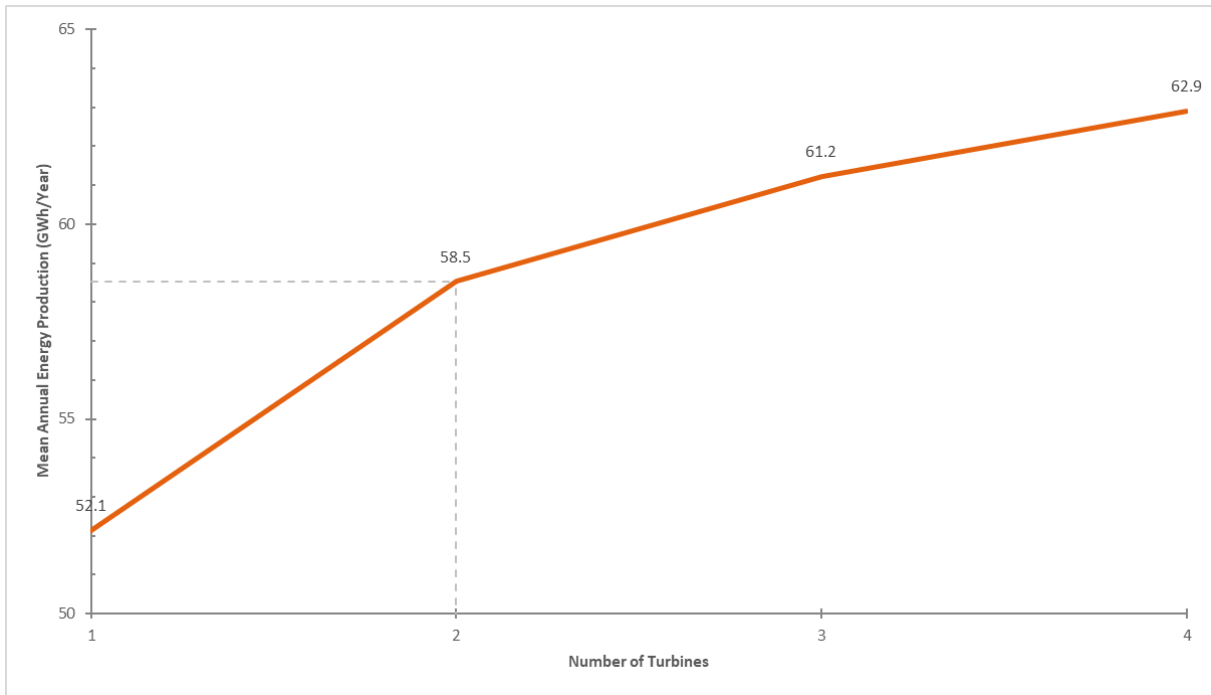


Figure 6.9: Energy Production vs Number of Pelton Turbine Units in the Powerhouse

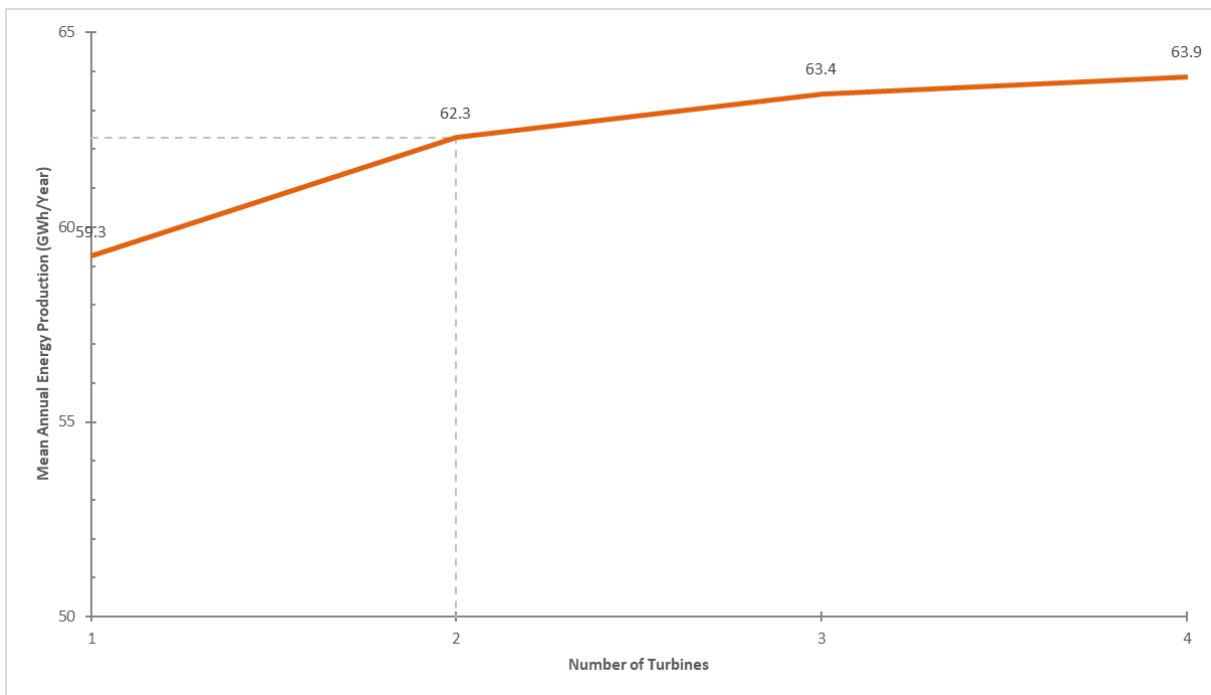


Table 6.5: Power plant Design Flow and Turbine Type Results for Piedras Negras HPP

| Parameter | Francis Turbine | Pelton Turbine |
|--|-----------------|----------------|
| Design Flow (m ³ /s) | 10.0 | 10.0 |
| Gross Head (m) | 283.6 | 281.5 |
| Net Head (m) | 268.0 | 265.9 |
| Total Head Losses as Gross Head Percentage | 5.5% | 5.5% |
| Number of Turbine Units | 2 | 2 |
| Installed Capacity (MW) | 25.0 | 24.0 |
| Energy Production (GWh/year) | 58.53 | 62.30 |
| Capacity Factor | 26.7% | 29.6% |

With the results in Table 6.5, Figure 6.6 and Figure 6.7, the following points can be deduced:

- The selected design flow for Piedras Negras HPP which maximizes the energy production is 10 m³/s.
- Even though the Francis turbines works with more head, Pelton turbines deliver 6.4% more energy production.
- Pelton turbines are better adapted to the hydrological behavior of San José river, this is reflected in the extra 2.9% capacity factor in comparison with Francis turbine.
- For both Francis and Pelton, two units resulted in the biggest marginal increment of the energy production.
- For later analysis, powerhouses with two Pelton units will be considered.

6.6 Optimal Diameter and Turbine Size Combination

This point involved an iterative analysis in which both pipes diameters and a combination of turbines of varied sizes were successively evaluated.

To select the size of the turbine units, different combinations of unit sizes were evaluated and the one that resulted in the highest energy production was selected.

Due to its extension and complexity, the optimal diameter evaluation will be explained in its own Title.

6.6.1 Optimal Diameter Analysis

In most cases, an optimization process involves a minimization of the most relevant costs in the analysis. For the case of this point, the most relevant items analyzed were: The cost of the pipe itself and the cost of less energy production due to the hydraulic head losses.

The cost of the pipe is decided by the amount of material needed to withstand its own weight and the internal and external pressures acting on the conduit. The head losses are linked to the pipe diameter, the bigger the diameter, the smaller the head losses and vice versa.

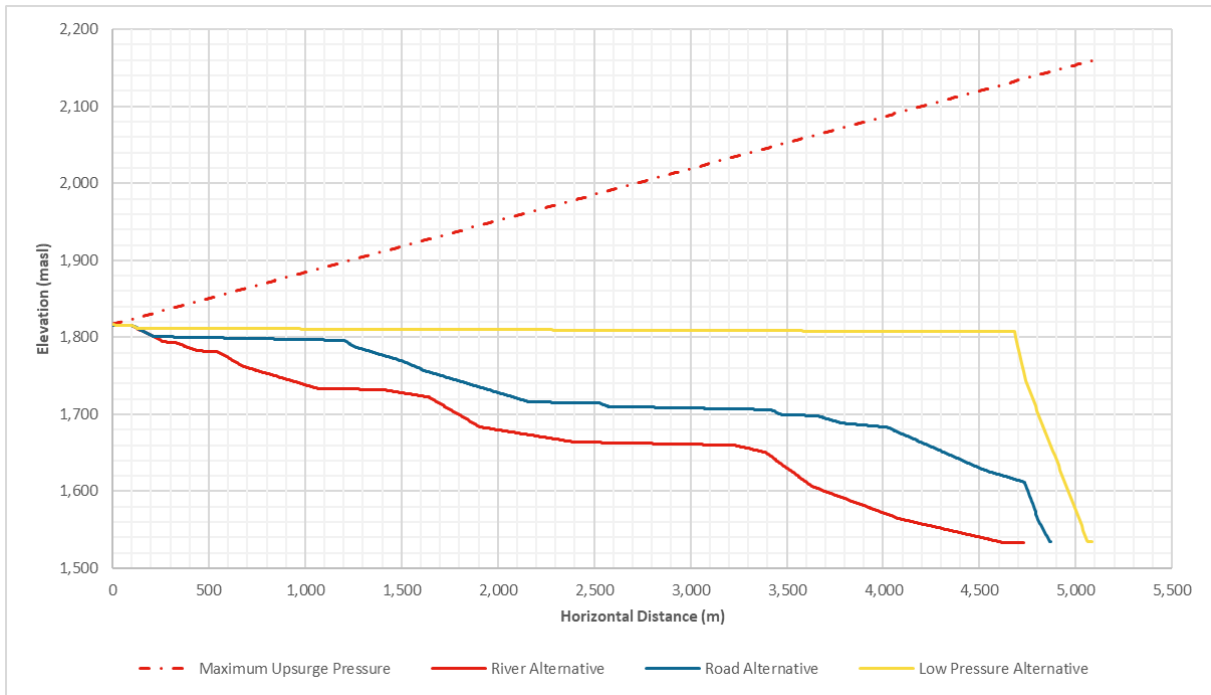
6.6.1.1 Design Pressure

To be able to calculate to define the wall thickness, in the case of steel pipes, or the nominal pressure class in the case of GRP pipes, it must be first defined the working pressure of the conduit. In this regard, it was decided to use the maximum pressure of the water hammer.

Because a detailed analysis of the water hammer phenomena escapes the scope of this Thesis and considering Pelton turbines, the maximum upsurge pressure was calculated as 20% of the static pressure at the inlet point to the powerhouse. For the rest of the alignment, the piezometric line decreases linearly until it reaches the water surface elevation at the entrance of the conduit.

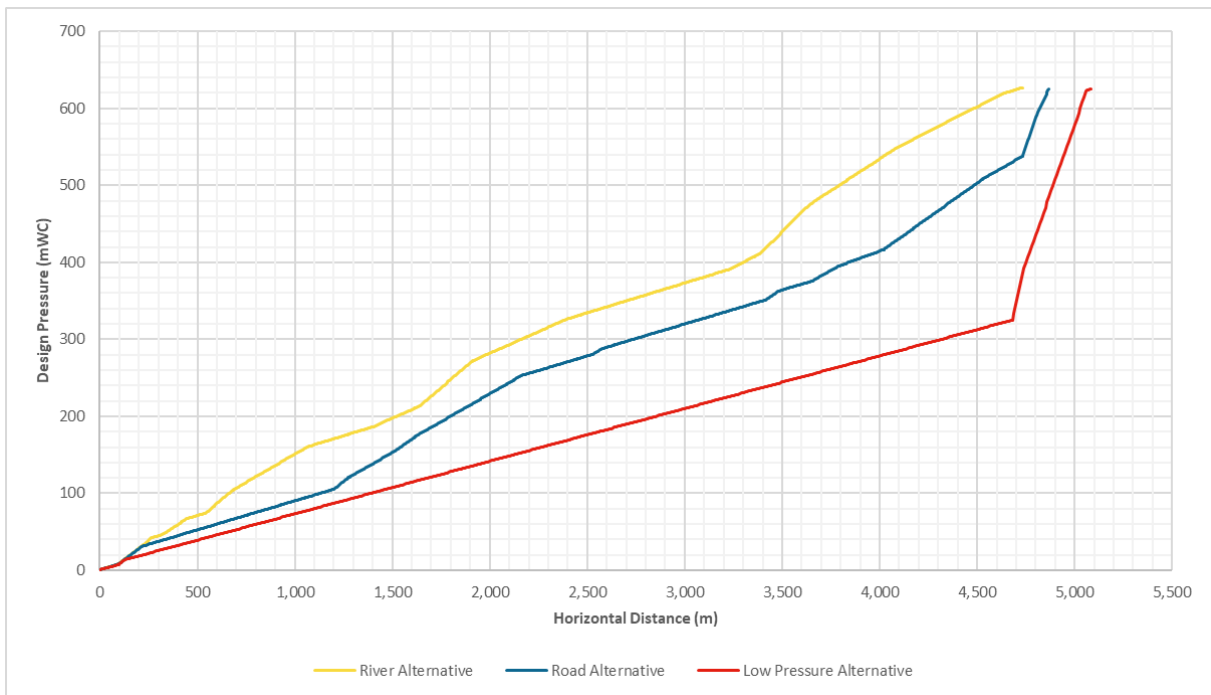
Figure 6.10 shows the considered maximum upsurge piezometric line and the vertical alignments of each of the studied alternatives.

Figure 6.10: Design Piezometric Line for Alignment Alternatives



For reference, Figure 6.11 shows the design pressure in mWC (Meter of Water Column) of each conduit along its alignment.

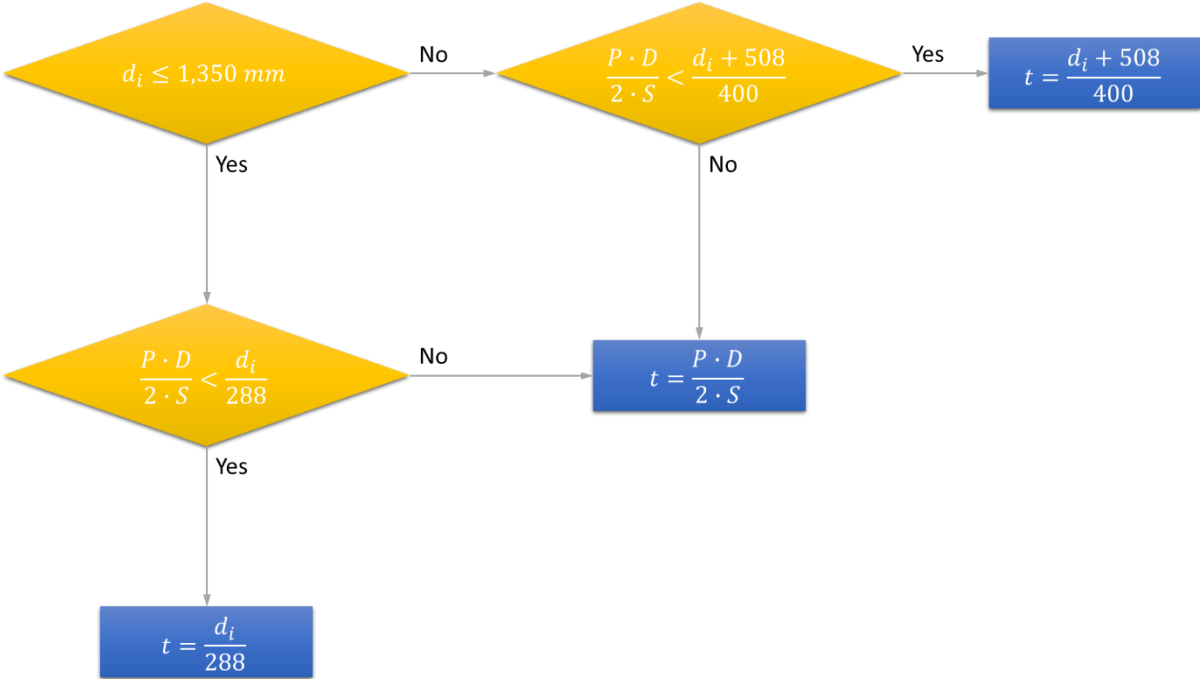
Figure 6.11: Design Conduit Pressure for Alignment Alternatives



6.6.1.2 Steel Pipe Thickness

The criterion and recommendations included in (American Water Works Association, 2004) were followed and the resulting process flowchart applied to calculate the steel pipe thickness is shown in Figure 6.12.

Figure 6.12: Calculation Flowchart of Steel Conduit Wall Thickness



With:

$$D = d_i + 2 \cdot t$$

$$S = 0.75 \cdot \sigma$$

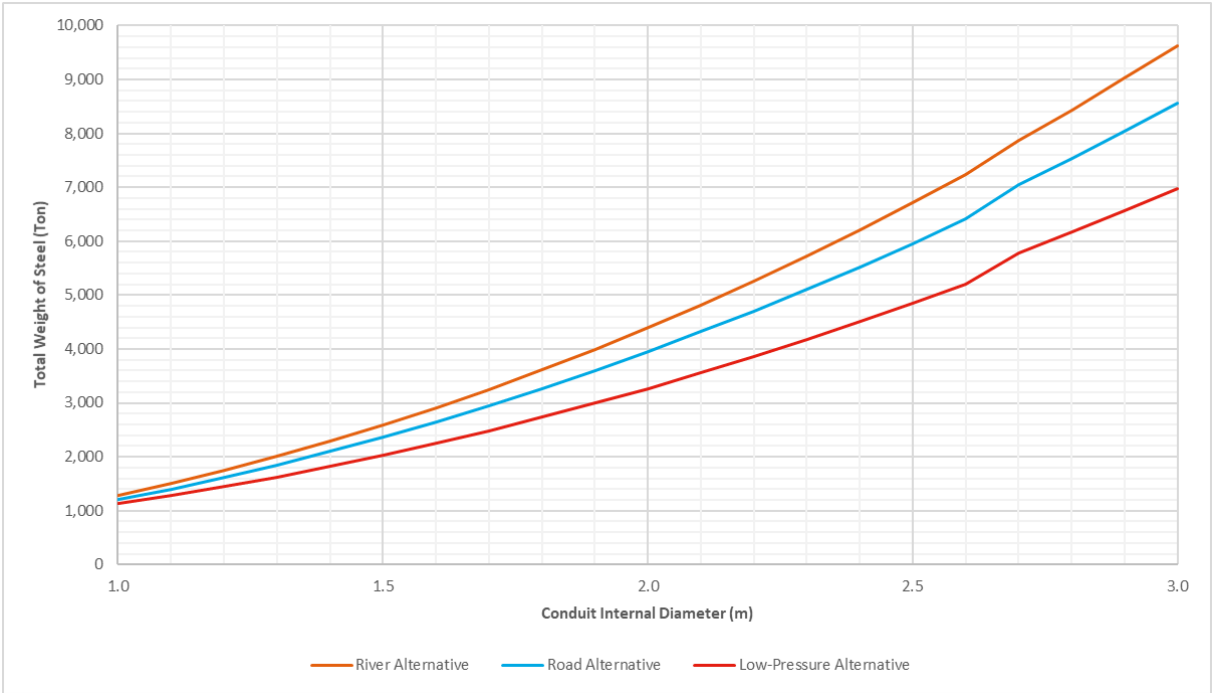
Where:

- d_i : Internal diameter of the conduit (mm).
- D : External diameter of the conduit (mm).
- P : Design pressure (MPa).
- S : Allowable design stress (MPa).
- t : Wall thickness (mm).
- σ : Yield stress of steel (MPa).

For the steel yield stress, a value of $\sigma = 248.2 \text{ MPa}$ was adopted, this corresponds to the typical value of an ASTM A36 / A36M carbon steel, which is commonly used in this type of conduits.

The resulting wall thickness for the three alignment alternatives was in the range from 8 mm up to 52 mm. In this regard, Figure 6.13 shows the total amount of steel needed for each alternative under analysis.

Figure 6.13: Total Required Weight of Steel for Alignment Alternatives Conduits



6.6.1.3 GRP Pipes

The GRP pipes were selected according to the nominal pressure class that governs their fabrication standard, that is, a PN6 pipe is designed to handle an internal pressure of up to 60 mWC approximately.

In this regard, six GRP pipe classes were considered: PN6, PN10, PN16, PN20, PN25, and PN32.

However, and looking at Figure 6.11, the maximum design pressure for the conduits is approximately 626 mWC. This means that it is not possible to design an alignment entirely in

GRP. In the last section of the conduit, where the design pressure exceeds 320 mWC, mandatorily the pipe material must be changed to steel until the conduit reaches the powerhouse.

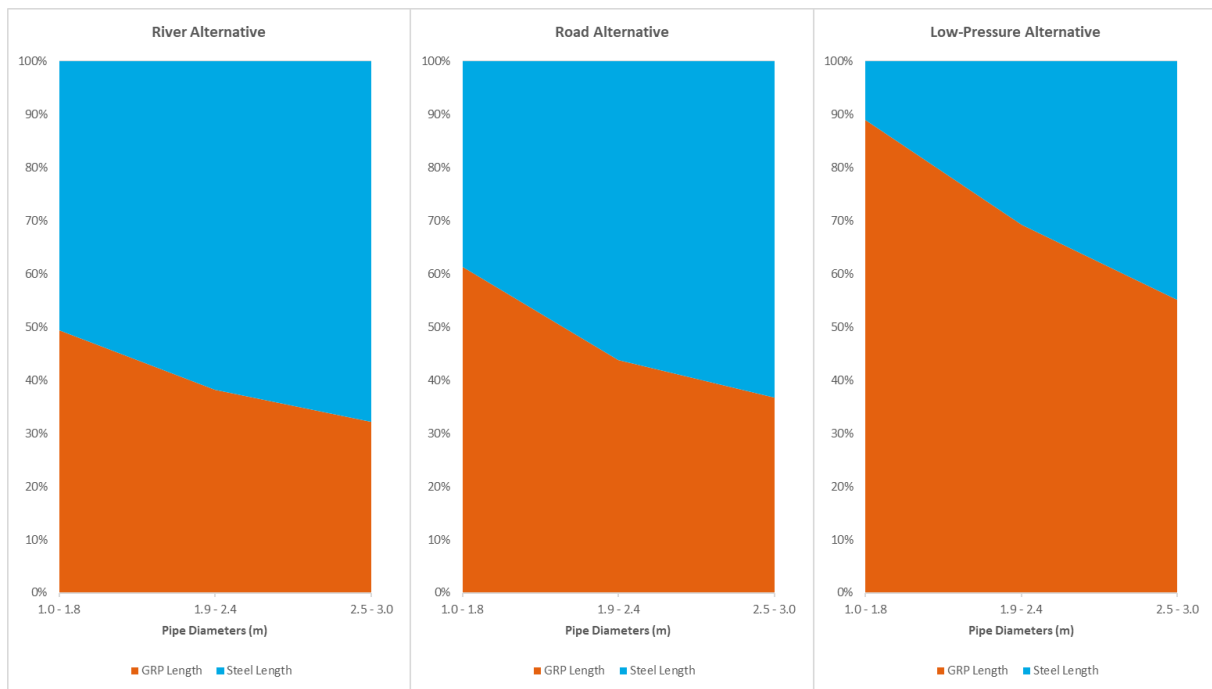
It is also important to mention that the GRP pipe suppliers reduce the maximum commercially available diameter as the nominal pressure class increases. After consulting the catalogs from several suppliers, the following distribution in Table 6.6 was considered:

Table 6.6: Maximum Commercially Available GRP Pipe Diameters

| GRP Nominal Pressure Class | Maximum Commercially Available Diameter (m) |
|-----------------------------------|--|
| PN6 | 3.4 |
| PN10 | 3.4 |
| PN16 | 3.4 |
| PN20 | 3.0 |
| PN25 | 2.4 |
| PN32 | 1.8 |

With these considerations, Figure 6.14 includes the percentage of the total lengths of GRP and Steel for each of considered alignment alternatives.

Figure 6.14: Percentage of the Conduit Length in GRP and Steel for Alignment Alternatives



6.6.1.4 Costs

As mentioned, the aim of the optimization is to find the pipe diameter that produces the minimum total cost, which is the addition of the pipe and energy losses cost.

For this, the following prices were considered:

- For steel, 1.90 USD/kg. This price was reported by Anpac Energía.
- For GRP, NVE cost curves Fig. 4.7.2 were used with a price update factor from Jan 2015 to Feb 2018 of 1.02 (Norges vassdrags-og energidirektorat, 2016).
- The energy sale price was considered at 60 USD/MWh. This price was reported by Anpac Energía.

6.6.2 Results

Figure 6.15, Figure 6.16 and Figure 6.17 shows the optimal diameter analysis results for the river, road, and low-pressure alternatives respectively.

Figure 6.15: Optimal Diameter for River Alternative

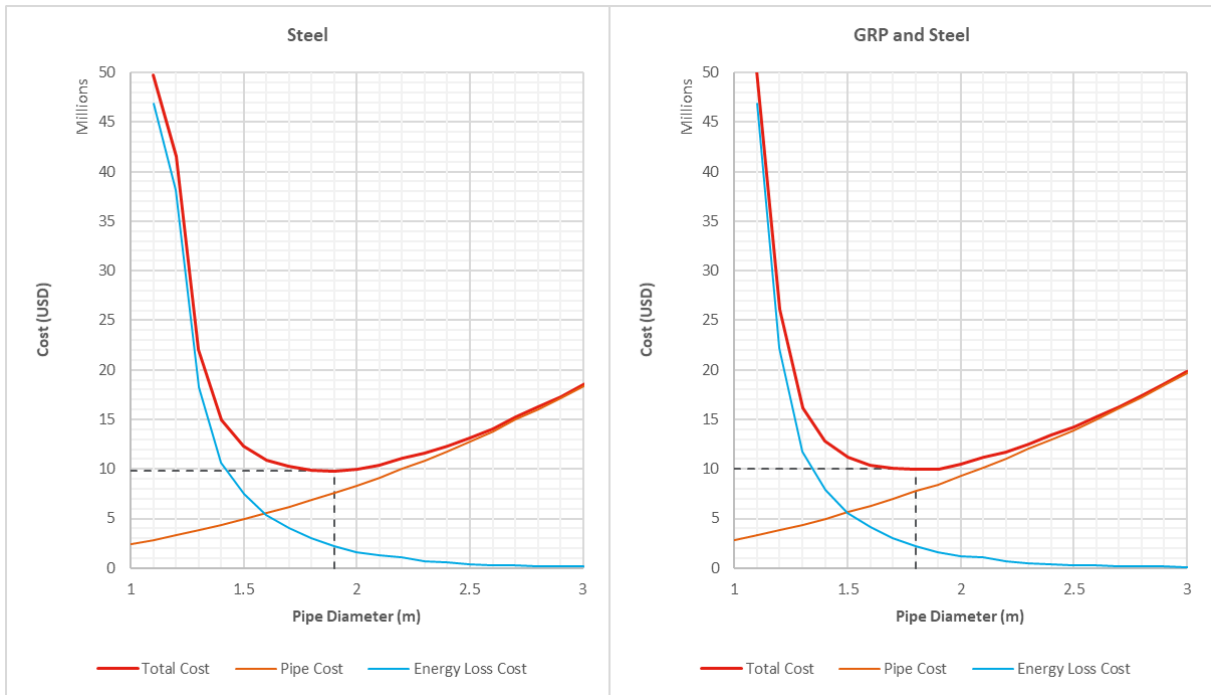


Figure 6.16: Optimal Diameter for Road Alternative

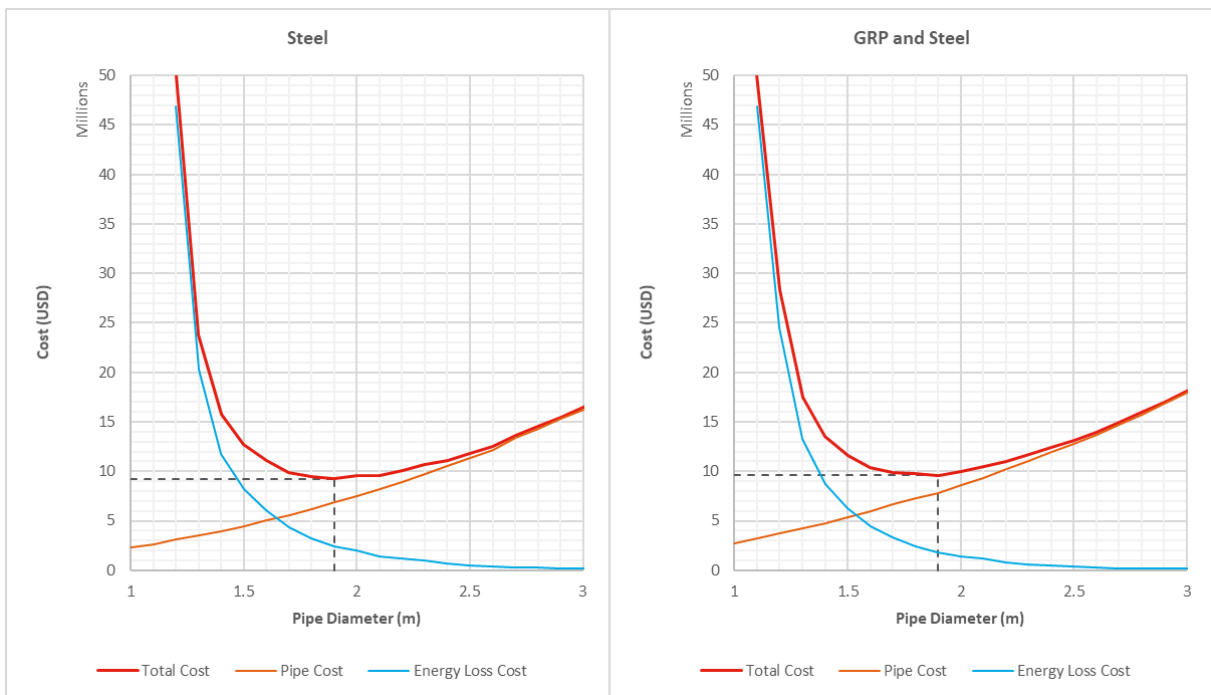
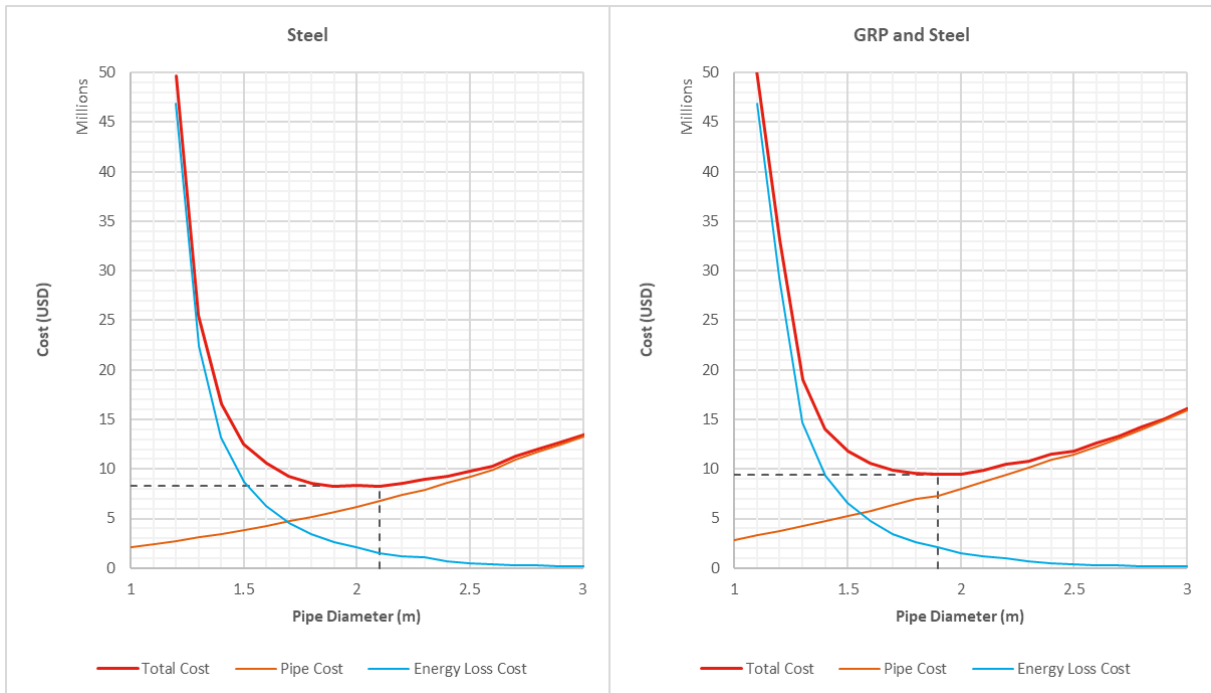


Figure 6.17: Optimal Diameter for Low-Pressure Alternative



The results from testing different combinations of turbine sizes for the river, road and low-pressure alternative, considering the optimal diameter of the conduits and its material, are shown in Figure 6.18, Figure 6.19 and Figure 6.20 respectively.

Figure 6.18: Turbine Size Combination for River Alternative

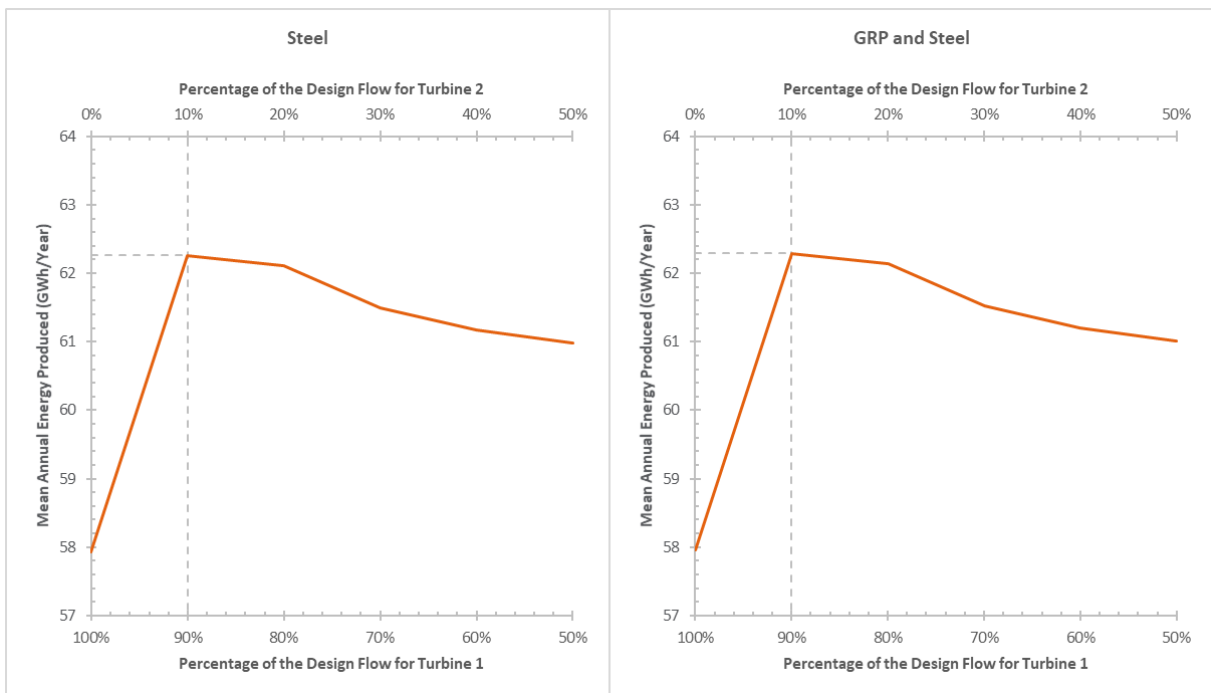


Figure 6.19: Turbine Size Combination for Road Alternative

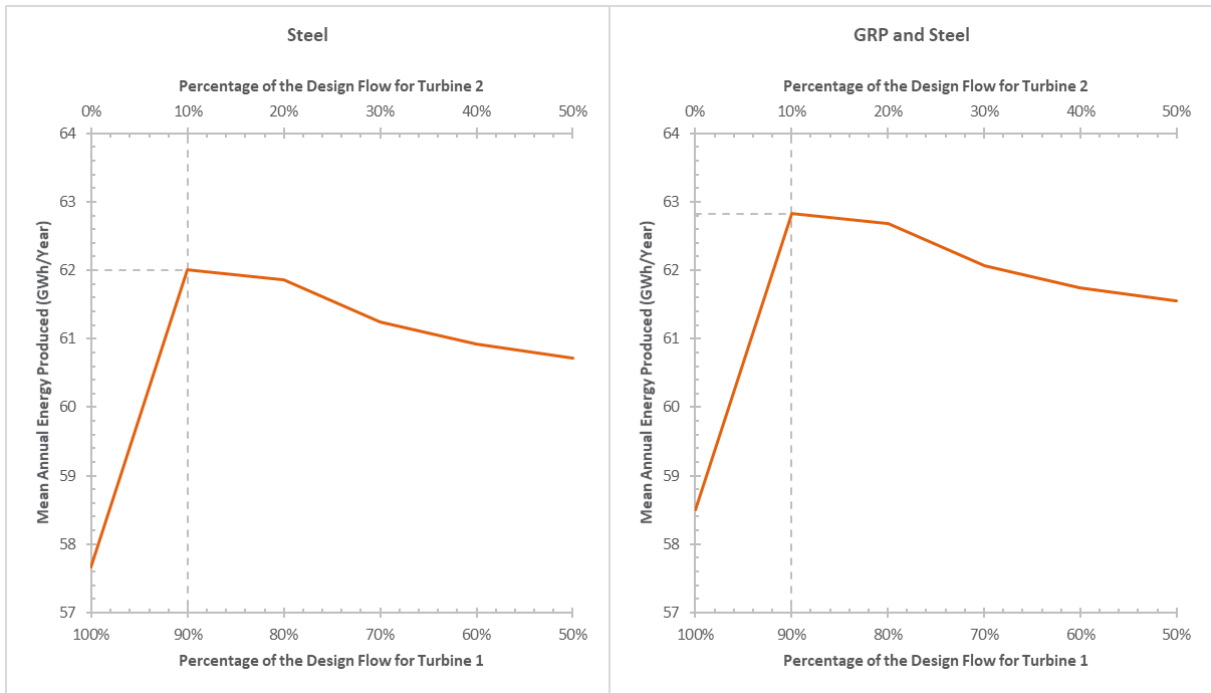
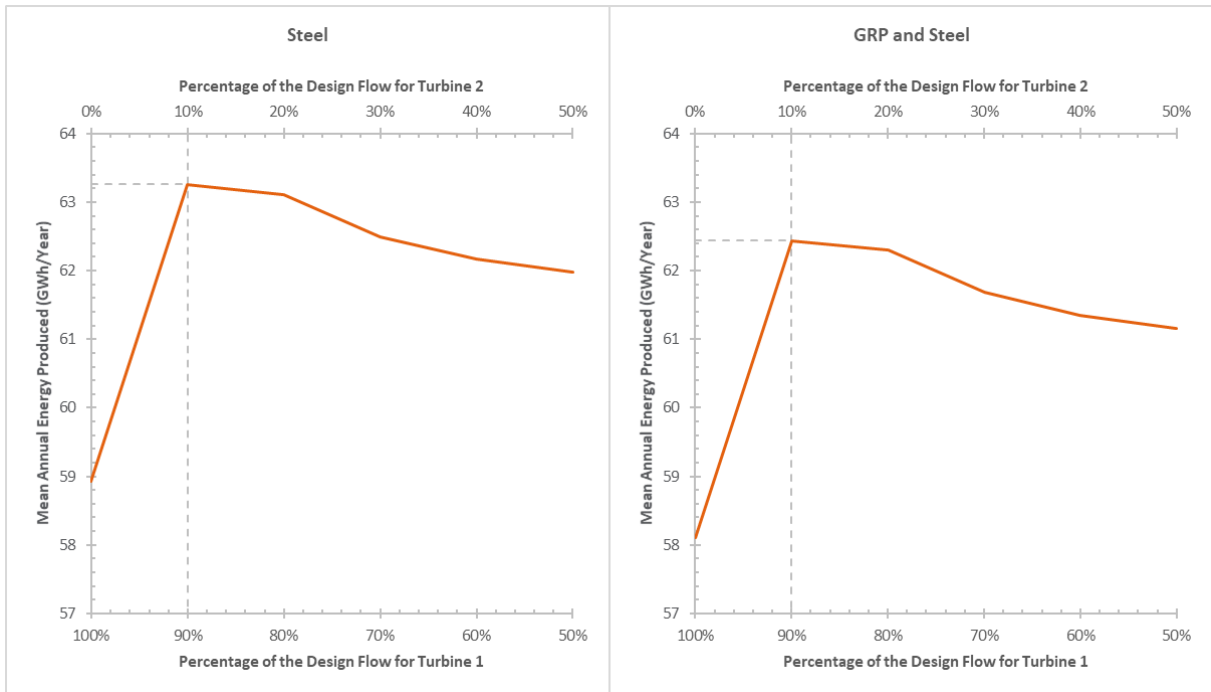


Figure 6.20: Turbine Size Combination for Low-Pressure Alternative



6.7 Minimum Flow Impact on Energy Generation

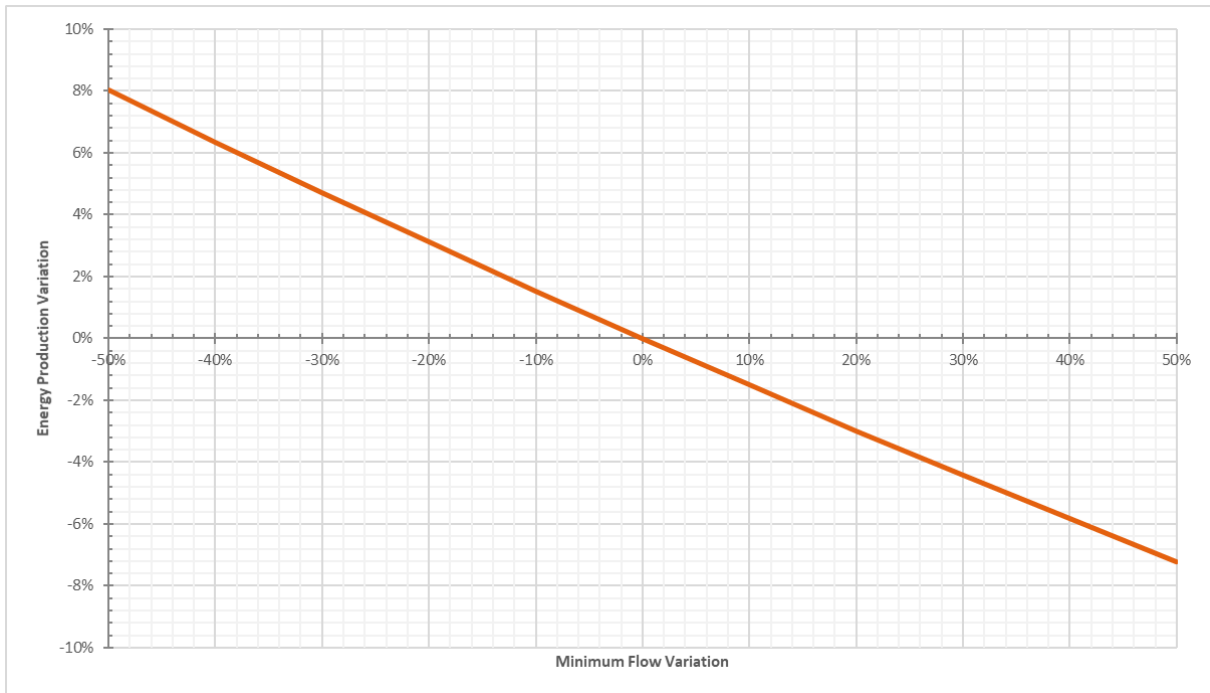
As mentioned above, water rights stipulate a minimum flow that must be bypassed through the intake to keep as much as possible the hydraulic conditions of the intervened river.

This minimum flow included in the water right has been determined by the DGA solely based on the hydrological statistics of the San José river, which means that it does not consider the potential consequences on the aquatic habitat conditions for the affected river section. In this regard, this environmental impact is later evaluated by the Environmental Assessment Service (SEA, Servicio de Evaluación Ambiental) once the pertinent permits are introduced to begin construction of the power plant.

Normally the SEA considers the minimum flow defined by the DGA as a starting point to define its own environmental flow, this means that the minimum flow defined by the DGA is usually increased by the SEA. This results in a decrease, on occasion of considerable magnitude, in the projected energy production of the power plant.

In this sense, a sensitivity analysis was carried out varying the minimum flows included in Table 6.1 within a range of $\pm 50\%$ to see the impact that this would have on the energy production. Figure 6.21 shows the result of this analysis for all the alternatives.

Figure 6.21: Minimum Flow Variation Impact on Energy Production



6.8 Results Summary and Final Remarks

A summary of the most relevant results obtained from the energy production model is included in Table 6.7.

From these results, the following comments arise:

- The design flow for all schemes is equal to 10 m³/s. This is 2.5 times the mean annual flow of the river.
- The greatest energy production power plant alternative is the low-pressure alignment with steel conduits.
- The road alternative with GRP and steel conduits is the second to have biggest energy production, followed closely by the low-pressure GRP and steel and the river alternative.
- The installed capacity values of the alternatives lie between 23 MW and 24 MW.
- All the alternatives have a mean capacity factor of 31%.
- The optimum diameter for the alternatives ranges from 1.8 m to 2.1 m.
- For the optimum diameter, the average flow velocity value is 3.5 m/s.
- The resulting combination for the size of the turbines is outstanding.

From the point of view of the discharges, and considering the duration curve of the inflow to the turbine (Figure 6.22), this means that Unit 2 (the smallest) will work 31% of the time approximately, that is, when the inflow is between 0.15 m³/s and 1.0 m³/s or when it exceeds 9.0 m³/s.

It is also important to mention that between the maximum flow of the smallest turbine (1.0 m³/s) and the minimum flow of the largest turbine (1.35 m³/s) there is a gap of 0.35 m³/s that will be spilled. In this regard, Figure 6.23 shows the mean annual spilled volume due to the turbine size, meaning, the inflow that had to be spilled because it was outside the working range of both turbine units. What this Figure shows is the selected turbine size combination minimize the annual spilled volume.

- Installing distinct size units increase the energy production by 2.1% in comparison with same-size turbines.
- The average head losses stand for an 8.5% of the gross head.
- If the minimum flow requirements increase up to 50%, compared with the actual conditions, the energy production will decrease by 7.2%. This is true for all alternatives with either steel or GRP and steel conduits.

Table 6.7: Energy Production Model Results Summary

| | Turbine Type Selection | | River Alternative | | Road Alternative | | Low-Pressure Alternative | |
|------------------------------------|------------------------|---------|-------------------|---------------|------------------|---------------|--------------------------|---------------|
| | Francis | Pelton | Steel | GRP and Steel | Steel | GRP and Steel | Steel | GRP and Steel |
| Basic Powerplant Data | | | | | | | | |
| Design Flow (m ³ /s) | 10.0 | 10.0 | 10.0 | 10.0 | 10.0 | 10.0 | 10.0 | 10.0 |
| Installed Capacity (MW) | 25.0 | 24.0 | 23.0 | 23.0 | 23.0 | 24.0 | 23.0 | 23.0 |
| Energy Production (GWh/Year) | 58.53 | 62.30 | 62.26 | 62.29 | 62.00 | 62.83 | 63.26 | 62.44 |
| Capacity Factor (%) | 26.7% | 29.6% | 30.9% | 30.9% | 30.7% | 29.9% | 30.1% | 31.0% |
| Penstock | | | | | | | | |
| Headrace Penstock Length (m) | 0 | 0 | 0 | 0 | 4,743 | 4,743 | 4,684 | 4,684 |
| High Pressure Penstock Length (m) | 4,747 | 4,747 | 4,747 | 4,747 | 158 | 158 | 493 | 493 |
| Inner Diameter (m) | 2.10 | 2.10 | 1.90 | 1.80 | 1.90 | 1.90 | 2.10 | 1.90 |
| Flow Velocity (m/s) | 2.89 | 2.89 | 3.53 | 3.93 | 3.53 | 3.53 | 2.89 | 3.53 |
| Turbine | | | | | | | | |
| Turbine Type | Francis | Pelton | Pelton | Pelton | Pelton | Pelton | Pelton | Pelton |
| Number of Units | 2 | 2 | 2 | 2 | 2 | 2 | 2 | 2 |
| Unit 1 Size | 50% | 50% | 90% | 90% | 90% | 90% | 90% | 90% |
| Unit 2 Size | 50% | 50% | 10% | 10% | 10% | 10% | 10% | 10% |
| Energy Losses | | | | | | | | |
| Intake Water Elevation (masl) | 1,813.0 | 1,813.0 | 1,813.0 | 1,813.0 | 1,813.0 | 1,813.0 | 1,813.0 | 1,813.0 |
| Turbine/Discharge Elevation (masl) | 1,529.4 | 1,531.5 | 1,531.5 | 1,531.5 | 1,531.5 | 1,531.5 | 1,531.5 | 1,531.5 |
| Gross Head (m) | 283.6 | 281.5 | 281.5 | 281.5 | 281.5 | 281.5 | 281.5 | 281.5 |
| Net Head (m) | 268.0 | 265.9 | 255.9 | 256.2 | 253.1 | 259.6 | 263.0 | 258.1 |
| Percentage of Gross Head | 5.5% | 5.5% | 9.1% | 9.0% | 10.1% | 7.8% | 6.6% | 8.3% |

Figure 6.22: Turbine Inflow Duration Curve

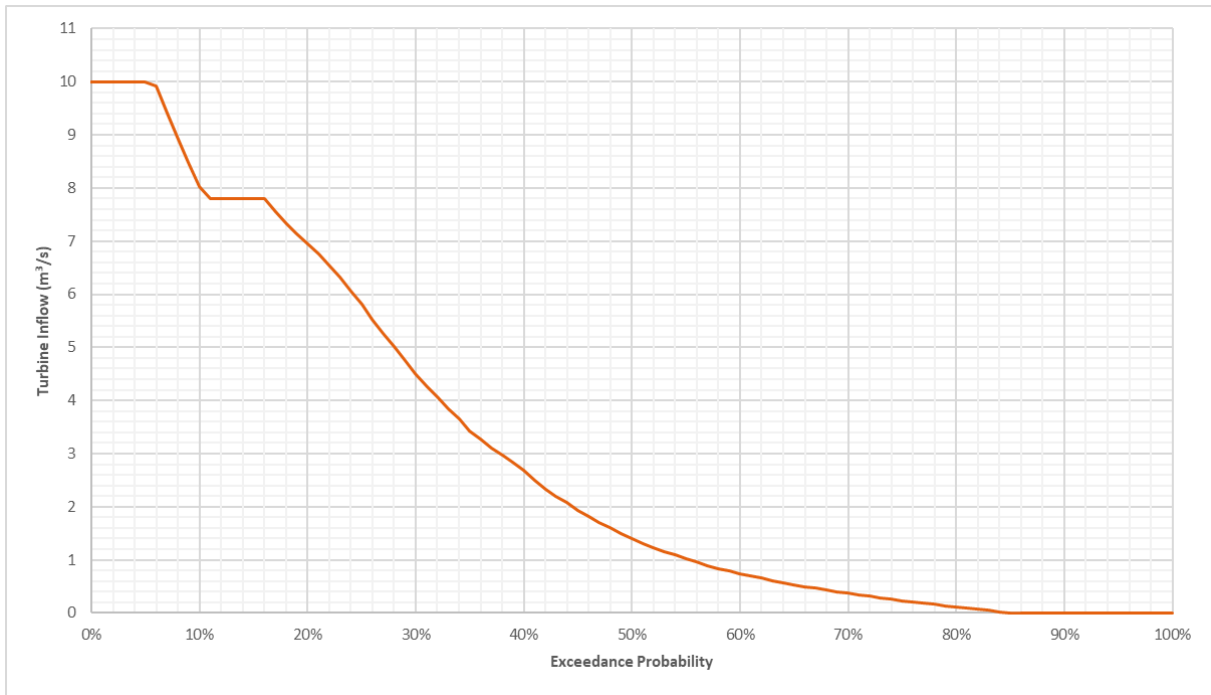
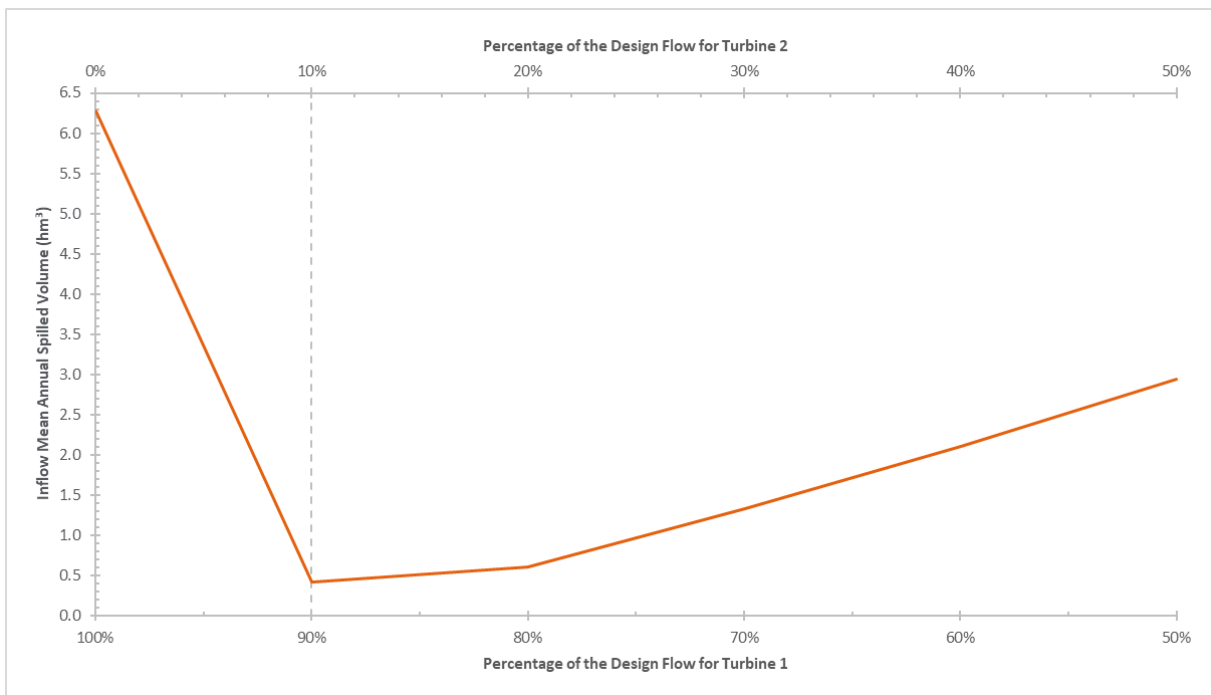


Figure 6.23: Spilled Volume of Inflow due to the Turbine Size Combination



(This page intentionally left blank)

7 Surge Chamber and Governor Stability Assessment

As mentioned before, a detailed analysis of the hydraulic transient phenomena and its management measures are beyond the scope of this Thesis, however, and considering a level of pre-feasibility engineering, the following points were analyzed.

7.1 Surge Chamber

In the description made of the alignment alternatives (Title 5.6.2), it was commented that the road and low-pressure alternatives have in its layout a surge chamber at the point of transition between the headrace conduit (low to medium pressure) and the penstock (high pressure).

For purposes of CAPEX, it was decided to pre-dimension this structure. To do this it should be remembered first that for the design pressure of the conduits it was decided an extra 20% of the static head include the effects of water hammer. Knowing that the gross head is equal to 281.5 m, this means that the maximum upsurge that can be inside the surge chamber should be 56.3 m.

With this consideration, the equation to calculate the maximum upsurge following instantaneously closing of the emergency valve in a frictionless system is (Chaudhry, 2014):

$$Z^* = Q \cdot \sqrt{\frac{L_t}{g \cdot A_S \cdot A_t}}$$

Where:

- Z^* : Maximum upsurge inside the surge chamber (m).
- Q : Design flow of the power plant (m³/s).
- L_t : Headrace conduit length (m).
- g : Gravitational acceleration (m/s²).
- A_S : Surge chamber cross-sectional area (m²).
- A_t : Headrace conduit cross-sectional area (m²).

Different surge chamber areas were tested until reaching an upsurge value of 56.3 m. Now, the resulting area was tested for stability by comparing it with the Thoma criterion, which expresses (Chaudhry, 2014):

$$A_{ST} = 0.01414 \cdot \frac{A_t^{5/3}}{n^2 \cdot H_n}$$

Where:

A_{ST} : Minimum surge chamber cross-sectional area (m²).

A_t : Headrace conduit cross-sectional area (m²).

n : Manning roughness coefficient for the headrace conduit.

H_n : Net head (m).

The parameters used, and the results are included in Table 7.1:

Table 7.1: Surge Chamber Pre-Dimensioning Results

| Parameter | Road Alternative | Low-Pressure Alternative |
|--|-------------------------|---------------------------------|
| Design flow (m ³ /s) | 10.0 | 10.0 |
| Net head (m) | 259.6 | 258.1 |
| Headrace conduit length (m) | 4,743 | 4,684 |
| Headrace conduit cross-sectional area (m ²) | 2.84 | 2.84 |
| Headrace conduit Manning roughness coefficient | 0.010 | 0.010 |
| Maximum surge chamber upsurge (m) | 54.6 | 54.2 |
| Maximum surge chamber upsurge elevation (masl) | 1,870 | 1,869 |
| Minimum surge chamber cross-sectional area (m ²) | 3.09 | 3.11 |
| Surge chamber cross-sectional area (m ²) | 5.73 | 5.76 |
| Surge chamber diameter (m) | 2.70 | 2.70 |
| Surge chamber length (m) | 308 | 32 |

For reference, Figure 7.1 and Figure 7.2 shows the disposition of the surge chamber in the road and low-pressure alternatives respectively.

Figure 7.1: Surge Chamber Alignment for Road Alternative

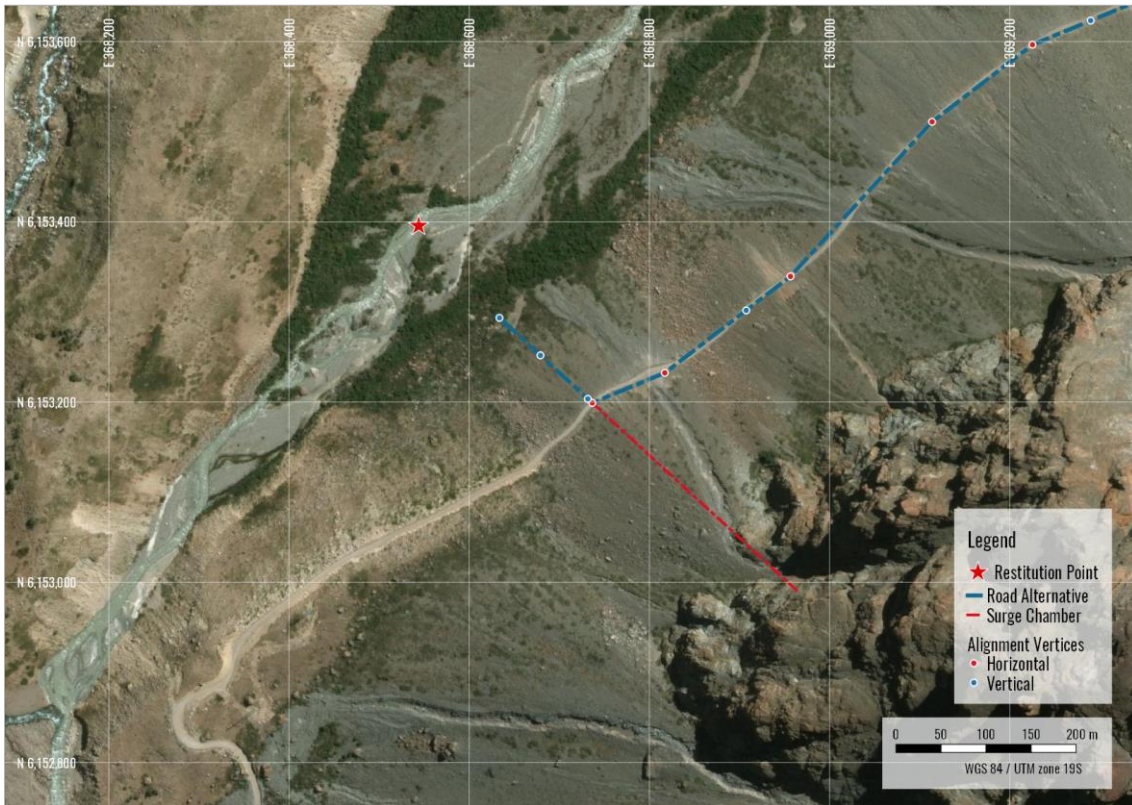
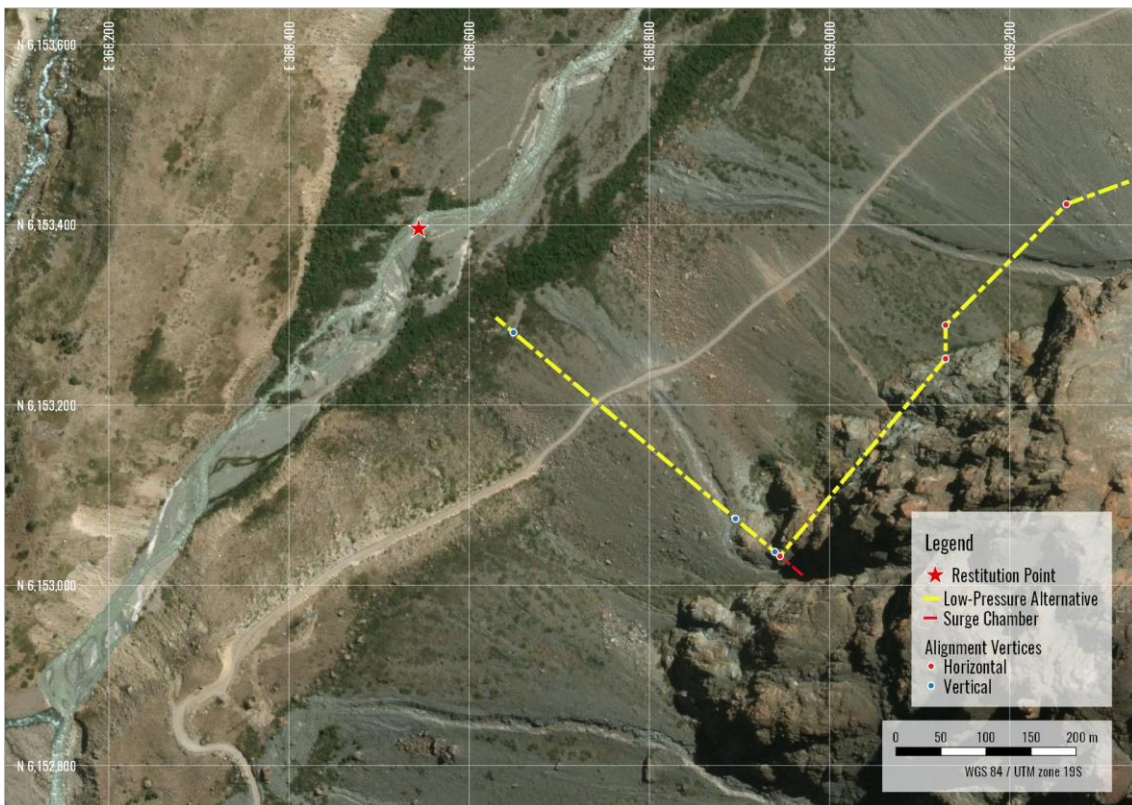


Figure 7.2: Surge Chamber Alignment for Low-Pressure Alternative



7.2 Governor Stability

The fundamental concept of electric production, in a very simplified way, is to achieve the rotation of a generator. The rotational speed of this electro-mechanical equipment must be in synchrony with the frequency of the electrical grid to which energy will be supplied.

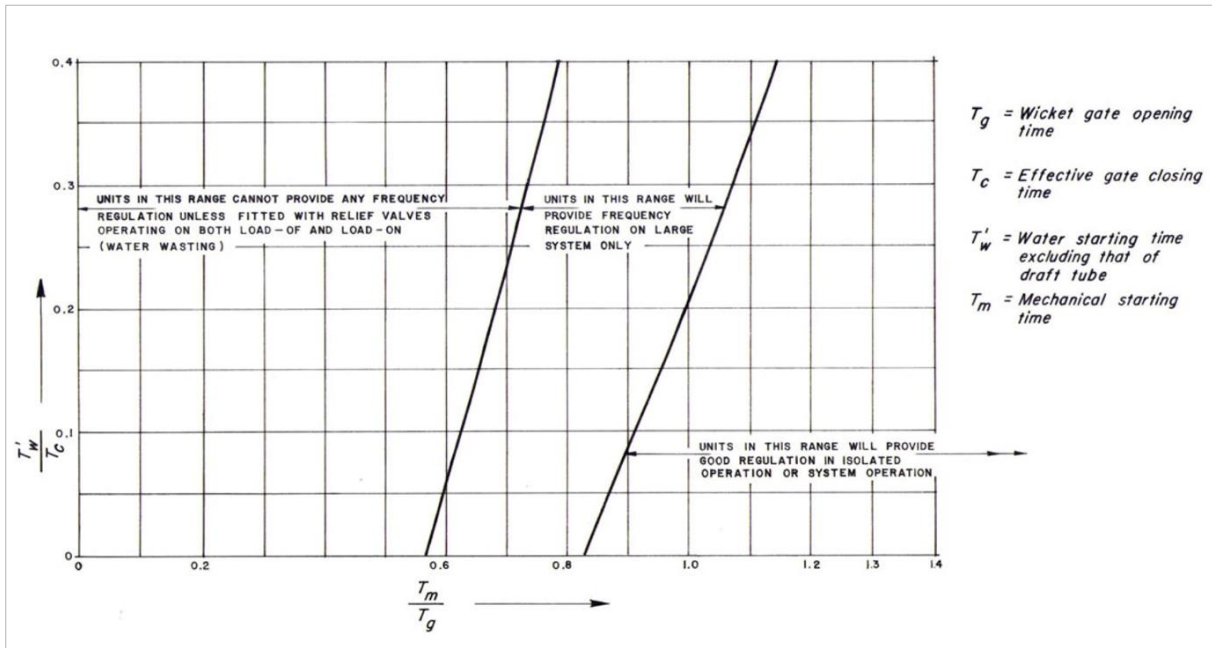
Since the operating conditions of the power plants vary over time, this synchronous rotational speed also suffers from variations which, depending on the size and amount of power plants in the grid, can affect the regulation of the electric frequency.

In the case of hydroelectric power plants, a governor is provided to keep the system constant by opening or closing the wicket gates as the turbine speed changes (Chaudhry, 2014).

Depending on the hydropower plant layout, the time it takes the governor to open or close the wickets gates, and therefore the time it takes to correct a deviation of the synchronous speed of the turbo-generator unit, will dictate whether the power plant is suitable to regulate the frequency of the electrical grid.

In order to make an assessment of the governor stability for the three alignment alternatives under study, the Gordon curves (Chaudhry, 2014)(Gordon, 1961) were used, which are shown in Figure 7.3 as a reference.

Figure 7.3: Gordon Stability Curves



Source: (Chaudhry, 2014)(Gordon, 1961)

To be able to use these curves it is necessary to calculate first the opening and closing times of the mechanical elements of the turbine, in addition to the hydraulic times linked to the flow inside the conduits. The steps taken to perform these calculations are explained next.

7.2.1 Synchronous Rotational Speed

The first step to assess the governor stability was to define the turbine synchronous rotational speed. This parameter was calculated using the following equation:

$$n_s = \frac{f \cdot 60}{Z_p}$$

Where:

- n_s : Synchronous rotational speed (rpm).
- f : Electrical grid frequency (Hz).
- Z_p : Number of poles pairs in the generator.

Having defined the design flow and the net head of the power plant, each type of turbine has a range of synchronous speeds for which its best efficiency can be achieved. The parameter that allows this evaluation is called the speed number and is calculated with the following expression:

$$\underline{\Omega} = \frac{\omega}{\sqrt{2 \cdot g \cdot H_n}} \cdot \sqrt{\frac{Q_T}{\sqrt{2 \cdot g \cdot H_n}}}$$

With:

$$\omega = \frac{2 \cdot \pi \cdot n_s}{60}$$

Where:

- $\underline{\Omega}$: Speed number.
- ω : Angular velocity (rad/s).
- g : Gravitational acceleration (m/s²).
- H_n : Net head (m).
- Q_T : Design discharge of the turbine (m³/s).
- n_s : Synchronous rotational speed (rpm).

In this regard, Table 7.2 shows the usual best efficiency range for the different types of turbines (Nielsen, n.d.):

Table 7.2: Speed Number Ranges for Best Efficiency in Turbines

| Turbine Type | Best Efficiency Speed Number Range |
|--------------|------------------------------------|
| Francis | 0,20 – 1,20 |
| Pelton | 0,05 – 0,15 |
| Kaplan | 1,50 – 2,50 |

With these considerations, Table 7.3 includes the results for the turbine synchronous rotational speed. It is important to mention that from each alignment alternative the greatest installed capacity or conduit diameter possibility along with the biggest unit was considered.

Table 7.3: Synchronous Rotational Speed and Speed Number for Pelton Turbines

| Parameter | River Alternative | Road Alternative | Low-Pressure Alternative |
|---|-------------------|------------------|--------------------------|
| Design discharge of the turbine (m ³ /s) | 9.0 | 9.0 | 9.0 |
| Net head (m) | 255.9 | 259.6 | 263.0 |
| Electrical grid frequency (Hz) | 50 | 50 | 50 |
| Number of poles pairs in the generator | 11 | 11 | 11 |
| Synchronous rotational speed (rpm) | 272.7 | 272.7 | 272.7 |
| Speed number | 0.144 | 0.142 | 0.141 |

7.2.2 Inertia of Electro-Mechanical Elements

To estimate the total inertia of the turbo-generator group, the following expressions were used (Chaudhry, 2014):

- Generator Inertia:

$$I_G = 15,000 \cdot \left(\frac{S}{n_s^{1.5}} \right)^{1.25}$$

With:

$$S = \frac{P_T \cdot 10^3}{P_f}$$

- Turbine Inertia:

$$I_T = 1,446 \cdot \left(\frac{P_T \cdot 10^3}{n_s^{1.5}} \right)^{1.25}$$

Where:

- I_G : Generator inertia (kg·m²).
- I_T : Turbine inertia (kg·m²).
- S : Generator apparent power (kVA).
- n_s : Synchronous rotational speed (rpm).
- P_T : Turbine installed capacity (MW).
- P_f : Power factor.

The estimated turbo-generator inertia results are included in Table 7.4:

Table 7.4: Total Inertia for the Turbo-Generator Group

| Parameter | River Alternative | Road Alternative | Low-Pressure Alternative |
|--|-------------------|------------------|--------------------------|
| Turbine installed capacity (MW) | 20.7 | 21.6 | 21.6 |
| Synchronous rotational speed (rpm) | 272.7 | 272.7 | 272.7 |
| Power factor | 0.95 | 0.95 | 0.95 |
| Generator apparent power (kVA) | 21,789 | 22,737 | 22,737 |
| Generator inertia (kg·m ²) | 107,624 | 113,504 | 113,504 |
| Turbine inertia (kg·m ²) | 9,731 | 10,262 | 10,262 |
| Total inertia (kg·m ²) | 117,355 | 123,766 | 123,766 |

7.2.3 Water and Mechanic Starting Times

The water starting time is defined as the time to accelerate the flow inside a conduit from zero to its nominal velocity under a constant pressure head (Chaudhry, 2014). The following expression was used to calculate it:

$$T_w = \frac{Q_T}{g \cdot H_n} \cdot \sum_{i=1}^m \frac{L_i}{A_i}$$

Where:

- T_w : Water starting time (s).
 Q_T : Design discharge of the turbine (m³/s).
 g : Gravitational acceleration (m/s²).
 H_n : Net head (m).
 L_i : Length of the penstock section (m)
 A_i : Inner area of the penstock section (m²).

Similarly, the mechanical starting time is the time in which the unit is accelerated from zero to a rated speed when rated torque is applied (Chaudhry, 2014). To calculate it the following expression was used:

$$T_m = \frac{I \cdot n_s^2}{91.2 \cdot 10^6 \cdot P_T}$$

Where:

- T_m : Mechanical starting time (s).
 I : Total inertia of turbo-generator group (kg·m²).
 n_s : Synchronous rotational speed (rpm).
 P_T : Turbine installed capacity (MW).

The used parameters and the results are included in Table 7.5.

Table 7.5: Hydraulic and Mechanical Starting Times

| Parameter | River Alternative | Road Alternative | Low-Pressure Alternative |
|---|-------------------|------------------|--------------------------|
| Design discharge of the turbine (m ³ /s) | 20.7 | 21.6 | 21.6 |
| Net head (m) | 255.9 | 259.6 | 263.0 |
| Penstock length (m) | 4,747 | 158 | 493 |
| Inner penstock area (m ²) | 2.84 | 2.84 | 3.46 |
| Turbo-generator group inertia (kg·m ²) | 117,355 | 123,766 | 123,766 |
| Synchronous rotational speed (rpm) | 272.7 | 272.7 | 272.7 |
| Turbine installed capacity (MW) | 20.7 | 21.6 | 21.6 |

| Parameter | River Alternative | Road Alternative | Low-Pressure Alternative |
|------------------------------|--------------------------|-------------------------|---------------------------------|
| Water starting time (s) | 6.0 | 0.2 | 0.5 |
| Mechanical starting time (s) | 4.6 | 4.7 | 4.7 |

7.2.4 Wicket, Gate Times, and Governor Stability Results

Once the water and mechanical starting times were defined, to use Gordon curves (Figure 7.3) is necessary to estimate the effective gate-closing and wicket-gate opening time.

The wicket-gate opening time, as suggested by (Chaudhry, 2014), was defined as the effective gate-opening time plus 1.5 s to include the cushion stroke time.

The same effective gate-opening and closing time were considered, and to define them a trial and error procedure was done until the coordinates in the Gordon stability curve were set on the boundary between the regions of “frequency regulation on large system only” and “good regulation in isolated operation or system operation”. Any effective gate-opening and closing value greater than the one picked will allocate the governor stability in the “frequency regulation on large system only” region, on the contrary, a smaller number will move the result to the “good regulation in isolated operation or system operation” region.

The resulting effective gate-opening and closing times for each alignment alternative are included in Table 7.6, while Figure 7.4, Figure 7.5 and Figure 7.6 show the results plotted in the Gordon curves for each alternative.

Table 7.6: Gate Operation Time and Gordon Curves Stability Parameters

| Parameter | River Alternative | Road Alternative | Low-Pressure Alternative |
|-----------------------------------|--------------------------|-------------------------|---------------------------------|
| Gate opening and closing time (s) | 15.0 | 3.9 | 3.5 |
| Wicket gate opening time (s) | 16.5 | 5.4 | 5.0 |
| T_m/T_g | 0.28 | 0.87 | 0.93 |
| T_w/T_c | 0.40 | 0.05 | 0.14 |

Figure 7.4: Governor Stability Result for River Alternative

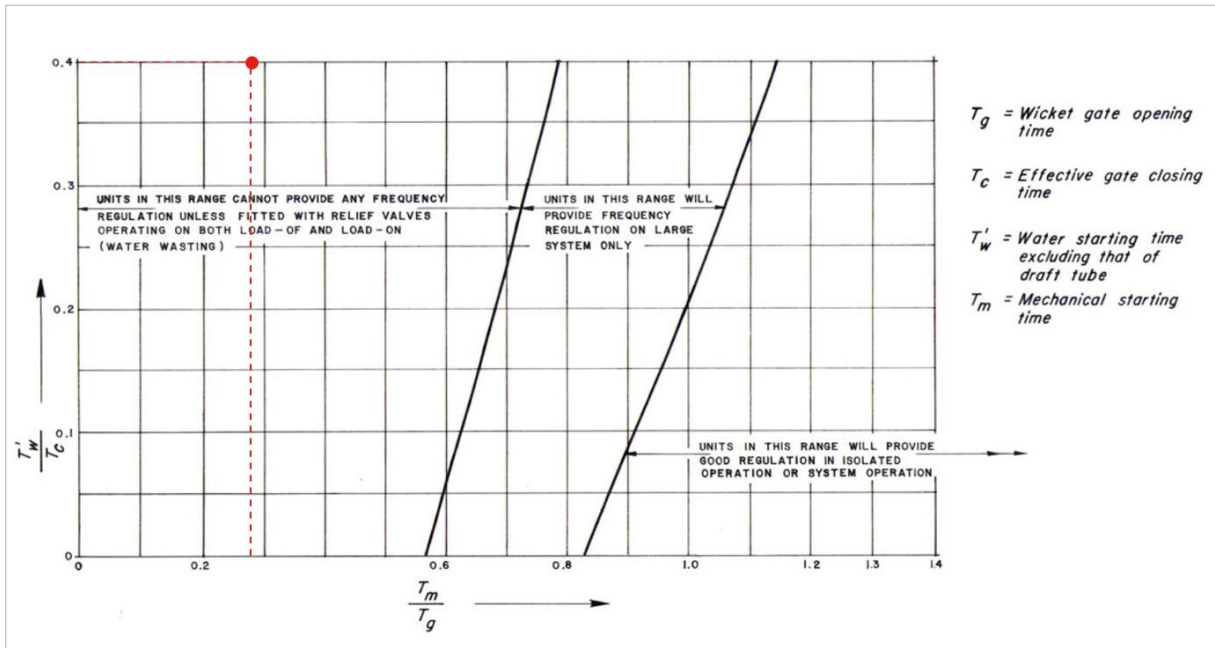


Figure 7.5: Governor Stability Result for Road Alternative

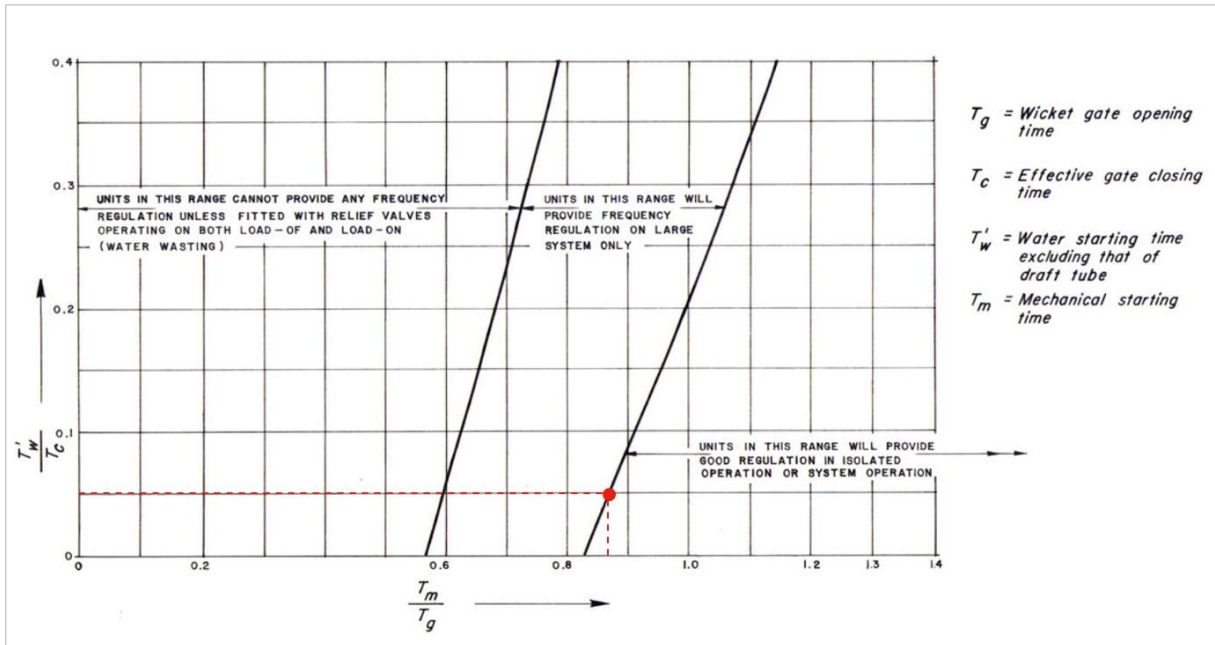
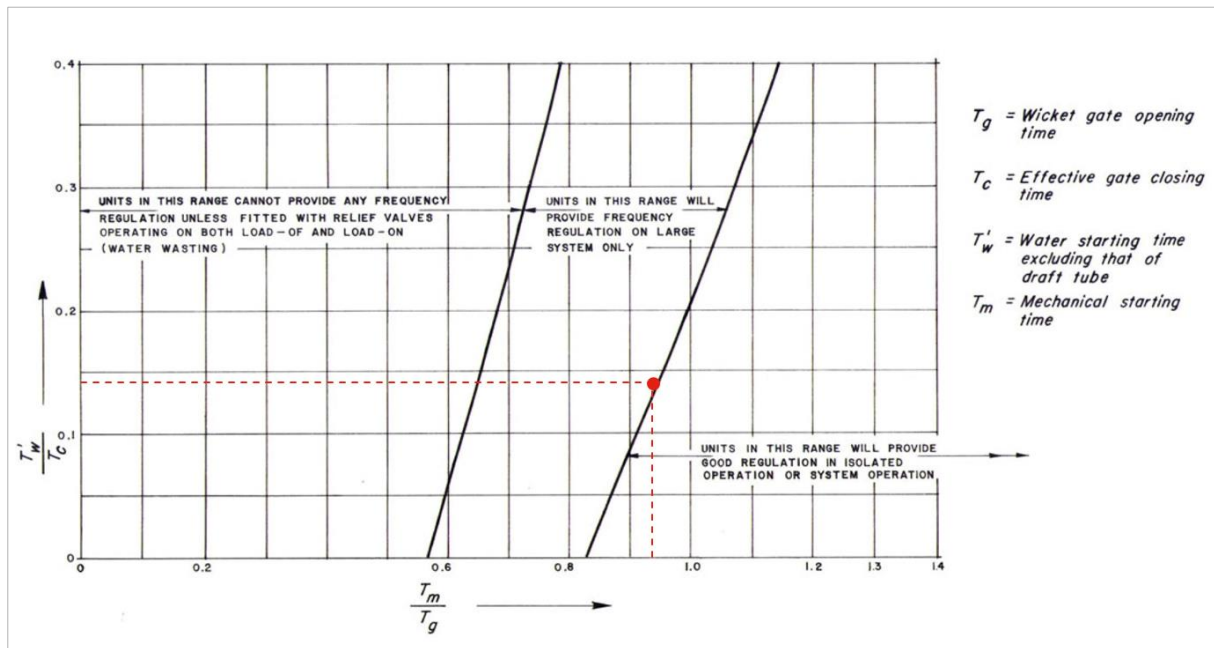


Figure 7.6: Governor Stability Result for Low-Pressure Alternative



7.3 Final Remarks

It is particularly important to note that in a later stage of engineering for this project a detailed study of the effects of hydraulic transients in the system must be made, placing special emphasis on the extreme pressure envelope and its damping mechanisms.

Although this phenomenon affects the three alignment alternatives, the river alternative is considered especially susceptible due to its long pressure conduit.

Regarding the governor stability results, only the road and low-pressure alternative can bring frequency regulation even to isolated grids.

The great length of the river alternative prevents it to perform any type of electrical frequency regulation to the network to which it will be connected. To adapt the design of this alternative to provide frequency regulation to large networks, one possibility could be adding a flywheel to the turbo-generator with the idea of increasing its inertia, however, this would require that this element had an inertia greater than 210,000 kg·m², that is, 1.8 times the value of the turbo-generator, which makes it unfeasible. Another possibility could involve the construction of a surge chamber with the aim of shortening the penstock to a maximum length of 1,400 m.

8 Cost Analysis

To be able to compare the alignment alternatives from a financial point of view, a CAPEX estimation for each one of them was carried out.

If it is not explicitly mentioned, all costs were calculated using the curves prepared by NVE with a price level on January 2010 (SWECO Norge AS, 2012b, 2012a). To update the prices, a factor of 1.37 derived from the price of the US dollar to January 2018 was applied.

The analysis carried out considered the following elements.

8.1 Direct Costs

8.1.1 Intake

For all the alternatives, a concrete gravity dam with a height of 3.5 m and a length of 35 m was considered. The following items were included:

- Stripping, clearing, and grubbing and removal of material.
- Concrete, reinforcement, and its formwork.
- Four trashracks of 5.0 m² each.
- One sliding gate of 10 m².
- Contractor expenses.

8.1.2 Settling Basin and Forebay

Considering the design showed in the Title 5.5.2, the following items were included:

- Stripping, clearing, and grubbing and removal of material.
- Terrain excavations.
- Settling basin and forebay concrete, reinforcement, and its formwork.
- Two flushing gates of 2.5 m² for each chamber of the settling basin.
- One trashrack and one sliding emergency gate of 4.0 m² each in the forebay.

8.1.3 Headrace Conduit and Penstock

This item was considered the main differentiator between the alternatives. The following elements were included:

- Each alternative had two CAPEX: One for steel pipes and the second for the combination of GRP and steel. The optimal diameter included in Table 6.7 was considered.
- For steel pipes, a price of 1.90 USD/kg reported by Anpac Energía was used.
- The river and road alternatives considered trenches of 6.0 m in depth and a basal width of 2.5 m. In the low-pressure alternative, the depth of the trench was 5.0 m.
- The river and road alternatives had 80% of the trench excavated in soil and the rest 20% in rock. The low-pressure alternative has 65% in soil and 35% in rock.
- Due to its location in the floodplains of San José river, a total of 655 m critical sections of the river alternative penstock distributed along its alignment were encapsulated in concrete to protect it against potential floods or terrain landslides.
- As explained in Title 7.1, the road and low-pressure alternative included the cost of a surge chamber.
- All alternatives included the contractor expenses.

8.1.4 Powerhouse

- The turbine cost including a distributor pipe, inlet valve, and frequency governor.
- Electro-technical equipment was considered including control-auxiliary system, two power units, outgoing lines from the plant, switchgear of a conventional type with a single bus bar and one circuit breaker.
- Miscellaneous mechanical equipment such as hall crane, cooling, and drainage system.
- Civil works cost for the powerhouse building itself and its discharge channel. This cost was derived from similar Chilean projects.
- The transmission line cost was not included because a connection to the existing line coming from San Andrés was considered.

8.2 Indirect Costs

For the mechanical and electrical equipment of the project, the following percentages, taken from other Chilean projects with similar characteristics as Piedras Negras, were added to their direct cost to cover the following aspects:

- A 5.0% of all prefabricated elements (i.e.: trashracks, gates, pipes, turbines, etc.) to include transport and insurance.
- Items manufactured outside Chile (i.e.: turbines and electro-technical equipment) included 4.0% for customs and taxes.
- Mechanical equipment such as gates, turbines and the miscellaneous powerhouse equipment considered 3.0% for spare parts.

The future project stages and its engineering were considered with the following percentages applied to the total direct cost (SWECO Norge AS, 2012).

- 1.5% for the pre-engineering phase.
- 2.5% for tender documents.
- 8.0% for detailed engineering.
- 8.0% for local construction management.

With experience in similar projects in Chile, a price of USD 1.6 million was considered to cover the power plant commissioning costs.

Finally, the costs associated with all personnel directly employed by Anpac Energía, or by contracting for work that is involved in the project such as administrators, technicians, consultants, human resources, etc. were considered as "owner's costs" and represent 2.0% of the total sum of direct and indirect costs till this point.

8.3 Unforeseen Expenses

To cover any unforeseen cost during the construction of the Piedras Negras power plant, or cost not contemplated in the CAPEX calculation, an added 20% of the sum of the direct and indirect costs was considered.

8.4 Results

Table 8.1, Table 8.2 and Table 8.3 include the main cost results values for the river, road, and low-pressure alternatives respectively.

Table 8.1: Cost Results for River Alternative

| Item | Steel Option | GRP and Steel Option |
|--------------------------------------|---------------------|-----------------------------|
| Intake (MM USD) | 0.8 | 0.8 |
| Settling Basin & Forebay (MM USD) | 2.5 | 2.5 |
| Headrace Conduit & Penstock (MM USD) | 30.7 | 33.9 |
| Powerhouse (MM USD) | 11.7 | 11.7 |
| Direct Costs Total (MM USD) | 45.7 | 48.9 |
| Indirect Costs Total (MM USD) | 13.7 | 14.8 |
| Unforeseen Expenses (MM USD) | 11.9 | 12.7 |
| Total (MM USD) | 71.3 | 76.4 |

Table 8.2: Cost Results for Road Alternative

| Item | Steel Option | GRP and Steel Option |
|--------------------------------------|---------------------|-----------------------------|
| Intake (MM USD) | 0.8 | 0.8 |
| Settling Basin & Forebay (MM USD) | 2.5 | 2.5 |
| Headrace Conduit & Penstock (MM USD) | 32.3 | 37.2 |
| Powerhouse (MM USD) | 11.7 | 12.1 |
| Direct Costs Total (MM USD) | 47.3 | 52.6 |
| Indirect Costs Total (MM USD) | 14.1 | 15.7 |
| Unforeseen Expenses (MM USD) | 12.3 | 13.7 |
| Total (MM USD) | 73.7 | 81.9 |

Table 8.3: Cost Results for Low-Pressure Alternative

| Item | Steel Option | GRP and Steel Option |
|--------------------------------------|--------------|----------------------|
| Intake (MM USD) | 0.8 | 0.8 |
| Settling Basin & Forebay (MM USD) | 2.5 | 2.5 |
| Headrace Conduit & Penstock (MM USD) | 33.0 | 36.6 |
| Powerhouse (MM USD) | 12.1 | 11.7 |
| Direct Costs Total (MM USD) | 48.4 | 51.6 |
| Indirect Costs Total (MM USD) | 14.3 | 15.3 |
| Unforeseen Expenses (MM USD) | 12.5 | 13.4 |
| Total (MM USD) | 75.2 | 80.3 |

The same costs included in the prior Tables are graphically showed next.

Figure 8.1: Cost Results for River Alternative

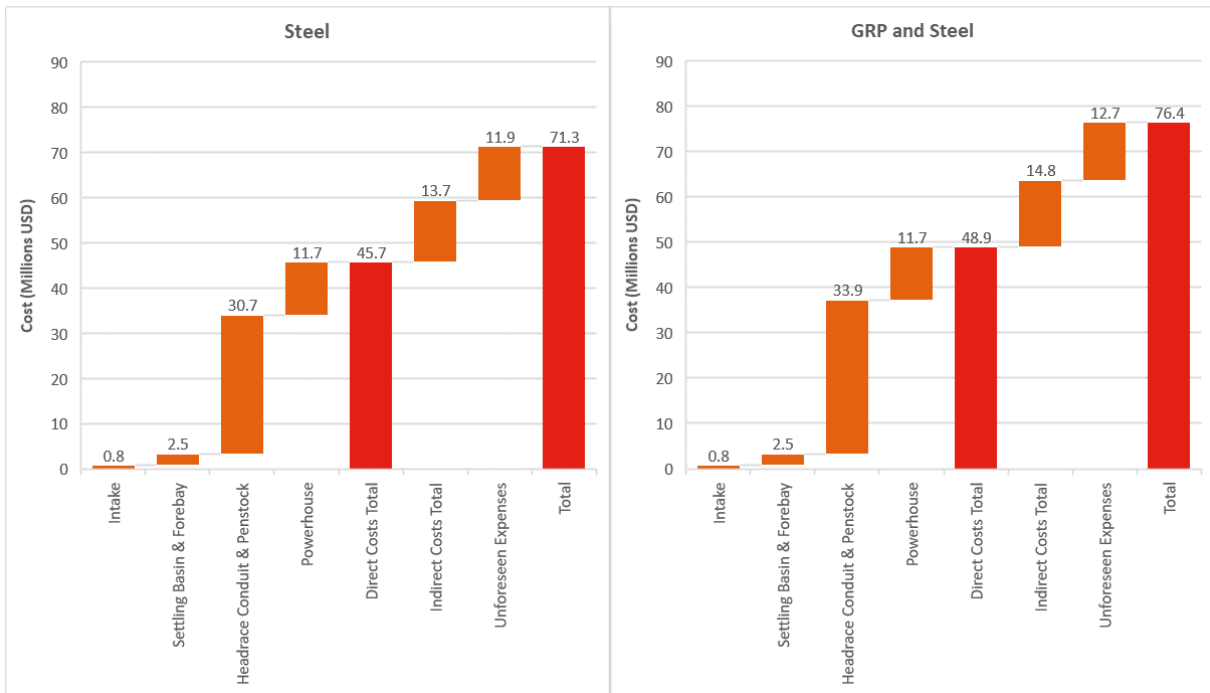


Figure 8.2: Cost Results for Road Alternative

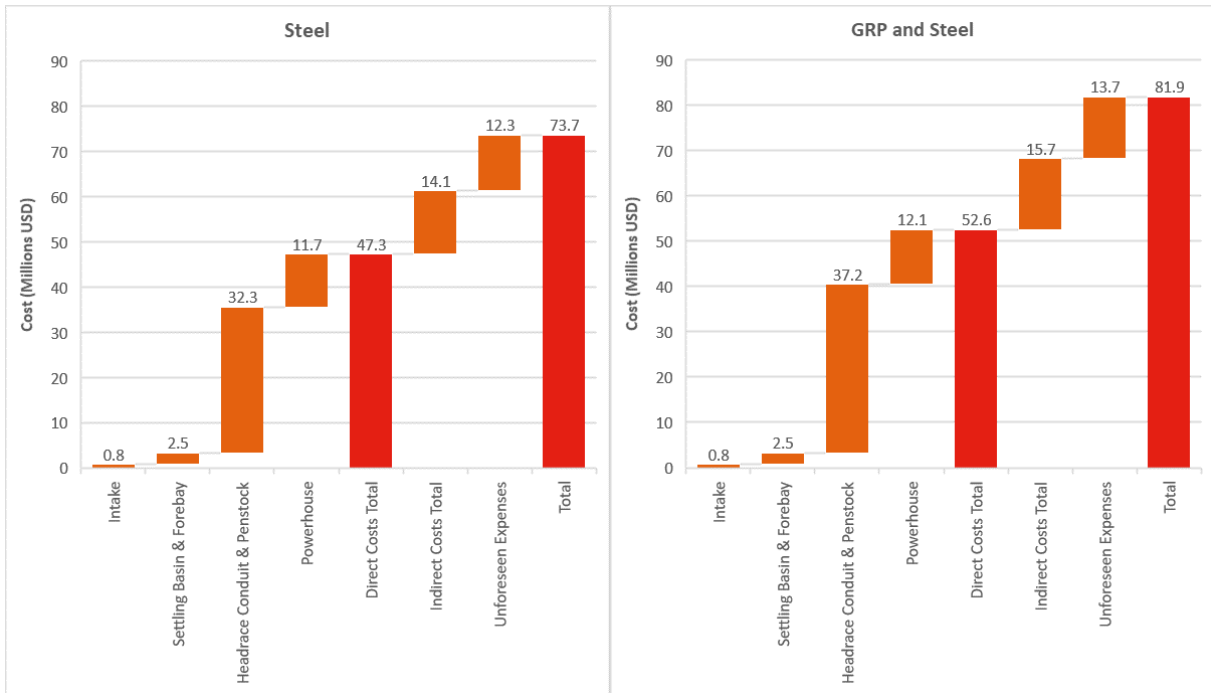
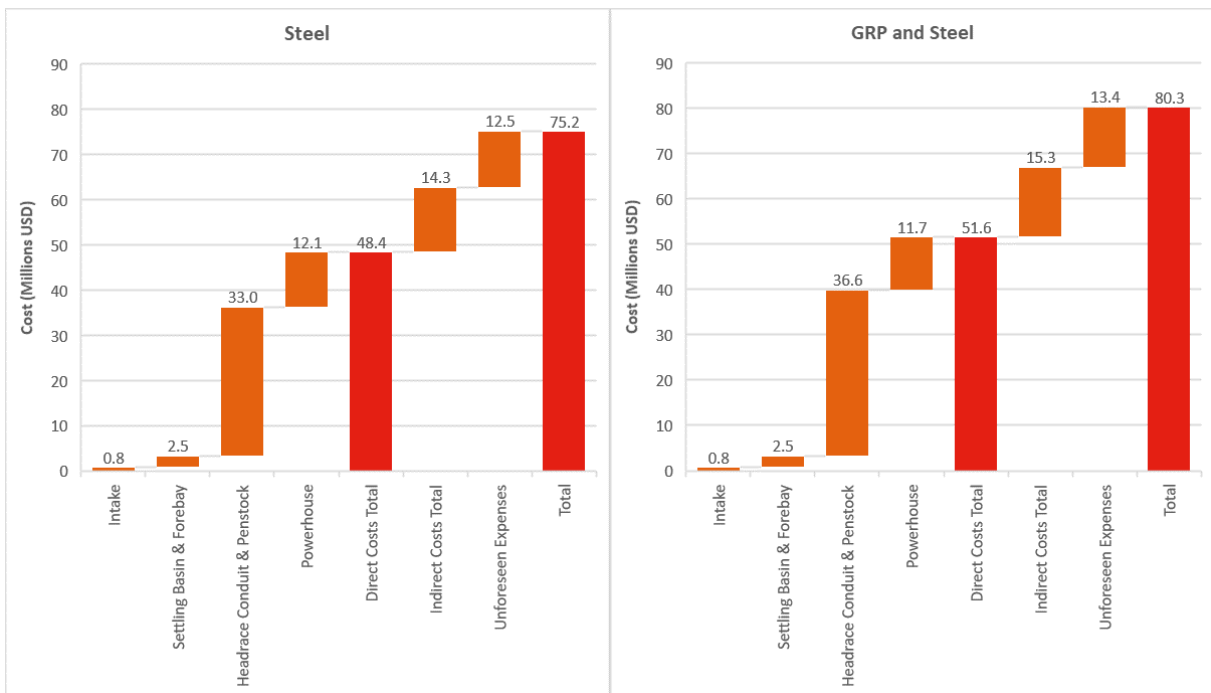


Figure 8.3: Cost Results for Low-Pressure Alternative



The detailed cost analysis Tables are included in Appendix VIII

Observing these values, and as expected, the most expensive item of the power plant alternatives is given by the headrace conduit and penstock, reaching an average of 44% of the total cost of the power plant.

As a reference, the top 5 of the most expensive items of direct costs are listed below by alternative.

- River and Road Alternatives:
 1. Headrace conduit and penstock contractor costs
 2. Pipe cost.
 3. Powerhouse electrotechnical equipment.
 4. Large turbine unit.
 5. Trench in the soil for the headrace conduit and penstock.

- Low-Pressure Alternative
 1. Headrace conduit and penstock contractor costs
 2. Pipe cost.
 3. Powerhouse electrotechnical equipment.
 4. Trench in rock for the headrace conduit.
 5. Large turbine unit.

Finally, if energy generation is considered, it is possible to obtain the unit cost of energy production for each alternative. This is included in Table 8.4.

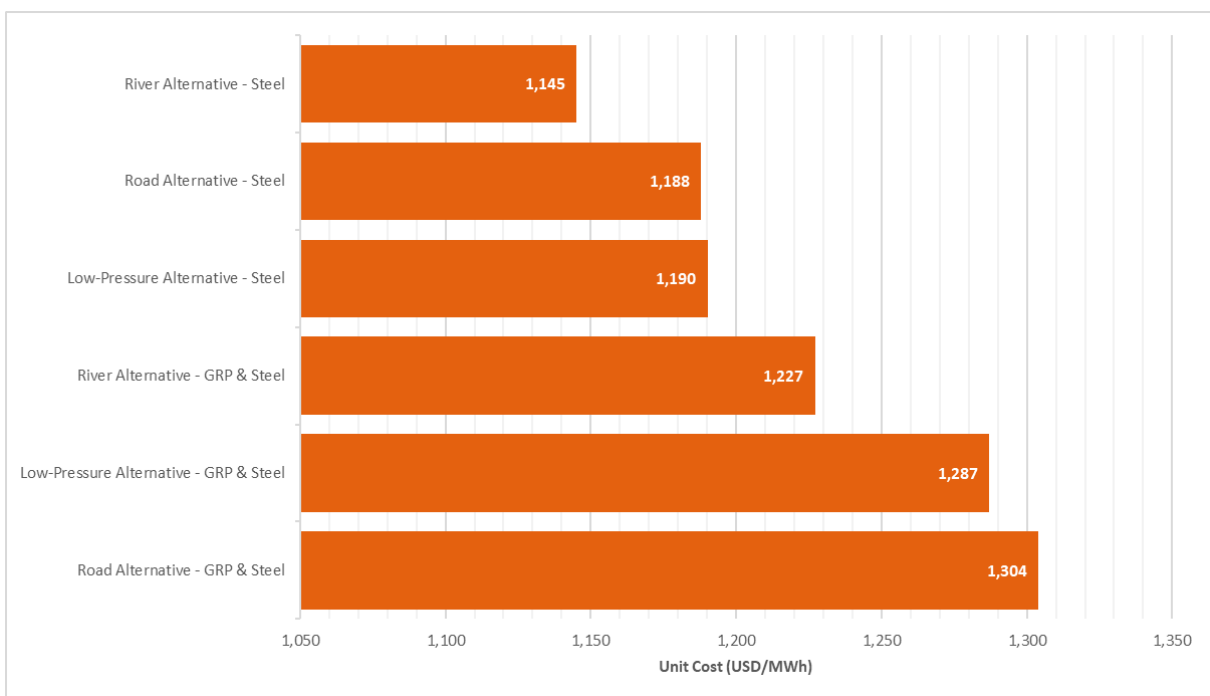
Table 8.4: Unit Cost of Generation per Alternative

| | River Alternative | | Road Alternative | | Low-Pressure Alternative | |
|------------------------------|-------------------|---------------|------------------|---------------|--------------------------|---------------|
| | Steel | GRP and Steel | Steel | GRP and Steel | Steel | GRP and Steel |
| Installed Capacity (MW) | 23.0 | 23.0 | 23.0 | 24.0 | 24.0 | 23.0 |
| Energy Production (GWh/Year) | 62.26 | 62.29 | 62.00 | 62.83 | 63.26 | 62.44 |
| CAPEX (MM USD) | 71.3 | 76.4 | 73.7 | 81.9 | 75.2 | 80.3 |

| | River Alternative | | Road Alternative | | Low-Pressure Alternative | |
|----------------------------|-------------------|---------------|------------------|---------------|--------------------------|---------------|
| | Steel | GRP and Steel | Steel | GRP and Steel | Steel | GRP and Steel |
| Unit Cost (USD/MWh) | 1,145 | 1,227 | 1,188 | 1,304 | 1,190 | 1,287 |

Figure 8.4 shows the same results as Table 8.4 but in a graphical way sorted from the lowest (most attractive) to the highest (least attractive) unit cost.

Figure 8.4: Sorted Unit Cost Results per Alternative



8.5 Final Remarks

Observing the results of Table 8.4 and Figure 8.4, it is possible to see that although the river alternative - steel is not the option with the greatest energy production, when evaluating its costs it becomes the most attractive alternative of all.

The alternatives that follow are the road alternative - steel and the low - pressure alternative - steel, both with almost the same unit price of generation.

From an operational point of view, the results translate into that for Piedras Negras HPP, there is an economic alternative that does not have the capacity of regulating the electrical frequency of the grid to which will be connected and another two alternatives 4% more expensive (in terms of unit cost) that will allow performing this task.

Despite this, and as already mentioned in Title 7, the alternatives presented here will need a detailed analysis of the transient phenomenon at a later engineering stage. This could cause the alternatives to need tailor-made solutions to reduce this phenomenon, having a differentiated impact on their final cost.

(This page intentionally left blank)

9 Climate Change Impact in Energy Production

In the climate change chapter (Title 4), it was shown that for the scenarios RCP4.5 and RCP8.5, the mean annual runoff of the San José river would increase by 25% and 38% respectively.

With the aim evaluate the impact that this increase in the average runoff will have in the energy production and considering only the three most economical hydroelectric power plant alternatives from the earlier chapter, this is: River, road, and low-pressure alternatives with steel conduits, a simulation of the hydroelectric generation was done considering the projected runoff from the year 2021 till 2070.

It is good to mention that the characteristics of each power plant were not altered for this analysis. The only change made to the models consisted in updating the hydrology of the river.

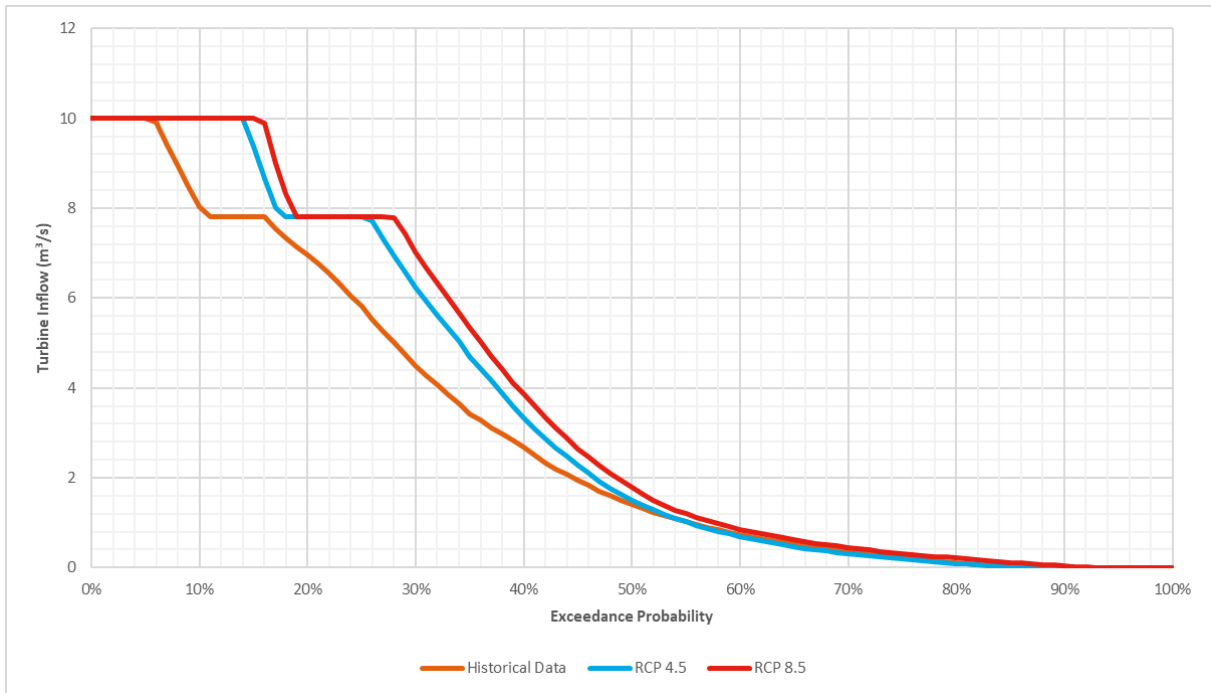
The energy production results for the three alternatives are included in Table 9.1

Table 9.1: Energy Production Results with Climate Change

| | River Alternative Steel | Road Alternative Steel | Low-Pressure Alternative Steel |
|-------------------------------|--------------------------------|-------------------------------|---------------------------------------|
| Historical Hydrology | | | |
| Capacity Factor (%): | 30.9% | 30.7% | 30.1% |
| Energy Production (GWh/Year): | 62.26 | 62.00 | 63.26 |
| Climate Change RCP4.5 | | | |
| Capacity Factor (%): | 35.8% | 35.1% | 34.5% |
| Energy Production (GWh/Year): | 72.28 | 70.80 | 72.57 |
| Climate Change RCP8.5 | | | |
| Capacity Factor (%): | 38.1% | 37.0% | 36.4% |
| Energy Production (GWh/Year): | 76.74 | 74.63 | 76.55 |

Is also interesting to see in Figure 9.1 how the inflow to the turbines will evolve with the climate change scenarios.

Figure 9.1: Turbine Inflow Comparison: Historical vs Climate Change Scenarios



Similarly, Figure 9.2, Figure 9.3, and Figure 9.4 shows the duration curve evolution of the energy production for the river, road, and low-pressure alternative respectively.

Figure 9.2: Historical and Climate Change Energy Production for River Alternative

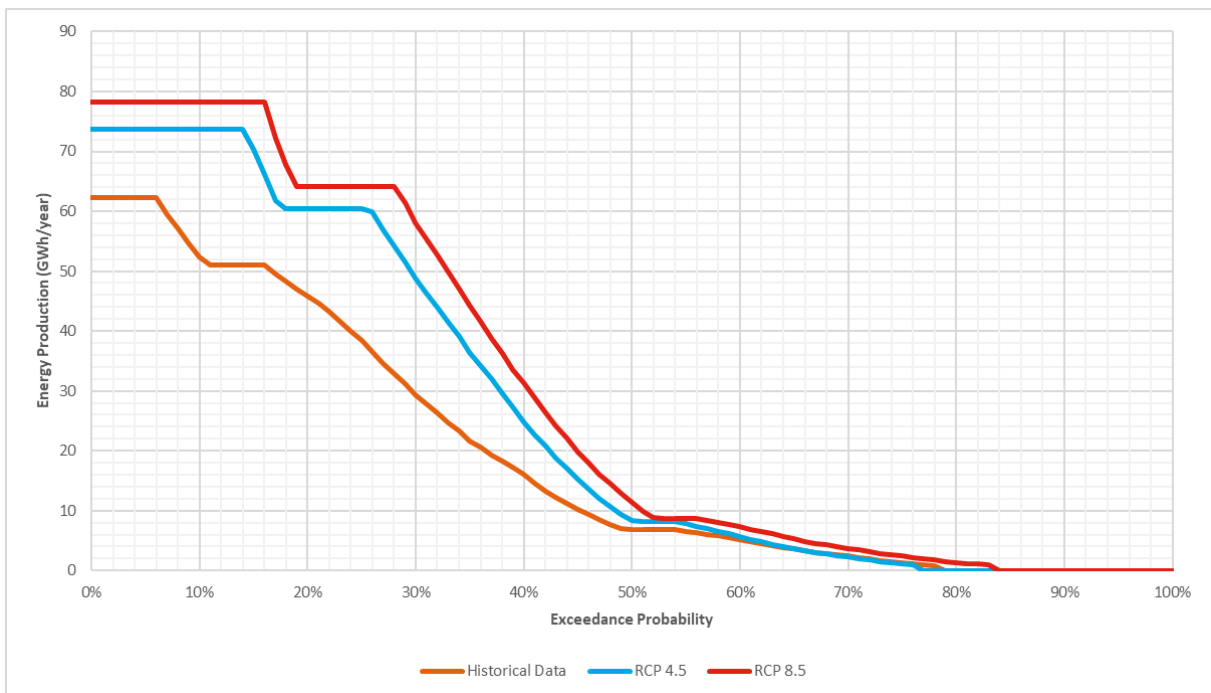


Figure 9.3: Historical and Climate Change Energy Production for Road Alternative

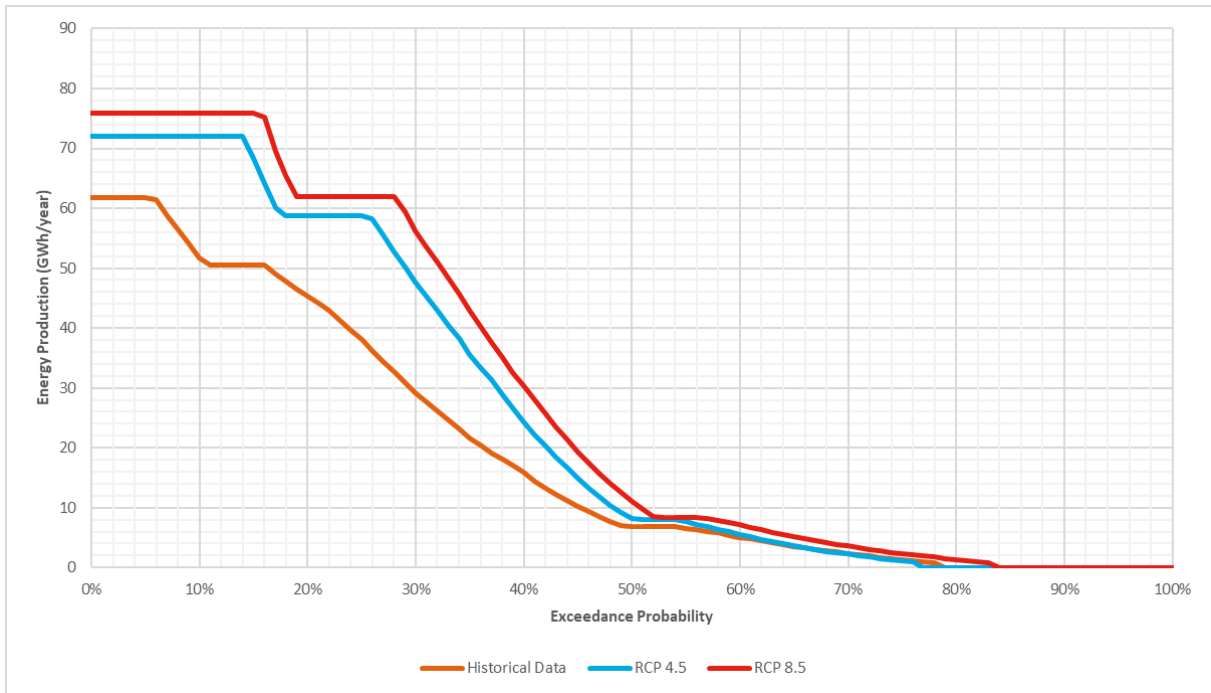
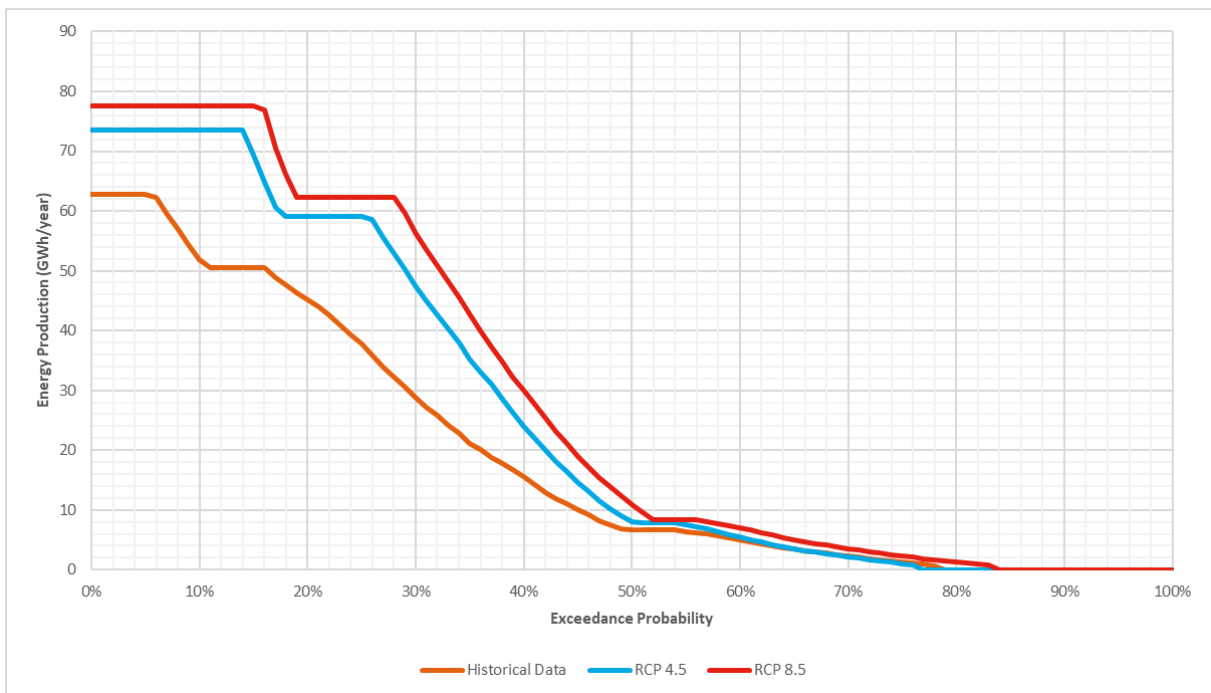


Figure 9.4: Historical and Climate Change Energy Production for Low-Pressure Alternative



Observing these results, the first thing that can be seen is how the energy production increases, especially for the most extreme climate change scenario, the RCP8.5. As a reference, the increase percentage in generation is included in Table 9.2.

Table 9.2: Energy Production Increment with Climate Change

| Energy Production | River Alternative Steel | Road Alternative Steel | Low-Pressure Alternative Steel |
|--------------------------|--------------------------------|-------------------------------|---------------------------------------|
| Historical vs RCP4.5 | 16% | 14% | 15% |
| Historical vs RCP8.5 | 23% | 20% | 21% |

10 Results Summary and Recommendations

10.1 Results Summary

Throughout this Thesis work, diverse types of studies have been done and explained with the main goal of assessing the best alternative to exploit the hydropower potential of Anpac water rights and continue in this way the hydroelectrical development of the San José river in Chile. In this regard, a summary of the most relevant results of the Piedras Negras power plant project are:

- The definition for the location of the intake follows the requirements established by the water rights owned by Anpac Energía and, at the same time, does not interfere with a third-party water right found in the same area.
- 28% of the area of the intake catchment is covered by the Universidad glacier, meaning that the runoff regime of San José river is highly dependent on the melting process of this ice body.
- A hydrological model, specifically the HBV model, was used to obtain 39 years (ranging from 1978 till 2017) of mean daily runoff data at the intake point of the power plant.
- At the intake point, San José river has a mean annual runoff of 4.0 m³/s.
- Flood events occur most often during the summer season, specifically between December and February.
- To assess the effects of climate change, five different models and two scenarios were taken into consideration: RCP4.5 and RCP8.5. The goal was to project an envelope of the climate conditions from the year 2021 till 2070, the expected lifetime of the power plant.
- The results from the climate change analysis show a 26% average reduction of precipitation and an average temperature increase of 1.3°C (46%) considering both scenarios.
- The increment in temperature will increase the snow and glacier melting with it, potentially reducing the area of the ice body over the years and making the river hydrology more extreme.
- Nevertheless, the combination of future climatic conditions will result in an increment of the runoff in San José river: 25% for RCP4.5 and 38% for RCP8.5.

- Regarding the intake design, the construction of a dam to create a regulation reservoir was discarded. Instead, a typical run-of-the-river scheme with a low dam across the river and a lateral intake structure was considered.
- One main challenge that will affect the operation of the power plant is the sediments management. A settling basin was designed, but as seen in San Andrés HPP found upstream of the project site, this structure will mitigate but not end the sediment problems, especially the abrasion of the electro-mechanical components.
- Three alternatives of power plants were studied: One going through the floodplain of the San José river, the second following the access road alignment to San Andrés HPP, and the third following the contour line at stilling basin outlet. These alternatives were named river, road a low-pressure respectively.
- Each one of these alternatives contemplated pressure conduits to carry the water from the intake to the powerhouse. Steel and a combination of GRP and steel where the materials chosen for the conduits.
- An energy production model was created to define the main aspects of the power plant. According to the results, Pelton turbines are better suited for this project than Francis and the design flow of the power plant was set in 10 m³/s.
- For the three alternatives under analysis, and for each of the conduit materials studied, the obtained installed capacities were 23 MW and 24 MW, the energy production ranged between 62.0 GWh/year and 63.3 GWh/year. The optimal conduit diameters are 1.80 m, 1.90 m, and 2.10 m.
- All alternatives contemplated two Pelton units with 90%-10% size combination.
- The governor stability assessment showed that only the road and low-pressure alternative were suitable for frequency regulation of the electrical system. These two alternatives also consider a surge chamber to dampen the transient effects in the system.
- Cost analysis showed the most attractive power plant layout is the river alternative closely followed by the road alternative and the low-pressure alternative, all with steel conduits.
- Considering climate change, the energy production of the most cost-attractive alternatives will increase 15% for RCP4.5 and 22% for RCP8.5.

The main results data from this Thesis are included as a summary in Table 10.1.

Table 10.1: Piedras Negras Hydropower Plant Results Summary

| | River Alternative | | Road Alternative | | Low-Pressure Alternative | |
|--|-------------------|---------------|------------------|---------------|--------------------------|---------------|
| | Steel | GRP and Steel | Steel | GRP and Steel | Steel | GRP and Steel |
| Basic Powerplant Data | | | | | | |
| Design Flow (m ³ /s) | 10.0 | 10.0 | 10.0 | 10.0 | 10.0 | 10.0 |
| Installed Capacity (MW) | 23.0 | 23.0 | 23.0 | 24.0 | 24.0 | 23.0 |
| Energy Production (GWh/Year) | 62.26 | 62.29 | 62.00 | 62.83 | 63.26 | 62.44 |
| Capacity Factor (%) | 30.9% | 30.9% | 30.7% | 29.9% | 30.1% | 31.0% |
| Penstock | | | | | | |
| Headrace Penstock Length (m) | 0 | 0 | 4,743 | 4,743 | 4,684 | 4,684 |
| High Pressure Penstock Length (m) | 4,747 | 4,747 | 158 | 158 | 493 | 493 |
| Inner Diameter (m) | 1.90 | 1.80 | 1.90 | 1.90 | 2.10 | 1.90 |
| Flow Velocity (m/s) | 3.53 | 3.93 | 3.53 | 3.53 | 2.89 | 3.53 |
| Turbine | | | | | | |
| Turbine Type | Pelton | Pelton | Pelton | Pelton | Pelton | Pelton |
| Number of Units | 2 | 2 | 2 | 2 | 2 | 2 |
| Unit 1 Size | 90% | 90% | 90% | 90% | 90% | 90% |
| Unit 2 Size | 10% | 10% | 10% | 10% | 10% | 10% |
| Production Increment from Different Size Units | 2.10% | 2.10% | 2.10% | 2.08% | 2.07% | 2.09% |
| Energy Losses | | | | | | |
| Intake Water Elevation (masl) | 1,813.0 | 1,813.0 | 1,813.0 | 1,813.0 | 1,813.0 | 1,813.0 |
| Turbine/Discharge Elevation (masl) | 1,531.5 | 1,531.5 | 1,531.5 | 1,531.5 | 1,531.5 | 1,531.5 |
| Gross Head (m) | 281.5 | 281.5 | 281.5 | 281.5 | 281.5 | 281.5 |
| Net Head (m) | 255.9 | 256.2 | 253.1 | 259.6 | 263.0 | 258.1 |
| Percentage of Gross Head | 9.1% | 9.0% | 10.1% | 7.8% | 6.6% | 8.3% |
| CAPEX | | | | | | |
| Direct Costs (MM USD) | 45.7 | 48.9 | 47.3 | 52.6 | 48.4 | 51.6 |
| Indirect Costs (MM USD) | 13.7 | 14.8 | 14.1 | 15.7 | 14.3 | 15.3 |
| CAPEX (MM USD) | 71.3 | 76.4 | 73.7 | 81.9 | 75.2 | 80.3 |
| Unit Cost (USD/MW/h) | 1,145 | 1,227 | 1,188 | 1,304 | 1,190 | 1,287 |
| Climate Change | | | | | | |
| Energy Production RCP4.5 (GWh/Year) | 72.28 | - | 70.80 | - | 72.57 | - |
| Energy Production RCP8.5 (GWh/Year) | 76.74 | - | 74.63 | - | 76.55 | - |

10.2 Recommendations

Based on the different analysis and the results, the author of this Thesis recommends the following:

- From the hydrological point of view, one of the biggest challenges is the modeling of the future behavior of the Universidad glacier. Although in this Thesis the HBV model did an excellent job during the calibration of historical runoff of the San José river, one of the consequences of climate change will be the shrinking process over time of the glacier size, a topic that the HBV model cannot simulate. In this regard, the recommendation is to have a specific study of the glacier behavior in the future to which the base flows could be compared.
- Related to the above, with climate change the energy production of the power plant will increase. Therefore, it is worth considering at a later stage of engineering an increase in the installed capacity of the power plant to take advantage of this effect.
- Although a high-quality LIDAR topography is available in the project sector, it is also recommended to perform a bathymetry of San José riverbed that allows a more precise hydraulic modeling.
- Sediment management should not be overlooked. Although its detailed study could involve non-depreciable cost, having fewer operation interruptions or fewer repairs jobs of electro-mechanical components can result in greater economic benefits during the lifetime of the power plant. In this sense, the possibility of having a sedimentation pond that, due to its size, allows daily regulation of the discharge used by the plant should be analyzed. Also, a sedimentological behavior study of the San José river as well as the quartz concentration at different flow stages and seasons of the year is recommended. This data will be of special interest to specialists in sediment management.
- For a future stage of engineering of the project, it is imperative to have a detailed analysis of the transient phenomenon in the headrace conduit and penstock, which shall include the maximum and minimum pressure envelope and attenuation measures of the phenomena. This is especially critical if its decided to continue with the development of the river alternative in steel, the most attractive alternative from the cost analysis point of view.

- It is also recommended an environmental assessment study of the sector, that in addition to following the environmental requirements of the Chilean laws, focus on the aquatic habitat aiming to define more precisely an environmental flow, and thus, reduce the uncertainty this parameter could have on the energy generation.
- Finally, an electrical connection study must be carried out to evaluate if the existing line from the San Andrés HPP can absorb the energy production of Piedras Negras HPP.

(This page intentionally left blank)

11 References

- American Water Works Association. (2004). *Steel pipe: A Guide for Design and Installation*. AWWA.
- ARCADIS Geotécnica. (2010). *Declaración de Impacto Ambiental Aumento de Potencia Central Hidroeléctrica San Andrés - Capítulo 2 Descripción del Proyecto - 3321- 0000- MA-INF-001-0*. Santiago.
- Bouvard, M. (1984). Barrages mobiles et ouvrages de dérivation, à partir de rivières transportant des matériaux solides, 388.
- Brekke, H. (1995). *Hydropower Development - Volume 12 Mechanical Equipment*. Trondheim: Norwegian Institute of Technology Division of Hydraulic Engineering.
- Camp, T. R. (1946). Sedimentation and the design of settling tanks. *ASCE*, 111, 895–958.
- Chaudhry, M. H. (2014). *Transient-Flow Equations. Applied Hydraulic Transients*. New York, NY: Springer New York.
- Chow, V. Te. (1959). *Open-channel hydraulics*. McGraw-Hill Book Company.
- Corporación Nacional Forestal. (n.d.). Sistema de Información Territorial - CONAF 2016. Retrieved September 26, 2017, from <https://sit.conaf.cl/>
- Cortes, G., McPhee, J., & Baldo, E. (2017). *Cambio Climático y Vulnerabilidad a Sequías Cuenca Alta Río Tinguiritica - Informe Etapa II - Ver. 1*.
- CR2, C. for C. and R. R.-. (n.d.). Bases de Datos. Retrieved January 2, 2018, from <http://www.cr2.cl/recursos-y-publicaciones/bases-de-datos/>
- Cuffey, K. M., & Paterson, W. S. . B. (2010). *Physics of Glaciers, Fourth Edition. The Physics of Glaciers*.
- European Network for Earth System modelling. (2016). CORDEX Data Structure. Retrieved April 26, 2018, from <https://portal.enes.org/data/enes-model-data/cordex/datastructure>
- Ferguson, R., & Church, M. (2004). A Simple Universal Equation for Grain Settling Velocity. *Journal of Sedimentary Research*, 74(6), 933–937. Retrieved from <https://pubs.geoscienceworld.org/sepm/jsedres/article-abstract/74/6/933/99413>
- Flato, G., Marotzke, J., Abiodun, B., Braconnot, P., Chou, S. C., Collins, W. J., ... Eyring, V. (2013). Evaluation of climate models. In: climate change 2013: the physical science basis. Contribution of working group I to the fifth assessment report of the intergovernmental panel on climate change. *Climate Change 2013*, 5, 741–866.
- Goodell, C. (2012). The RAS Solution: How to draw cross sections. Retrieved May 2, 2018,

- from <http://hecrasmodel.blogspot.no/2012/07/how-to-draw-cross-sections.html>
- Gordon, J. L. (1961). Determination of Generator inertia. In *Eastern Zone Meeting, Hydraulic Power Section, Canadian Electrical Association, Halifax*.
- Gudmundsson, L. (2016). Statistical Transformations for Post-Processing Climate Model Output, 36. Retrieved from <https://cran.r-project.org/web/packages/qmap/qmap.pdf>
- Killingtveit, Å., & Sælthun, N. (1995). *Hydropower Development - Volume 7 Hydrology*. Trondheim: Norwegian Institute of Technology Division of Hydraulic Engineering.
- Kirk, J. T. O. (1994). *Light and photosynthesis in aquatic ecosystems*. Cambridge university press.
- Krause, P., Boyle, D. P., & Bäse, F. (2005). Comparison of different efficiency criteria for hydrological model assessment. *Advances in Geosciences*, 5, 89–97.
- Mays, L. W. (1999). *Hydraulic design handbook*. McGraw-Hill Professional Publishing.
- Méndez, M. V. (1995). *Tuberías a Presión en los Sistemas de Abastecimiento de Agua*. Publicaciones UCAB.
- METI, & NASA. (2011). Aster Gdem 2.0. *Terra ASTER*, 12–13. Retrieved from <https://lpdaac.usgs.gov/>
- Ministerio de Energía. (2014). *Agenda de Energía - Resumen*. Santiago. Retrieved from http://www.energia.gob.cl/sites/default/files/agenda_de_energia_-_resumen_en_espanol.pdf
- Ministerio de Justicia. DFL-1122 (1981) Código de Aguas, Pub. L. No. DFL1122 (2018). Retrieved from <https://www.leychile.cl/Navegar?idNorma=5605>
- Moss, R. H., Edmonds, J. A., Hibbard, K. A., Manning, M. R., Rose, S. K., Van Vuuren, D. P., ... Wilbanks, T. J. (2010). The next generation of scenarios for climate change research and assessment. *Nature*, 463(7282), 747–756.
- Nielsen, T. K. (n.d.). Speed Number – Classification of Turbines. Trondheim.
- Pascual-ferrer, J., & Candela, L. (2015). *Water Balance on the Central Rift Valley Water Balance on the Central Rift Valley Global Dimension in Engineering Education*. GDEE. Retrieved from <https://upcommons.upc.edu/handle/2117/89152>
- Raup, B., Racoviteanu, A., Khalsa, S. J. S., Helm, C., Armstrong, R., & Arnaud, Y. (2007). The GLIMS geospatial glacier database: A new tool for studying glacier change. *Global and Planetary Change*, 56(1–2), 101–110.
- SWECO Norge AS. (2012a). *Cost base for hydropower plants (over 10 000 kW)*. (J. Slapgård, Ed.). Oslo: Norwegian Water Resources and Energy Directorate. Retrieved from

- http://publikasjoner.nve.no/veileder/2012/veileder2012_03.pdf
- SWECO Norge AS. (2012b). *Cost base for small-scale hydropower plants (up to 10 000 kW)*. (J. Slapgård, Ed.). Oslo: Norwegian Water Resources and Energy Directorate. Retrieved from http://publikasjoner.nve.no/veileder/2012/veileder2012_02.pdf
- Swedish Meteorological and Hydrological Institute. (n.d.). HBV | SMHI. Retrieved April 16, 2018, from <https://www.smhi.se/en/research/research-departments/hydrology/hbv-1.90007>
- Tercera, L. (2017, May 12). Costo de la electricidad baja 60% en tres años de la Agenda de la Energía. Retrieved April 26, 2018, from <http://www2.latercera.com/noticia/costo-la-electricidad-baja-60-tres-anos-la-agenda-energia/>
- USACE. (2016). *HEC-RAS, River Analysis System Hydraulic Reference Manual Version 5.0*.
- WMO. (2018). IPCC - Intergovernmental Panel on Climate Change. Retrieved April 25, 2018, from <http://www.ipcc.ch/organization/organization.shtml>
- World Meteorological Organization. (2010). *Manual on Stream Gauging: Volume II - computation of discharge* (Vol. II). Geneva: WMO.
- Xoren Earth. (2018a). *AInforme Geotécnico Proyecto Hidroeléctrico Piedras Negras Rev. A*.
- Xoren Earth. (2018b). *Informe Geológico Proyecto Hidroeléctrico Piedras Negras Rev. B*.

(This page intentionally left blank)

12 Appendix

(This page intentionally left blank)

Appendix I

Monthly Summary of Precipitation Data

Total Monthly Precipitation at La Rufina (mm)

| | Jan | Feb | Mar | Apr | May | Jun | Jul | Aug | Sep | Oct | Nov | Dec |
|------|------|------|-------|-------|-------|-------|-------|-------|-------|-------|-------|-------|
| 1978 | 0.0 | 0.0 | 0.0 | 0.0 | 75.0 | 246.9 | 767.0 | 54.0 | 85.0 | 61.0 | 168.0 | 0.0 |
| 1979 | 0.0 | 0.0 | 0.0 | 23.0 | 138.0 | 22.0 | 380.0 | 232.0 | 196.0 | 3.0 | 124.0 | 150.0 |
| 1980 | 0.0 | 59.0 | 14.0 | 336.0 | 385.7 | 306.0 | 302.0 | 51.0 | 93.3 | 0.0 | 20.0 | 7.0 |
| 1981 | 0.0 | 0.0 | 0.0 | 83.0 | 553.0 | 97.6 | 110.0 | 81.0 | 65.0 | 23.7 | 15.0 | 0.0 |
| 1982 | 0.0 | 0.0 | 26.0 | 15.0 | 270.0 | 718.2 | 480.0 | 213.0 | 256.5 | 95.5 | 8.0 | 0.0 |
| 1983 | 15.0 | 3.0 | 0.0 | 36.0 | 128.0 | 227.0 | 218.0 | 143.0 | 81.0 | 8.2 | 0.0 | 0.0 |
| 1984 | 0.0 | 0.0 | 4.3 | 3.8 | 320.7 | 129.5 | 464.1 | 140.5 | 145.0 | 104.3 | 33.4 | 0.0 |
| 1985 | 0.0 | 0.0 | 21.2 | 23.0 | 192.7 | 53.4 | 206.2 | 14.1 | 56.3 | 113.1 | 0.0 | 0.0 |
| 1986 | 0.0 | 0.0 | 17.0 | 113.5 | 385.3 | 414.4 | 35.3 | 220.6 | 12.2 | 36.4 | 70.1 | 0.0 |
| 1987 | 0.0 | 0.0 | 5.2 | 26.3 | 161.7 | 92.4 | 587.2 | 274.6 | 105.7 | 124.4 | 0.0 | 0.0 |
| 1988 | 0.0 | 0.0 | 30.0 | 18.0 | 17.7 | 164.7 | 148.9 | 249.2 | 55.3 | 5.1 | 28.3 | 0.0 |
| 1989 | 0.0 | 0.0 | 2.1 | 20.2 | 74.6 | 63.4 | 175.7 | 367.4 | 32.2 | 20.2 | 4.1 | 13.1 |
| 1990 | 0.0 | 0.0 | 100.3 | 35.3 | 62.1 | 39.2 | 142.2 | 114.2 | 123.7 | 43.1 | 44.1 | 0.0 |
| 1991 | 0.0 | 0.0 | 0.0 | 62.0 | 218.7 | 279.6 | 273.5 | 33.0 | 125.2 | 50.0 | 3.1 | 103.2 |
| 1992 | 0.0 | 0.0 | 12.1 | 174.5 | 516.7 | 453.7 | 58.2 | 158.1 | 84.1 | 10.1 | 18.1 | 0.0 |
| 1993 | 2.0 | 0.0 | 0.0 | 121.1 | 360.3 | 460.1 | 220.0 | 67.1 | 47.0 | 35.0 | 38.0 | 56.0 |
| 1994 | 0.0 | 0.0 | 0.0 | 120.0 | 209.0 | 203.1 | 461.2 | 17.0 | 87.8 | 27.1 | 0.0 | 36.0 |
| 1995 | 0.0 | 9.0 | 0.0 | 180.1 | 22.0 | 360.1 | 242.0 | 122.2 | 48.0 | 44.0 | 0.0 | 0.0 |
| 1996 | 0.0 | 0.0 | 0.0 | 67.1 | 37.0 | 219.2 | 79.1 | 232.2 | 16.0 | 24.1 | 5.0 | 9.0 |
| 1997 | 0.3 | 0.0 | 15.1 | 98.0 | 272.1 | 638.8 | 155.2 | 258.4 | 267.0 | 218.0 | 54.2 | 10.0 |
| 1998 | 0.0 | 0.0 | 0.0 | 85.4 | 58.2 | 91.1 | 0.0 | 0.0 | 77.1 | 0.0 | 0.0 | 0.0 |
| 1999 | 0.0 | 7.1 | 12.1 | 9.1 | 52.2 | 148.1 | 110.3 | 309.1 | 322.2 | 30.1 | 0.0 | 0.0 |
| 2000 | 0.0 | 77.1 | 0.0 | 9.0 | 28.0 | 875.5 | 118.0 | 19.1 | 278.5 | 5.0 | 16.0 | 0.0 |
| 2001 | 2.0 | 0.0 | 5.0 | 62.1 | 376.4 | 62.4 | 583.1 | 282.1 | 21.1 | 0.0 | 0.0 | 0.0 |
| 2002 | 0.0 | 0.0 | 20.1 | 23.0 | 276.1 | 272.1 | 237.0 | 574.1 | 144.0 | 56.0 | 14.0 | 0.0 |
| 2003 | 64.0 | 0.0 | 0.0 | 0.0 | 158.0 | 334.0 | 169.0 | 10.0 | 138.0 | 50.0 | 103.0 | 0.0 |
| 2004 | 0.0 | 0.0 | 70.0 | 116.0 | 22.0 | 189.0 | 191.0 | 80.0 | 146.0 | 52.0 | 72.0 | 0.0 |

| | Jan | Feb | Mar | Apr | May | Jun | Jul | Aug | Sep | Oct | Nov | Dec |
|------------|-------------|-------------|--------------|--------------|--------------|--------------|--------------|--------------|--------------|--------------|--------------|--------------|
| 2005 | 0.0 | 0.0 | 20.0 | 6.0 | 281.0 | 472.0 | 162.0 | 377.0 | 13.0 | 19.0 | 48.0 | 7.0 |
| 2006 | 0.0 | 0.0 | 0.0 | 57.0 | 122.5 | 321.0 | 416.0 | 170.5 | 69.0 | 116.0 | 0.0 | 0.0 |
| 2007 | 0.0 | 31.0 | 10.0 | 0.0 | 29.0 | 142.0 | 149.0 | 103.6 | 0.0 | 5.0 | 19.0 | 0.0 |
| 2008 | 0.0 | 0.0 | 23.0 | 62.0 | 411.5 | 199.0 | 167.0 | 359.0 | 41.0 | 0.0 | 0.0 | 0.0 |
| 2009 | 0.0 | 0.0 | 0.0 | 0.0 | 122.0 | 220.0 | 49.5 | 227.1 | 213.0 | 90.9 | 17.0 | 0.0 |
| 2010 | 0.0 | 0.0 | 0.0 | 0.0 | 74.0 | 281.0 | 124.0 | 14.0 | 11.0 | 46.0 | 35.0 | 6.0 |
| 2011 | 0.0 | 0.0 | 27.0 | 145.0 | 0.0 | 141.0 | 141.0 | 143.0 | 33.9 | 11.0 | 18.0 | 0.0 |
| 2012 | 0.0 | 8.0 | 0.0 | 11.0 | 161.0 | 398.0 | 10.0 | 82.0 | 0.0 | 98.0 | 0.0 | 123.0 |
| 2013 | 0.0 | 0.0 | 0.0 | 0.0 | 236.0 | 75.0 | 55.0 | 80.0 | 40.0 | 10.0 | 0.0 | 0.0 |
| 2014 | 13.0 | 0.0 | 24.0 | 23.0 | 93.1 | 163.0 | 80.0 | 152.0 | 101.0 | 15.0 | 28.0 | 17.0 |
| 2015 | 0.0 | 0.0 | 18.0 | 0.0 | 10.6 | 72.0 | 237.0 | 308.0 | 43.7 | 149.0 | 5.0 | 0.0 |
| 2016 | 16.0 | 0.0 | 0.0 | 300.0 | 67.0 | 46.0 | 181.0 | 23.0 | 17.1 | 72.0 | 6.0 | 2.0 |
| 2017 | 0.0 | 0.0 | 1.4 | 11.9 | 85.9 | 131.0 | 74.1 | 101.0 | 24.5 | 0.0 | | |
| Min | 0.0 | 0.0 | 0.0 | 0.0 | 0.0 | 22.0 | 0.0 | 0.0 | 0.0 | 0.0 | 0.0 | 0.0 |
| Ave | 2.8 | 4.9 | 11.9 | 61.9 | 176.6 | 245.6 | 219.0 | 161.4 | 92.9 | 46.8 | 26.0 | 13.8 |
| Max | 64.0 | 77.1 | 100.3 | 336.0 | 553.0 | 875.5 | 767.0 | 574.1 | 322.2 | 218.0 | 168.0 | 150.0 |

Appendix II

Monthly Summary of Temperature Data

Average Monthly Temperature at Termas del Flaco (°C)

| | Jan | Feb | Mar | Apr | May | Jun | Jul | Aug | Sep | Oct | Nov | Dec |
|------|------|------|------|------|-----|------|------|------|------|-----|------|------|
| 1978 | 9.3 | 10.2 | 9.7 | 10.3 | 7.2 | 1.9 | 0.1 | -1.6 | 0.9 | 3.6 | 6.2 | 11.7 |
| 1979 | 12.9 | 10.6 | 10.6 | 7.6 | 4.3 | 2.8 | 3.6 | 2.4 | 1.1 | 6.4 | 7.6 | 10.0 |
| 1980 | 12.7 | 10.2 | 13.1 | 5.6 | 6.2 | 2.9 | 1.5 | 3.0 | 4.8 | 4.9 | 7.2 | 10.3 |
| 1981 | 10.4 | 11.9 | 11.0 | 6.4 | 2.4 | 0.6 | 2.4 | 2.9 | 3.8 | 4.5 | 7.5 | 11.1 |
| 1982 | 12.1 | 10.2 | 10.3 | 8.6 | 4.0 | -0.9 | -1.3 | 0.5 | 1.2 | 2.5 | 6.2 | 11.8 |
| 1983 | 11.5 | 12.2 | 10.9 | 7.1 | 2.1 | -1.8 | -1.4 | -0.7 | -0.4 | 6.0 | 9.4 | 12.5 |
| 1984 | 12.4 | 12.2 | 10.5 | 7.7 | 1.2 | -2.0 | -0.5 | -1.7 | 1.2 | 4.5 | 6.6 | 9.7 |
| 1985 | 10.3 | 12.8 | 10.4 | 6.9 | 5.2 | 4.3 | 1.1 | 2.2 | 4.5 | 3.4 | 10.0 | 11.6 |
| 1986 | 12.5 | 11.9 | 11.1 | 7.6 | 2.7 | 0.5 | 4.2 | 1.6 | 2.6 | 5.1 | 6.5 | 12.5 |
| 1987 | 13.3 | 14.0 | 11.0 | 8.2 | 1.5 | 2.1 | -1.2 | -2.1 | -0.2 | 2.7 | 9.1 | 10.2 |
| 1988 | 11.8 | 13.1 | 11.7 | 8.4 | 4.0 | 1.8 | 1.5 | 0.5 | 1.3 | 5.6 | 10.0 | 11.6 |
| 1989 | 13.3 | 14.5 | 10.8 | 8.5 | 5.2 | 3.2 | 2.8 | 0.5 | 1.2 | 6.2 | 9.8 | 11.3 |
| 1990 | 13.0 | 12.5 | 10.2 | 6.6 | 4.7 | 3.6 | 2.0 | 5.3 | 2.9 | 5.3 | 9.1 | 11.1 |
| 1991 | 11.7 | 13.4 | 12.4 | 8.0 | 5.3 | 0.9 | -0.1 | 1.0 | 4.2 | 4.3 | 7.8 | 8.0 |
| 1992 | 13.0 | 11.6 | 11.4 | 5.5 | 1.1 | -0.4 | -0.7 | 1.3 | 4.3 | 5.8 | 7.2 | 10.2 |
| 1993 | 12.5 | 12.4 | 12.3 | 6.6 | 0.4 | 1.4 | 0.8 | 2.8 | 2.8 | 5.6 | 7.4 | 11.1 |
| 1994 | 12.5 | 11.9 | 12.2 | 7.6 | 5.6 | 1.6 | 0.1 | 1.6 | 5.2 | 4.3 | 8.5 | 11.7 |
| 1995 | 11.4 | 11.3 | 11.0 | 7.7 | 8.0 | 1.7 | -1.3 | 0.8 | 4.5 | 5.1 | 8.8 | 12.3 |
| 1996 | 10.6 | 11.7 | 11.0 | 6.5 | 6.5 | 1.7 | 4.4 | 3.1 | 5.4 | 5.9 | 9.7 | 10.1 |
| 1997 | 11.8 | 13.4 | 11.9 | 9.7 | 6.4 | -2.2 | 1.4 | 1.5 | 2.2 | 1.7 | 6.4 | 9.5 |
| 1998 | 12.9 | 10.8 | 10.0 | 5.8 | 6.0 | 2.6 | 4.8 | 3.5 | 2.8 | 8.6 | 8.6 | 11.3 |
| 1999 | 11.3 | 13.8 | 10.3 | 8.0 | 6.4 | 1.7 | 2.4 | 1.9 | 2.9 | 6.1 | 7.8 | 10.2 |
| 2000 | 12.0 | 10.5 | 10.5 | 8.8 | 4.2 | -0.7 | 1.5 | 1.6 | 1.3 | 5.8 | 6.2 | 10.6 |
| 2001 | 11.9 | 15.3 | 11.6 | 7.1 | 1.9 | 1.7 | 0.4 | 1.0 | 1.8 | 6.6 | 6.7 | 12.6 |
| 2002 | 11.7 | 12.7 | 11.0 | 6.1 | 4.0 | -0.3 | 0.7 | 1.0 | 2.2 | 4.9 | 7.7 | 9.9 |
| 2003 | 12.3 | 12.6 | 12.8 | 8.4 | 6.0 | 3.2 | 1.1 | 4.0 | 4.2 | 7.7 | 8.6 | 9.9 |
| 2004 | 13.8 | 12.7 | 12.2 | 6.6 | 5.2 | 2.7 | 1.5 | 2.8 | 4.7 | 4.6 | 7.1 | 10.7 |

| | Jan | Feb | Mar | Apr | May | Jun | Jul | Aug | Sep | Oct | Nov | Dec |
|------------|-------------|-------------|-------------|-------------|------------|-------------|-------------|-------------|-------------|-------------|-------------|-------------|
| 2005 | 12.2 | 14.8 | 9.8 | 7.4 | 1.8 | 1.7 | 1.0 | 1.3 | 0.6 | 4.0 | 8.5 | 11.0 |
| 2006 | 13.5 | 13.4 | 11.4 | 9.6 | 7.6 | 1.7 | 2.3 | 1.4 | 4.4 | 5.6 | 8.6 | 11.2 |
| 2007 | 13.1 | 10.6 | 10.5 | 7.8 | 4.1 | -0.4 | -1.2 | -2.2 | 3.1 | 5.4 | 8.6 | 11.2 |
| 2008 | 12.2 | 12.5 | 11.1 | 8.1 | 4.3 | 0.8 | 2.5 | 0.0 | 2.6 | 5.0 | 9.9 | 11.9 |
| 2009 | 13.0 | 12.5 | 13.4 | 11.6 | 7.1 | 2.2 | 0.5 | 1.3 | 0.9 | 4.8 | 6.0 | 10.2 |
| 2010 | 13.5 | 12.6 | 12.5 | 7.9 | 4.6 | 0.6 | -2.5 | 1.2 | 1.8 | 5.0 | 6.9 | 9.3 |
| 2011 | 11.9 | 12.4 | 10.7 | 8.0 | 7.4 | -0.2 | -0.7 | -0.8 | 4.1 | 3.8 | 8.1 | 12.0 |
| 2012 | 12.5 | 12.2 | 13.1 | 7.0 | 6.4 | 1.2 | 1.5 | 0.9 | 5.3 | 3.4 | 8.6 | 9.3 |
| 2013 | 13.5 | 12.2 | 10.3 | 8.6 | 4.4 | 1.8 | 1.9 | 1.8 | 1.7 | 5.7 | 8.0 | 13.0 |
| 2014 | 13.4 | 11.3 | 10.2 | 7.8 | 4.3 | -0.1 | 2.2 | 4.3 | 2.7 | 7.2 | 7.4 | 10.1 |
| 2015 | 14.3 | 12.2 | 12.7 | 10.1 | 6.3 | 4.2 | 0.7 | 1.0 | 1.9 | 2.3 | 5.9 | 11.1 |
| 2016 | 12.5 | 14.1 | 12.7 | 5.5 | 4.5 | 1.7 | 2.2 | 4.0 | 7.2 | 4.5 | 9.3 | 10.8 |
| 2017 | 14.6 | 13.0 | 10.6 | 6.5 | 2.2 | 1.3 | 1.6 | 0.1 | 2.4 | -2.8 | | |
| Min | 9.3 | 10.2 | 9.7 | 5.5 | 0.4 | -2.2 | -2.5 | -2.2 | -0.4 | -2.8 | 5.9 | 8.0 |
| Ave | 12.4 | 12.3 | 11.3 | 7.7 | 4.6 | 1.3 | 1.1 | 1.4 | 2.8 | 4.8 | 7.9 | 10.9 |
| Max | 14.6 | 15.3 | 13.4 | 11.6 | 8.0 | 4.3 | 4.8 | 5.3 | 7.2 | 8.6 | 10.0 | 13.0 |

Appendix III

Monthly Summary of Calibration Runoff Data

Average Monthly Runoff at Aquaflow (m³/s)

| | Jan | Feb | Mar | Apr | May | Jun | Jul | Aug | Sep | Oct | Nov | Dec |
|------------|-------------|-------------|-------------|------------|------------|------------|------------|------------|------------|------------|-------------|-------------|
| 2010 | | | | 6.2 | 4.4 | 3.8 | 3.4 | 3.3 | 3.7 | 6.4 | 11.8 | 15.3 |
| 2011 | 20.9 | 21.5 | 14.7 | 8.4 | 5.1 | 4.4 | 3.3 | 3.1 | 4.0 | 6.1 | 12.2 | 20.9 |
| 2012 | 19.8 | 14.0 | 10.7 | 5.4 | 4.0 | 5.7 | 5.1 | 4.7 | 5.4 | 5.5 | 12.3 | 19.4 |
| 2013 | 28.1 | 23.8 | 12.0 | 5.9 | 3.4 | 2.9 | 2.7 | 2.9 | 3.7 | 4.4 | 12.7 | 19.2 |
| 2014 | 16.6 | 8.8 | 4.7 | 1.9 | 2.8 | 2.4 | 2.2 | 2.3 | 2.4 | 5.5 | 14.4 | 19.5 |
| 2015 | 27.3 | 19.3 | | | | | | | | | | |
| Min | 16.6 | 8.8 | 4.7 | 1.9 | 2.8 | 2.4 | 2.2 | 2.3 | 2.4 | 4.4 | 11.8 | 15.3 |
| Ave | 22.5 | 17.5 | 10.5 | 5.6 | 3.9 | 3.8 | 3.4 | 3.3 | 3.8 | 5.6 | 12.7 | 18.9 |
| Max | 28.1 | 23.8 | 14.7 | 8.4 | 5.1 | 5.7 | 5.1 | 4.7 | 5.4 | 6.4 | 14.4 | 20.9 |

(This page intentionally left blank)

Appendix IV

Monthly Summary of Runoff Data at the Intake

Average Monthly Runoff at Intake (m³/s)

| | Jan | Feb | Mar | Apr | May | Jun | Jul | Aug | Sep | Oct | Nov | Dec |
|------|------|------|------|------|------|-----|-----|-----|-----|-----|-----|-----|
| 1978 | | | | 3.9 | 2.8 | 1.3 | 0.8 | 0.4 | 0.2 | 0.3 | 1.0 | 4.1 |
| 1979 | 10.0 | 7.8 | 6.6 | 4.1 | 2.0 | 1.2 | 1.2 | 0.9 | 0.6 | 1.5 | 1.9 | 4.8 |
| 1980 | 9.1 | 10.8 | 11.1 | 7.2 | 3.1 | 1.9 | 0.9 | 0.5 | 1.2 | 1.1 | 2.0 | 4.8 |
| 1981 | 4.9 | 6.8 | 9.6 | 4.0 | 1.4 | 0.9 | 0.4 | 0.5 | 0.7 | 1.0 | 1.8 | 4.1 |
| 1982 | 8.4 | 7.9 | 5.7 | 3.9 | 2.6 | 1.1 | 0.8 | 0.4 | 0.3 | 0.2 | 0.8 | 4.7 |
| 1983 | 9.5 | 9.4 | 7.8 | 4.6 | 1.8 | 0.8 | 0.5 | 0.2 | 0.2 | 0.8 | 2.0 | 9.2 |
| 1984 | 10.0 | 11.1 | 8.8 | 4.5 | 1.5 | 0.6 | 0.5 | 0.2 | 0.2 | 0.4 | 1.1 | 3.1 |
| 1985 | 4.9 | 6.8 | 10.2 | 3.8 | 2.0 | 1.5 | 1.0 | 0.6 | 0.8 | 1.1 | 2.6 | 6.6 |
| 1986 | 9.5 | 11.2 | 7.5 | 4.3 | 3.0 | 1.2 | 0.5 | 0.4 | 0.5 | 0.7 | 1.7 | 6.0 |
| 1987 | 11.6 | 16.5 | 13.4 | 4.6 | 1.8 | 0.8 | 0.8 | 0.6 | 0.3 | 0.3 | 1.8 | 4.6 |
| 1988 | 7.4 | 10.5 | 9.2 | 6.9 | 2.0 | 0.9 | 0.6 | 0.5 | 0.3 | 0.8 | 3.6 | 5.3 |
| 1989 | 11.6 | 16.8 | 10.5 | 5.1 | 2.3 | 1.3 | 0.9 | 0.7 | 0.4 | 0.7 | 2.4 | 5.5 |
| 1990 | 10.0 | 14.3 | 7.9 | 3.8 | 1.9 | 1.3 | 1.0 | 1.1 | 0.8 | 1.2 | 2.7 | 6.7 |
| 1991 | 10.3 | 11.1 | 12.0 | 5.7 | 2.6 | 1.2 | 0.6 | 0.3 | 0.5 | 0.8 | 1.6 | 2.7 |
| 1992 | 7.5 | 9.0 | 11.7 | 4.0 | 1.5 | 0.8 | 0.4 | 0.2 | 0.3 | 0.8 | 1.7 | 3.1 |
| 1993 | 8.2 | 11.7 | 9.7 | 4.9 | 1.7 | 0.7 | 0.4 | 0.3 | 0.6 | 1.5 | 1.7 | 4.0 |
| 1994 | 9.1 | 8.8 | 10.8 | 4.9 | 2.8 | 1.3 | 0.7 | 0.4 | 0.4 | 0.8 | 1.8 | 5.5 |
| 1995 | 7.9 | 8.6 | 6.8 | 4.2 | 2.6 | 1.7 | 0.7 | 0.4 | 0.5 | 0.7 | 2.2 | 6.0 |
| 1996 | 7.5 | 7.2 | 7.8 | 3.7 | 3.0 | 1.6 | 0.9 | 1.0 | 1.1 | 1.5 | 2.8 | 4.7 |
| 1997 | 8.5 | 10.1 | 13.8 | 12.4 | 10.1 | 2.2 | 0.9 | 0.5 | 0.4 | 0.4 | 1.1 | 3.1 |
| 1998 | 7.8 | 7.9 | 5.7 | 3.9 | 2.5 | 1.5 | 1.1 | 0.7 | 0.6 | 1.6 | 2.8 | 5.1 |
| 1999 | 7.3 | 13.3 | 8.8 | 3.6 | 2.3 | 1.1 | 0.6 | 0.8 | 0.8 | 1.4 | 2.1 | 3.6 |
| 2000 | 7.3 | 7.4 | 6.1 | 5.0 | 2.2 | 1.3 | 0.9 | 0.4 | 0.4 | 0.8 | 1.4 | 4.1 |
| 2001 | 7.1 | 18.1 | 14.6 | 6.3 | 1.8 | 0.9 | 0.7 | 0.4 | 0.3 | 0.8 | 1.2 | 6.9 |
| 2002 | 8.6 | 10.9 | 8.7 | 3.4 | 1.7 | 0.9 | 0.4 | 0.4 | 0.3 | 0.5 | 1.2 | 3.1 |
| 2003 | 7.0 | 11.0 | 11.7 | 6.6 | 3.1 | 1.2 | 0.7 | 0.6 | 1.0 | 1.8 | 2.8 | 4.3 |
| 2004 | 11.7 | 12.0 | 11.5 | 5.9 | 2.7 | 1.4 | 0.9 | 0.8 | 1.4 | 1.7 | 1.9 | 4.4 |

| | Jan | Feb | Mar | Apr | May | Jun | Jul | Aug | Sep | Oct | Nov | Dec |
|------------|-------------|-------------|-------------|-------------|-------------|------------|------------|------------|------------|------------|------------|------------|
| 2005 | 11.1 | 14.4 | 10.2 | 3.7 | 1.8 | 0.8 | 0.5 | 0.3 | 0.3 | 0.5 | 1.5 | 4.5 |
| 2006 | 9.7 | 17.0 | 8.6 | 5.8 | 4.5 | 1.6 | 1.0 | 0.5 | 0.5 | 1.3 | 2.5 | 4.5 |
| 2007 | 11.6 | 8.6 | 7.7 | 4.4 | 1.9 | 0.8 | 0.4 | 0.2 | 0.2 | 0.7 | 2.0 | 5.3 |
| 2008 | 10.1 | 10.3 | 7.3 | 4.9 | 2.4 | 1.2 | 0.5 | 0.4 | 0.3 | 0.4 | 2.2 | 5.8 |
| 2009 | 10.9 | 12.1 | 13.2 | 9.9 | 4.5 | 1.5 | 0.5 | 0.3 | 0.2 | 0.4 | 1.1 | 2.9 |
| 2010 | 8.8 | 13.0 | 11.1 | 6.6 | 2.4 | 1.1 | 0.5 | 0.2 | 0.2 | 0.5 | 1.4 | 2.5 |
| 2011 | 5.9 | 10.4 | 9.0 | 4.9 | 3.2 | 1.3 | 0.6 | 0.3 | 0.4 | 0.8 | 1.5 | 5.3 |
| 2012 | 11.5 | 11.8 | 11.3 | 6.1 | 2.1 | 1.3 | 0.5 | 0.2 | 0.9 | 0.9 | 2.4 | 3.5 |
| 2013 | 9.5 | 11.5 | 7.2 | 4.9 | 2.7 | 1.2 | 0.6 | 0.4 | 0.7 | 0.8 | 1.8 | 7.4 |
| 2014 | 17.8 | 9.8 | 6.5 | 3.6 | 2.0 | 0.9 | 0.4 | 0.6 | 0.6 | 1.4 | 2.5 | 4.0 |
| 2015 | 11.1 | 15.1 | 13.9 | 6.5 | 3.4 | 1.4 | 0.8 | 0.5 | 0.4 | 0.3 | 0.9 | 3.5 |
| 2016 | 9.4 | 13.9 | 12.7 | 4.8 | 1.9 | 0.9 | 0.6 | 0.7 | 1.6 | 1.8 | 3.5 | 5.7 |
| 2017 | 13.8 | 15.5 | 9.7 | | | | | | | | | |
| Min | 4.9 | 6.8 | 5.7 | 3.4 | 1.4 | 0.6 | 0.4 | 0.2 | 0.2 | 0.2 | 0.8 | 2.5 |
| Ave | 9.3 | 11.3 | 9.7 | 5.2 | 2.6 | 1.2 | 0.7 | 0.5 | 0.5 | 0.9 | 1.9 | 4.8 |
| Max | 17.8 | 18.1 | 14.6 | 12.4 | 10.1 | 2.2 | 1.2 | 1.1 | 1.6 | 1.8 | 3.6 | 9.2 |

Appendix V

Maximum Runoff per Year at Aquaflow

| Year | Maximum Runoff (m ³ /s) |
|------|------------------------------------|
| 1978 | 9.5 |
| 1979 | 12.2 |
| 1980 | 14.6 |
| 1981 | 14.7 |
| 1982 | 11.3 |
| 1983 | 13.1 |
| 1984 | 14.1 |
| 1985 | 17.7 |
| 1986 | 15.4 |
| 1987 | 22.3 |
| 1988 | 13.0 |
| 1989 | 19.0 |
| 1990 | 20.1 |
| 1991 | 17.2 |
| 1992 | 14.7 |
| 1993 | 15.1 |
| 1994 | 14.3 |
| 1995 | 12.8 |
| 1996 | 11.7 |
| 1997 | 33.5 |
| 1998 | 11.0 |
| 1999 | 17.8 |
| 2000 | 11.4 |
| 2001 | 24.6 |
| 2002 | 13.3 |
| 2003 | 13.3 |
| 2004 | 15.9 |
| 2005 | 18.8 |

| Year | Maximum Runoff (m³/s) |
|-------------|---|
| 2006 | 19.6 |
| 2007 | 15.9 |
| 2008 | 14.2 |
| 2009 | 16.3 |
| 2010 | 18.0 |
| 2011 | 13.5 |
| 2012 | 16.1 |
| 2013 | 16.6 |
| 2014 | 26.0 |
| 2015 | 20.0 |
| 2016 | 18.9 |
| 2017 | 24.6 |

Appendix VI

Monthly Summary of Runoff Data with Climate Change at the Intake

Average Monthly Runoff at Intake for RCP4.5 (m³/s)

| | Jan | Feb | Mar | Apr | May | Jun | Jul | Aug | Sep | Oct | Nov | Dec |
|------|------|------|------|-----|-----|-----|-----|-----|-----|-----|-----|-----|
| 2021 | 7.9 | 13.4 | 12.5 | 5.7 | 2.1 | 0.8 | 0.4 | 0.3 | 0.4 | 0.6 | 1.8 | 5.4 |
| 2022 | 10.5 | 13.6 | 9.9 | 4.0 | 1.6 | 0.7 | 0.4 | 0.3 | 0.3 | 0.7 | 2.0 | 4.9 |
| 2023 | 11.7 | 12.5 | 11.2 | 6.8 | 2.7 | 1.0 | 0.5 | 0.3 | 0.3 | 0.6 | 1.9 | 6.1 |
| 2024 | 11.3 | 14.1 | 9.8 | 4.9 | 2.2 | 0.9 | 0.5 | 0.4 | 0.3 | 0.6 | 2.0 | 6.7 |
| 2025 | 11.0 | 15.1 | 11.4 | 5.1 | 2.2 | 1.0 | 0.5 | 0.4 | 0.4 | 0.9 | 2.4 | 6.1 |
| 2026 | 11.9 | 13.9 | 10.8 | 5.2 | 2.1 | 0.8 | 0.5 | 0.3 | 0.3 | 0.7 | 1.6 | 4.6 |
| 2027 | 10.4 | 15.5 | 10.0 | 5.2 | 1.8 | 0.8 | 0.4 | 0.3 | 0.4 | 0.7 | 2.1 | 6.0 |
| 2028 | 10.8 | 13.4 | 10.0 | 5.7 | 2.0 | 1.0 | 0.6 | 0.4 | 0.4 | 0.7 | 2.3 | 6.6 |
| 2029 | 10.4 | 13.0 | 8.9 | 4.8 | 1.9 | 1.0 | 0.5 | 0.4 | 0.5 | 0.8 | 2.2 | 5.5 |
| 2030 | 10.1 | 13.1 | 9.7 | 4.7 | 2.4 | 1.1 | 0.6 | 0.4 | 0.5 | 0.7 | 1.9 | 4.9 |
| 2031 | 11.0 | 14.2 | 11.8 | 5.9 | 2.0 | 0.9 | 0.5 | 0.4 | 0.5 | 0.8 | 1.9 | 4.8 |
| 2032 | 10.7 | 17.3 | 11.9 | 5.5 | 2.2 | 0.9 | 0.6 | 0.4 | 0.4 | 1.1 | 2.1 | 5.6 |
| 2033 | 11.3 | 15.4 | 12.2 | 4.6 | 1.8 | 0.8 | 0.4 | 0.4 | 0.5 | 1.0 | 2.9 | 6.4 |
| 2034 | 12.2 | 14.8 | 11.2 | 4.8 | 2.0 | 0.8 | 0.4 | 0.4 | 0.6 | 1.1 | 3.0 | 6.8 |
| 2035 | 11.6 | 13.9 | 10.3 | 4.7 | 2.0 | 0.9 | 0.5 | 0.4 | 0.5 | 0.8 | 2.9 | 7.1 |
| 2036 | 14.7 | 18.8 | 11.1 | 6.0 | 2.6 | 0.9 | 0.5 | 0.3 | 0.3 | 0.7 | 2.2 | 6.3 |
| 2037 | 11.9 | 14.5 | 13.9 | 6.3 | 1.9 | 0.9 | 0.5 | 0.4 | 0.6 | 0.9 | 2.2 | 6.3 |
| 2038 | 15.0 | 17.1 | 10.6 | 5.6 | 2.5 | 1.0 | 0.6 | 0.5 | 0.5 | 0.9 | 2.1 | 6.9 |
| 2039 | 11.4 | 14.0 | 9.4 | 5.1 | 2.0 | 1.1 | 0.6 | 0.4 | 0.4 | 1.0 | 3.2 | 7.3 |
| 2040 | 10.2 | 14.3 | 11.0 | 5.4 | 2.0 | 0.9 | 0.5 | 0.4 | 0.6 | 1.2 | 3.6 | 8.9 |
| 2041 | 13.5 | 15.3 | 12.0 | 5.9 | 2.0 | 1.0 | 0.6 | 0.5 | 0.5 | 0.8 | 2.3 | 7.4 |
| 2042 | 11.7 | 14.0 | 10.7 | 5.3 | 2.2 | 1.1 | 0.6 | 0.4 | 0.5 | 0.8 | 2.0 | 6.1 |
| 2043 | 11.5 | 16.1 | 11.7 | 6.5 | 2.2 | 1.1 | 0.6 | 0.4 | 0.3 | 0.8 | 1.7 | 6.2 |
| 2044 | 11.3 | 12.8 | 10.5 | 5.9 | 2.3 | 1.0 | 0.6 | 0.6 | 0.8 | 0.9 | 2.4 | 5.4 |
| 2045 | 9.8 | 12.5 | 10.5 | 5.4 | 2.2 | 0.9 | 0.5 | 0.4 | 0.6 | 1.4 | 3.7 | 6.3 |
| 2046 | 10.7 | 14.5 | 11.3 | 6.7 | 2.4 | 1.0 | 0.6 | 0.4 | 0.5 | 0.9 | 2.6 | 6.7 |
| 2047 | 12.6 | 15.6 | 10.3 | 5.3 | 2.0 | 0.9 | 0.5 | 0.4 | 0.6 | 1.1 | 2.1 | 5.6 |

| | Jan | Feb | Mar | Apr | May | Jun | Jul | Aug | Sep | Oct | Nov | Dec |
|------------|-------------|-------------|-------------|------------|------------|------------|------------|------------|------------|------------|------------|-------------|
| 2048 | 11.5 | 16.0 | 11.4 | 4.9 | 2.5 | 1.4 | 0.7 | 0.5 | 0.6 | 0.9 | 1.9 | 6.4 |
| 2049 | 11.1 | 14.5 | 10.9 | 6.0 | 2.2 | 0.9 | 0.5 | 0.4 | 0.5 | 1.0 | 3.3 | 8.6 |
| 2050 | 13.3 | 17.6 | 11.4 | 6.0 | 2.4 | 1.2 | 0.6 | 0.5 | 0.5 | 1.0 | 2.5 | 7.2 |
| 2051 | 14.8 | 16.4 | 11.9 | 6.1 | 2.3 | 1.1 | 0.6 | 0.5 | 0.8 | 1.1 | 2.2 | 6.7 |
| 2052 | 13.8 | 14.8 | 12.7 | 6.6 | 2.4 | 1.1 | 0.5 | 0.5 | 0.6 | 0.9 | 1.9 | 6.1 |
| 2053 | 12.7 | 13.8 | 10.6 | 5.6 | 2.2 | 1.0 | 0.5 | 0.5 | 0.6 | 1.1 | 2.8 | 6.4 |
| 2054 | 13.0 | 18.1 | 12.4 | 5.1 | 2.5 | 1.2 | 0.7 | 0.5 | 0.6 | 0.8 | 2.3 | 6.1 |
| 2055 | 13.1 | 15.1 | 12.7 | 6.6 | 2.7 | 1.2 | 0.6 | 0.5 | 0.5 | 0.8 | 2.7 | 7.6 |
| 2056 | 15.5 | 15.7 | 12.3 | 6.2 | 2.0 | 0.9 | 0.5 | 0.3 | 0.6 | 1.2 | 3.3 | 6.7 |
| 2057 | 13.7 | 16.2 | 12.1 | 6.9 | 2.7 | 1.0 | 0.5 | 0.5 | 0.5 | 0.8 | 1.9 | 6.4 |
| 2058 | 15.2 | 15.2 | 12.1 | 6.9 | 2.3 | 1.0 | 0.6 | 0.4 | 0.6 | 1.5 | 2.8 | 7.5 |
| 2059 | 12.8 | 13.9 | 13.6 | 7.6 | 2.6 | 1.0 | 0.5 | 0.5 | 0.7 | 0.9 | 2.3 | 6.7 |
| 2060 | 14.4 | 15.2 | 12.4 | 6.2 | 2.5 | 1.1 | 0.5 | 0.4 | 0.4 | 0.9 | 2.6 | 7.2 |
| 2061 | 17.4 | 15.9 | 10.4 | 6.6 | 2.4 | 1.0 | 0.6 | 0.4 | 0.7 | 1.0 | 2.8 | 9.5 |
| 2062 | 14.8 | 16.8 | 11.9 | 5.5 | 2.5 | 1.3 | 0.7 | 0.5 | 0.5 | 1.1 | 2.5 | 7.3 |
| 2063 | 14.0 | 16.1 | 13.0 | 6.9 | 3.0 | 1.2 | 0.7 | 0.4 | 0.5 | 1.0 | 3.6 | 11.7 |
| 2064 | 17.7 | 15.4 | 11.6 | 6.3 | 2.3 | 0.9 | 0.6 | 0.5 | 0.5 | 1.0 | 2.5 | 7.1 |
| 2065 | 15.5 | 16.6 | 11.2 | 5.7 | 2.3 | 0.9 | 0.5 | 0.3 | 0.4 | 0.9 | 2.3 | 6.1 |
| 2066 | 13.6 | 16.1 | 12.3 | 6.9 | 2.8 | 1.1 | 0.6 | 0.5 | 0.6 | 0.9 | 2.4 | 7.0 |
| 2067 | 14.2 | 16.4 | 14.6 | 7.1 | 2.5 | 1.0 | 0.6 | 0.6 | 0.6 | 1.1 | 2.9 | 8.7 |
| 2068 | 15.3 | 15.2 | 11.6 | 6.3 | 2.7 | 1.3 | 0.7 | 0.5 | 0.7 | 1.1 | 2.5 | 8.1 |
| 2069 | 15.0 | 18.8 | 12.8 | 5.6 | 2.5 | 1.1 | 0.6 | 0.4 | 0.6 | 1.2 | 2.3 | 7.5 |
| 2070 | 16.6 | 17.9 | 12.1 | 5.9 | 2.1 | 1.0 | 0.6 | 0.5 | 0.5 | 0.9 | 2.8 | 7.0 |
| Min | 7.9 | 12.5 | 8.9 | 4.0 | 1.6 | 0.7 | 0.4 | 0.3 | 0.3 | 0.6 | 1.6 | 4.6 |
| Ave | 12.7 | 15.2 | 11.5 | 5.8 | 2.3 | 1.0 | 0.5 | 0.4 | 0.5 | 0.9 | 2.4 | 6.7 |
| Max | 17.7 | 18.8 | 14.6 | 7.6 | 3.0 | 1.4 | 0.7 | 0.6 | 0.8 | 1.5 | 3.7 | 11.7 |

Average Monthly Runoff at Intake for RCP8.5 (m³/s)

| | Jan | Feb | Mar | Apr | May | Jun | Jul | Aug | Sep | Oct | Nov | Dec |
|------|------------|------------|------------|------------|------------|------------|------------|------------|------------|------------|------------|------------|
| 2021 | 8.4 | 15.8 | 10.9 | 5.3 | 1.9 | 0.9 | 0.5 | 0.5 | 0.5 | 0.6 | 1.4 | 4.9 |
| 2022 | 12.2 | 14.6 | 9.2 | 5.6 | 2.3 | 1.0 | 0.7 | 0.4 | 0.5 | 1.0 | 2.9 | 6.7 |
| 2023 | 11.5 | 15.8 | 10.5 | 4.9 | 2.0 | 1.0 | 0.6 | 0.5 | 0.5 | 0.9 | 2.2 | 5.9 |
| 2024 | 10.1 | 13.8 | 9.7 | 4.9 | 1.9 | 1.0 | 0.6 | 0.5 | 0.6 | 1.1 | 2.0 | 5.9 |
| 2025 | 10.4 | 15.2 | 11.8 | 5.2 | 1.9 | 0.8 | 0.4 | 0.4 | 0.5 | 1.0 | 2.0 | 5.4 |
| 2026 | 14.7 | 17.9 | 12.4 | 5.9 | 2.2 | 1.0 | 0.5 | 0.4 | 0.3 | 0.6 | 1.9 | 7.1 |
| 2027 | 11.5 | 13.2 | 10.3 | 5.1 | 2.2 | 0.9 | 0.6 | 0.5 | 0.5 | 0.9 | 2.6 | 5.8 |
| 2028 | 10.9 | 15.5 | 11.2 | 6.5 | 2.5 | 1.1 | 0.5 | 0.4 | 0.4 | 0.8 | 1.7 | 7.0 |
| 2029 | 12.0 | 13.8 | 9.5 | 5.5 | 2.4 | 1.0 | 0.5 | 0.4 | 0.4 | 0.6 | 1.7 | 5.9 |
| 2030 | 12.3 | 14.5 | 11.6 | 5.3 | 2.0 | 0.8 | 0.5 | 0.4 | 0.4 | 0.8 | 2.1 | 5.6 |
| 2031 | 11.2 | 15.4 | 11.8 | 5.5 | 1.9 | 0.9 | 0.5 | 0.4 | 0.6 | 1.0 | 2.4 | 6.2 |
| 2032 | 12.9 | 14.9 | 11.1 | 5.5 | 2.0 | 0.9 | 0.6 | 0.5 | 0.7 | 0.9 | 2.4 | 7.0 |
| 2033 | 10.9 | 14.5 | 10.2 | 5.4 | 2.3 | 1.0 | 0.6 | 0.4 | 0.3 | 0.7 | 2.7 | 7.1 |
| 2034 | 11.6 | 13.4 | 10.9 | 5.3 | 2.3 | 1.0 | 0.6 | 0.5 | 0.6 | 0.7 | 1.8 | 6.5 |
| 2035 | 10.8 | 14.1 | 11.8 | 6.4 | 2.4 | 1.0 | 0.5 | 0.4 | 0.5 | 1.2 | 2.7 | 7.1 |
| 2036 | 12.2 | 16.3 | 11.3 | 5.2 | 2.2 | 1.0 | 0.5 | 0.4 | 0.5 | 0.9 | 2.6 | 7.5 |
| 2037 | 14.2 | 14.0 | 10.4 | 4.3 | 1.9 | 0.9 | 0.5 | 0.4 | 0.4 | 0.8 | 2.1 | 6.8 |
| 2038 | 11.9 | 16.7 | 11.6 | 5.8 | 2.5 | 1.3 | 0.7 | 0.4 | 0.6 | 1.0 | 2.9 | 7.5 |
| 2039 | 13.6 | 16.9 | 12.5 | 5.8 | 2.1 | 0.9 | 0.5 | 0.4 | 0.4 | 0.9 | 2.7 | 7.5 |
| 2040 | 12.8 | 17.7 | 14.1 | 6.2 | 2.4 | 1.0 | 0.5 | 0.4 | 0.5 | 1.1 | 2.7 | 7.3 |
| 2041 | 11.8 | 15.7 | 12.6 | 7.2 | 2.5 | 1.0 | 0.5 | 0.4 | 0.5 | 0.8 | 2.4 | 7.9 |
| 2042 | 17.3 | 21.5 | 14.9 | 6.7 | 2.9 | 1.2 | 0.8 | 1.0 | 0.7 | 1.0 | 2.5 | 6.2 |
| 2043 | 11.3 | 16.1 | 10.5 | 6.2 | 2.7 | 1.3 | 0.7 | 0.4 | 0.5 | 1.0 | 3.0 | 8.3 |
| 2044 | 16.6 | 18.8 | 11.0 | 5.7 | 2.3 | 1.1 | 0.7 | 0.5 | 0.7 | 1.1 | 2.5 | 8.0 |
| 2045 | 13.1 | 15.7 | 12.4 | 6.7 | 2.5 | 1.2 | 0.7 | 0.6 | 0.7 | 1.3 | 2.8 | 7.8 |
| 2046 | 16.2 | 18.8 | 13.4 | 6.5 | 2.2 | 1.0 | 0.6 | 0.4 | 0.5 | 0.9 | 2.7 | 7.2 |
| 2047 | 11.8 | 16.4 | 13.4 | 7.4 | 3.0 | 1.4 | 0.9 | 0.7 | 0.7 | 1.1 | 2.7 | 7.8 |
| 2048 | 13.2 | 15.4 | 11.8 | 6.9 | 2.4 | 1.0 | 0.5 | 0.4 | 0.6 | 1.0 | 2.9 | 8.4 |
| 2049 | 14.9 | 14.3 | 12.4 | 6.0 | 2.2 | 0.9 | 0.5 | 0.4 | 0.5 | 0.9 | 2.8 | 6.7 |
| 2050 | 13.9 | 16.6 | 14.3 | 6.9 | 2.6 | 1.6 | 0.7 | 0.5 | 0.6 | 1.0 | 2.1 | 6.5 |

| | Jan | Feb | Mar | Apr | May | Jun | Jul | Aug | Sep | Oct | Nov | Dec |
|------------|-------------|-------------|-------------|------------|------------|------------|------------|------------|------------|------------|------------|-------------|
| 2051 | 12.5 | 17.4 | 12.3 | 6.5 | 2.8 | 1.2 | 0.7 | 0.5 | 0.5 | 1.2 | 2.5 | 7.2 |
| 2052 | 14.5 | 15.9 | 11.3 | 6.7 | 3.0 | 1.2 | 0.8 | 0.5 | 0.7 | 1.2 | 3.8 | 8.0 |
| 2053 | 17.6 | 17.9 | 12.1 | 5.7 | 2.4 | 1.4 | 0.9 | 0.7 | 0.8 | 1.3 | 3.1 | 9.0 |
| 2054 | 14.4 | 19.9 | 16.7 | 7.2 | 2.4 | 1.1 | 0.6 | 0.5 | 0.6 | 1.0 | 2.9 | 9.7 |
| 2055 | 18.5 | 17.9 | 13.0 | 6.9 | 3.2 | 1.1 | 0.6 | 0.5 | 0.7 | 1.3 | 3.1 | 7.7 |
| 2056 | 14.2 | 18.0 | 13.2 | 6.4 | 2.5 | 1.2 | 0.8 | 0.6 | 1.0 | 2.0 | 3.5 | 8.0 |
| 2057 | 14.2 | 15.1 | 11.7 | 7.5 | 2.8 | 1.3 | 0.7 | 0.6 | 0.8 | 1.2 | 2.8 | 8.5 |
| 2058 | 14.8 | 17.8 | 13.0 | 7.6 | 3.1 | 1.3 | 0.7 | 0.5 | 0.7 | 1.1 | 4.6 | 9.8 |
| 2059 | 17.4 | 20.9 | 15.9 | 6.8 | 2.9 | 1.2 | 0.7 | 0.6 | 0.8 | 1.2 | 3.4 | 8.8 |
| 2060 | 14.2 | 16.8 | 12.4 | 6.5 | 2.7 | 1.3 | 0.9 | 0.6 | 0.6 | 1.2 | 3.7 | 8.2 |
| 2061 | 17.3 | 17.1 | 13.1 | 6.5 | 2.9 | 1.3 | 0.6 | 0.6 | 0.9 | 1.5 | 4.4 | 10.9 |
| 2062 | 17.3 | 16.0 | 14.9 | 6.2 | 2.4 | 1.0 | 0.5 | 0.5 | 0.8 | 1.1 | 3.6 | 9.2 |
| 2063 | 18.7 | 19.7 | 16.5 | 6.7 | 2.6 | 1.1 | 0.6 | 0.5 | 0.8 | 1.4 | 3.3 | 9.6 |
| 2064 | 15.2 | 18.1 | 13.3 | 6.8 | 2.8 | 1.2 | 0.6 | 0.6 | 0.8 | 1.4 | 3.7 | 10.6 |
| 2065 | 19.7 | 20.8 | 14.1 | 6.6 | 2.5 | 1.3 | 0.8 | 0.5 | 0.6 | 1.1 | 3.0 | 8.8 |
| 2066 | 17.9 | 22.0 | 15.2 | 7.8 | 3.3 | 1.3 | 0.7 | 0.7 | 0.7 | 1.2 | 3.2 | 10.5 |
| 2067 | 22.8 | 22.8 | 14.8 | 6.4 | 2.6 | 1.3 | 0.9 | 0.8 | 1.0 | 1.4 | 3.5 | 8.8 |
| 2068 | 19.4 | 19.7 | 14.8 | 7.5 | 3.3 | 1.5 | 0.9 | 0.7 | 0.9 | 1.4 | 3.9 | 10.9 |
| 2069 | 19.3 | 20.0 | 15.4 | 7.1 | 2.8 | 1.1 | 0.9 | 0.6 | 0.8 | 1.5 | 3.4 | 8.7 |
| 2070 | 16.2 | 20.7 | 15.4 | 7.5 | 3.0 | 1.3 | 0.6 | 0.6 | 0.8 | 1.3 | 3.5 | 8.8 |
| Min | 8.4 | 13.2 | 9.2 | 4.3 | 1.9 | 0.8 | 0.4 | 0.4 | 0.3 | 0.6 | 1.4 | 4.9 |
| Ave | 14.2 | 17.0 | 12.6 | 6.2 | 2.5 | 1.1 | 0.6 | 0.5 | 0.6 | 1.1 | 2.8 | 7.7 |
| Max | 22.8 | 22.8 | 16.7 | 7.8 | 3.3 | 1.6 | 0.9 | 1.0 | 1.0 | 2.0 | 4.6 | 10.9 |

Appendix VII

Hydraulic Simulation Results

Hydraulic Characteristics San José River Complete Reach

| Cross Section | Return Period | Riverbed El. (masl) | W.S. El. (masl) | Energy El. (masl) | Flow Vel. (m/s) | Flow Depth (m) | Froude |
|---------------|---------------|---------------------|-----------------|-------------------|-----------------|----------------|--------|
| 5,600 | Tr5y | 1,828.1 | 1,829.0 | 1,830.5 | 5.37 | 0.88 | 2.18 |
| | Tr100y | 1,828.1 | 1,829.2 | 1,831.3 | 6.47 | 1.08 | 2.29 |
| | Tr200y | 1,828.1 | 1,829.3 | 1,831.5 | 6.69 | 1.12 | 2.31 |
| 5,500 | Tr5y | 1,815.9 | 1,816.8 | 1,818.5 | 5.75 | 0.97 | 2.35 |
| | Tr100y | 1,815.9 | 1,817.0 | 1,819.5 | 6.93 | 1.17 | 2.46 |
| | Tr200y | 1,815.9 | 1,817.1 | 1,819.7 | 7.16 | 1.21 | 2.48 |
| 5,400 | Tr5y | 1,810.0 | 1,810.9 | 1,811.9 | 4.36 | 0.90 | 1.79 |
| | Tr100y | 1,810.0 | 1,811.1 | 1,812.5 | 5.20 | 1.11 | 1.88 |
| | Tr200y | 1,810.0 | 1,811.2 | 1,812.6 | 5.36 | 1.15 | 1.90 |
| 5,300 | Tr5y | 1,802.6 | 1,803.8 | 1,805.1 | 5.01 | 1.20 | 1.92 |
| | Tr100y | 1,802.6 | 1,804.1 | 1,805.9 | 6.00 | 1.44 | 1.99 |
| | Tr200y | 1,802.6 | 1,804.1 | 1,806.1 | 6.19 | 1.49 | 2.00 |
| 5,200 | Tr5y | 1,792.6 | 1,793.7 | 1,794.9 | 4.86 | 1.08 | 2.21 |
| | Tr100y | 1,792.6 | 1,793.9 | 1,795.6 | 5.87 | 1.24 | 2.32 |
| | Tr200y | 1,792.6 | 1,793.9 | 1,795.8 | 6.07 | 1.28 | 2.34 |
| 5,100 | Tr5y | 1,781.0 | 1,781.9 | 1,783.3 | 5.30 | 0.86 | 2.41 |
| | Tr100y | 1,781.0 | 1,782.0 | 1,784.1 | 6.34 | 1.03 | 2.50 |
| | Tr200y | 1,781.0 | 1,782.1 | 1,784.2 | 6.53 | 1.07 | 2.52 |
| 5,000 | Tr5y | 1,770.3 | 1,771.2 | 1,772.8 | 5.65 | 0.84 | 2.33 |
| | Tr100y | 1,770.3 | 1,771.4 | 1,773.7 | 6.77 | 1.03 | 2.45 |
| | Tr200y | 1,770.3 | 1,771.4 | 1,773.8 | 6.99 | 1.07 | 2.47 |
| 4,900 | Tr5y | 1,763.3 | 1,764.4 | 1,765.8 | 5.25 | 1.04 | 1.91 |
| | Tr100y | 1,763.3 | 1,764.6 | 1,766.5 | 6.12 | 1.32 | 1.99 |
| | Tr200y | 1,763.3 | 1,764.7 | 1,766.7 | 6.31 | 1.36 | 2.01 |
| 4,800 | Tr5y | 1,756.7 | 1,757.8 | 1,758.6 | 3.98 | 1.07 | 1.82 |
| | Tr100y | 1,756.7 | 1,757.9 | 1,759.1 | 4.82 | 1.23 | 1.92 |
| | Tr200y | 1,756.7 | 1,758.0 | 1,759.2 | 4.98 | 1.26 | 1.94 |

| Cross Section | Return Period | Riverbed El. (masl) | W.S. El. (masl) | Energy El. (masl) | Flow Vel. (m/s) | Flow Depth (m) | Froude |
|----------------------|----------------------|----------------------------|------------------------|--------------------------|------------------------|-----------------------|---------------|
| 4,700 | Tr5y | 1,751.1 | 1,751.8 | 1,752.5 | 3.72 | 0.75 | 1.72 |
| | Tr100y | 1,751.1 | 1,752.0 | 1,753.0 | 4.48 | 0.91 | 1.81 |
| | Tr200y | 1,751.1 | 1,752.0 | 1,753.1 | 4.63 | 0.94 | 1.82 |
| 4,600 | Tr5y | 1,743.0 | 1,743.9 | 1,745.1 | 4.75 | 0.93 | 1.96 |
| | Tr100y | 1,743.0 | 1,744.1 | 1,745.8 | 5.68 | 1.13 | 2.02 |
| | Tr200y | 1,743.0 | 1,744.2 | 1,745.9 | 5.85 | 1.17 | 2.03 |
| 4,500 | Tr5y | 1,733.1 | 1,734.1 | 1,735.6 | 5.43 | 1.00 | 2.20 |
| | Tr100y | 1,733.1 | 1,734.3 | 1,736.4 | 6.47 | 1.22 | 2.28 |
| | Tr200y | 1,733.1 | 1,734.4 | 1,736.6 | 6.67 | 1.26 | 2.30 |
| 4,400 | Tr5y | 1,726.1 | 1,727.0 | 1,728.1 | 4.65 | 0.85 | 1.94 |
| | Tr100y | 1,726.1 | 1,727.2 | 1,728.7 | 5.55 | 1.05 | 2.04 |
| | Tr200y | 1,726.1 | 1,727.2 | 1,728.9 | 5.73 | 1.08 | 2.06 |
| 4,300 | Tr5y | 1,719.6 | 1,720.5 | 1,721.4 | 4.22 | 0.95 | 1.83 |
| | Tr100y | 1,719.6 | 1,720.7 | 1,722.0 | 5.11 | 1.12 | 1.93 |
| | Tr200y | 1,719.6 | 1,720.7 | 1,722.2 | 5.28 | 1.16 | 1.94 |
| 4,200 | Tr5y | 1,714.0 | 1,714.6 | 1,715.1 | 3.15 | 0.63 | 1.61 |
| | Tr100y | 1,714.0 | 1,714.8 | 1,715.4 | 3.62 | 0.77 | 1.66 |
| | Tr200y | 1,714.0 | 1,714.8 | 1,715.5 | 3.72 | 0.80 | 1.67 |
| 4,100 | Tr5y | 1,711.0 | 1,711.9 | 1,712.2 | 2.70 | 0.85 | 1.12 |
| | Tr100y | 1,711.0 | 1,712.1 | 1,712.6 | 3.15 | 1.07 | 1.14 |
| | Tr200y | 1,711.0 | 1,712.1 | 1,712.7 | 3.24 | 1.11 | 1.14 |
| 4,000 | Tr5y | 1,707.4 | 1,708.3 | 1,708.8 | 3.13 | 0.88 | 1.33 |
| | Tr100y | 1,707.4 | 1,708.5 | 1,709.2 | 3.78 | 1.06 | 1.40 |
| | Tr200y | 1,707.4 | 1,708.5 | 1,709.3 | 3.91 | 1.09 | 1.41 |
| 3,900 | Tr5y | 1,699.0 | 1,699.6 | 1,700.4 | 4.08 | 0.55 | 2.01 |
| | Tr100y | 1,699.0 | 1,699.7 | 1,700.9 | 4.92 | 0.69 | 2.10 |
| | Tr200y | 1,699.0 | 1,699.7 | 1,701.0 | 5.09 | 0.72 | 2.13 |
| 3,800 | Tr5y | 1,693.7 | 1,694.7 | 1,695.3 | 3.44 | 0.93 | 1.55 |
| | Tr100y | 1,693.7 | 1,694.8 | 1,695.7 | 4.06 | 1.10 | 1.62 |
| | Tr200y | 1,693.7 | 1,694.9 | 1,695.8 | 4.19 | 1.13 | 1.63 |

| Cross Section | Return Period | Riverbed El. (masl) | W.S. El. (masl) | Energy El. (masl) | Flow Vel. (m/s) | Flow Depth (m) | Froude |
|----------------------|----------------------|----------------------------|------------------------|--------------------------|------------------------|-----------------------|---------------|
| 3,700 | Tr5y | 1,688.9 | 1,689.8 | 1,690.5 | 3.70 | 0.92 | 1.56 |
| | Tr100y | 1,688.9 | 1,690.0 | 1,691.0 | 4.45 | 1.11 | 1.62 |
| | Tr200y | 1,688.9 | 1,690.1 | 1,691.1 | 4.59 | 1.15 | 1.63 |
| 3,600 | Tr5y | 1,684.8 | 1,685.6 | 1,686.1 | 3.05 | 0.89 | 1.44 |
| | Tr100y | 1,684.8 | 1,685.8 | 1,686.5 | 3.57 | 1.05 | 1.51 |
| | Tr200y | 1,684.8 | 1,685.8 | 1,686.5 | 3.67 | 1.08 | 1.52 |
| 3,500 | Tr5y | 1,679.5 | 1,680.6 | 1,681.2 | 3.41 | 1.06 | 1.54 |
| | Tr100y | 1,679.5 | 1,680.8 | 1,681.6 | 4.08 | 1.23 | 1.61 |
| | Tr200y | 1,679.5 | 1,680.8 | 1,681.7 | 4.21 | 1.26 | 1.62 |
| 3,400 | Tr5y | 1,675.0 | 1,675.8 | 1,676.4 | 3.43 | 0.76 | 1.56 |
| | Tr100y | 1,675.0 | 1,675.9 | 1,676.8 | 4.10 | 0.93 | 1.63 |
| | Tr200y | 1,675.0 | 1,676.0 | 1,676.9 | 4.23 | 0.96 | 1.64 |
| 3,300 | Tr5y | 1,670.5 | 1,671.5 | 1,672.1 | 3.58 | 0.98 | 1.48 |
| | Tr100y | 1,670.5 | 1,671.7 | 1,672.6 | 4.17 | 1.20 | 1.53 |
| | Tr200y | 1,670.5 | 1,671.7 | 1,672.7 | 4.30 | 1.24 | 1.55 |
| 3,200 | Tr5y | 1,666.8 | 1,667.7 | 1,668.1 | 3.00 | 0.88 | 1.38 |
| | Tr100y | 1,666.8 | 1,667.8 | 1,668.5 | 3.58 | 1.04 | 1.46 |
| | Tr200y | 1,666.8 | 1,667.9 | 1,668.6 | 3.71 | 1.07 | 1.47 |
| 3,100 | Tr5y | 1,662.0 | 1,663.0 | 1,663.7 | 3.82 | 0.96 | 1.50 |
| | Tr100y | 1,662.0 | 1,663.2 | 1,664.2 | 4.50 | 1.20 | 1.52 |
| | Tr200y | 1,662.0 | 1,663.3 | 1,664.3 | 4.62 | 1.25 | 1.52 |
| 3,000 | Tr5y | 1,658.6 | 1,659.6 | 1,659.9 | 2.53 | 0.97 | 1.26 |
| | Tr100y | 1,658.6 | 1,659.7 | 1,660.2 | 3.07 | 1.10 | 1.34 |
| | Tr200y | 1,658.6 | 1,659.7 | 1,660.2 | 3.19 | 1.13 | 1.36 |
| 2,900 | Tr5y | 1,655.1 | 1,656.0 | 1,656.5 | 3.16 | 0.85 | 1.30 |
| | Tr100y | 1,655.1 | 1,656.2 | 1,656.9 | 3.74 | 1.06 | 1.32 |
| | Tr200y | 1,655.1 | 1,656.2 | 1,657.0 | 3.85 | 1.11 | 1.32 |
| 2,800 | Tr5y | 1,650.0 | 1,650.9 | 1,651.8 | 4.08 | 0.93 | 1.59 |
| | Tr100y | 1,650.0 | 1,651.2 | 1,652.4 | 4.86 | 1.17 | 1.63 |
| | Tr200y | 1,650.0 | 1,651.2 | 1,652.5 | 5.00 | 1.22 | 1.63 |

| Cross Section | Return Period | Riverbed El. (masl) | W.S. El. (masl) | Energy El. (masl) | Flow Vel. (m/s) | Flow Depth (m) | Froude |
|----------------------|----------------------|----------------------------|------------------------|--------------------------|------------------------|-----------------------|---------------|
| 2,700 | Tr5y | 1,646.0 | 1,646.8 | 1,647.3 | 3.17 | 0.78 | 1.46 |
| | Tr100y | 1,646.0 | 1,647.0 | 1,647.7 | 3.81 | 0.94 | 1.54 |
| | Tr200y | 1,646.0 | 1,647.0 | 1,647.8 | 3.94 | 0.97 | 1.56 |
| 2,600 | Tr5y | 1,639.7 | 1,640.7 | 1,641.6 | 4.19 | 0.96 | 1.71 |
| | Tr100y | 1,639.7 | 1,640.9 | 1,642.2 | 5.00 | 1.17 | 1.76 |
| | Tr200y | 1,639.7 | 1,640.9 | 1,642.3 | 5.16 | 1.21 | 1.77 |
| 2,500 | Tr5y | 1,631.1 | 1,632.0 | 1,633.4 | 5.21 | 0.92 | 2.10 |
| | Tr100y | 1,631.1 | 1,632.2 | 1,634.1 | 6.15 | 1.14 | 2.17 |
| | Tr200y | 1,631.1 | 1,632.2 | 1,634.3 | 6.34 | 1.18 | 2.19 |
| 2,400 | Tr5y | 1,625.0 | 1,625.9 | 1,627.0 | 4.50 | 0.89 | 1.83 |
| | Tr100y | 1,625.0 | 1,626.1 | 1,627.7 | 5.45 | 1.10 | 1.92 |
| | Tr200y | 1,625.0 | 1,626.2 | 1,627.8 | 5.63 | 1.14 | 1.94 |
| 2,300 | Tr5y | 1,619.4 | 1,620.8 | 1,622.0 | 4.81 | 1.42 | 1.64 |
| | Tr100y | 1,619.4 | 1,621.1 | 1,622.8 | 5.70 | 1.73 | 1.68 |
| | Tr200y | 1,619.4 | 1,621.2 | 1,622.9 | 5.87 | 1.79 | 1.69 |
| 2,200 | Tr5y | 1,614.3 | 1,615.0 | 1,615.8 | 4.02 | 0.71 | 1.73 |
| | Tr100y | 1,614.3 | 1,615.2 | 1,616.4 | 4.86 | 0.89 | 1.83 |
| | Tr200y | 1,614.3 | 1,615.2 | 1,616.5 | 5.02 | 0.93 | 1.85 |
| 2,100 | Tr5y | 1,608.6 | 1,609.5 | 1,610.1 | 3.37 | 0.97 | 1.63 |
| | Tr100y | 1,608.6 | 1,609.7 | 1,610.4 | 3.66 | 1.16 | 1.63 |
| | Tr200y | 1,608.6 | 1,609.7 | 1,610.5 | 3.74 | 1.19 | 1.66 |
| 2,000 | Tr5y | 1,605.5 | 1,606.3 | 1,606.6 | 2.44 | 0.71 | 1.26 |
| | Tr100y | 1,605.5 | 1,606.4 | 1,606.8 | 2.92 | 0.85 | 1.32 |
| | Tr200y | 1,605.5 | 1,606.4 | 1,606.9 | 3.03 | 0.87 | 1.33 |
| 1,900 | Tr5y | 1,601.1 | 1,602.8 | 1,603.4 | 3.44 | 1.72 | 0.94 |
| | Tr100y | 1,601.1 | 1,603.2 | 1,604.0 | 4.04 | 2.15 | 0.96 |
| | Tr200y | 1,601.1 | 1,603.3 | 1,604.1 | 4.15 | 2.25 | 0.96 |
| 1,800 | Tr5y | 1,592.4 | 1,593.4 | 1,594.9 | 5.51 | 0.96 | 2.20 |
| | Tr100y | 1,592.4 | 1,593.6 | 1,595.8 | 6.69 | 1.16 | 2.33 |
| | Tr200y | 1,592.4 | 1,593.6 | 1,596.0 | 6.92 | 1.20 | 2.36 |

| Cross Section | Return Period | Riverbed El. (masl) | W.S. El. (masl) | Energy El. (masl) | Flow Vel. (m/s) | Flow Depth (m) | Froude |
|----------------------|----------------------|----------------------------|------------------------|--------------------------|------------------------|-----------------------|---------------|
| 1,700 | Tr5y | 1,584.0 | 1,584.6 | 1,585.4 | 3.91 | 0.64 | 2.01 |
| | Tr100y | 1,584.0 | 1,584.8 | 1,585.9 | 4.70 | 0.76 | 2.13 |
| | Tr200y | 1,584.0 | 1,584.8 | 1,586.0 | 4.86 | 0.79 | 2.15 |
| 1,600 | Tr5y | 1,579.0 | 1,579.9 | 1,580.7 | 3.82 | 0.94 | 1.53 |
| | Tr100y | 1,579.0 | 1,580.2 | 1,581.2 | 4.49 | 1.18 | 1.56 |
| | Tr200y | 1,579.0 | 1,580.2 | 1,581.3 | 4.62 | 1.22 | 1.56 |
| 1,500 | Tr5y | 1,571.6 | 1,572.4 | 1,573.3 | 4.37 | 0.79 | 1.96 |
| | Tr100y | 1,571.6 | 1,572.5 | 1,573.9 | 5.28 | 0.95 | 2.07 |
| | Tr200y | 1,571.6 | 1,572.6 | 1,574.1 | 5.46 | 0.98 | 2.09 |
| 1,400 | Tr5y | 1,564.3 | 1,565.3 | 1,566.0 | 3.62 | 1.05 | 1.73 |
| | Tr100y | 1,564.3 | 1,565.5 | 1,566.3 | 3.94 | 1.22 | 1.85 |
| | Tr200y | 1,564.3 | 1,565.5 | 1,566.3 | 4.03 | 1.24 | 1.85 |
| 1,300 | Tr5y | 1,559.4 | 1,560.3 | 1,560.9 | 3.44 | 0.90 | 1.52 |
| | Tr100y | 1,559.4 | 1,560.5 | 1,561.3 | 4.08 | 1.09 | 1.56 |
| | Tr200y | 1,559.4 | 1,560.5 | 1,561.4 | 4.20 | 1.12 | 1.56 |
| 1,200 | Tr5y | 1,554.1 | 1,554.8 | 1,555.4 | 3.39 | 0.70 | 1.63 |
| | Tr100y | 1,554.1 | 1,554.9 | 1,555.8 | 4.10 | 0.85 | 1.71 |
| | Tr200y | 1,554.1 | 1,555.0 | 1,555.9 | 4.23 | 0.88 | 1.73 |
| 1,100 | Tr5y | 1,549.1 | 1,550.0 | 1,550.7 | 3.79 | 0.85 | 1.55 |
| | Tr100y | 1,549.1 | 1,550.2 | 1,551.2 | 4.50 | 1.07 | 1.59 |
| | Tr200y | 1,549.1 | 1,550.2 | 1,551.3 | 4.63 | 1.11 | 1.60 |
| 1,000 | Tr5y | 1,544.8 | 1,545.9 | 1,546.5 | 3.34 | 1.16 | 1.45 |
| | Tr100y | 1,544.8 | 1,546.1 | 1,546.9 | 4.04 | 1.34 | 1.53 |
| | Tr200y | 1,544.8 | 1,546.1 | 1,547.0 | 4.17 | 1.38 | 1.54 |
| 900 | Tr5y | 1,539.2 | 1,540.5 | 1,540.9 | 2.78 | 1.24 | 0.99 |
| | Tr100y | 1,539.2 | 1,540.5 | 1,541.5 | 4.60 | 1.22 | 1.64 |
| | Tr200y | 1,539.2 | 1,540.5 | 1,541.7 | 4.86 | 1.24 | 1.72 |
| 800 | Tr5y | 1,535.6 | 1,536.5 | 1,537.0 | 3.05 | 0.96 | 1.37 |
| | Tr100y | 1,535.6 | 1,536.7 | 1,537.4 | 3.71 | 1.12 | 1.45 |
| | Tr200y | 1,535.6 | 1,536.7 | 1,537.5 | 3.84 | 1.15 | 1.47 |

| Cross Section | Return Period | Riverbed El. (masl) | W.S. El. (masl) | Energy El. (masl) | Flow Vel. (m/s) | Flow Depth (m) | Froude |
|----------------------|----------------------|----------------------------|------------------------|--------------------------|------------------------|-----------------------|---------------|
| 700 | Tr5y | 1,532.0 | 1,533.0 | 1,533.4 | 2.78 | 0.99 | 1.30 |
| | Tr100y | 1,532.0 | 1,533.1 | 1,533.7 | 3.38 | 1.14 | 1.38 |
| | Tr200y | 1,532.0 | 1,533.2 | 1,533.8 | 3.50 | 1.17 | 1.40 |
| 600 | Tr5y | 1,528.1 | 1,528.9 | 1,529.3 | 2.71 | 0.77 | 1.39 |
| | Tr100y | 1,528.1 | 1,529.0 | 1,529.6 | 3.26 | 0.89 | 1.46 |
| | Tr200y | 1,528.1 | 1,529.0 | 1,529.6 | 3.37 | 0.91 | 1.48 |
| 500 | Tr5y | 1,523.7 | 1,524.5 | 1,524.9 | 2.66 | 0.78 | 1.41 |
| | Tr100y | 1,523.7 | 1,524.6 | 1,525.2 | 3.19 | 0.90 | 1.48 |
| | Tr200y | 1,523.7 | 1,524.7 | 1,525.2 | 3.29 | 0.93 | 1.49 |
| 400 | Tr5y | 1,520.2 | 1,521.2 | 1,521.6 | 2.93 | 1.01 | 1.26 |
| | Tr100y | 1,520.2 | 1,521.4 | 1,522.0 | 3.50 | 1.20 | 1.30 |
| | Tr200y | 1,520.2 | 1,521.4 | 1,522.1 | 3.61 | 1.23 | 1.31 |
| 300 | Tr5y | 1,517.8 | 1,518.8 | 1,519.1 | 2.64 | 0.93 | 1.15 |
| | Tr100y | 1,517.8 | 1,519.1 | 1,519.4 | 2.42 | 1.28 | 0.83 |
| | Tr200y | 1,517.8 | 1,519.2 | 1,519.4 | 2.39 | 1.35 | 0.79 |
| 200 | Tr5y | 1,515.1 | 1,516.2 | 1,516.6 | 2.81 | 1.04 | 1.15 |
| | Tr100y | 1,515.1 | 1,516.4 | 1,516.9 | 3.37 | 1.25 | 1.20 |
| | Tr200y | 1,515.1 | 1,516.4 | 1,517.0 | 3.48 | 1.29 | 1.21 |
| 100 | Tr5y | 1,512.6 | 1,513.5 | 1,513.9 | 2.67 | 0.93 | 1.19 |
| | Tr100y | 1,512.6 | 1,513.7 | 1,514.2 | 3.24 | 1.09 | 1.27 |
| | Tr200y | 1,512.6 | 1,513.7 | 1,514.3 | 3.37 | 1.12 | 1.29 |
| 0 | Tr5y | 1,510.0 | 1,510.7 | 1,511.1 | 2.57 | 0.70 | 1.18 |
| | Tr100y | 1,510.0 | 1,510.9 | 1,511.4 | 3.11 | 0.86 | 1.25 |
| | Tr200y | 1,510.0 | 1,510.9 | 1,511.4 | 3.21 | 0.89 | 1.26 |

Hydraulic Characteristics San José River Powerhouse Reach

| Cross Section | Return Period | Riverbed El. (masl) | W.S. El. (masl) | Energy El. (masl) | Flow Vel. (m/s) | Flow Depth (m) | Froude |
|----------------------|----------------------|----------------------------|------------------------|--------------------------|------------------------|-----------------------|---------------|
| 1,500 | Tr5y | 1,572.0 | 1,572.8 | 1,573.5 | 3.85 | 0.77 | 1.73 |
| | Tr100y | 1,572.0 | 1,573.0 | 1,574.0 | 4.62 | 0.95 | 1.81 |
| | Tr200y | 1,572.0 | 1,573.0 | 1,574.1 | 4.76 | 0.98 | 1.82 |
| 1,475 | Tr5y | 1,569.2 | 1,570.3 | 1,571.5 | 4.91 | 1.13 | 1.98 |
| | Tr100y | 1,569.2 | 1,570.6 | 1,572.0 | 5.36 | 1.38 | 2.12 |
| | Tr200y | 1,569.2 | 1,570.6 | 1,572.1 | 5.47 | 1.42 | 2.13 |
| 1,450 | Tr5y | 1,568.0 | 1,568.7 | 1,569.4 | 3.68 | 0.70 | 1.80 |
| | Tr100y | 1,568.0 | 1,568.9 | 1,569.9 | 4.40 | 0.84 | 1.93 |
| | Tr200y | 1,568.0 | 1,568.9 | 1,570.0 | 4.55 | 0.87 | 1.95 |
| 1,425 | Tr5y | 1,566.2 | 1,567.0 | 1,567.9 | 4.10 | 0.83 | 1.76 |
| | Tr100y | 1,566.2 | 1,567.3 | 1,568.1 | 4.04 | 1.13 | 1.69 |
| | Tr200y | 1,566.2 | 1,567.4 | 1,568.2 | 4.08 | 1.17 | 1.75 |
| 1,400 | Tr5y | 1,564.6 | 1,565.8 | 1,566.1 | 2.39 | 1.29 | 1.00 |
| | Tr100y | 1,564.6 | 1,566.1 | 1,566.4 | 2.64 | 1.54 | 0.98 |
| | Tr200y | 1,564.6 | 1,566.1 | 1,566.5 | 2.70 | 1.58 | 0.99 |
| 1,375 | Tr5y | 1,563.0 | 1,564.0 | 1,564.4 | 2.54 | 1.03 | 1.00 |
| | Tr100y | 1,563.0 | 1,564.3 | 1,564.7 | 2.96 | 1.28 | 1.01 |
| | Tr200y | 1,563.0 | 1,564.3 | 1,564.8 | 3.00 | 1.34 | 0.99 |
| 1,350 | Tr5y | 1,562.0 | 1,563.2 | 1,563.5 | 2.49 | 1.15 | 0.99 |
| | Tr100y | 1,562.0 | 1,563.5 | 1,563.8 | 2.59 | 1.45 | 1.03 |
| | Tr200y | 1,562.0 | 1,563.5 | 1,563.9 | 2.60 | 1.50 | 1.00 |
| 1,325 | Tr5y | 1,560.6 | 1,561.6 | 1,562.2 | 3.52 | 0.99 | 1.64 |
| | Tr100y | 1,560.6 | 1,561.8 | 1,562.6 | 3.91 | 1.19 | 1.61 |
| | Tr200y | 1,560.6 | 1,561.8 | 1,562.6 | 3.99 | 1.23 | 1.60 |
| 1,300 | Tr5y | 1,559.6 | 1,560.5 | 1,561.1 | 3.34 | 0.91 | 1.51 |
| | Tr100y | 1,559.6 | 1,560.7 | 1,561.4 | 3.87 | 1.10 | 1.53 |
| | Tr200y | 1,559.6 | 1,560.7 | 1,561.5 | 3.94 | 1.14 | 1.51 |
| 1,275 | Tr5y | 1,558.1 | 1,559.4 | 1,559.8 | 2.73 | 1.31 | 0.99 |
| | Tr100y | 1,558.1 | 1,559.4 | 1,560.4 | 4.34 | 1.32 | 1.56 |

| Cross Section | Return Period | Riverbed El. (masl) | W.S. El. (masl) | Energy El. (masl) | Flow Vel. (m/s) | Flow Depth (m) | Froude |
|----------------------|----------------------|----------------------------|------------------------|--------------------------|------------------------|-----------------------|---------------|
| | Tr200y | 1,558.1 | 1,559.5 | 1,560.5 | 4.43 | 1.37 | 1.56 |
| 1,250 | Tr5y | 1,556.8 | 1,557.9 | 1,558.6 | 3.70 | 1.08 | 1.61 |
| | Tr100y | 1,556.8 | 1,558.0 | 1,559.1 | 4.54 | 1.24 | 1.76 |
| | Tr200y | 1,556.8 | 1,558.1 | 1,559.2 | 4.68 | 1.28 | 1.77 |
| 1,225 | Tr5y | 1,555.8 | 1,556.9 | 1,557.5 | 3.37 | 1.12 | 1.49 |
| | Tr100y | 1,555.8 | 1,557.1 | 1,557.9 | 3.91 | 1.32 | 1.51 |
| | Tr200y | 1,555.8 | 1,557.1 | 1,557.9 | 4.01 | 1.36 | 1.52 |
| 1,200 | Tr5y | 1,554.0 | 1,555.2 | 1,555.5 | 2.40 | 1.22 | 0.99 |
| | Tr100y | 1,554.0 | 1,555.2 | 1,556.1 | 4.34 | 1.15 | 1.89 |
| | Tr200y | 1,554.0 | 1,555.2 | 1,556.2 | 4.56 | 1.17 | 1.96 |
| 1,175 | Tr5y | 1,552.7 | 1,553.7 | 1,554.4 | 3.73 | 1.03 | 1.49 |
| | Tr100y | 1,552.7 | 1,554.0 | 1,554.8 | 3.94 | 1.28 | 1.64 |
| | Tr200y | 1,552.7 | 1,554.0 | 1,554.8 | 4.05 | 1.31 | 1.65 |
| 1,150 | Tr5y | 1,551.1 | 1,552.2 | 1,553.1 | 4.22 | 1.07 | 1.76 |
| | Tr100y | 1,551.1 | 1,552.4 | 1,553.5 | 4.55 | 1.34 | 1.70 |
| | Tr200y | 1,551.1 | 1,552.5 | 1,553.5 | 4.54 | 1.40 | 1.66 |
| 1,125 | Tr5y | 1,550.0 | 1,551.1 | 1,551.9 | 3.72 | 1.10 | 1.54 |
| | Tr100y | 1,550.0 | 1,551.4 | 1,552.3 | 4.21 | 1.34 | 1.61 |
| | Tr200y | 1,550.0 | 1,551.4 | 1,552.4 | 4.29 | 1.38 | 1.62 |
| 1,100 | Tr5y | 1,549.0 | 1,550.1 | 1,550.8 | 3.82 | 1.05 | 1.49 |
| | Tr100y | 1,549.0 | 1,550.3 | 1,551.3 | 4.29 | 1.32 | 1.50 |
| | Tr200y | 1,549.0 | 1,550.4 | 1,551.4 | 4.39 | 1.37 | 1.50 |
| 1,075 | Tr5y | 1,548.2 | 1,549.2 | 1,549.9 | 3.65 | 0.98 | 1.44 |
| | Tr100y | 1,548.2 | 1,549.5 | 1,550.4 | 4.29 | 1.22 | 1.48 |
| | Tr200y | 1,548.2 | 1,549.5 | 1,550.5 | 4.41 | 1.26 | 1.49 |
| 1,050 | Tr5y | 1,547.0 | 1,548.0 | 1,548.8 | 3.93 | 0.97 | 1.60 |
| | Tr100y | 1,547.0 | 1,548.2 | 1,549.3 | 4.65 | 1.18 | 1.66 |
| | Tr200y | 1,547.0 | 1,548.3 | 1,549.4 | 4.79 | 1.23 | 1.67 |
| 1,025 | Tr5y | 1,546.2 | 1,547.3 | 1,547.9 | 3.69 | 1.05 | 1.45 |
| | Tr100y | 1,546.2 | 1,547.5 | 1,548.3 | 4.44 | 1.24 | 1.56 |

| Cross Section | Return Period | Riverbed El. (masl) | W.S. El. (masl) | Energy El. (masl) | Flow Vel. (m/s) | Flow Depth (m) | Froude |
|----------------------|----------------------|----------------------------|------------------------|--------------------------|------------------------|-----------------------|---------------|
| 1,000 | Tr200y | 1,546.2 | 1,547.5 | 1,548.4 | 4.59 | 1.28 | 1.58 |
| | Tr5y | 1,545.1 | 1,546.0 | 1,546.8 | 4.14 | 0.92 | 1.65 |
| | Tr100y | 1,545.1 | 1,546.2 | 1,547.3 | 4.84 | 1.13 | 1.72 |
| 975 | Tr200y | 1,545.1 | 1,546.2 | 1,547.4 | 4.95 | 1.18 | 1.72 |
| | Tr5y | 1,544.0 | 1,544.9 | 1,545.6 | 3.65 | 0.90 | 1.63 |
| | Tr100y | 1,544.0 | 1,545.1 | 1,546.0 | 4.28 | 1.08 | 1.68 |
| 950 | Tr200y | 1,544.0 | 1,545.1 | 1,546.1 | 4.41 | 1.12 | 1.69 |
| | Tr5y | 1,542.0 | 1,543.1 | 1,543.5 | 2.71 | 1.11 | 1.00 |
| | Tr100y | 1,542.0 | 1,543.0 | 1,544.3 | 5.08 | 1.00 | 1.97 |
| 925 | Tr200y | 1,542.0 | 1,543.0 | 1,544.4 | 5.19 | 1.04 | 1.96 |
| | Tr5y | 1,541.0 | 1,541.9 | 1,542.2 | 2.29 | 0.93 | 0.99 |
| | Tr100y | 1,541.0 | 1,541.9 | 1,542.7 | 3.79 | 0.91 | 1.65 |
| 900 | Tr200y | 1,541.0 | 1,541.9 | 1,542.7 | 3.92 | 0.94 | 1.67 |
| | Tr5y | 1,539.5 | 1,540.6 | 1,541.1 | 3.17 | 1.09 | 1.39 |
| | Tr100y | 1,539.5 | 1,540.7 | 1,541.5 | 3.76 | 1.27 | 1.49 |
| 875 | Tr200y | 1,539.5 | 1,540.8 | 1,541.5 | 3.88 | 1.30 | 1.51 |
| | Tr5y | 1,538.0 | 1,539.1 | 1,539.9 | 4.13 | 1.07 | 1.63 |
| | Tr100y | 1,538.0 | 1,539.4 | 1,540.4 | 4.50 | 1.37 | 1.54 |
| 850 | Tr200y | 1,538.0 | 1,539.4 | 1,540.5 | 4.60 | 1.43 | 1.56 |
| | Tr5y | 1,537.6 | 1,538.6 | 1,539.1 | 3.08 | 1.06 | 1.37 |
| | Tr100y | 1,537.6 | 1,538.8 | 1,539.5 | 3.61 | 1.24 | 1.48 |
| 825 | Tr200y | 1,537.6 | 1,538.8 | 1,539.5 | 3.64 | 1.28 | 1.45 |
| | Tr5y | 1,536.5 | 1,537.7 | 1,538.2 | 3.07 | 1.17 | 1.36 |
| | Tr100y | 1,536.5 | 1,537.9 | 1,538.6 | 3.61 | 1.35 | 1.38 |
| 800 | Tr200y | 1,536.5 | 1,537.9 | 1,538.6 | 3.71 | 1.40 | 1.37 |
| | Tr5y | 1,535.9 | 1,536.7 | 1,537.2 | 3.20 | 0.81 | 1.48 |
| | Tr100y | 1,535.9 | 1,536.9 | 1,537.6 | 3.80 | 0.98 | 1.53 |
| 775 | Tr200y | 1,535.9 | 1,536.9 | 1,537.7 | 3.89 | 1.02 | 1.52 |
| | Tr5y | 1,535.0 | 1,536.0 | 1,536.4 | 3.05 | 0.92 | 1.26 |
| | Tr100y | 1,535.0 | 1,536.2 | 1,536.8 | 3.60 | 1.13 | 1.28 |

| Cross Section | Return Period | Riverbed El. (masl) | W.S. El. (masl) | Energy El. (masl) | Flow Vel. (m/s) | Flow Depth (m) | Froude |
|----------------------|----------------------|----------------------------|------------------------|--------------------------|------------------------|-----------------------|---------------|
| 750 | Tr200y | 1,535.0 | 1,536.2 | 1,536.9 | 3.70 | 1.18 | 1.28 |
| | Tr5y | 1,534.0 | 1,535.0 | 1,535.7 | 3.56 | 1.00 | 1.37 |
| | Tr100y | 1,534.0 | 1,535.3 | 1,536.1 | 3.98 | 1.30 | 1.35 |
| 725 | Tr200y | 1,534.0 | 1,535.4 | 1,536.2 | 4.07 | 1.35 | 1.34 |
| | Tr5y | 1,533.0 | 1,534.1 | 1,534.5 | 2.85 | 1.07 | 1.05 |
| | Tr100y | 1,533.0 | 1,534.1 | 1,534.3 | 2.56 | 1.07 | 0.94 |
| 700 | Tr200y | 1,533.0 | 1,534.1 | 1,534.3 | 2.68 | 1.09 | 0.97 |
| | Tr5y | 1,532.1 | 1,533.0 | 1,533.3 | 2.82 | 0.86 | 1.27 |
| | Tr100y | 1,532.1 | 1,533.1 | 1,533.6 | 3.33 | 1.03 | 1.31 |
| 675 | Tr200y | 1,532.1 | 1,533.2 | 1,533.6 | 3.41 | 1.07 | 1.30 |
| | Tr5y | 1,531.4 | 1,532.3 | 1,532.7 | 2.99 | 0.86 | 1.35 |
| | Tr100y | 1,531.4 | 1,532.4 | 1,532.9 | 3.47 | 1.01 | 1.41 |
| 650 | Tr200y | 1,531.4 | 1,532.4 | 1,533.0 | 3.57 | 1.04 | 1.43 |
| | Tr5y | 1,530.0 | 1,530.9 | 1,531.6 | 3.80 | 0.93 | 1.64 |
| | Tr100y | 1,530.0 | 1,531.2 | 1,532.0 | 4.19 | 1.16 | 1.57 |
| 625 | Tr200y | 1,530.0 | 1,531.2 | 1,532.0 | 4.26 | 1.20 | 1.57 |
| | Tr5y | 1,529.0 | 1,529.8 | 1,530.5 | 3.46 | 0.84 | 1.54 |
| | Tr100y | 1,529.0 | 1,530.0 | 1,530.9 | 4.07 | 1.02 | 1.64 |
| 600 | Tr200y | 1,529.0 | 1,530.1 | 1,531.0 | 4.19 | 1.06 | 1.65 |
| | Tr5y | 1,528.4 | 1,529.1 | 1,529.5 | 2.91 | 0.75 | 1.43 |
| | Tr100y | 1,528.4 | 1,529.3 | 1,529.8 | 3.34 | 0.92 | 1.45 |
| 575 | Tr200y | 1,528.4 | 1,529.3 | 1,529.8 | 3.42 | 0.95 | 1.45 |
| | Tr5y | 1,527.2 | 1,528.0 | 1,528.3 | 2.49 | 0.84 | 1.27 |
| | Tr100y | 1,527.2 | 1,528.1 | 1,528.6 | 3.10 | 0.96 | 1.39 |
| 550 | Tr200y | 1,527.2 | 1,528.1 | 1,528.7 | 3.21 | 0.98 | 1.41 |
| | Tr5y | 1,526.3 | 1,527.0 | 1,527.3 | 2.62 | 0.71 | 1.43 |
| | Tr100y | 1,526.3 | 1,527.1 | 1,527.6 | 3.15 | 0.81 | 1.54 |
| 525 | Tr200y | 1,526.3 | 1,527.1 | 1,527.6 | 3.24 | 0.83 | 1.54 |
| | Tr5y | 1,525.0 | 1,525.6 | 1,526.0 | 2.96 | 0.56 | 1.65 |
| | Tr100y | 1,525.0 | 1,525.7 | 1,526.2 | 3.49 | 0.67 | 1.72 |

| Cross Section | Return Period | Riverbed El. (masl) | W.S. El. (masl) | Energy El. (masl) | Flow Vel. (m/s) | Flow Depth (m) | Froude |
|----------------------|----------------------|----------------------------|------------------------|--------------------------|------------------------|-----------------------|---------------|
| 500 | Tr200y | 1,525.0 | 1,525.7 | 1,526.3 | 3.60 | 0.69 | 1.73 |
| | Tr5y | 1,523.9 | 1,524.7 | 1,525.0 | 2.65 | 0.78 | 1.37 |
| | Tr100y | 1,523.9 | 1,524.8 | 1,525.3 | 3.06 | 0.91 | 1.43 |
| 475 | Tr200y | 1,523.9 | 1,524.9 | 1,525.3 | 3.13 | 0.94 | 1.44 |
| | Tr5y | 1,523.0 | 1,523.7 | 1,524.1 | 2.76 | 0.69 | 1.40 |
| | Tr100y | 1,523.0 | 1,523.9 | 1,524.3 | 3.20 | 0.84 | 1.44 |
| 450 | Tr200y | 1,523.0 | 1,523.9 | 1,524.4 | 3.28 | 0.87 | 1.45 |
| | Tr5y | 1,522.0 | 1,522.9 | 1,523.2 | 2.51 | 0.90 | 1.35 |
| | Tr100y | 1,522.0 | 1,523.0 | 1,523.5 | 2.90 | 1.03 | 1.39 |
| 425 | Tr200y | 1,522.0 | 1,523.1 | 1,523.5 | 2.98 | 1.05 | 1.39 |
| | Tr5y | 1,521.0 | 1,522.0 | 1,522.3 | 2.50 | 0.99 | 1.34 |
| | Tr100y | 1,521.0 | 1,522.2 | 1,522.6 | 2.90 | 1.12 | 1.37 |
| 400 | Tr200y | 1,521.0 | 1,522.2 | 1,522.6 | 2.97 | 1.15 | 1.37 |
| | Tr5y | 1,520.4 | 1,521.6 | 1,521.7 | 1.85 | 1.13 | 0.90 |
| | Tr100y | 1,520.4 | 1,521.7 | 1,522.0 | 2.45 | 1.22 | 1.08 |
| 375 | Tr200y | 1,520.4 | 1,521.7 | 1,522.0 | 2.56 | 1.24 | 1.11 |
| | Tr5y | 1,520.0 | 1,521.1 | 1,521.3 | 2.01 | 1.06 | 0.99 |
| | Tr100y | 1,520.0 | 1,521.3 | 1,521.5 | 2.35 | 1.22 | 0.99 |
| 350 | Tr200y | 1,520.0 | 1,521.3 | 1,521.6 | 2.42 | 1.25 | 1.00 |
| | Tr5y | 1,519.1 | 1,520.1 | 1,520.4 | 2.60 | 1.01 | 1.28 |
| | Tr100y | 1,519.1 | 1,520.3 | 1,520.7 | 2.83 | 1.17 | 1.33 |
| 325 | Tr200y | 1,519.1 | 1,520.3 | 1,520.7 | 2.93 | 1.20 | 1.34 |
| | Tr5y | 1,518.6 | 1,519.4 | 1,519.6 | 2.02 | 0.74 | 0.98 |
| | Tr100y | 1,518.6 | 1,519.5 | 1,519.8 | 2.37 | 0.89 | 1.00 |
| 300 | Tr200y | 1,518.6 | 1,519.6 | 1,519.9 | 2.44 | 0.92 | 1.01 |
| | Tr5y | 1,518.0 | 1,518.9 | 1,519.1 | 2.06 | 0.93 | 1.01 |
| | Tr100y | 1,518.0 | 1,519.1 | 1,519.4 | 2.42 | 1.08 | 1.07 |
| 275 | Tr200y | 1,518.0 | 1,519.1 | 1,519.4 | 2.50 | 1.10 | 1.07 |
| | Tr5y | 1,517.0 | 1,517.8 | 1,518.2 | 2.69 | 0.82 | 1.36 |
| | Tr100y | 1,517.0 | 1,518.0 | 1,518.5 | 3.11 | 0.97 | 1.35 |

| Cross Section | Return Period | Riverbed El. (masl) | W.S. El. (masl) | Energy El. (masl) | Flow Vel. (m/s) | Flow Depth (m) | Froude |
|----------------------|----------------------|----------------------------|------------------------|--------------------------|------------------------|-----------------------|---------------|
| 250 | Tr200y | 1,517.0 | 1,518.0 | 1,518.5 | 3.18 | 1.00 | 1.35 |
| | Tr5y | 1,516.0 | 1,517.2 | 1,517.4 | 2.04 | 1.20 | 0.87 |
| | Tr100y | 1,516.0 | 1,517.4 | 1,517.7 | 2.36 | 1.40 | 0.88 |
| 225 | Tr200y | 1,516.0 | 1,517.5 | 1,517.7 | 2.43 | 1.45 | 0.88 |
| | Tr5y | 1,516.0 | 1,516.8 | 1,517.1 | 2.26 | 0.84 | 1.00 |
| | Tr100y | 1,516.0 | 1,517.0 | 1,517.4 | 2.67 | 1.03 | 1.00 |
| 200 | Tr200y | 1,516.0 | 1,517.1 | 1,517.4 | 2.74 | 1.07 | 1.01 |
| | Tr5y | 1,515.0 | 1,516.2 | 1,516.5 | 2.41 | 1.22 | 0.99 |
| | Tr100y | 1,515.0 | 1,516.5 | 1,516.8 | 2.71 | 1.46 | 0.99 |
| 175 | Tr200y | 1,515.0 | 1,516.5 | 1,516.9 | 2.76 | 1.51 | 1.00 |
| | Tr5y | 1,514.7 | 1,515.8 | 1,516.1 | 2.43 | 1.12 | 1.00 |
| | Tr100y | 1,514.7 | 1,516.0 | 1,516.4 | 2.85 | 1.34 | 1.01 |
| 150 | Tr200y | 1,514.7 | 1,516.0 | 1,516.5 | 2.93 | 1.39 | 1.01 |
| | Tr5y | 1,514.0 | 1,514.7 | 1,515.2 | 3.05 | 0.67 | 1.40 |
| | Tr100y | 1,514.0 | 1,514.8 | 1,515.5 | 3.69 | 0.83 | 1.47 |
| 125 | Tr200y | 1,514.0 | 1,514.9 | 1,515.6 | 3.80 | 0.87 | 1.48 |
| | Tr5y | 1,513.2 | 1,514.1 | 1,514.5 | 2.87 | 0.89 | 1.13 |
| | Tr100y | 1,513.2 | 1,514.4 | 1,514.9 | 3.08 | 1.17 | 1.16 |
| 100 | Tr200y | 1,513.2 | 1,514.4 | 1,514.9 | 3.17 | 1.21 | 1.16 |
| | Tr5y | 1,512.9 | 1,513.7 | 1,514.0 | 2.30 | 0.81 | 1.03 |
| | Tr100y | 1,512.9 | 1,513.9 | 1,514.3 | 2.73 | 0.99 | 1.05 |
| 75 | Tr200y | 1,512.9 | 1,513.9 | 1,514.3 | 2.99 | 0.98 | 1.15 |
| | Tr5 | 1,512.1 | 1,513.1 | 1,513.4 | 2.09 | 1.06 | 0.81 |
| | Tr100 | 1,512.1 | 1,513.2 | 1,513.7 | 3.13 | 1.12 | 1.16 |
| 50 | Tr200 | 1,512.1 | 1,513.2 | 1,513.8 | 3.20 | 1.16 | 1.16 |
| | Tr5 | 1,511.6 | 1,512.5 | 1,512.8 | 2.51 | 0.87 | 1.26 |
| | Tr100 | 1,511.6 | 1,512.6 | 1,513.1 | 3.00 | 1.01 | 1.30 |
| 25 | Tr200 | 1,511.6 | 1,512.7 | 1,513.1 | 3.09 | 1.04 | 1.30 |
| | Tr5 | 1,511.0 | 1,511.8 | 1,512.1 | 2.52 | 0.80 | 1.25 |
| | Tr100 | 1,511.0 | 1,512.0 | 1,512.4 | 3.06 | 0.94 | 1.32 |

| Cross Section | Return Period | Riverbed El. (masl) | W.S. El. (masl) | Energy El. (masl) | Flow Vel. (m/s) | Flow Depth (m) | Froude |
|----------------------|----------------------|----------------------------|------------------------|--------------------------|------------------------|-----------------------|---------------|
| 0 | Tr200 | 1,511.0 | 1,512.0 | 1,512.5 | 3.13 | 0.97 | 1.31 |
| | Tr5 | 1,510.0 | 1,510.7 | 1,511.2 | 3.01 | 0.69 | 1.47 |
| | Tr100 | 1,510.0 | 1,510.9 | 1,511.5 | 3.53 | 0.85 | 1.50 |
| | Tr200 | 1,510.0 | 1,510.9 | 1,511.6 | 3.62 | 0.88 | 1.49 |

(This page intentionally left blank)

Appendix VIII

Detailed Cost Analysis Results

Cost Analysis River Alternative - Steel

| Item | Units | Units Number | Unit Cost (USD) | Cost (USD) |
|--|-------|--------------|-----------------|-------------------|
| Direct Costs | | | | |
| Intake | | | | 752,182 |
| Stripping - L:35 m | Lm | 35 | 279 | 9,767 |
| Formwork - L:35 m | Lm | 35 | 1,919 | 67,148 |
| Concrete - L:35 m | Lm | 35 | 4,883 | 170,922 |
| Reinforcement - L:35 m | Lm | 35 | 165 | 5,763 |
| Trashracks - 5 m ² | gl | 4 | 13,004 | 52,015 |
| Sliding Gate - 10 m ² | gl | 1 | 215,824 | 215,824 |
| Contractor Expenses - H:3.5 m L:35 m | Lm | 35 | 6,593 | 230,742 |
| Settling Basin & Forebay | | | | 2,546,788 |
| Stripping - L: 128 m | Lm | 128 | 279 | 35,719 |
| Excavations - L: 128 m | Lm | 128 | 1,842 | 235,747 |
| Settling Basin Concrete - L:95 m | Lm | 95 | 12,209 | 1,159,830 |
| Forebay Concrete - L:33 m | Lm | 33 | 2,965 | 97,844 |
| Formwork - L: 128 m | Lm | 128 | 4,988 | 638,482 |
| Reinforcement - L: 128 m | Lm | 128 | 318 | 40,720 |
| Flushing Gates - 2.5 m ² | gl | 2 | 98,997 | 197,994 |
| Trashracks - 4 m ² | gl | 1 | 11,515 | 11,515 |
| Forebay Emergency Gate - 4 m ² | gl | 1 | 128,937 | 128,937 |
| Headrace Conduit & Penstock | | | | 30,696,527 |
| Pipe Cost - Steel - D:1.9 m | ton | 3,998 | 1,900 | 7,596,466 |
| Trench in Soil - H:6.0 m B:2.5 m | Lm | 3,797 | 775 | 2,943,811 |
| Trench in Rock - H:6.0 m B:2.5 m | Lm | 949 | 2,644 | 2,509,855 |
| Segments Protected with Concrete | Lm | 655 | 652 | 427,253 |
| Contractor Costs | m | 4,747 | 3,628 | 17,219,141 |
| Powerhouse | | | | 11,711,298 |
| Turbine 1 (Dist., Inlet Valve, Freq. Gov.) - Q:9 m ³ /s H:282 m | kW | 20,700 | 158 | 3,278,023 |
| Turbine 2 (Dist., Inlet Valve, Freq. Gov.) - Q:1 m ³ /s H:282 m | kW | 2,300 | 632 | 1,453,045 |
| Electro Technical Work (Gen., Trans., Control, Etc.) | gl | 1 | 6,366,990 | 6,366,990 |
| Miscellaneous Mechanical Equipment | kW | 23,000 | 22 | 513,240 |
| Civil Works | gl | 1 | 100,000 | 100,000 |
| Direct Costs Total | | | | 45,706,795 |

| Item | Units | Units Number | Unit Cost (USD) | Cost (USD) |
|---|-------|--------------|-----------------|-------------------|
| Indirect Costs | | | | |
| Transport and Insurance of Equipment (5%) | gl | - | - | 990,702 |
| Equipment Customs Taxes (4%) | gl | - | - | 443,922 |
| Equipment Spare Parts (3%) | gl | - | - | 364,622 |
| Pre-Engineering (1.5%) | gl | - | - | 685,602 |
| Tender Documents (2.5%) | gl | - | - | 1,142,670 |
| Detailed Engineering (8%) | gl | - | - | 3,656,544 |
| Construction Management (8%) | gl | - | - | 3,656,544 |
| Power Plant Commissioning | gl | - | - | 1,600,000 |
| Owner's Costs (2%) | gl | - | - | 1,164,948 |
| Indirect Costs Total | | | | 13,705,553 |
| Unforeseen Expenses (20%) | gl | - | - | 11,882,470 |
| Total | | | | 71,294,818 |
| Unit Cost (USD/MWh) | | | | 1,145 |

Cost Analysis River Alternative – GRP and Steel

| Item | Units | Units Number | Unit Cost (USD) | Cost (USD) |
|--|-------|--------------|-----------------|-------------------|
| Direct Costs | | | | |
| Intake | | | | 752,182 |
| Stripping - L:35 m | Lm | 35 | 279 | 9,767 |
| Formwork - L:35 m | Lm | 35 | 1,919 | 67,148 |
| Concrete - L:35 m | Lm | 35 | 4,883 | 170,922 |
| Reinforcement - L:35 m | Lm | 35 | 165 | 5,763 |
| Trashracks - 5 m ² | gl | 4 | 13,004 | 52,015 |
| Sliding Gate - 10 m ² | gl | 1 | 215,824 | 215,824 |
| Contractor Expenses - H:3.5 m L:35 m | Lm | 35 | 6,593 | 230,742 |
| Settling Basin & Forebay | | | | 2,546,788 |
| Stripping - L: 128 m | Lm | 128 | 279 | 35,719 |
| Excavations - L: 128 m | Lm | 128 | 1,842 | 235,747 |
| Settling Basin Concrete - L:95 m | Lm | 95 | 12,209 | 1,159,830 |
| Forebay Concrete - L:33 m | Lm | 33 | 2,965 | 97,844 |
| Formwork - L: 128 m | Lm | 128 | 4,988 | 638,482 |
| Reinforcement - L: 128 m | Lm | 128 | 318 | 40,720 |
| Flushing Gates - 2.5 m ² | gl | 2 | 98,997 | 197,994 |
| Trashracks - 4 m ² | gl | 1 | 11,515 | 11,515 |
| Forebay Emergency Gate - 4 m ² | gl | 1 | 128,937 | 128,937 |
| Headrace Conduit & Penstock | | | | 33,930,830 |
| Pipe Cost - GRP+Steel - D:1.8 m | gl | 1 | 7,784,305 | 7,784,305 |
| Trench in Soil - H:6.0 m B:2.5 m | Lm | 3,797 | 775 | 2,943,811 |
| Trench in Rock - H:6.0 m B:2.5 m | Lm | 949 | 2,644 | 2,509,855 |
| Segments Protected with Concrete | Lm | 655 | 652 | 427,253 |
| Contractor Costs | m | 4,747 | 4,270 | 20,265,605 |
| Powerhouse | | | | 11,711,298 |
| Turbine 1 (Dist., Inlet Valve, Freq. Gov.) - Q:9 m ³ /s H:282 m | kW | 20,700 | 158 | 3,278,023 |
| Turbine 2 (Dist., Inlet Valve, Freq. Gov.) - Q:1 m ³ /s H:282 m | kW | 2,300 | 632 | 1,453,045 |
| Electro Technical Work (Gen., Trans., Control, Etc.) | gl | 1 | 6,366,990 | 6,366,990 |
| Miscellaneous Mechanical Equipment | kW | 23,000 | 22 | 513,240 |
| Civil Works | gl | 1 | 100,000 | 100,000 |
| Direct Costs Total | | | | 48,941,098 |
| Indirect Costs | | | | |
| Transport and Insurance of Equipment (5%) | gl | - | - | 1,000,094 |
| Equipment Customs Taxes (4%) | gl | - | - | 755,294 |
| Equipment Spare Parts (3%) | gl | - | - | 364,622 |

| Item | Units | Units Number | Unit Cost (USD) | Cost (USD) |
|------------------------------|-------|--------------|-----------------|-------------------|
| Pre-Engineering (1.5%) | gl | - | - | 734,116 |
| Tender Documents (2.5%) | gl | - | - | 1,223,527 |
| Detailed Engineering (8%) | gl | - | - | 3,915,288 |
| Construction Management (8%) | gl | - | - | 3,915,288 |
| Power Plant Commissioning | gl | - | - | 1,600,000 |
| Owner's Costs (2%) | gl | - | - | 1,248,987 |
| Indirect Costs Total | | | | 14,757,217 |
| Unforeseen Expenses (20%) | gl | - | - | 12,739,663 |
| Total | | | | 76,437,977 |
| Unit Cost (USD/MWh) | | | | 1,227 |

Cost Analysis Road Alternative – Steel

| Item | Units | Units Number | Unit Cost (USD) | Cost (USD) |
|--|-------|--------------|-----------------|-------------------|
| Direct Costs | | | | |
| Intake | | | | 752,182 |
| Stripping - L:35 m | Lm | 35 | 279 | 9,767 |
| Formwork - L:35 m | Lm | 35 | 1,919 | 67,148 |
| Concrete - L:35 m | Lm | 35 | 4,883 | 170,922 |
| Reinforcement - L:35 m | Lm | 35 | 165 | 5,763 |
| Trashracks - 5 m ² | gl | 4 | 13,004 | 52,015 |
| Sliding Gate - 10 m ² | gl | 1 | 215,824 | 215,824 |
| Contractor Expenses - H:3.5 m L:35 m | Lm | 35 | 6,593 | 230,742 |
| Settling Basin & Forebay | | | | 2,546,788 |
| Stripping - L: 128 m | Lm | 128 | 279 | 35,719 |
| Excavations - L: 128 m | Lm | 128 | 1,842 | 235,747 |
| Settling Basin Concrete - L:95 m | Lm | 95 | 12,209 | 1,159,830 |
| Forebay Concrete - L:33 m | Lm | 33 | 2,965 | 97,844 |
| Formwork - L: 128 m | Lm | 128 | 4,988 | 638,482 |
| Reinforcement - L: 128 m | Lm | 128 | 318 | 40,720 |
| Forebay Flushing Gates - 2.5 m ² | gl | 2 | 98,997 | 197,994 |
| Trashracks - 4 m ² | gl | 1 | 11,515 | 11,515 |
| Forebay Emergency Gate - 4 m ² | gl | 1 | 128,937 | 128,937 |
| Headrace Conduit & Penstock | | | | 32,266,932 |
| Pipe Cost - Steel - D:1.9 m | ton | 3,595 | 1,900 | 6,830,258 |
| Trench in Soil - H:6.0 m B:2.5 m | Lm | 3,920 | 775 | 3,039,339 |
| Trench in Rock - H:6.0 m B:2.5 m | Lm | 980 | 2,644 | 2,591,302 |
| Surge Chamber Shaft - D:2.7 m L:308 m | Lm | 308 | 1,412 | 434,756 |
| Surge Chamber Inner Lining - D:2.7 m L:308 m | Lm | 308 | 5,173 | 1,593,366 |
| Contractor Costs | m | 4,901 | 3,628 | 17,777,912 |
| Powerhouse | | | | 11,711,298 |
| Turbine 1 (Dist., Inlet Valve, Freq. Gov.) - Q:9 m ³ /s H:282 m | kW | 20,700 | 158 | 3,278,023 |
| Turbine 2 (Dist., Inlet Valve, Freq. Gov.) - Q:1 m ³ /s H:282 m | kW | 2,300 | 632 | 1,453,045 |
| Electro Technical Work (Gen., Trans., Control, Etc.) | gl | 1 | 6,366,990 | 6,366,990 |
| Miscellaneous Mechanical Equipment | kW | 23,000 | 22 | 513,240 |
| Civil Works | gl | 1 | 100,000 | 100,000 |
| Direct Costs Total | | | | 47,277,200 |
| Indirect Costs | | | | |
| Transport and Insurance of Equipment (5%) | gl | - | - | 1,032,060 |
| Equipment Customs Taxes (4%) | gl | - | - | 443,922 |

| Item | Units | Units Number | Unit Cost (USD) | Cost (USD) |
|------------------------------|-------|--------------|-----------------|-------------------|
| Equipment Spare Parts (3%) | gl | - | - | 364,622 |
| Pre-Engineering (1.5%) | gl | - | - | 709,158 |
| Tender Documents (2.5%) | gl | - | - | 1,181,930 |
| Detailed Engineering (8%) | gl | - | - | 3,782,176 |
| Construction Management (8%) | gl | - | - | 3,782,176 |
| Power Plant Commissioning | gl | - | - | 1,600,000 |
| Owner's Costs (2%) | gl | - | - | 1,203,465 |
| Indirect Costs Total | | | | 14,099,509 |
| Unforeseen Expenses (20%) | gl | - | - | 12,275,342 |
| Total | | | | 73,652,051 |
| Unit Cost (USD/MWh) | | | | 1,188 |

Cost Analysis Road Alternative – GRP and Steel

| Item | Units | Units Number | Unit Cost (USD) | Cost (USD) |
|--|-------|--------------|-----------------|-------------------|
| Direct Costs | | | | |
| Intake | | | | 752,182 |
| Stripping - L:35 m | Lm | 35 | 279 | 9,767 |
| Formwork - L:35 m | Lm | 35 | 1,919 | 67,148 |
| Concrete - L:35 m | Lm | 35 | 4,883 | 170,922 |
| Reinforcement - L:35 m | Lm | 35 | 165 | 5,763 |
| Trashracks - 5 m ² | gl | 4 | 13,004 | 52,015 |
| Sliding Gate - 10 m ² | gl | 1 | 215,824 | 215,824 |
| Contractor Expenses - H:3.5 m L:35 m | Lm | 35 | 6,593 | 230,742 |
| Settling Basin & Forebay | | | | 2,546,788 |
| Stripping - L: 128 m | Lm | 128 | 279 | 35,719 |
| Excavations - L: 128 m | Lm | 128 | 1,842 | 235,747 |
| Settling Basin Concrete - L:95 m | Lm | 95 | 12,209 | 1,159,830 |
| Forebay Concrete - L:33 m | Lm | 33 | 2,965 | 97,844 |
| Formwork - L: 128 m | Lm | 128 | 4,988 | 638,482 |
| Reinforcement - L: 128 m | Lm | 128 | 318 | 40,720 |
| Forebay Flushing Gates - 2.5 m ² | gl | 2 | 98,997 | 197,994 |
| Trashracks - 4 m ² | gl | 1 | 11,515 | 11,515 |
| Forebay Emergency Gate - 4 m ² | gl | 1 | 128,937 | 128,937 |
| Headrace Conduit & Penstock | | | | 37,154,163 |
| Pipe Cost - GRP+Steel - D:1.9 m | gl | 1 | 7,794,383 | 7,794,383 |
| Trench in Soil - H:6.0 m B:2.5 m | Lm | 3,920 | 775 | 3,039,339 |
| Trench in Rock - H:6.0 m B:2.5 m | Lm | 980 | 2,644 | 2,591,302 |
| Surge Chamber Shaft - D:2.7 m L:308 m | Lm | 308 | 1,412 | 434,756 |
| Surge Chamber Inner Lining - D:2.7 m L:308 m | Lm | 308 | 5,173 | 1,593,366 |
| Contractor Costs | m | 4,901 | 4,428 | 21,701,018 |
| Powerhouse | | | | 12,117,753 |
| Turbine 1 (Dist., Inlet Valve, Freq. Gov.) - Q:9 m ³ /s H:282 m | kW | 21,600 | 158 | 3,420,545 |
| Turbine 2 (Dist., Inlet Valve, Freq. Gov.) - Q:1 m ³ /s H:282 m | kW | 2,400 | 632 | 1,516,221 |
| Electro Technical Work (Gen., Trans., Control, Etc.) | gl | 1 | 6,545,432 | 6,545,432 |
| Miscellaneous Mechanical Equipment | kW | 24,000 | 22 | 535,555 |
| Civil Works | gl | 1 | 100,000 | 100,000 |
| Direct Costs Total | | | | 52,570,887 |
| Indirect Costs | | | | |
| Transport and Insurance of Equipment (5%) | gl | - | - | 1,100,589 |
| Equipment Customs Taxes (4%) | gl | - | - | 771,063 |

| Item | Units | Units Number | Unit Cost (USD) | Cost (USD) |
|------------------------------|-------|--------------|-----------------|-------------------|
| Equipment Spare Parts (3%) | gl | - | - | 376,815 |
| Pre-Engineering (1.5%) | gl | - | - | 788,563 |
| Tender Documents (2.5%) | gl | - | - | 1,314,272 |
| Detailed Engineering (8%) | gl | - | - | 4,205,671 |
| Construction Management (8%) | gl | - | - | 4,205,671 |
| Power Plant Commissioning | gl | - | - | 1,600,000 |
| Owner's Costs (2%) | gl | - | - | 1,338,671 |
| Indirect Costs Total | | | | 15,701,316 |
| Unforeseen Expenses (20%) | gl | - | - | 13,654,441 |
| Total | | | | 81,926,643 |
| Unit Cost (USD/MWh) | | | | 1,304 |

Cost Analysis Low-Pressure Alternative – Steel

| Item | Units | Units Number | Unit Cost (USD) | Cost (USD) |
|--|-------|--------------|-----------------|-------------------|
| Direct Costs | | | | |
| Intake | | | | 752,182 |
| Stripping - L:35 m | Lm | 35 | 279 | 9,767 |
| Formwork - L:35 m | Lm | 35 | 1,919 | 67,148 |
| Concrete - L:35 m | Lm | 35 | 4,883 | 170,922 |
| Reinforcement - L:35 m | Lm | 35 | 165 | 5,763 |
| Trashracks - 5 m ² | gl | 4 | 13,004 | 52,015 |
| Sliding Gate - 10 m ² | gl | 1 | 215,824 | 215,824 |
| Contractor Expenses - H:3.5 m L:35 m | Lm | 35 | 6,593 | 230,742 |
| Settling Basin & Forebay | | | | 2,546,788 |
| Stripping - L: 128 m | Lm | 128 | 279 | 35,719 |
| Excavations - L: 128 m | Lm | 128 | 1,842 | 235,747 |
| Settling Basin Concrete - L:95 m | Lm | 95 | 12,209 | 1,159,830 |
| Forebay Concrete - L:33 m | Lm | 33 | 2,965 | 97,844 |
| Formwork - L: 128 m | Lm | 128 | 4,988 | 638,482 |
| Reinforcement - L: 128 m | Lm | 128 | 318 | 40,720 |
| Forebay Flushing Gates - 2.5 m ² | gl | 2 | 98,997 | 197,994 |
| Trashracks - 4 m ² | gl | 1 | 11,515 | 11,515 |
| Forebay Emergency Gate - 4 m ² | gl | 1 | 128,937 | 128,937 |
| Headrace Conduit & Penstock | | | | 32,999,840 |
| Pipe Cost - Steel - D:2.1 m | ton | 3,557 | 1,900 | 6,757,845 |
| Trench in Soil - H:5.0 m B:2.5 m | Lm | 3,365 | 722 | 2,428,311 |
| Trench in Rock - H:5.0 m B:2.5 m | Lm | 1,812 | 2,065 | 3,740,964 |
| Surge Chamber Shaft - D:2.7 m L:32 m | Lm | 32 | 1,412 | 45,169 |
| Surge Chamber Inner Lining - D:2.7 m L:32 m | Lm | 32 | 5,173 | 165,545 |
| Contractor Costs | m | 5,176 | 3,837 | 19,862,006 |
| Powerhouse | | | | 12,117,753 |
| Turbine 1 (Dist., Inlet Valve, Freq. Gov.) - Q:9 m ³ /s H:282 m | kW | 21,600 | 158 | 3,420,545 |
| Turbine 2 (Dist., Inlet Valve, Freq. Gov.) - Q:1 m ³ /s H:282 m | kW | 2,400 | 632 | 1,516,221 |
| Electro Technical Work (Gen., Trans., Control, Etc.) | gl | 1 | 6,545,432 | 6,545,432 |
| Miscellaneous Mechanical Equipment | kW | 24,000 | 22 | 535,555 |
| Civil Works | gl | 1 | 100,000 | 100,000 |
| Direct Costs Total | | | | 48,416,564 |
| Indirect Costs | | | | |
| Transport and Insurance of Equipment (5%) | gl | - | - | 977,371 |
| Equipment Customs Taxes (4%) | gl | - | - | 459,288 |

| Item | Units | Units Number | Unit Cost (USD) | Cost (USD) |
|------------------------------|-------|--------------|-----------------|-------------------|
| Equipment Spare Parts (3%) | gl | - | - | 376,815 |
| Pre-Engineering (1.5%) | gl | - | - | 726,248 |
| Tender Documents (2.5%) | gl | - | - | 1,210,414 |
| Detailed Engineering (8%) | gl | - | - | 3,873,325 |
| Construction Management (8%) | gl | - | - | 3,873,325 |
| Power Plant Commissioning | gl | - | - | 1,600,000 |
| Owner's Costs (2%) | gl | - | - | 1,230,267 |
| Indirect Costs Total | | | | 14,327,055 |
| Unforeseen Expenses (20%) | gl | - | - | 12,548,724 |
| Total | | | | 75,292,342 |
| Unit Cost (USD/MWh) | | | | 1,190 |

Cost Analysis Low-Pressure Alternative – GRP and Steel

| Item | Units | Units Number | Unit Cost (USD) | Cost (USD) |
|--|-------|--------------|-----------------|-------------------|
| Direct Costs | | | | |
| Intake | | | | 752,182 |
| Stripping - L:35 m | Lm | 35 | 279 | 9,767 |
| Formwork - L:35 m | Lm | 35 | 1,919 | 67,148 |
| Concrete - L:35 m | Lm | 35 | 4,883 | 170,922 |
| Reinforcement - L:35 m | Lm | 35 | 165 | 5,763 |
| Trashracks - 5 m ² | gl | 4 | 13,004 | 52,015 |
| Sliding Gate - 10 m ² | gl | 1 | 215,824 | 215,824 |
| Contractor Expenses - H:3.5 m L:35 m | Lm | 35 | 6,593 | 230,742 |
| Settling Basin & Forebay | | | | 2,546,788 |
| Stripping - L: 128 m | Lm | 128 | 279 | 35,719 |
| Excavations - L: 128 m | Lm | 128 | 1,842 | 235,747 |
| Settling Basin Concrete - L:95 m | Lm | 95 | 12,209 | 1,159,830 |
| Forebay Concrete - L:33 m | Lm | 33 | 2,965 | 97,844 |
| Formwork - L: 128 m | Lm | 128 | 4,988 | 638,482 |
| Reinforcement - L: 128 m | Lm | 128 | 318 | 40,720 |
| Forebay Flushing Gates - 2.5 m ² | gl | 2 | 98,997 | 197,994 |
| Trashracks - 4 m ² | gl | 1 | 11,515 | 11,515 |
| Forebay Emergency Gate - 4 m ² | gl | 1 | 128,937 | 128,937 |
| Headrace Conduit & Penstock | | | | 36,636,476 |
| Pipe Cost - GRP+Steel - D:1.9 m | gl | 1 | 7,333,926 | 7,333,926 |
| Trench in Soil - H:5.0 m B:2.5 m | Lm | 3,365 | 722 | 2,428,311 |
| Trench in Rock - H:5.0 m B:2.5 m | Lm | 1,812 | 2,065 | 3,740,964 |
| Surge Chamber Shaft - D:2.7 m L:32 m | Lm | 32 | 1,412 | 45,169 |
| Surge Chamber Inner Lining - D:2.7 m L:32 m | Lm | 32 | 5,173 | 165,545 |
| Contractor Costs | m | 5,176 | 4,428 | 22,922,561 |
| Powerhouse | | | | 11,711,298 |
| Turbine 1 (Dist., Inlet Valve, Freq. Gov.) - Q:9 m ³ /s H:282 m | kW | 20,700 | 158 | 3,278,023 |
| Turbine 2 (Dist., Inlet Valve, Freq. Gov.) - Q:1 m ³ /s H:282 m | kW | 2,300 | 632 | 1,453,045 |
| Electro Technical Work (Gen., Trans., Control, Etc.) | gl | 1 | 6,366,990 | 6,366,990 |
| Miscellaneous Mechanical Equipment | kW | 23,000 | 22 | 513,240 |
| Civil Works | gl | 1 | 100,000 | 100,000 |
| Direct Costs Total | | | | 51,646,744 |
| Indirect Costs | | | | |
| Transport and Insurance of Equipment (5%) | gl | - | - | 985,853 |
| Equipment Customs Taxes (4%) | gl | - | - | 737,279 |

| Item | Units | Units Number | Unit Cost (USD) | Cost (USD) |
|------------------------------|-------|--------------|-----------------|-------------------|
| Equipment Spare Parts (3%) | gl | - | - | 364,622 |
| Pre-Engineering (1.5%) | gl | - | - | 774,701 |
| Tender Documents (2.5%) | gl | - | - | 1,291,169 |
| Detailed Engineering (8%) | gl | - | - | 4,131,739 |
| Construction Management (8%) | gl | - | - | 4,131,739 |
| Power Plant Commissioning | gl | - | - | 1,600,000 |
| Owner's Costs (2%) | gl | - | - | 1,313,277 |
| Indirect Costs Total | | | | 15,330,379 |
| Unforeseen Expenses (20%) | gl | - | - | 13,395,425 |
| Total | | | | 80,372,548 |
| Unit Cost (USD/MWh) | | | | 1,287 |